Unravelling Carbon Formation on high Temperature Alloys and Coatings

Ontrafelen Coke Vorming op Hoge Temperatuur Legeringen en Coatings

Stamatis A. Sarris

Promotoren: prof. dr. ir. K.M. Van Geem, Prof. dr. Marie-Françoise Reyniers
Proefschrift ingediend tot het behalen van de graad van
Doctor in de Ingenieurswetenschappen: Chemische Technologie

Vakgroep Materialen, Textiel en Chemische Proceskunde
Voorzitter: prof. dr. ir. Guy B. Marin
Faculteit Ingenieurswetenschappen en Architectuur
Academiejaar 2017 – 2018

Promotoren:

Prof. dr. ir. Kevin M. Van Geem
Vakgroep Materialen, Textiel en Chemische Proceskunde
Faculteit Ingenieurswetenschappen en Architectuur
Universiteit Gent

Prof. dr. Marie-Françoise Reyniers
Vakgroep Materialen, Textiel en Chemische Proceskunde
Faculteit Ingenieurswetenschappen en Architectuur
Universiteit Gent

Decaan: Prof. dr. ir. Rik Van de Walle

Rector: Prof. dr. Anne De Paepe

De auteur genoot tijdens de onderzoeksactiviteiten de steun van de langdurige en structurele *Methusalem* financiering van de Vlaamse Overheid BOF09/01M00409.

EXAMENCOMMISSIE

Leescommissie

Dr. Marjolein Vanoppen
Faculteit Bio-ingenieurswetenschappen
Vakgroep Toegepaste Analytische en Fysische Chemie
Universiteit Gent

Prof. Dr. ir. Kim Verbeken
Vakgroep Materialen, Textiel en Chemische Proceskunde
Faculteit Ingenieurswetenschappen en Architectuur
Universiteit Gent

Prof. Dr. ir. Nikolaos Papayannakos
Department of Process Analysis and Plant Design
School of Chemical Engineering
National Technical University of Athens

Dr. ir. Valérie Vanrysselberghe
Raffinage-Chimie
Division Procédés & Avant-Projets
Département Procédés Raffinage & Base Chem
Total Research & Technology Feluy

Prof. Dr. ir. Guy B. Marin [promotor]
Vakgroep Materialen, Textiel en Chemische Proceskunde
Faculteit Ingenieurswetenschappen en Architectuur
Universiteit Gent

Andere leden

Prof. dr. ir. Kevin M. Van Geem [promotor]
Vakgroep Materialen, Textiel en Chemische Proceskunde
Faculteit Ingenieurswetenschappen en Architectuur
Universiteit Gent

Prof. dr. Marie-Françoise Reyniers [promotor]
Vakgroep Materialen, Textiel en Chemische Proceskunde
Faculteit Ingenieurswetenschappen en Architectuur
Universiteit Gent

Prof. dr. ir. Luc Taerwe [voorzitter]
Vakgroep Bouwkundige Constructies
Universiteit Gent

Having no limitation as limitation

Αφιερωμένο στην οικογένεια μου και σε εσένα Αλεξάνδρα

Acknowledgement

More than four years of dedicated and passionate work, there is a long list of people that I would like to express my gratitude for the help and support in proceeding along the hard path of a PhD in Chemical Engineering.

First of all, I would like to thank professor Guy B. Marin and my two promotors Kevin Van Geem and Marie-Françoise Reyniers, for giving me such a unique opportunity to be a part of their group and to evolve as a person, both professionally and emotionally. Your effort, knowledge, professional experience and motivation supported and inspired me to improve through this evolving procedure.

Kevin, I personally thank you for giving me all this support and belief in my ideas and passion for the last four years. You have been an ideal coach, talking with me like a great friend, helping me picking the proper solutions for my scientific obstacles. Your speed, efficiency and practicality have been eventually my most valuable professional engineering standards thanks to your guidance. Marie-Françoise, of course, thank you for our endless discussions that helped me thinking in a much more fundamental way every phenomenon that I had met during my research. For both, it has been a pleasure working with you.

I would like to express my strong appreciation – and sincere apologies if I have been too strict – to my master students. Sara and Matthias, Emma, Blerta and Annelies, Koen, Hanne and Steffen. I hope I managed to convey to you at least the knowledge you gave me through coaching you.

Acknowledgement

Infinite appreciation to my colleagues at LCT. Your support and constant energy in and out of the lab created an amazing working and social environment. Kaustav, Marita, Hassan, Max and Kristy, David and Pieter Reyniers, Carl, Nick, Michael, Marcel, Hence, Gilles, Gonzalo, the two Rubens, Jelena, Aditya, Chanakya, Stefanie and Lukas…Above all else, my partners in crime: Marko, Nenad, Steffen, Arturo and Aleksandar. Хвала, Dank u wel, Gracias!

Στην ελληνική παρέα της Γάνδης ένα τεράστιο ευχαριστώ για τις απίστευτες στιγμές που μου χαρίσατε. Τάκη, Μαγλοτζόνιδες, Κώστα, Μαρία και Πάνο, Βάιε, Άγγελε, Γιώργο, Γιάννη, Μαριάννα, Ρούμπεν, Εύα...σας ευχαριστώ. Ζαρρίκο, Δημήτριε, Μπάμπη, Σταύρο και Βασίλη θα συνεχίσουμε να τα λέμε για πάντα είμαι βέβαιος!

Κύριε καθηγητά, σας ευχαριστώ για τις γεμάτες ουσία και βάθος συζητήσεις μας και την φιλοσοφική αναζήτηση των τελευταίων μηνών. Είναι μεγάλη μου τιμή που σας έχω γνωρίσει και με βοηθάτε να βελτιώνομαι σαν οντότητα επιστημονικά και μη.

Τελευταίοι μα καθόλα σημαντικοί, θα ήθελα να ευχαριστήσω την οικογένεια μου, τους ανθρώπους που με στηρίζουν όλα αυτά τα χρόνια με αγάπη και συγκατάβαση σε ότι επιλέξω. Πατέρα και μητέρα, σας ευχαριστώ για την τεράστια συναισθηματική και ηθική στήριξη σε όλη μου τη ζωή. Μαριεττάκι είμαι περήφανος που έχω μία τέτοια αδερφή. Γιώργο και Μάικ η υποστήριξη σας ήταν πάντα παρούσα και χωρίς σύνορα. Αλεξία μου χωρίς την απεριόριστη και άνευ όρων σου αγάπη δεν θα έφτανα ποτέ εδώ σήμερα. Σε ευχαριστώ για όλα και το παρόν αυστηρά αφιερωμένο.

Ευχαριστώ, Thank you, Хвала вам пуно, Muchas gracias, dank u wel…

Stamatis Sarris

Gent, 2018

Contents

Notation

Roman

A	Pre-exponential factor of a reaction with order n	[$kg \cdot s^{-1} \cdot m^{-2} \cdot m_r^{3n} \cdot mol^{-n}$]
A_i	Peak area of compound i on a chromatogram	[$\mu V \cdot s$]
C_i	Concentration of component i	[$mol \cdot m^{-3}$]
CIP	Coil inlet pressure	[Pa]
CIT	Coil inlet temperature	[$^{\circ}C$]
COP	Coil outlet pressure	[Pa]
COT	Coil outlet temperature	[$^{\circ}C$]
$\#C_i$	Carbon number of compound i	[-]
$\#C_{i,eff}$	Effective carbon number of compound i	[-]
Ea	Activation energy	[$kJ \cdot mol^{-1}$]
Ei	Activation energy for reaction i	[$kJ \cdot mol^{-1}$]
F_i	Mass flow rate of component i	[$kg \cdot s^{-1}$]
f_i	Response factor for component i relative to methane	[-]
K	Strain rate	[s^{-1}]
M_i	Molar mass of a compound i	[$kg \cdot mol^{-1}$]
M_s	Molar mass of a reference compound i	[$kg \cdot mol^{-1}$]
$\dot{m}_i$	mass flow rate of compound i	[$kg \cdot s^{-1}$]

N_{Ci}	Number of carbon atoms in a molecule of compound i	[-]
P	Pressure	[Pa]
R	Universal gas constant	8.314 [$J \cdot mol^{-1} \cdot K^{-1}$]
R•	Surface radical	[-]
R_a	Mean surface roughness	[µm]
R_c	Coking rate	[$kg \cdot s^{-1} \cdot m^{-2}$]
$R_{c,asym}$	Asymptotic coking rate	[$kg \cdot s^{-1} \cdot m^{-2}$]
$R_{c,\,pyr}$	Pyrolytic coking rate	[$kg \cdot s^{-1} \cdot m^{-2}$]
$R_{c,cat}$	Rate of growth of catalytic cokes	[$kg \cdot s^{-1} \cdot m^{-2}$]
$R_{c,init}$	Initial coking rate	[$kg \cdot s^{-1} \cdot m^{-2}$]
T	Temperature	[K]
t	Time	[s]
$T_{process,gas}$	Process gas temperature	[K]
x_i	Weight fraction of compound i	[wt %]
X_i	Mole fraction of component i	[mol%]
y_i	Weight fraction of compound i	[wt %]

Greek

δ	Dilution	[-]
σ	standard deviation	
ρ	Volumetric density	[$kg \cdot m^{-3}$]
τ	Mean residence time	[s]

Acronyms

AGO	Atmospheric gas oil
CIT	Coil inlet temperature
CFD	Computational fluid dynamics
COP	Coil outlet pressure
COT	Coil outlet temperature
CSTR	Continuously stirred tank reactor
EDX	Energy-dispersive X-ray spectroscopy
FID	Flame ionization detector
GC	Gas chromatography
HRTEM	High-resolution transmission electro microscopy
JSR	Jet stirred reactor
MFC	Mass flow controller
MOT	Maximum operating temperature
PFR	Plug-flow reactor
RGA	Refinery gas analyzer
SEM	Scanning eletron microscopy

TCD	Thermal conductivity detector
VGO	Vacuum gas oil
WDS	Wavelength-dispersive spectroscopy
XPS	X-ray photoelectron spectroscopy
XRD	X-Ray Diffraction

Subscripts

E	Ethylene
Int. std.	Internal standard
M	Methane
P	Propylene
r	Reactor
Rel st dev	Relative standard deviation
St dev	Standard deviation

Summary

Nowadays, steam cracking of hydrocarbons is still one of the most vital chemical processes for the production of many key-building blocks of the chemical industry. In steam cracking, feedstocks, ranging from ethane and propane over LPG and naphtha to light gasoil, are converted in a high temperature process to ethylene, propylene and several other valuable components. To date, almost 200 million tons of ethylene are manufactured globally per year, underlining the process significance.

The formation of carbonaceous deposits on the inner wall of the reactor forces industrial steam crackers to regularly interrupt production to remove the coke via combustion with a steam/air mixture. The reduction of coke formation is one of the most promising ways of further improving steam cracker efficiency. In an effort to mitigate coke formation several anti-coking technologies have been evolved over the years, namely 3-D reactor technologies, application of additives and use of advanced surface technologies.

The focus of this is put on the last two categories. Finding the optimal process conditions to operate and knowing the effect of extreme carburization and oxidation on a broad range of innovative commercially available materials constitutes its core. Being a corpus of published journal papers and manuscripts that are planned to be submitted for publication this work is therefore written in chapters in the form of one or multiple manuscripts on similar subject areas, having independently a short introduction describing their relevant context.

Initially, in Chapter 2, the non-trivial effect of pretreatment of the reactor coil is evaluated. Eight different pretreatments are tested on a Ni/Cr 35/25 high temperature alloy measuring on-line its coking resistance using a thermogravimetric set-up with a jet stirred reactor under industrially relevant ethane steam cracking conditions (dilution 0.33 kg H2O/ kg C2H6, continuous addition of 41 ppmw S/HC at T=1160 K, equivalent ethane conversion 68 %). The order of the preoxidation and steam pretreatment, together with presulfiding was evaluated. The coking observations confirmed that a high temperature preoxidation, followed by a steam/air pretreatment at 1173 K of 15 minutes has the best coking performance under ethane cracking conditions. Optimization of the pretreatment can lead to a factor 5 reduction of the coking rate. Based on SEM and EDX observations, the uniformity of the oxide layers formed, consisting of Cr and Mn, causes passivation of the alloy catalytic behavior. The presence of Fe and Ni leads to pronounced coking rates, which was the case in particular when presulfiding was applied. Optimization of the pretreatment is expected to be different per the starting material.

In Chapter 3, the unmapped effect of surface roughness on the coking tendency of a 35/25 Ni/Cr wt % alloy is investigated in the same quartz electro-balance set-up, under industrially relevant ethane steam cracking conditions. A lot of work has been done proving qualitatively that the composition and micro-structure of the inner surface of an ethylene cracker is detrimental for its coking behavior. Nevertheless, in the tests, surface roughness and cyclic aging proved to have a quantitative effect mainly on the catalytic coking behavior in a Ra roughness range of 0.15 to 7 μm. A minor effect on the pyrolytic coking rates was found. Surface characterization showed that increased homogeneity of the surface composition together with the formation of Cr_2O_3 and $MnCr_2O_4$ lead to a stable coking behavior, while oxidation of the surface proved to be independent of the surface roughness.

Finding the material with the best anti-coking performance is a typical industrial challenge. In chapter 4, the coking behavior of several innovative allyos, three Fe-Ni-Cr and one Al-content is evaluated under several different conditions. The studies were performed in the jet stirred reactor set up (JSR) evaluating on-line the coking behavior of the super alloys under multiple industrially representative conditions. Together with the effect of continuous addition of DMDS and the cracking temperature, the effect of increasing Ni-Cr content or the effect of Al addition was evaluated. Carbon formation measurements combined with EDX analyses proved that by increasing the Ni-Cr content the coking resistance is improved by even a factor 2 during the most industrially representative conditions.

In an attempt to find alternatives of the typically used Fe-Ni-Cr alloys, the coking performance of a Ti-base alloy under ethane steam cracking conditions is also tested, in the Chapter 5. As a first step, the optimal pretreatment for Fe-Ni-Cr Alloys was applied and compared with a pretreatment at increased temperature, aiming at a better oxidation of the surface and thus coking behavior of the material. The results indicated decreased coking rates of the Ti-base alloy at the expense of the pronounced formation of carbon oxides. Additionally, the tested coupons showed crack propagation after application of cyclic aging and cooling down back to ambient conditions, making it an industrially indifferent choice for steam cracking reactor alloy.

Surface novelties to suppress coke formation in the ethylene industry are one of the key research topics in this field. In the Chapter 6, a commercial coating CoatAlloyTM has been compared to a typically used uncoated base material. Examination of the samples was assessed using online thermogravimetry, scanning electron microscopy and energy diffractive X-ray for surface and cross-section analysis together with X-ray photoelectron spectroscopy and wavelength-dispersive X-ray spectroscopy for surface analysis. Improved coking

behavior of the coating in comparison with the reference Ni-Cr Fe-base alloy after application of the optimized pretreatment was noted with no effect on the product distribution.

Chapter 7 studies the duration of the service time of an industrial cracker. The latter is strongly dependent on the long-term coking behavior and microstructure stability of the reactor coil alloy. Super alloys are known to withstand temperatures up to even 1400 K, however an experimental comparison of different alloys after exposure to extreme oxidation conditions is not available in literature. In chapter 6, several commercially available alloys have been first exposed to a long term oxidation at 1423 K for 500 h, namely metallurgic aging. Their coking behavior was evaluated in-situ at a thermogravimetric setup in a jet stirred reactor under ethane steam cracking conditions (Tgasphase = 1173 K, Ptot = 0.1 MPa, XC2H6 = 70 %, continuous addition of 41 ppmw S/HC of DMDS, dilution δ= 0.33 kgH2O/kgHC) and compared with their initial "fresh" coking behavior. The tested samples were also examined using scanning electron microscopy and energy diffractive X-ray for surface and cross-section analysis. No effect of the alloy microstructure on coking rates was found.

In chapter 8, the conclusions are given and based on these future studies and ideas are outlined.

Samenvatting

Vandaag de dag is stoomkraken nog steeds een van de meest essentiële chemische processen voor de productie van meerdere sleutelcomponenten in de chemische industrie. Bij stoomkraken worden koolwaterstofvoedingen, gaande van ethaan en propaan over LPG en nafta tot lichte gasolie, omgezet naar ethyleen, propyleen en andere waardevolle componenten door kortstondige blootstelling aan hoge temperaturen. Op dit moment wordt er jaarlijks bijna 200 miljoen ton ethyleen geproduceerd, een cijfer dat het belang van dit proces bevestigt.

De vorming van een koolstofhoudende afzetting, genaamd cokes, op de binnenwand van de reactor dwingt de operatoren van industriële stoomkraakinstallaties om regelmatig de productie te onderbreken zodat de gevormde cokes kan worden verwijderd door verbranding met een stoom/lucht mengsel. Het verminderen van cokesvorming is een van de meest veelbelovende opties om de efficiëntie van stoomkraakinstallaties verder te verbeteren. In de afgelopen jaren zijn er verschillende technologieën ontwikkeld om de vorming van cokes te onderdrukken, in het bijzonder 3D reactorgeometrieën, het toevoegen van additieven en het toepassen van geavanceerde oppervlakbehandelingen.

In dit werk ligt de focus vooral op de laatste twee technologieën. De hoofddoelen waren het vinden van optimale procescondities voor het bedrijven van industriële stoomkraakinstallaties en het onderzoeken van het effect van extreme carburatie en oxidatie op een wijd bereik aan innovatieve commercieel beschikbare reactormaterialen. Aangezien dit document is samengesteld uit in vaktijdschriften gepubliceerde en nog te publiceren manuscripten, bestaan

de hoofdstukken uit een dergelijk manuscript of een combinatie van meerdere dergelijke manuscripten met een gelijkaardig onderwerp. Elk van de hoofdstukken heeft een eigen introductie die de context en relevantie toelicht.

Om te beginnen wordt in Hoofdstuk 2 de niet-triviale effecten van het voorbehandelen van de reactorbuis geëvalueerd. Acht verschillende voorbehandelingen zijn getest op een Ni/Cr 35/25 legering bestand tegen hoge temperaturen, waarbij de weerstand tegen cokesvorming online werd gemeten aan de hand van een thermogravimetrische opstelling gecombineerd met een straalgemengde reactor (*jet stirred reactor*, JSR) tijdens het stoomkraken van ethaan bij industrieel relevante condities (verdunning 0.33 kg H_2O/kg C_2H_6, continu toevoegen van 41 ppmw S/HC bij T=1160 K, equivalente ethaanconversie van 68 %). De volgorde van de preoxidatie, de voorbehandeling met stoom en de eventuele presulfidatie werd gevarieerd en het effect ervan onderzocht. De observaties met betrekking tot cokesvorming bevestigden dat een preoxidatie bij hoge temperatuur gevolgd door een voorbehandeling met een water/lucht mengsel bij 1173 K gedurende 15 minuten het beste resultaat oplevert tijdens het stoomkraken van ethaan, met andere woorden deze combinatie vertoonde de hoogste weerstand tegen cokesvorming. Het optimaliseren van de voorbehandeling kan leiden tot een daling van de snelheid van cokesvorming met een factor 5. Op basis van observaties met rasterelektronenmicroscopie (*scanning electron microscopy*, SEM) en energie-dispersieve X-stralenspectroscopie (*energy dispersive X-ray spectroscopy*, EDX) werd vastgesteld dat de gelijkmatigheid van de gevormde oxidelaag, bestaande uit oxides van Cr en Mn, ervoor zorgt dat de het oppervlak wordt gepassiveerd en de vorming van cokes niet meer wordt gekatalyseerd. De aanwezigheid van Fe en Ni leidt tot hoge snelheden voor cokesvorming, wat in het bijzonder voorkwam als het oppervlak werd gepresulfideerd. De optimale voorbehandeling van de reactorbuis is vanzelfsprekend materiaalafhankelijk.

In Hoofdstuk 3 wordt het effect van de ruwheid van het oppervlak op de snelheid van cokesvorming onderzocht voor een 35/25 Ni/Cr legering aan de hand van dezelfde opstelling met kwartsreactor en elektrobalans tijdens het stoomkraken van ethaan bij industrieel relevante condities. Er is reeds veel kwalitatieve informatie beschikbaar die het belang aantoont van de samenstelling en de microstructuur van het oppervlak de stoomkraakreactorwand voor de snelheid van cokesvorming. Desalniettemin kon aan de hand van experimenten vastgesteld worden dat de ruwheid van het oppervlak en cyclische veroudering een kwantificeerbare invloed heeft in een Ra ruwheidsbereik tussen 0.15 μm en 7 μm, in het bijzonder voor de gekatalyseerde vorming van cokes. De invloed op de vormingssnelheid van pyrolytische cokes was beperkt. Karakterisering van het oppervlak toonde aan dat een toenemende uniformiteit van de metallurgische samenstelling van het oppervlak in combinatie met de vorming van Cr_2O_3 en $MnCr_2O_4$ leiden tot een stabiel cokesvormingsgedrag. De oxidatie van het oppervlak bleek onafhankelijk te zijn van de ruwheid van het oppervlak.

Een uitdaging voor de industrie is het vinden van het reactormateriaal met de grootste weerstand tegen cokesvorming. In Hoofdstuk 4 wordt de snelheid van cokesvorming onderzocht voor een aantal innovatieve materialen: drie Fe-Ni-Cr gebaseerde legeringen en een legering die daarnaast ook Al bevat. De experimenten werden uitgevoerd in de straalgemengde reactor (*jet stirred reactor*, JSR) waarbij de snelheid van cokesvorming voor de verschillende superlegeringen online werd gemeten bij verschillende industrieel relevante procescondities. De invloed van het verhogen van de hoeveelheid Ni-Cr in de legering en het toevoegen van Al werd onderzocht, evenals de invloed van de bedrijfstemperatuur en van het continu toevoegen van dimethyldisulfide (DMDS). Metingen van de hoeveelheid gevormde cokes in combinatie met EDX-analyses toonden aan dat de weerstand tegen cokesvorming

verhoogt bij toenemende hoeveelheid Ni-Cr. Bij de meest industrieel relevante condities werd de snelheid van cokesvorming gereduceerd met een factor 2.

In een poging om een alternatief te vinden voor de typische Fe-Ni-Cr legeringen werd de snelheid van cokesvorming onderzocht voor een Ti-gebaseerde legering tijdens het stoomkraken van ethaan. De resultaten worden beschreven in Hoofdstuk 5. De geoptimaliseerde voorbehandeling voor Fe-Ni-Cr legeringen werd toegepast en vergeleken met een voorbehandeling bij verhoogde temperatuur met als doel de oxidatie van het oppervlak te verbeteren en aldus een hogere weerstand tegen cokesvorming te ontwikkelen. De resultaten van deze test wezen inderdaad op lagere snelheden voor cokesvorming van de Ti-gebaseerde legeringen, dit echter ten koste van significant hogere snelheden voor de vorming van koolstofoxides (CO, CO_2). Daarbovenop vertoonden de geteste coupons scheurpropagatie na cyclische veroudering en terug afkoelen naar kamertemperatuur, wat de legering ongeschikt maakt als constructiemateriaal voor industriële reactorbuizen.

Geavanceerde oppervlakbehandelingen voor het onderdrukken van cokesvorming is een van de belangrijkste onderzoeksdomeinen in de stoomkraakindustrie. In Hoofdstuk 6 wordt de commercieel beschikbare coating CoatAlloyTM onderzocht door het cokesvormingsgedrag te vergelijken met dat van een ongecoat basismateriaal. De proefstukken werden onderzocht op basis van online thermogravimetrie, rasterelektronenmicroscopie en energie-dispersieve X-stralenspectroscopie voor analyses van het oppervlak en de doorsnede en op basis van X-stralen fotoelektronspectroscopie en golflengte-dispersieve X-stralenspectroscopie voor verdere analyses van het oppervlak. Na het toepassen van de geoptimaliseerde voorbehandeling werd een lagere snelheid van cokesvorming vastgesteld voor de gecoate coupons in vergelijking met de referentie, zijnde een ongecoat coupon bestaande uit een Ni-Cr Fe-gebaseerde legering, en dit zonder veranderingen in de productdistributie.

In Hoofdstuk 7 wordt de levensduur van een industriële reactorbuis bestudeerd. Deze is sterk afhankelijk van het cokesvormingsgedrag en de microstructurele stabiliteit van het constructiemateriaal van de reactor op lange termijn. Het is geweten dat superlegeringen bestand zijn tegen temperaturen tot 1400 K maar een experimentele vergelijking van verschillende legeringen na blootstelling aan extreme oxidatieve condities is niet beschikbaar in de literatuur. Daarom werden coupons van verschillende commercieel beschikbare legeringen langdurig blootgesteld aan een oxidatieve atmosfeer bij 1423 K gedurende 500 h om metallische veroudering te induceren. In-situ metingen van het cokesvormingsgedrag van de coupons werden bekomen in een thermogravimetrische opstelling gecombineerd met een straalgemengde reactor tijdens het stoomkraken van ethaan (T_gasfase = 1173 K, P_tot = 0.1 MPa, X_C_2H_6 = 70%, continu toevoegen van 41 ppmw S/HC via DMDS, verdunning δ = 0.33 kg H_2O/kg C_2H_6) en vergeleken met metingen van het initiële cokesvormingsgedrag van de coupons voor veroudering. Het oppervlak en de doorsnede van de geteste proefstukken werden ook onderzocht aan de hand van rasterelektronenmicroscopie en energie-dispersieve X-stralenspectroscopie. De snelheid van cokesvorming bleek onafhankelijk van de microstructuur van de legering.

Tot slot vat Hoofdstuk 8 de belangrijkste conclusies van de doctoraatsthesis samen, aangevuld met een aantal aanbevelingen voor de toekomst.

Chapter 1: Introduction and Outline

1.1. Introduction

For the last 20 years a dramatic increase of the energy consumption has been noticed globally in particular in China [1-3]. Luckily improved energy efficiency, the key to ensure a safe reliable, affordable and sustainable energy system, passivates this growth compared to previous decades. China will have the largest share in the energy demand growth until mid-2020's, when its population and financial growth is expected to slow down. In the meantime, other countries or regions, such as India, Southeast Asia, the Middle East together with parts of Africa and Latin America are going to emerge as the dominant regions for energy demand [1-3], as it is shown in Figure 1.1. 1. Crude oil, natural gas and coal are currently the main resources for energy with oil providing at least the one third of the total world's energy usage. Wind and solar energy will play an important role in the upcoming decades, as summarized in Table 1.1. 1.

The cumulative world oil production is expected to increase until 2020 and level off until 2030. After that a decrease is projected until 2050. In contrast, as far as the U.S. are concerned, a rapid increase is anticipated until 2050. The total world oil supply will increase by roughly 15 million barrels/day to almost 110 million barrels/day in 2040 [1-3] See Figure 1.1. 2.

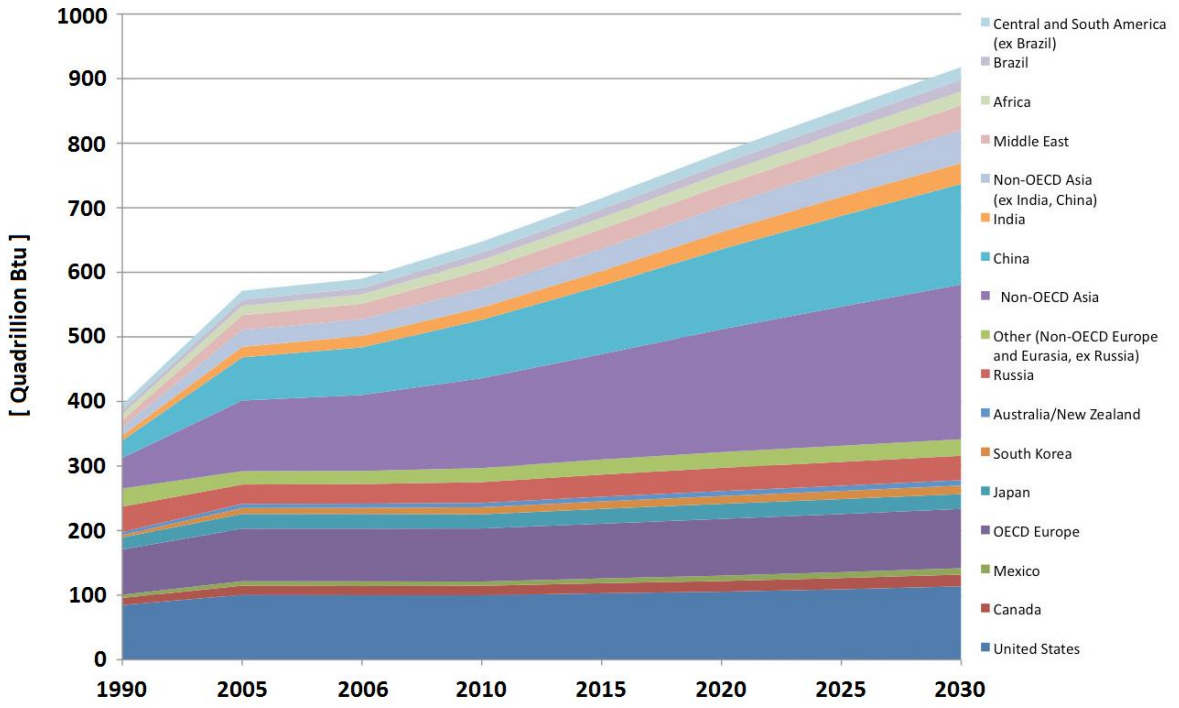

Figure 1.1. 1. World Total Primary energy Consumption as a function of time by Region for 1990 to 2030.[2]

Table 1.1. 1. World Energy Consumption, projected until 2050. [1-3]

World Energy Consumption (Mtoe)	2000	2010	2020	2030	2040	2050
Oil and Biofuels	3588	4080	4485	4387	3999	3440
Natural Gas	2185	2887	3460	3694	3475	3003
Coal	2379	3634	3917	4138	4240	4107
Nuclear	584	626	687	888	1009	1129
Hydro, Geothermal and Biomass	644	869	1149	1321	1522	1723
Wind and Solar	7	85	565	1301	2066	2833
Total	**9388**	**12181**	**14264**	**15729**	**16311**	**16234**
World GDP (billion $)	62548	90494	124340	156483	184150	207212
GDP per Capita ($)	10229	13069	16027	18408	20110	21307
Energy Efficiency ($/toe)	6662	7429	8717	9949	11290	12764
Carbon Dioxide Emissions (Mt)	24010	31507	34941	35939	34665	31460

"Oil" consumption exludes biofuels, Mt: million metric tons of oil-equivalent, $: constant 2011 international dollars, $/toe : constant 2011 international dollars per metric ton of oil-equivalent.

As illustrated in Figure 1.1. 3, Crude oil is mostly used for transportation purposes with gasoline, diesel and jet fuel making up more than three-quarters of current oil usage. Only about 10% of global oil production is used for the production of chemicals. The main

petroleum cuts used for chemicals production are petroleum gasses and naphtha, a petroleum cut with a boiling range between 300 and 470 K.

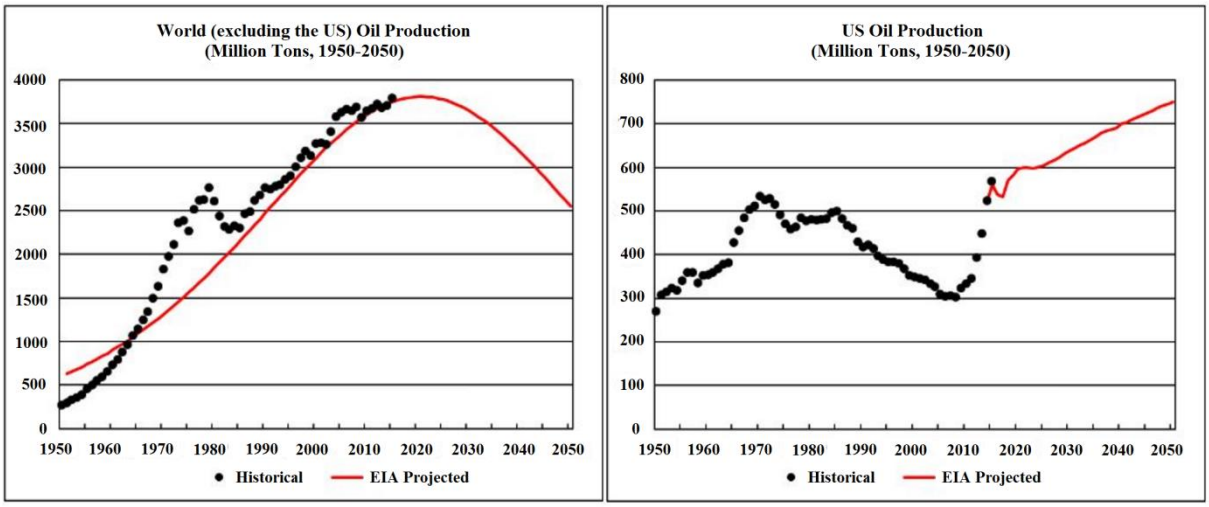

Figure 1.1. 2. Cumulative oil production growth as a function of time. In the left figure the world oil production is shown excluding U.S., while on the right the trend regarding only U.S. is presented.[3]

All major regions, except Europe, will contribute to a more than 50% rise in natural gas output to 2040 [1]. Currently the third largest energy contributor, natural gas, will be the world's fastest growing major energy source through 2040 and is expected to surpass coal as second most important energy source. The share of unconventional gas will increase by 10%. Purified natural gas is mainly used for electricity production, residential heating and as an industrial fuel. Natural gas liquids, e.g. ethane, propane and butanes, and gas condensates obtained during natural gas treatment, are often used for the production of base chemicals. With the rise of new technologies such as hydraulic fracking, the production of natural gas trapped in shale formations, i.e. shale gas, has boomed over recent years. As shale gas can contain more than 20 mol% of C_2+ molecules, it is expected to increase natural gas liquids production by more than 40 % [4].

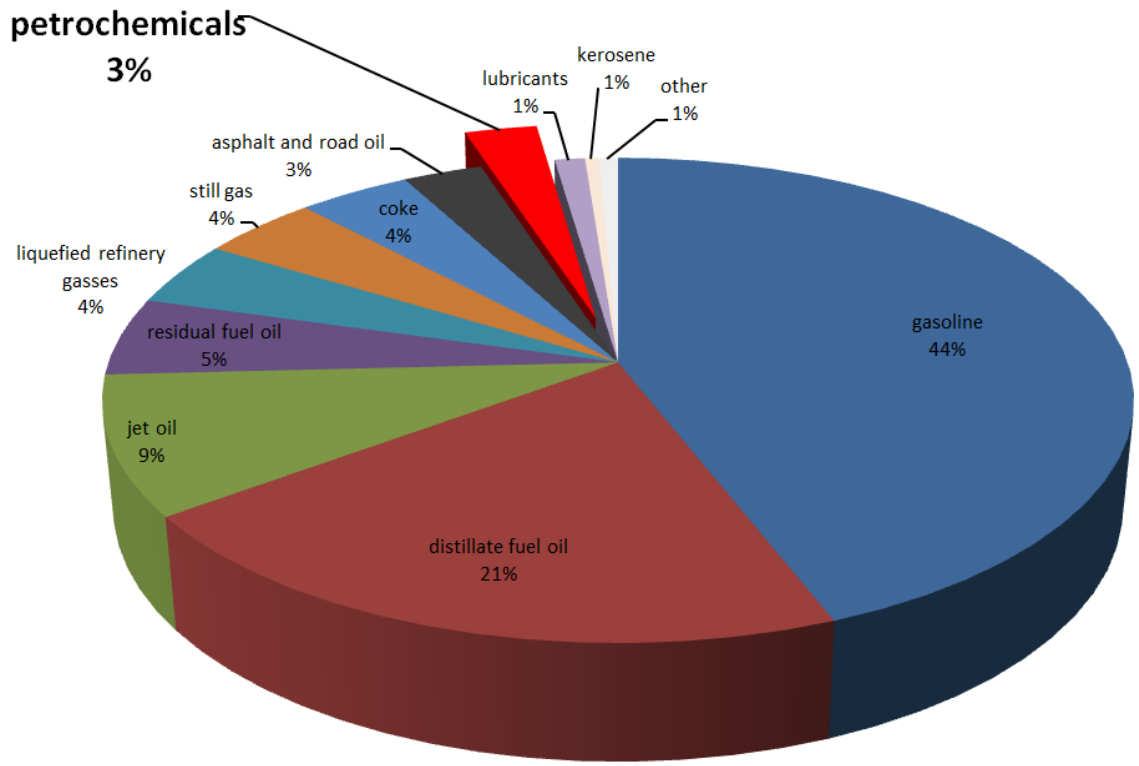

Figure 1.1. 3. Global Crude oil uses[5-18]

1.2. Petrochemistry and Steam Cracking

Even though the fraction of natural gas and oil consumption used for the production of chemicals and materials is relatively small compared to the fraction used for transportation, heating and electricity production, the economic significance due to the higher added value of chemicals compared to fuels and electricity is clear. The Petrochemical sector is responsible for the highest growth in oil demand, consumption increasing by more than 5 mb/d to reach 15 mb/d in 2040, an annual growth rate of 1.6 %. This is closely linked to the output of the most important petrochemical intermediary product, ethylene, whose output grows by close to 2% per year, due to robust demand for resins, fibres and plastics as a relatively low-cost, versatile and resistant packaging material. The majority of the high-value chemicals and materials are derived from a limited number of base chemicals. These main base chemicals involve hydrogen, olefins such as ethylene, propylene and 1,3-butadiene, and aromatics such

as benzene, toluene and xylenes, often supplemented with some heteroatom-containing chemicals such as ammonia, chlorine and sulfuric acid. Ethylene is the raw material used to the manufacture poly(ethene), oxirane, 1,2-dichloroethane, poly(ethene terephthalate), poly(1-chloroethene) and polystyrene as well as fibers and other organic chemicals. Global ethylene capacity in 2012 was nearly 150 million metric tons per year (tpy) [19]. This capacity is expected to rise by 35 million tpy in 2017 with production surpassing 160 million tpy. The sudden economic crisis in 2008 influenced substantially the demand, which picked up in and after 2010 and continues to grow over the medium term. In total 33 Mtpy capacity is to be added by the end of 2017. China leads the growth with more than 14 Mtpy. More than 6 Mtpy of capacity, i.e. 1/5th of global capacity addition is projected to be added in the Middle East. The Middle East shows increased availability of cheap feedstocks which results to a considerable growth of the ethylene market in this region.

Nevertheless, global oil use in this sector grows more slowly than over the past two decades (when annual growth was over 3%) as a consequence of saturation effects in developed countries, coal gaining ground as a feedstock in China, and of the higher recycling rates that are anticipated in the future. Most feedstock for petrochemical products originates from steam crackers or from refinery units (catalytic reforming and catalytic cracking).

Certainly, the dominant process to produce light olefins, such as ethylene and propylene, is steam cracking of hydrocarbons. Steam cracking of hydrocarbons is one of the foremost important processes of petrochemical industry. It allows the production of many chemical building blocks such as ethylene, propylene, butadiene and benzene from feedstocks ranging from ethane to heavy gasoil. The most important oil-based feedstock for steam cracking is naphtha, which currently accounts for more than half of all inputs[1-3, 20], as illustrated in Figure 1.1. 4. Even though naphtha demand for petrochemicals can grow by around 2 mb/d over the period to 2040, mainly because of the higher consumption in Asia, the relative

importance of naphtha declines. This is a consequence of the quickly growing demand for lighter feedstocks – LPG and ethane – particularly in North America and the Middle East.

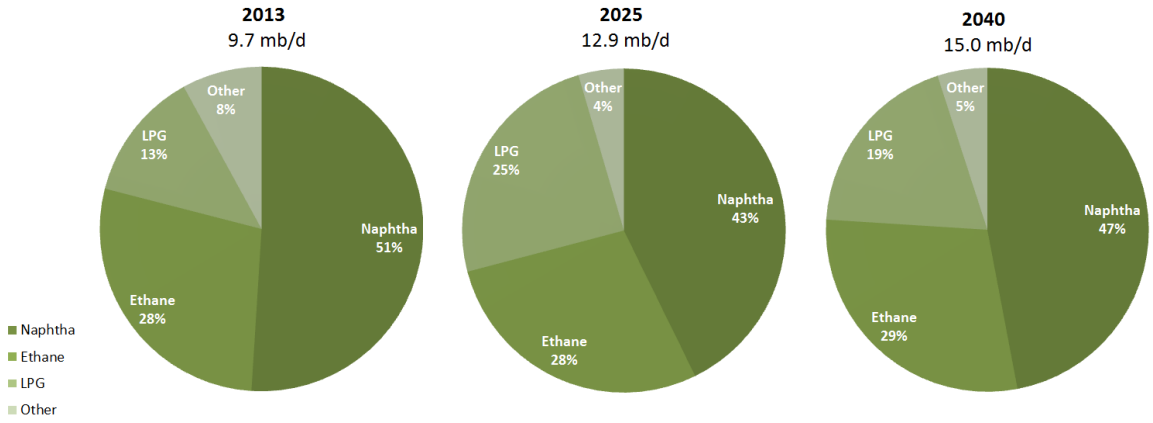

Figure 1.1. 4 Global demand for petrochemical feedstocks. [20].

Currently, there are four major licensors of steam cracker plants: KBR, Technip, Linde and Lummus [21-25]. A standard steam cracking plant is separated into two sections, generally called the "hot" and the "cold" section. In the hot section, the hydrocarbon feed is mixed with a diluent , typically steam, and introduced into cracking furnaces. Within the furnace the hydrocarbon feed is converted into a gaseous mixture of hydrocarbon components, of which light olefins and benzene are the most important [26]. A representative schematic description of a typical steam cracker is displayed in Figure 1.1. 5.

The radiation section comprises long adjacent tubes which serve as a reactor. The reactions occurring in the cracker are highly endothermic, meaning supplemental heat must be provided to sustain the process.

Rice and coworkers[27, 28] showed that steam cracking of hydrocarbons proceeds through a free radical mechanism and that three reaction families can be distinguished:

- Carbon-carbon and carbon-hydrogen bond scissions of molecules and the reverse radical-radical recombinations:

$$R_1 - R_2 \rightleftharpoons R_1^{\bullet} + R_2^{\bullet} \qquad [1.\ 1]$$

- Hydrogen abstraction reactions, both intra- and intermolecular:

$$R_1 - H + R_2^{\bullet} \rightleftharpoons R_1^{\bullet} + R_2 - H \qquad [1.2]$$

- Radical addition to olefins and the reverse β scission of radicals, both intra- and intermolecular:

$$R_1^{\bullet} + R_2 = R_3 \rightleftharpoons R_1 - R_2 - R_3^{\bullet} \qquad [1.3]$$

Steam cracking of hydrocarbons is initiated by breaking the molecule into radicals. n-Paraffins and olefins lead to the formation of 2 radicals, naphthenic compounds can lead to a biradical through ring opening. Substituted aromatics generally split off a small group in the side chain leading to a paraffinic radical and an aromatic radical. Evidently the scission of the bond occurs first on the weakest bond in the molecule. In other words, the scission of a molecule in which a more stable radical is formed is more favored.

The C-C scission reactions and C-H scission reactions of molecules and the reverse recombination reactions are very important reactions for steam cracking because they determine the total radical concentration in the reaction mixture. Hence, these reactions determine to a large extent the rate of disappearance of the molecules.

The two main categories of reactions taking place in a steam cracker are the cracking of C-C bonds, where alkanes and alkenes are formed, and the cracking of C-H bonds where an alkene and hydrogen are formed[29]. This latter type is often termed a dehydrogenation. Both reactions lead to the formation of α-olefins, the base products of the cracking process.

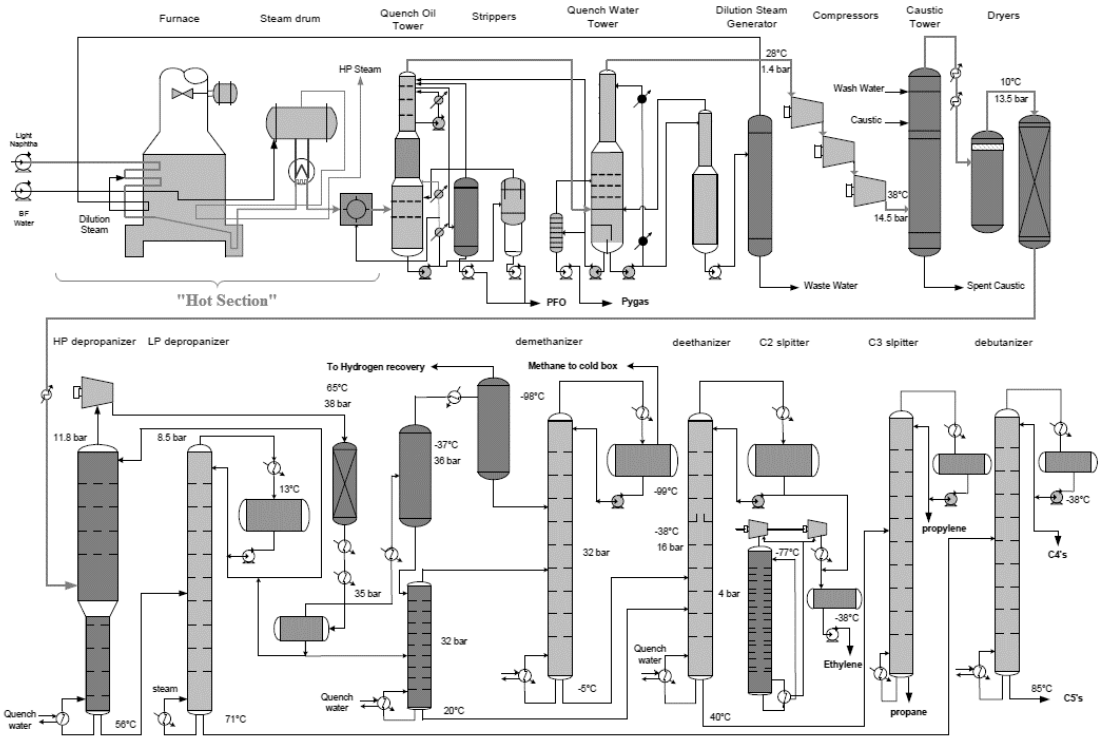

Figure 1.1. 5: Overview of depropanizer first naphtha cracker with front-end hydrogenation [30].

Besides these main reactions, side reactions such as isomerizations, cyclizations and polymerizations, electrocyclizations [31] take place. Typically, cyclodehydrogenations lead to the formation of coke, the primary drawback of the process.

Temperatures of 1000 to 1200 K are used to reach a conversion of 60 to 80% per pass, which affects the choice of reactor material[32]. Normally, steam cracking is performed in fired tubular reactors constructed out of Fe-Ni-Cr alloys. The heat of the furnace's flue gas is recovered in the convection section by preheating the feed. High pressure steam is produced in the convection section. The next zone is the TLE section in which the effluent of the furnace is quenched by oil and water. The purpose of this section is to cool the effluent to terminate the reactions. The heat is recovered as steam so it can be energetically intergrated in the petrochemical complex[26]. Typical residence times in the reactor deviate from 0.1 to 0.5 seconds, required to obtain the desired selectivity towards the main products, ethylene and

propylene[32-34]. An economical limit for naphtha is set here by the decreasing propene yield at higher severity resulting in typical P/E-values between 0.40 and 0.65. Plehiers and Froment [35] showed that lower residence times require higher temperatures to obtain the desired cracking severity.

1.3. Coke formation and mitigation

It is well accepted that the cracking of hydrocarbons at elevated temperature, proceeds mainly through a radical reaction mechanism [27, 36]. The gas-phase cracking reactions are escorted by the formation of a carbonaceous layer on the reactor inner wall [37]. The latter demonstrates a number of negative effects on the process' finance [38]. The growing coke layer eventually reduces the cross-sectional flow reactor area resulting in an elevated pressure drop over the coil length. The higher pressure has a detrimental effect on the selectivity to ethylene, while coke is highly insulating and forms an additional resistance to the heat transfer from the furnace to the process gas. To maintain the cracking severity, the fuel flow rate to the furnace burners is increased over time and as a result the external tube metal temperature (TMT) increases over time. When the TMT reaches the maximum allowable value or when the venturi pressure ratio (VPR) reaches a maximum permitted value (typically 0.9), the reactors are typically decoked on-line for about 48 hours using steam, steam and hydrogen[39] or - more commonly - a steam/air mixture[40-42]. Many alternative decoking technologies have been developed over the past years for tubular heaters or reactors[43-53] and some best practices have been summarized by Sullivan[41]. Obviously, these periodic production interruptions if a plant is furnace limited have a negative effect on the process economics. Furthermore, the reactor material deteriorates with successive coking-decoking cycles by tube corrosion, carburization and erosion [54-57], so the reactor coils need replacement every 4 to 10 years. Given the negative impact of coking on the process economics, a fundamental understanding of coke formation and the dependency of coke

formation on process conditions is important for plant design and optimization. The coke deposited in steam cracking reactors is formed via three different mechanisms: the catalytic, the radical non-catalytic and the homogeneous non-catalytic coke formation mechanism. When the gas-phase hydrocarbons are in direct contact with the reactor alloy, coke is formed through a catalytic mechanism with the alloy providing catalytic active sites [58-61]. Evidently, the reactor surface composition greatly influences the rate of coke formation during this catalytic coke formation [57, 62-64]. During this mechanism, a hydrocarbon molecule chemisorbs on an active site, dehydrogenating to form $-CH_3$, $-CH_2$ and -CH groups on the surface allowing hydrogen in the gas-phase [60]. Dissolution and diffusion of the carbon in and through the alloy follows. Whereas catalytic coke formation decreases over time due to encapsulation of the active sites, the heterogeneous, non-catalytic mechanism proceeds throughout the entire run of the reactors. As such, the run length of industrial reactors is mainly determined by the heterogeneous, non-catalytic coke formation [65]. In this mechanism, gas-phase species react with the coke layer itself through a radical mechanism. Wauters and Marin [38] suggested five families of reversible elementary reactions: hydrogen abstraction from the coke layer by a gas-phase radical, substitution reaction of a gas-phase radical on the coke layer, radical addition of a gas-phase radical to a surface olefinic bond, addition of a gas-phase olefinic bond to a surface radical and cyclization of a surface radical. In theory, all gas-phase radicals and molecules could react with the coke layer, but given their respective reactivity caused by their reactive groups and their concentration, a limited number of components, i.e. the coke precursors, dictate coke formation at least for ethane. In the third and last mechanism, i.e. the homogeneous, non-catalytic coke formation, small droplets prevalent in the process gas impinge on the reactor inner wall. These droplets can rebound, splash or stick [66]. The sticky droplets consist of polyaromatic hydrocarbons (PAH) either present in the feed or formed through secondary condensation reactions [67]. Although this

mechanism is very relevant for coke formation in the TLEs and in the convection section, its importance in the reactors is limited to heavy feed cracking [67]. Because of the many adverse effects of coke formation on the profitability of steam cracking units, the large scale of the process and low profit margins, many technologies to reduce coke formation have been developed and installed commercially over the last decades.

To date, the available anti-coking technologies can be roughly divided into three groups: feed additives, surface technologies and three-dimensional reactor technologies. The first category of feed additives is one of the most widely and easily applied techniques to minimize coke formation. For some additives a combination of an on-line pretreatment of the reactor with their continuous injection is applied[39, 43-46, 68], while for others only continuous addition is beneficial. Sulfur-containing compounds are the most widely studied group of additives [69-76]. The role of sulfur additives on diminishing carbon monoxide formation is well established, but their effect on coke formation is debated [69]. Besides sulfur-containing additives, components with phosphor [77-79] and silicon [70, 80] have also been investigated.

The category of surface technologies comprises high performance alloys and coatings application. Steam cracking reactors are typically made out of heat-resistant Ni-Cr alloys aiming at a limited catalytic coke formation because of the formation of a chromia oxide layer at the surface [57, 81]. Often aluminum and manganese are added to enhance the coking resistance of the alloys by forming a protective alumina or a manganese chromite ($MnCr_2O_4$) spinel layer respectively [81, 82]. However, the relative performance of the different elements has not been evaluated. Alternatively, a thin layer of a coating can be deposited on the reactor base alloy surface. Barrier coatings [55, 83-89] passivate the inner wall, and catalytic coatings [90-93] aim at the conversion of coke to carbon oxides and hydrogen by reaction with dilution steam. A barrier coating passivates the base alloy by covering the catalytically active sites and prevents catalytic coke formation. However, non-catalytic coke formation is still possible.

Recently developed catalytic coatings[94] eliminate catalytic coke formation by covering the active sites and convert non-catalytically formed coke to carbon oxides and hydrogen by reaction with steam. Therefore, a positive catalytic activity is added besides the elimination of the negative catalytic activity of the base alloy. However, the relative coking performance of each individual catalytic element is not tested, while the performance of these coatings under sever cyclic cracking decoking carburizing and oxidizing conditions has also not been evaluated yet.

In the last category of three-dimensional reactor technologies, the reactor tube inner geometry is altered from the conventional bare, straight tube to a more complex geometry to enhance convective heat transfer and/or increase heat transfer area. For example, finned tubes [47, 95], ribbed [50] or partially ribbed [51] tubes and swirl flow tubes [49] have been investigated to enhance heat transfer to reduce the tube metal temperature. As all these technologies lead to an increased pressure drop compared to conventional bare tubes, the selectivity towards light olefins is probably reduced [52]. The beneficial effect on coking rates and run lengths by these technologies is well established. However, the quantification of the effect on product selectivity is still a challenge. Indeed, measurement of the selectivity loss in an industrial unit is difficult as differences in the order of 0.1 wt% are to be expected which are within the uncertainty of the measurement. Furthermore, for a fair comparison, two similar furnaces, one with and one without a 3D technology, cracking the same feedstock at the same severity, at identical time on stream, should be compared which is practically impossible to achieve. Quantification of the selectivity loss in pilot plant experiments is also questionable due to the difference in tube diameter and attainable Reynolds numbers between a pilot plant and an industrial unit.

In the present thesis, a quite extensive experimental investigation has been performed unveiling the effect of several different unexplored or partially explored parameters of the

scientific work done in the field of coke formation during steam cracking. The quantitative effect of application of different pretreatments, materials and special coatings under different conditions of carburization, nitration, oxidation and sulfiding together with the effect of roughness added a special stone on the temple of anti-coking technologies science.

1.4. Outline

This thesis is a collection of published journal papers and manuscripts that have been submitted or are planned to be submitted for publication in the near future. Therefore, every chapter is written in the form of one or multiple manuscripts in similar subject areas, having independently a short introduction describing their relevant context.

In Chapter 2, the crucial effect of pretreatment of the reactor coil is evaluated. For that, eight different pretreatments are tested on a classical Ni/Cr 35/25 high temperature alloy coking resistance in a thermogravimetric set-up with a jet stirred reactor under industrially relevant ethane steam cracking conditions (dilution 0.33 kg H2O/ kg C2H6, continuous addition of 41 ppmw S/HC at T=1160 K, equivalent ethane conversion 68 %). The sequence of the preoxidation and steam pretreatment, together with presulfiding was evaluated.

In chapter 3, the unexplored effect of surface roughness on the coking tendency of a 35/25 Ni/Cr wt % alloy is investigated in a quartz electro-balance set-up with a jet stirred reactor, under industrially relevant ethane steam cracking conditions; Tgasphase = 1173 K, Ptot = 0.1 MPa and XC2H6 = 70 %. The composition and micro-structure of the inner surface of an ethylene cracker is detrimental for its coking behavior. In the tests, surface roughness and cyclic aging proved to have an effect mainly on the catalytic coking behavior in an Ra roughness range of 0.15 to 7 μm.

In the first part of Chapter 4, the coking behavior of four innovative alloys is evaluated under several different conditions. Finding the material with the best anti-coking performance is a typical industrial challenge, therefore a study was performed in the jet stirred reactor set up

(JSR) evaluating on-line the coking behavior of several Ni-Cr Fe-base commercial super alloys under multiple industrially representative conditions. Together with the effect of continuous addition of DMDS and the cracking temperature increase, the effect of increasing Ni-Cr content or the effect of Al addition was evaluated.

In an attempt to find alternatives of the typically used Fe-Ni-Cr alloys, the coking performance of a Ti-base Alloy under ethane steam cracking conditions is tested, in the second chapter of Chapter 4. As a first step, the optimal pretreatment for Fe-Ni-Cr Alloys was applied and compared with a pretreatment at increased temperature, aiming at a better oxidation of the surface and thus coking behavior of the material.

In chapter 5, several novel coatings are tested. Surface innovations to suppress coke formation in the ethylene industry is one of the key research topics. In the first chapter, a commercial coating CoatAlloyTM has been compared to a typically used uncoated base material. The tested samples were examined using online thermogravimetry, scanning electron microscopy and energy diffractive X-ray for surface and cross-section analysis together with X-ray photoelectron spectroscopy and wavelength-dispersive X-ray spectroscopy for surface analysis.

The service time of an industrial cracker is strongly dependent on the long-term coking behavior and microstructure stability of the reactor coil alloy. Super alloys are known to withstand temperatures up to even 1400 K. In chapter 6, several commercially available alloys have been first exposed to a long term oxidation at 1423 K for 500 h, namely metallurgic aging. Subsequently, their coking behavior was evaluated in-situ at a thermogravimetric setup in a jet stirred reactor under ethane steam cracking conditions (Tgasphase = 1173 K, Ptot = 0.1 MPa, XC2H6 = 70 %, continuous addition of 41 ppmw S/HC of DMDS, dilution δ= 0.33 kgH2O/kgHC) and compared with their initial “fresh” coking behavior. The tested samples

were also examined using scanning electron microscopy and energy diffractive X-ray for surface and cross-section analysis.

In chapter 7, the conclusions are reviewed and based on these future studies and ideas are outlined.

1.5. References

1. *International Energy Agency, World Energy Outlook 2014*. 2014.
2. Lab, F.C. *World total primary energy consumption*. 2017; Available from: http://www.ftrctlb.com/node/196.
3. *Peak Oil Barrel. World Energy 2014-2050 (Part 1).* 2014.
4. Foster, J. *Can shale gas save the naphtha crackers?* 2013.
5. Hewitt, G.F. and F. Coletti, *Preface*, in *Crude Oil Fouling*. 2015, Gulf Professional Publishing: Boston. p. ix-x.
6. Crittenden, B.D., et al., *Chapter Three - Experimental Generation of Fouling Deposits*, in *Crude Oil Fouling*. 2015, Gulf Professional Publishing: Boston. p. 51-94.
7. Coletti, F., et al., *Chapter One - Introduction*, in *Crude Oil Fouling*. 2015, Gulf Professional Publishing: Boston. p. 1-22.
8. Coletti, F. and G.F. Hewitt, *Chapter Six - Concluding Remarks*, in *Crude Oil Fouling*. 2015, Gulf Professional Publishing: Boston. p. 321-323.
9. Coletti, F., B.D. Crittenden, and S. Macchietto, *Chapter Two - Basic Science of the Fouling Process*, in *Crude Oil Fouling*. 2015, Gulf Professional Publishing: Boston. p. 23-50.
10. Coletti, F., et al., *Chapter Five - Modeling of Fouling from Molecular to Plant Scale*, in *Crude Oil Fouling*. 2015, Gulf Professional Publishing: Boston. p. 179-320.
11. Chew, J., et al., *Chapter Four - Deposit Characterization and Measurements A2 - Coletti, Francesco*, in *Crude Oil Fouling*, G.F. Hewitt, Editor. 2015, Gulf Professional Publishing: Boston. p. 95-178.
12. Chew, J., et al., *List of Contributors*, in *Crude Oil Fouling*. 2015, Gulf Professional Publishing: Boston. p. vii-viii.
13. *Index A2 - Coletti, Francesco*, in *Crude Oil Fouling*, G.F. Hewitt, Editor. 2015, Gulf Professional Publishing: Boston. p. 361-366.
14. *References A2 - Coletti, Francesco*, in *Crude Oil Fouling*, G.F. Hewitt, Editor. 2015, Gulf Professional Publishing: Boston. p. 329-360.

15. *Appendix 1 A2 - Coletti, Francesco*, in *Crude Oil Fouling*, G.F. Hewitt, Editor. 2015, Gulf Professional Publishing: Boston. p. 325-328.

16. *Nomenclature A2 - Coletti, Francesco*, in *Crude Oil Fouling*, G.F. Hewitt, Editor. 2015, Gulf Professional Publishing: Boston. p. xi-xvii.

17. *Copyright A2 - Coletti, Francesco*, in *Crude Oil Fouling*, G.F. Hewitt, Editor. 2015, Gulf Professional Publishing: Boston. p. iv.

18. *Front Matter A2 - Coletti, Francesco*, in *Crude Oil Fouling*, G.F. Hewitt, Editor. 2015, Gulf Professional Publishing: Boston. p. iii.

19. *Asia Pacific Region will Continue to Dominate the Ethylene Market*. Chemical Engineering World 2013 May 2013 [cited 2014; Available from: http://chemtech-online.com/.

20. Tan, F. and S.L. Peng. *Exxon starts world's 1st crude-cracking petrochemical unit*. 2014 [cited 2014 September 17th, 2014].

21. Zimmermann, H. and R. Walzl, *Ethylene*, in *Ullmann*. 2012, Wiley: Weinheim.

22. Zimmermann, H. and R. Walzl, *''Ethylene''in Ullmann's Encyclopedia of Industrial Chemistry, vol. 12*. 2003, Wiley–VCH.

23. BREF, *Integrated Pollution Prevention and Control (IPPC): Reference Document on Best Available Techniques in the Large Volume Organic Chemical Industry*, in *Integrated Pollution Prevention and Control (IPPC)*, BREF, Editor. 2003, European Commission.

24. Ren, T., M. Patel, and K. Blok, *Olefins from conventional and heavy feedstocks: Energy use in steam cracking and alternative processes.* Energy, 2006. **31**(4): p. 425-451.

25. Sadrameli, S.M., *Thermal/catalytic cracking of hydrocarbons for the production of olefins: A state-of-the-art review I: Thermal cracking review.* Fuel, 2015. **140**: p. 102-115.

26. Gündür, S., *Rate-based modeling of steam ethane cracker* in *Department of Chemical Engineering*. 2015, Middle East Technical University: Istanbul, Turkey. p. 110.

27. Rice, F.O. and K.F. Herzfeld, *The Thermal Decomposition of Organic Compounds from the Standpoint of Free Radicals. VI. The Mechanism of Some Chain Reactions.* Journal of the American Chemical Society, 1934. **56**(2): p. 284-289.

28. Kossiakoff, A. and F.O. Rice, *Thermal Decomposition of Hydrocarbons, Resonance Stabilization and Isomerization of Free Radicals1*. Journal of the American Chemical Society, 1943. **65**(4): p. 590-595.

29. Jukić, A., *Petroleum Refining and Petrochemical Processes: Production of Olefins – Steam Cracking of Hydrocarbons*. 2013, Faculty of Chemical Engineering and Technology, University of Zagreb: Zagreb.

30. Van Geem, K.M., *Light Olefin Production*, in *Sustainable Chemical Production Processes*. 2015, UGent.

31. Schiess, P., M. Huys-Francotte, and C. Vogel, *Thermolytic ring opening of acyloxybenzocyclobutenes: an efficient route to 3-substituted isoquinolines.* Tetrahedron Letters, 1985. **26**(33): p. 3959-3962.

32. Pinter, A., et al., *A laboratory steam cracking reactor to qualify raw materials: Characterisation of the apparatus* International Journal of Chemical Reactor Engineering 2006. **2**.

33. Murzin, D.Y., *Chemical Reaction Technology*. 2015: De Gruyter.

34. Figueiredo, J.L. and M.L.G.M. Pinto, *Carbon Deposition in Steam Cracking*, in *Fouling Science and Technology*, L. Melo, T.R. Bott, and C. Bernardo, Editors. 2012, Springer Netherlands: Faculdade de Engenharia, Porto, Portugal.

35. Plehiers, P.M. and G.F. Froment, *Reversed split coil improves ethylene yields.* Oil & Gas Journal, 1987. **85**(33): p. 41-&.

36. Rice, F.O., *The Thermal Decomposition of Organic Compounds from the Standpoint of Free Radicals. I. Saturated Hydrocarbons.* Journal of the American Chemical Society, 1931. **53**(5): p. 1959-1972.

37. Bennett, M.J. and J.B. Price, *A physical and chemical examination of an ethylene steam cracker coke and of the underlying pyrolysis tube.* J. Mater. Sci., 1981. **16**(1): p. 170-188.

38. Wauters, S. and G.B. Marin, *Kinetic Modeling of Coke Formation during Steam Cracking.* Industrial & Engineering Chemistry Research, 2002. **41**(10): p. 2379-2391.

39. Kivlen, J.A. and I. Koszman, *Decoking of onstream thermal cracking tubes with h20 and h2*. 1971, Google Patents.

40. Chen, J. and M. Maddock, *Hydrocarbon Process*. Vol. 52. 1973. 147-151.

41. Sullivan, B.K., *Ethylene Cracking Heater Decoking Tutorial*, in *AIChE Spring Natl. Meet., Conf. Proc.* 2014: New Orleans, LA.

42. Heynderickx, G., E. Schools, and G. Marin, *Optimization of the decoking procedure of an ethane cracker with a steam/air mixture.* Industrial & engineering chemistry research, 2006. **45**(22): p. 7520-7529.

43. Lenglet, E., *Method of decoking an installation for steam cracking hydrocarbons, and a corresponding steam-cracking installation*. 1993, Google Patents.

44. *HAK Decoking Technology (HDT)*. 2015; Available from: http://www.a-hak-is.com/en/home/what_we_do/services/furnace_services/hak_decoking_technology_hdt.

45. Nunciato, D.J., N.H. White, and W.A. Woodburn, *Method for decoking fired heater tubes*. 1981, Google Patents.

46. J, D.W., *Decoking and cleaning tubular heaters*. 1954, Google Patents.

47. De Saegher, J.J., T. Detemmerman, and G.F. Froment, *Three dimensional simulation of high severity internally finned cracking coils for olefins production.* Revue De L'Institut Français Du Pétrole, 1996. **51**(2): p. 245-260.

48. Detemmerman, T. and G.F. Froment, *Three dimensional coupled simulation of furnaces and reactor tubes for the thermal cracking of hydrocarbons.* Revue De L'Institut Français Du Pétrole, 1998. **53**(2): p. 181-194.

49. Schietekat, C.M., et al., *Swirl flow tube reactor technology: An experimental and computational fluid dynamics study.* Chemical Engineering Journal, 2014. **238**: p. 56-65.

50. Torigoe, T., et al. *Mixing element radiant tube (MERT) improves cracking furnace performance*. in *11th Ethylene Producers' Conference*. 1999. Houston, TX.

51. Györffy, M., et al. *MERT performance and technology update*. in *21st Ethylene Producers' Conference*. 2009. Tampa, FL.

52. Schietekat, C.M., et al., *Computational fluid dynamics-based design of finned steam cracking reactors.* AIChE J., 2014. **60**(2): p. 794-808.

53. Zimmermann, H. and R. Walzl, *Ethylene*, in *Ullmann's Encyclopedia of Industrial Chemistry*. 2000, Wiley-VCH Verlag GmbH & Co. KGaA.

54. Nishiyama, Y. and N. Otsuka, *Degradation of Surface Oxide Scale on Fe-Ni-Cr-Si Alloys upon Cyclic Coking and Decoking Procedures in a Simulated Ethylene Pyrolysis Gas Environment.* Corrosion, 2005. **61**(1): p. 84-93.

55. Zychlinski, W., K.A. Wynns, and B. Ganser, *Characterization of material samples for coking behavior of HP40 material both coated and uncoated using naphtha and ethane feedstock.* Materials and Corrosion-Werkstoffe Und Korrosion, 2002. **53**(1): p. 30-36.

56. Zimmermann, G., et al., *Absolute Rates of Coke Formation: A Relative Measure for the Assessment of the Chemical Behavior of High-Temperature Steels of Different Sources.* Ind. Eng. Chem. Res., 1998. **37**(11): p. 4302-4305.

57. Munoz Gandarillas, A.E., et al., *Influence of the Reactor Material Composition on Coke Formation during Ethane Steam Cracking.* Industrial & Engineering Chemistry Research, 2014. **53**(15): p. 6358-6371.

58. Rostrup-Nielsen, J. and D.L. Trimm, *Mechanisms of carbon formation on nickel-containing catalysts.* Journal of Catalysis, 1977. **48**(1–3): p. 155-165.

59. Baker, R.T.K., D.J.C. Yates, and J.A. Dumesic, *Filamentous Carbon Formation over Iron Surfaces*, in *Coke Formation on Metal Surfaces*. 1983, American Chemical Society. p. 1-21.

60. Snoeck, J.W., G.F. Froment, and M. Fowles, *Filamentous Carbon Formation and Gasification: Thermodynamics, Driving Force, Nucleation, and Steady-State Growth.* Journal of Catalysis, 1997. **169**(1): p. 240-249.

61. Reshetenko, T.V., et al., *Catalytic filamentous carbon: Structural and textural properties.* Carbon, 2003. **41**(8): p. 1605-1615.

62. Muñoz Gandarillas, A.E., et al., *Coking Resistance of Specialized Coil Materials during Steam Cracking of Sulfur-Free Naphtha.* Ind. Eng. Chem. Res., 2014. **53**(35): p. 13644-13655.

63. Geurts, P. and A. Vanderavoird, *Hartree-Fock-Slater-LCAO studies of the acetythylene-transition metal interaction. 2. Chemisorption on Fe and Cu - Cluster-models.* Surface Science, 1981. **103**(2-3): p. 416-430.

64. Geurts, P. and A. Vanderavoird, *Hartree-Fock-Slater-LCAO studies of the acetythylene-transition metal interaction. 2. Chemisorption on Ni surfaces - Cluster-models.* Surface Science, 1981. **102**(1): p. 185-206.

65. Reyniers, G., *Cokesvorming bij het thermisch kraken van koolwaterstoffen*. 1991, Ghent university.

66. Mahulkar, A.V., G.J. Heynderickx, and G.B. Marin, *Simulation of the coking phenomenon in the superheater of a steam cracker.* Chemical Engineering Science, 2014. **110**: p. 31-43.

67. Van Geem, K.M., et al., *Coke Formation in the Transfer Line Exchanger during Steam Cracking of Hydrocarbons.* Industrial & Engineering Chemistry Research, 2009. **48**(23): p. 10343-10358.

68. Sarris, S.A., et al., *Optimization of the in-situ pretreatment of high temperature Ni-Cr Alloys for Ethane steam cracking.* Ind. Eng. Chem. Res., 2017.

69. Wang, J., M.-F. Reyniers, and G.B. Marin, *Influence of Dimethyl Disulfide on Coke Formation during Steam Cracking of Hydrocarbons.* Ind. Eng. Chem. Res., 2007. **46**(12): p. 4134-4148.

70. Wang, J., et al., *Influence of Silicon and Silicon/Sulfur-Containing Additives on Coke Formation during Steam Cracking of Hydrocarbons.* Ind. Eng. Chem. Res., 2008. **47**(5): p. 1468-1482.

71. Reyniers, M. and G.F. Froment, *Influence of metal-surface and sulfur addition on coke deposition in the thermal cracking of hydrocarbons.* Industrial & Engineering Chemistry Research, 1995. **34**(3): p. 773-785.

72. Dhuyvetter, I., et al., *The influence of dimethyl disulfide on naphtha steam cracking.* Industrial & Engineering Chemistry Research, 2001. **40**(20): p. 4353-4362.

73. Bajus, M. and J. Baxa, *Coke formation during the pyrolysis of hydrocarbons in the presence of sulfur-compounds.* Collection of Czechoslovak Chemical Communications, 1985. **50**(12): p. 2903-2909.

74. Bajus, M., et al., *Steam cracking of hydrocarbons: 6. Effect of dibenzyl sulfide and dibenzyl disulfide on reaction-kinetics and coking.* Industrial & Engineering Chemistry Product Research and Development, 1983. **22**(2): p. 335-343.

75. Bajus, M. and V. Vesely, *Pyrolysis of hydrocarbons in the presence of elemental sulfur.* Collection of Czechoslovak Chemical Communications, 1980. **45**(1): p. 238-254.

76. Bajus, M., et al., *Steam cracking of hydrocarbons: 5. Effect of thiophene on reaction-kinetics and coking.* Industrial & Engineering Chemistry Product Research and Development, 1981. **20**(4): p. 741-745.

77. Wang, J.D., M.F. Reyniers, and G.B. Marin, *The influence of phosphorus containing compounds on steam cracking of n-hexane.* Journal of Analytical and Applied Pyrolysis, 2006. **77**(2): p. 133-148.

78. Vaish, S. and D. Kunzru, *Triphenyl phosphite as a coke inhibitor during naphtha pyrolysis.* Industrial & Engineering Chemistry Research, 1989. **28**(9): p. 1293-1299.

79. Ghosh, K.K. and D. Kunzru, *Reduction of coke formation during naphtha pyrolysis using triethyl phosphite.* Industrial & Engineering Chemistry Research, 1988. **27**(4): p. 559-565.

80. Brown, D.E., et al., *Inhibition of coke formation in ethylene steam cracking.* Acs Symposium Series, 1982. **202**: p. 23-43.

81. Verdier, G. and F. Carpentier, *Consider new materials for ethylene furnace applications.* Hydrocarbon Processing, 2011. **90**(5): p. 61-62.

82. Yan, J., et al., *Cyclic carburizing behaviour of Al modified high Si-containing HP40 alloy.* Corrosion Science, 2013. **67**(0): p. 161-168.

83. Ganser, B., K.A. Wynns, and A. Kurlekar, *Operational experience with diffusion coatings on steam cracker tubes.* Mater. Corros., 1999. **50**(12): p. 700-705.

84. Benum, L. *Achieving longer furnace runs at NOVA Chemicals*. in *2002 AIChE Spring Meeting*. 2002. New Orleans, LA.

85. Györffy, M., L. Benum, and L. Sakamoto. *Increased run length and furnace performance with Kubota and NOVA Chemicals' ANK 400 anticoking technology; data from current installations as well as technologyimprovements for higher thermal stability and decoking robustness*. in *2006 AIChE National Meeting*. 2006. Orlando, FL.

86. Bergeron, M., E. Maharajh, and T. McCall. *A low coking environment for pyrolysis furnace - CoatAlloy*. in *11th Annual Ethylene Producers' Conference*. 1999. Houston, TX.

87. Redmond, T., et al. *Performance of Coatalloy coating systems in ethylene pyrolysis furnaces using different feedstocks*. in *12th Annual Ethylene Producers' Conference*. 2000. Atlanta, GA.

88. Petrone, S., R. Mandyam, and A. Wysiekierski, *Surface alloyed high temperature alloys*, S.E.P. Corp., Editor. 1997.

89. Petrone, S., et al. *A "carbon-like" coating to improved coking resistance in pyrolysis furnaces*. in *10th Annual Ethylene Producers' Conference*. 1998. New Orleans, LA.

90. Petrone, S., et al. *Catalyzed-assisted manufacture of olefins (CAMOL): Realizing novel operational benefits from furnace coil surfaces*. in *20th Ethylene Producers' Conference*. 2008. New Orleans, LA.

91. Petrone, S., R. Deuis, and P. Unwin. *Catalyzed-assisted manufactur of olefins (CAMOL): Year-(4) update on commercial furnace installations*. in *22th Ethylene Producers's Conference* 2010. San Antonio, TX.

92. Rech, S. *Catalyzed-Assisted Manufacture of Olefins (CAMOL™): Updated for Use in Naphtha Service*. 2013 August 21, 2014].

93. SK-Corporation. *Coke Inhibition Technologies - Commercial Experience: F. SK Corporation - PY-COAT*. in *13th Ethylene Producers' Conference*. 2001. Houston, TX.

94. Schietekat, C.M., et al., *Catalytic Coating for Reduced Coke Formation in Steam Cracking Reactors.* Ind. Eng. Chem. Res., 2015. **54**(39): p. 9525-9535.

95. Detemmerman, T. and F. Froment, *Three dimensional coupled simulation of furnaces and reactor tubes for the thermal cracking of hydrocarbons.* Revue De L'Institut Français Du Pétrole, 1998. **53**(2): p. 181-194.

Chapter 2: Pretreatment Optimization

This chapter includes the following manuscript:

2. Optimization of the in-situ pretreatment of high temperature Ni-Cr Alloys for Ethane steam cracking

Stamatis A. Sarris[1], Natalia Olahova[1], Kim Verbeken[2], Marie-Françoise Reyniers[1], Guy B. Marin[1], Kevin M. Van Geem[1,*]

[1]Ghent University, Laboratory for Chemical Technology, Technologiepark 914, 9052 Gent, Belgium.

[2]Ghent University, Department of Materials Science and Engineering, Technologiepark 903, 9052 Gent, Belgium

DOI: 10.1021/acs.iecr.6b04537

2.1 Abstract

Coke inhibition of reactor materials is one of the major research areas in the field of steam cracking. Selecting the optimal in-situ pretreatment of a steam cracking coil depends on many different aspects such as the reactor material composition, the process conditions, the pretreatment duration, the atmosphere and the used additives. Therefore, the effect of eight

different pretreatments on the coking resistance of a classical Ni/Cr 35/25 high temperature alloy is evaluated in a thermogravimetric set-up with a jet stirred reactor under industrially relevant ethane steam cracking conditions (dilution 0.33 kg H_2O/ kg C_2H_6, continuous addition of 41 ppmw S/HC at T=1160 K, equivalent ethane conversion 68 %). Next to the sequence of the preoxidation and steam pretreatment, also presulfiding was evaluated. The coking results proved that a high temperature preoxidation, followed by a steam/air pretreatment at 1173 K for a duration of 15 min has the best coking performance under ethane cracking conditions. This pretreatment results in a factor 5 reduction of the coking rate compared to the standard pretreatment used as a reference case. SEM and EDX cross section and surface analyses show that the increased homogeneity of the oxide layer formed together with Cr and Mn layer passivates the catalytic behavior of the alloy, while the presence of Fe and Ni on the surface leads to increased catalytic and pyrolytic coke formation, which was the case when presulfiding was applied. Optimization of the pretreatment clearly pays off, however, the optimum will be different depending on the starting material.

Keywords: steam cracking, thermal cracking, presulfiding, pretreatment, jet stirred reactor, anti-coking technologies, Ni/Cr 35/25 Alloy

2.2 Introduction

Coke formation on the inner wall of tubular reactors in steam cracking furnaces has a strong negative impact on the economics of the process. As coke is formed, the cross-sectional area of the reactor is reduced, resulting in a higher pressure drop over the coil. This higher pressure drop negatively influences the product selectivities[1, 2] and, in addition, the highly insulating coke layer obstructs the heat transfer from the furnace to the reactor. To operate at a constant cracking severity over time, the fuel flow rate to the furnace burners has to be increased to compensate for

this supplementary conductive heat transfer resistance, leading to a temperature rise of the reactor tubes and consequently to an increased degradation of the tube material.

To avoid operation above the metallurgical maximum allowable temperatures or at the maximum pressure drop, the reactors are typically decoked on-line for about 48 hours using steam, steam and hydrogen[3] or - more commonly - a steam/air mixture[4-6]. Many alternative decoking technologies have been also developed over the past years for tubular heaters or reactors[7-16] and some best practices have been summarized by Sullivan[5]. In short, the target of decoking is to rapidly, safely and completely remove the coke deposited on the coil, forming a continuous oxide layer on the interface of the gas and coil. The focus in this work is on surface technologies, such as high performance alloys [17, 18] and coatings [19-21]. The cost of the reactors made out of these high temperature alloys is huge and hence maximizing their lifetime and anti-coking performance is vital. The use of additives, especially sulfur-containing ones, in combination with a pretreatment and/or continuous addition is therefore widely applied [22-37]. Classically, an oxidative pretreatment is applied before the material is used in the steam cracker.

High chrome-containing stainless steels can be selectively oxidized to enrich their surfaces in chromium by pretreatment at elevated temperatures (923 -1273 K) in H_2/H_2O, CO/CO_2 and $H_2/H_2O/CO/CO_2$ mixtures. Horsley and Cairns [38] pretreated high-alloy steels with these gaseous mixtures for 2-4 hours and evaluated their coke performance under dry hydrogen conditions observing a significant enrichment of Cr and Mn oxides at the surface of the alloy - namely $MnCr_2O_4$, MnO or Cr_2O_3, followed by a decreased absolute weight.

Luan and Eckert [39] tested several oxidizing gas mixtures on Incoloy 800 coupons concluding that temperature, duration, and composition of the pretreating gases are the pre-dominant factors affecting the surface composition and thickness of the formed layers after pretreatment. Cr concentrations at the surface increased rapidly in the initial phase of a pretreatment. As the

pretreatment continues, more Cr diffuses, however substantial amounts of Mn diffuse from the substrate to the surface. Transfer of Ti in considerable amounts seems strongly dependent on the preoxidation ability of the pretreating gas. Gases with higher oxidizing capacity seem to be needed to obtain substantial Ti diffusion. On the transfer of Si and Al, the authors were not able to make any conclusions, neither did these authors link composition with fouling tendencies.

Jakobi and Karduck [40, 41] performed comparative tests between different state-of-the-art spun cast alloys with a chromia- or spinel-based oxide protection and alloys which are protected by alumina. Preoxidation was observed for both materials during start up (H_2O 100 vol. % at 1123 K). Their results suggest that chromia forming alloys are protected by a complex system of oxide layers with a chromium-manganese spinel on top of the chromia layer and with a thin layer of SiO_2 at the oxide-metal interface forming a total oxide layer of 1 µm. Alumina-forming alloys displayed a rather thin protecting Al_2O_3 layer with a thickness of 100 nm. The latter provides increased corrosion and carburization resistance, especially if the temperature exceeds 1173 K, when transient alumina transforms into α-Al_2O_3, which is thermodynamically stable even under severe cracking conditions. No coking rates were determined in this study. Similarly, Asteman and Hartnagel [42] investigated the impact of the Al and Cr content in alloys and concluded that the Al_2O_3 forming alloy, containing 4 wt % Al (NiCr25Al4), has the best preoxidation properties with minimal spallation, compared to the Cr_2O_3 former (NiCr28), even after 500 h isothermal exposure. Adding more Al to the alloy (10 wt % Al: NiCr25Al10) results not only in an extremely poor machinability (hard and brittle) but it also results in a reduced carburization resistance. To the best of the authors' knowledge very limited information is available about the link between pretreatment and coke formation, not even in patents, where only vague claims about the combination of sulfur and other compounds were mentioned [43, 44]. Pretreatment times vary between 30 minutes and 4 hours at temperatures in the range of 873 to 1223 K.

Therefore, in this work eight different pretreatment sequences have been compared for a classical Fe-Ni-Cr high temperature alloy in a thermogravimetric set-up. The objective is hereby to optimize the coking resistance and to provide more precise guidelines for industrial operation. Detailed experimental coking rates and gas phase composition are obtained, supported by surface and cross-sectional SEM and EDX observations to assist with the interpretation of the experimental coking rates.

2.3 Experimental section

2.3.1 Electrobalance set-up Reactor model

The jet stirred reactor set-up has been extensively described by Muñoz et al. [17, 18], therefore, only a brief description is given here. The set-up consists out of three parts: a feed section, a reactor section and an analysis section as shown in Figure 2. 1. The mass flow rates of gasses and water are controlled by thermal mass flow controllers. All the lines in contact with sulfur are Sulfinert®-treated[45]. The water is vaporized to steam in an evaporator, mixed with the heated hydrocarbon feedstock and further heated before entering the reactor inlet at a temperature of 903 K. A jet stirred reactor made out of quartz is used, with a flat coupon in the center of the JSR suspended from the arm of an electrobalance. The coupon dimensions are 10 mm × 8 mm × 1 mm. The mass changes are tracked over time with a frequency of 1 Hz. Subsequently, the reactor effluent is quenched to prevent further cracking and its composition is measured with two gas chromatographs (GC) using nitrogen as internal standard i.e. a refinery gas analyzer dedicated to the analysis of components with less than 5 carbon atoms and a TRACE^{TM} Ultra GC detecting hydrocarbons ranging from methane to naphthalene. For ethane cracking no heavier products are measured than naphthalene. In detail, from the peak areas of the TCD-channel, experimentally determined calibration factors and the known amount of nitrogen, the flows of hydrogen,

methane, carbon oxides and C2 hydrocarbons are calculated. The calculated methane flow is subsequently used as internal standard for the flow determination of higher hydrocarbons in the FID-channels. A schematic representation of the use of internal standards is given in supporting information.

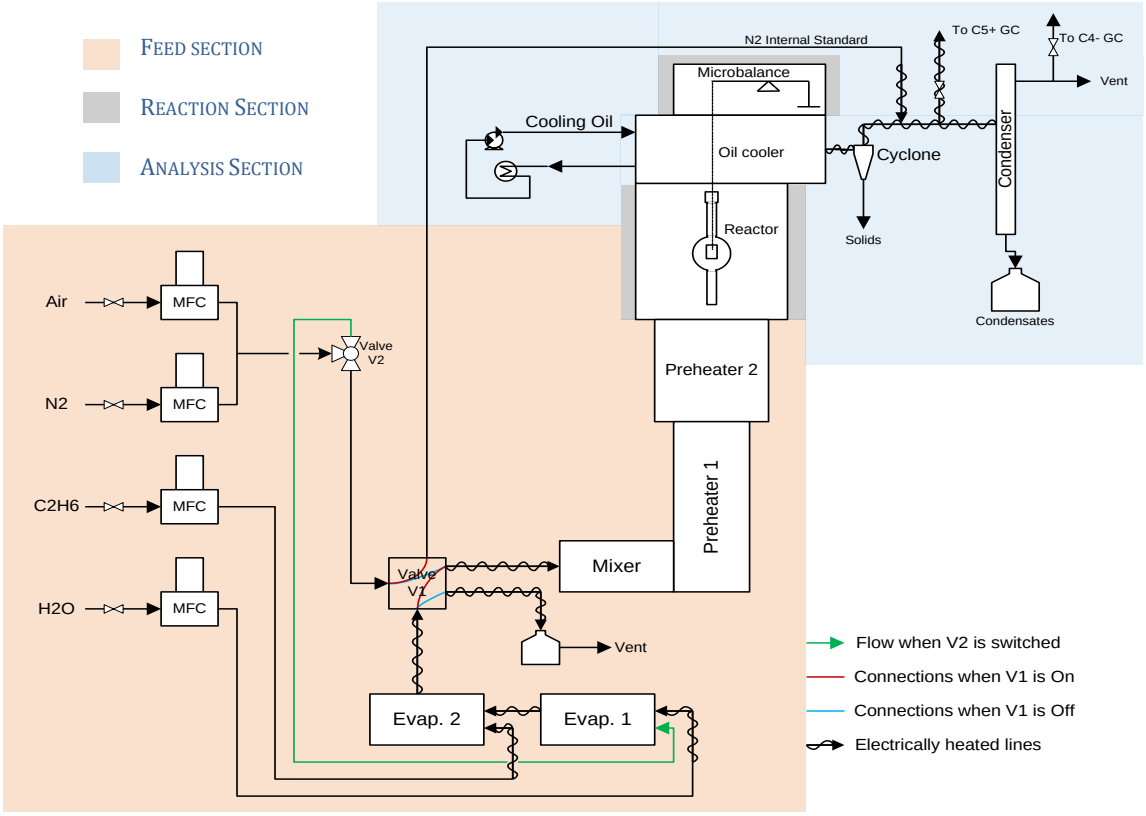

Figure 2. 1: Diagram of the thermogravimetric set-up for the study of coke deposition during steam cracking of ethane

2.3.2 Experimental procedures and conditions

Operating procedures and conditions used in this work are summarized in Table 2. 1. The experiments consisted of two cracking cycles of 6 h cracking and decoking. The heating ramp used during stabilization, heating and cooling of the set-up is 300 K · h^{-1}. Typically, before the first cycle, a pretreatment step, namely "OA", is performed to mimic the state of the alloy in an industrial steam cracker at start of run conditions.

Table 2. 1: Overview of the used pretreatments for ethane steam cracking: F_{HC}= 29.18 kg s^{-1}, δ= 0.33 kg_{H2O} kg^{-1}_{HC}, $T_{reactor}$= 1160 K, P= 101.35 kPa, F_{H2O}=9.72 kg s^{-1}, 41 ppmw S/HC

escription	id	Conditions		
		Temperature	Flows	Duration
Presulfiding	S.1 S.2	1100 K	$5.55 \cdot 10^{-6}$ kg s^{-1} of Steam with DMDS 500 ppmw DMDS/H_2O	60 min 30 min
Preoxidation with Air/N_2 mixture	OA	1023 K	$6.7 \cdot 10^{-3}$ Nl s-1 of Air	14 h
Preoxidation with Air/Steam	OAS.1 OAS.2	1173 K	$8.15 \cdot 10^{-3}$ Nl s^{-1} of Air and $6.67 \cdot 10^{-6}$ kg s^{-1} of Steam	15 min 60 min
Preoxidation with Steam	OS.1 OS.2	1173 K	$6.67 \cdot 10^{-6}$ kg s^{-1} of Steam	15 min 60 min
Decoke	DEC	from 1023 K to 1173 K	$8.15 \cdot 10^{-3}$ Nl s^{-1} of Air and $8.15 \cdot 10^{-3}$ Nl s^{-1} of N_2	30 min

Following the above, a mild preoxidation, with a mixture of air ($8.15 \cdot 10^{-3}$ Nl/s) and nitrogen ($8.15 \cdot 10^{-3}$ Nl/s) is conducted rising the temperature from 1023 K to 1173 K. Similarly, after every cracking cycle, the coupon is decoked according to a standardized procedure named pretreatment 'DEC', removing all the cokes formed in the reactor and on the sample. Table 2. 2

summarizes the eight pretreatments and in all cases the first step is identical, however, the following steps are different as it is clarified in Figure 2. 2.

Table 2. 2: Overview of the sequences of the tested pretreatments before the first cracking cycle: F_{HC}= 29.18 kg s^{-1}, δ= 0.33 kg_{H2O} kg^{-1}_{HC}, $T_{reactor}$= 1160 K, P= 101.35 kPa, F_{H2O}=9.72 kg s^{-1}, 41 ppmw S/HC.

Id	Sequence	Id	Sequence
A	**OA + DEC**	**E**	**A + OS.1**
B	**A + OAS.1**	**F**	**A + OS.2**
C	**A + OAS.2**	**G**	**A + OS.2 + S.1**
D	**A + OAS.1 + S.1**	**H**	**A + OS.2 + S.2**

*preoxidation at 1023 K is used as a primer pretreatment only before the 1st cc. For the 2nd cc is neglected

After the application of each pretreatment, the feed is switched back to nitrogen and the reactor temperature is increased to 1283 K. During heating, $9.7 \cdot 10^{-6}$ kg s^{-1} of a steam and $29.2 \cdot 10^{-6}$ kg s^{-1} ethane are sent to the evaporators and vented in order to get steady evaporation and mixing. A small amount of DMDS is co-fed with the steam by dissolving it in water at a concentration of $41 \cdot 10^{-6}$ kg DMDS/kg ethane. This value corresponds to typical amounts used in industrial ethane cracking furnaces to limit the formation of carbon oxides. Once the set temperature in the reactor is reached, the cracking mixture is sent to the reactor. The reactor temperature is set throughout the cracking runs at 1160 K, a value that is reached within 15 minutes after introducing the cracking mixture in the reactor. After cracking for 6 hours, the reactor temperature is set to 1023 K and the flow rate of ethane and steam is set to zero, leaving only nitrogen to purge the reactor. As mentioned above, once this temperature is reached the steam flow rate is set to $6.67 \cdot 10^{-6}$ kg

ID	Treatment				Cracking	Treatment			Cracking	Cooling down or Treatment
A	1023 K Air	1023 K->1173 K N2+Air			1160 K C_2H_6+H_2O	1023 K->1173 K N2+Air	1173 K		1160 K C_2H_6+H_2O	time
	OA - 14 h	DEC - 30 min	-	-	1st coking cycle - 6h	DEC - 30 min	-	-	2nd coking cycle - 6h	
B	1023 K Air	1023 K->1173 K N2+Air	1173 K Steam + Air		1160 K C_2H_6+H_2O	1023 K->1173 K N2+Air	1173 K Steam + Air		1160 K C_2H_6+H_2O	time
	OA - 14 h	DEC - 30 min	OAS.1 - 15 min	-	1st coking cycle - 6h	DEC - 30 min	OAS.1 - 15 min	-	2nd coking cycle - 6h	
C	1023 K Air	1023 K->1173 K N2+Air	1173 K Steam + Air		1160 K C_2H_6+H_2O	1023 K->1173 K N2+Air	1173 K Steam + Air		1160 K C_2H_6+H_2O	time
	OA - 14 h	DEC - 30 min	OAS.2 - 1 h	-	1st coking cycle - 6h	DEC 30 - min	OAS.2 - 1 h	-	2nd coking cycle - 6h	
D	1023 K Air	1023 K->1173 K N2+Air	1173 K Steam + Air	1100 K Steam + DMDS	1160 K C_2H_6+H_2O	1023 K->1173 K N2+Air	1173 K Steam + Air	1100 K Steam + DMDS	1160 K C_2H_6+H_2O	time
	OA - 14 h	DEC - 30 min	OAS.1 - 15 min	S.1 - 30 min	1st coking cycle - 6h	DEC - 30 min	OAS.1 - 15 min	S.1 - 30 min	2nd coking cycle - 6h	
E	1023 K Air	1023 K->1173 K N2+Air	1173 K Steam		1160 K C_2H_6+H_2O	1023 K->1173 K N2+Air	1173 K Steam		1160 K C_2H_6+H_2O	time
	OA - 14 h	DEC - 30 min	OS.1 - 15 min	-	1st coking cycle - 6h	DEC - 30 min	OS.1 - 15 min	-	2nd coking cycle - 6h	
F	1023 K Air	1023 K->1173 K N2+Air	1173 K Steam		1160 K C_2H_6+H_2O	1023 K->1173 K N2+Air	1173 K Steam		1160 K C_2H_6+H_2O	time
	OA - 14 h	DEC - 30 min	OS.2 - 1 h	-	1st coking cycle of 6h	DEC - 30 min	OS.2 - 1 h	-	2nd coking cycle - 6h	
G	1023 K Air	1023 K->1173 K N2+Air	1173 K Steam	1100 K Steam + DMDS	1160 K C_2H_6+H_2O	1023 K->1173 K N2+Air	1173 K Steam	1100 K Steam + DMDS	1160 K C_2H_6+H_2O	time
	OA - 14 h	DEC - 30 min	OS.2 - 1 h	S.1 - 30 min	1st coking cycle - 6h	DEC - 30 min	OS.2 - 1 h	S.1 - 30 min	2nd coking cycle - 6h	
H	1023 K Air	1023 K->1173 K N2+Air	1173 K Steam	1100 K Steam + DMDS	1160 K C_2H_6+H_2O	1023 K->1173 K N2+Air	1173 K Steam	1100 K Steam + DMDS	1160 K C_2H_6+H_2O	time
	OA - 14 h	DEC - 30 min	OS.2 - 1 h	S.2 - 1 h	1st coking cycle - 6h	DEC - 30 min	OS.2 - 1 h	S.2 - 1 h	2nd coking cycle - 6h	

weight change

Figure 2. 2: Simplified timelines of the coking−decoking experiments in the JSR Electrobalance set-up

s^{-1} and a mild preoxidation step with a mix of air and nitrogen fed to the reactor is conducted. During this decoking step, the reactor is heated to 1173 K.

Surface characteristics were determined by analyzing pretreated and coked samples by means of SEM and EDX at intermittent stages, additional experiments were performed with coupons that were for example only pretreated or not decoked. For both cases, while cooling down to room temperature, a He flow of $0.6 \cdot 10^{-6}$ kg $\cdot$ s^{-1} was used as inert gas while the ramp was set to 100 K per hour.

2.3.3 Coking rate calculation

The coke deposition on each sample is measured over time by continuously weighing the mass of the sample. This allows the determination of the total amount of coke after every cracking cycle, as well as the calculation of the initial catalytic coking rate and the asymptotic pyrolytic coking rate. Similarly with the work of Muñoz Gandarillas et al. [17, 18], the coking rate is determined as:

$$R_c = \frac{m_{t_2} - m_{t_1}}{t_2 - t_1} \frac{1}{S} \quad (1)$$

where R_c is the coking rate in $kg \cdot s^{-1} \cdot m^{-2}$, mt_j the mass of coke at time j in kg, t_j the experimental time at instant j in s and S the surface area of the coupon in m^2.

In this work, the mean value of the coking rate between 15 minutes and 60 minutes is defined as the initial or catalytic coking rate, i.e. characterizing the catalytic coking behavior of the sample. The asymptotic or pyrolytic coking rate is related to the pyrolytic coking mechanism and is reported as the mean measured coking rate between the 5^{th} and 6^{th} hour of cracking (see Figure 2. 3).

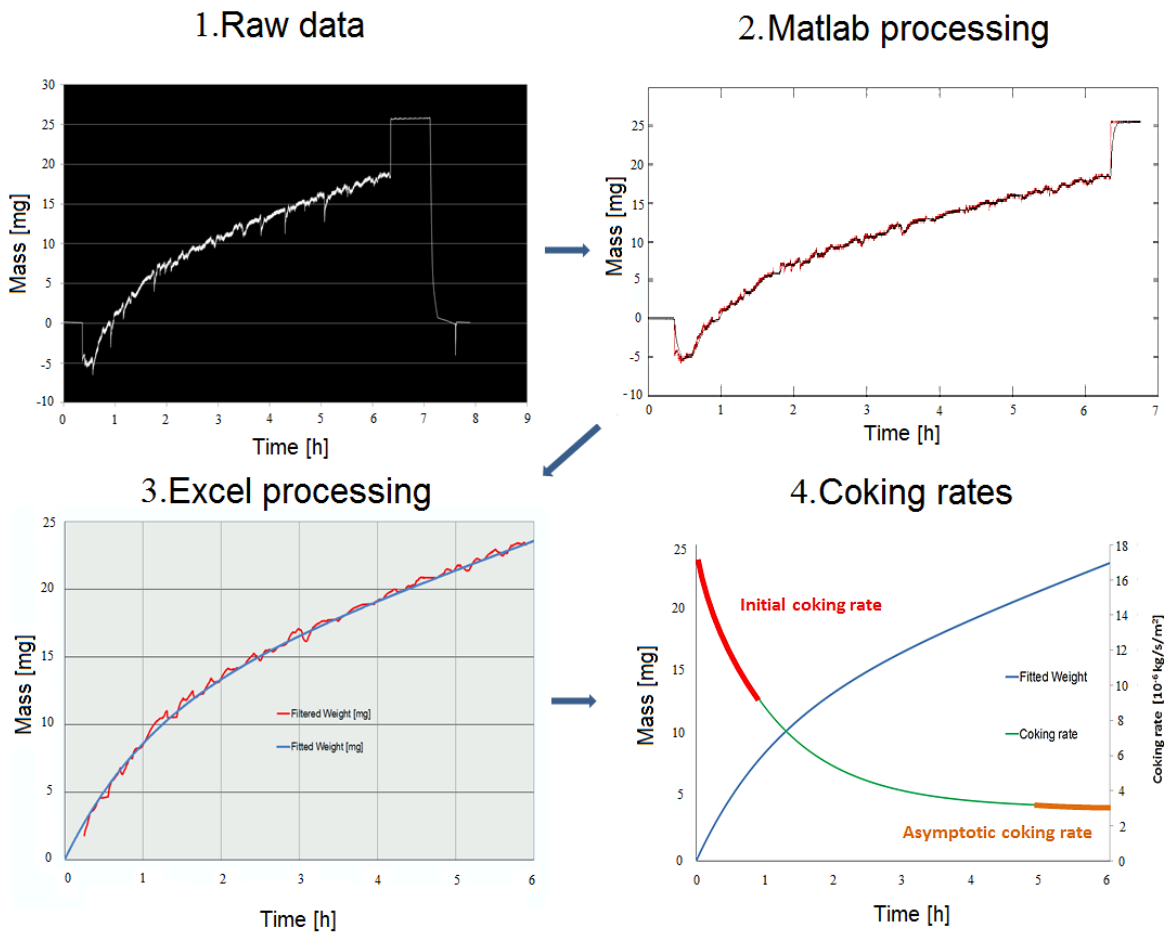

Figure 2. 3: Processing sequence for the coking rates determination

2.3.4 Scanning Electron Microscope and Energy Dispersive X-ray Analysis

Scanning Electron Microscopy (SEM) and Energy Dispersive X-ray Spectroscopy (EDX) are used to obtain information regarding the surface morphology and to perform chemical analysis. For the coked samples both top surface and cross sectional analyses were performed while for the pretreated samples only surface top-view analysis. As shown in Figure 2. 4, the top surface analyses gave a qualitative idea of the elemental composition of the surface, and was performed at 10 kV and 20 kV, while the cross sectional mappings evaluated the uniformity of the oxides

generated during each applied pretreatment. The surface composition is an average of EDX analyses on two different locations of the examined coupons. Analyses are performed for coked and pretreated samples.

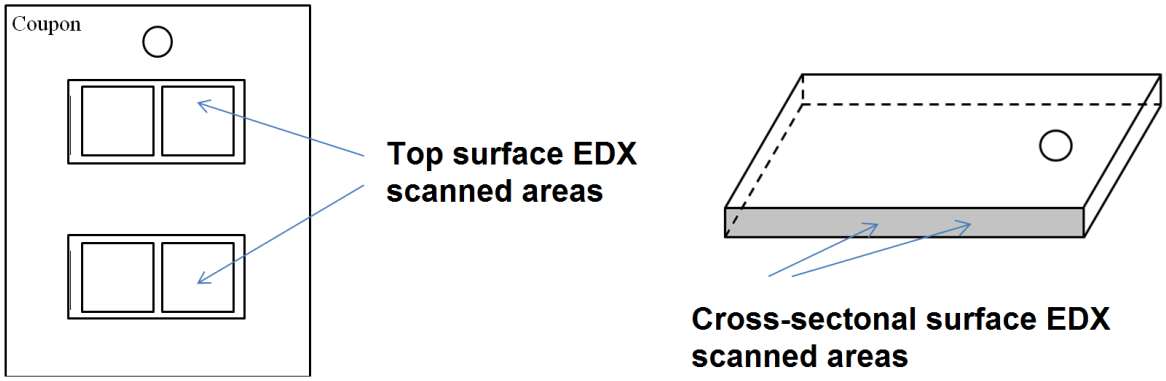

Figure 2. 4: Top surface (left) and cross-sectional (right) analysis of the examined coupons

2.3.5 Thermodynamic Calculations

To gain insight in the possibly formed, thermodynamically stable components on the surface of the samples, thermodynamic calculations are performed using the fresh coupon elemental composition and the one obtained by means of EDX. Additionally, calculations are performed with the aid of Ekvicalc [46]. The input values used were in line with the gas phase and surface composition and are given on Table S.1. in Supporting Information.

2.4 Experimental results

In Figure 2. 3, an overview of the total amount of coke formed after each cycle and each pretreatment is reported, next to the product yields of the main products averaged over 6 hours. For the total coke deposited huge differences are observed, up to a factor 5. However, for the product yields only a minor influence of the pretreatments can be observed, mainly for CO and CO_2. The conversion and selectivity of the main products is stable, while in line with previous

work [22, 24, 47], when using a pretreatment with sulfur – namely D, G and H - a significant decrease (at most a factor 2) of the CO yield is observed. The CO_2 yield – already small because of the continuous addition of DMDS - remains unaffected. Pretreatments B, C, E and F, that include a steam pretreatment before cracking, with or without air addition, show similar results in terms of cracked gas composition. A more detailed discussion for the effect of every pretreatment on the coking rates is made below.

Table 2. 3: Measured total coke and averaged product yields during ethane steam cracking: F_{HC} = 29.18 10^{-6} kg s^{-1}, δ = 0.33 kg_{H2O} kg^{-1}_{HC}, $T_{reactor}$ = 1160 K, p = 101.35 kPa, F_{H2O} =9.72 10^{-6} kg s^{-1}, CA of DMDS 41 ppmw S/HC, 2 cracking cycles (CC)

Pretreatment		**A**	**B**	**C**	**D**	**E**	**F**	**G**	**H**
CA (ppmw S/HC)		41							
Temperature (K)		1160							
Coke formed[a]	**1st cc**[b]	41.07	8.66	8.75	17.89	10.56	9.38	21.59	21.95
	2nd cc	15.84	5.69	5.84	12.85	7.25	6.84	18.32	18.44
Conversion		68.18	68.18	68.11	68.25	68.12	68.05	67.97	68.07
Component Yields[c] (weight %)	**H_2**	4.16	4.15	4.15	4.14	4.15	4.15	4.14	4.14
	CO	0.020	0.020	0.020	0.010	0.020	0.020	0.010	0.010
	CO_2	0.005	0.002	0.002	0.002	0.003	0.002	0.002	0.002
	CH_4	6.6	6.6	6.59	6.57	6.59	6.55	6.59	6.62
	C_2H_6	31.82	31.82	31.89	31.75	31.88	31.95	32.03	31.93
	C_2H_4	49.54	49.55	49.52	49.57	49.37	49.37	49.4	49.46
	C_3H_8	0.11	0.11	0.11	0.11	0.11	0.11	0.11	0.11
	C_3H_6	0.74	0.74	0.74	0.73	0.74	0.73	0.73	0.73
	C_2H_2	1.29	1.28	1.27	1.28	1.31	1.32	1.29	1.31
	1,3-C_4H_6	1.91	1.92	1.91	1.9	1.92	1.92	1.93	1.93
	Benzene	2.18	2.19	2.17	2.17	2.2	2.18	2.19	2.19

a relative error of 10 % is typically considered for the coking rates
b cracking cycle
c averaged values obtained for the first and the second cycle

2: The calculated coking rates over time based on the coking curves obtained for all the studied pretreatments are summarized in

3: Figure 2. **5**. Similar trends are observed for the catalytic as well as the asymptotic coking

rates for the performed experiments, suggesting that for a specific material catalytic and asymptotic coking rates are interrelated. For ethane cracking, it is known that the contributions of the heterogeneous catalytic coking and the homogeneous non catalytic coking mechanism to the total amount of coke formed during a complete run length are negligible[48] and that the coke is almost entirely formed via the homogeneous catalytic coking mechanism. Hence, the focus is on the latter, although the catalytic and asymptotic rates are both consistently reported. From

Figure 2. **5**, it is clear that pretreatments B and C lead to the lowest asymptotic coking rate, which is at least 30 % lower than the other investigated pretreatments. Also, for the second cycle a decrease of 30 % was observed in comparison with pretreatment E and F, the second best set of pretreatments. Clearly, a steam pretreatment combined with air leads to superior anti-coking behavior.

Based on the results, the duration of the steam/air pretreatment has a negligible effect on the coking rates (pretreatment B and C). It seems that the catalytic behavior of steam/air treated surfaces, after pretreatment B and C, is only mildly influenced by an additional presulfiding step such as in pretreatment D; in the case of a preceding steam/air pretreatment, presulfiding of the sample increased asymptotic coking rates with a factor 2 to 3, but not the initial coking rate. In contrast with the remaining pretreatments, the application of pure steam (pretreatment E and F) seems to mitigate the catalytic coking rate, but not the asymptotic. In these cases, the increase of the duration of the steam pretreatment leads to a further decrease of the catalytic coking rate. When steam pretreatment is not combined with air, presulfiding of the sample had a significantly negative effect on the initial coking rate, too. Increasing the duration of the presulfiding step does not cause a change to the coking rates as lengthening the duration of the steam pretreatment does. The coking rates after presulfiding for 30 minutes are identical to those in which the presulfiding

step is doubled in time. This supports the preposition that the amount of sulfur fed is probably excessive for the sample surface already after 30 min of pretreatment, so no additional effect is observed on the surface chemistry.

The surface characteristics of the metal or the carbonaceous surface during the initial coking steps exert a significant influence on coke formation. In this study, the roughness of the samples was kept fixed and will be investigated in a follow-up study. The roughness together with chemisorption and dehydrogenation properties of the surface are considered to play an important role in coke deposition on high temperature alloys containing Ni. [49-51]

Before evaluating the data measured by SEM and EDX, EkviCalc calculations are performed using as input the fresh coupon composition. This, to have an estimation on the thermodynamically stable phases expected by application of different conditions. As gas phase input, the conditions and composition of the last step of each pretreatment were used. In Table 2. 4, a summary of the results is given. Pretreatments including only air or steam/air without presulfiding, namely A, B and C, lead to increased amounts of Ni-based oxides. The rest show a pronounced amount of Ni on the surface, which is known to catalyze coke formation. Similar amounts of SiO_2 are simulated for all pretreatments. Judging by these results, A, B and C should be in principle the best pretreatments, while D to H should be the worst, with no differences observed among them in terms of surface composition. This is in line with the obtained results. However, clearly, EkviCalc cannot predict accurately the composition of a surface and additional SEM and EDX measurements are necessary.

SEM and EDX analyses allow to gain further insight in which variables affect the coking behavior of the samples. The overview of the results is summarized in Table 2. 5. Note that the 10 kV and 20 kV results are not always representative of the same depth on the alloy because of

the different elemental composition of the surface. However, from the amounts measured, some clear conclusions can still be extracted.

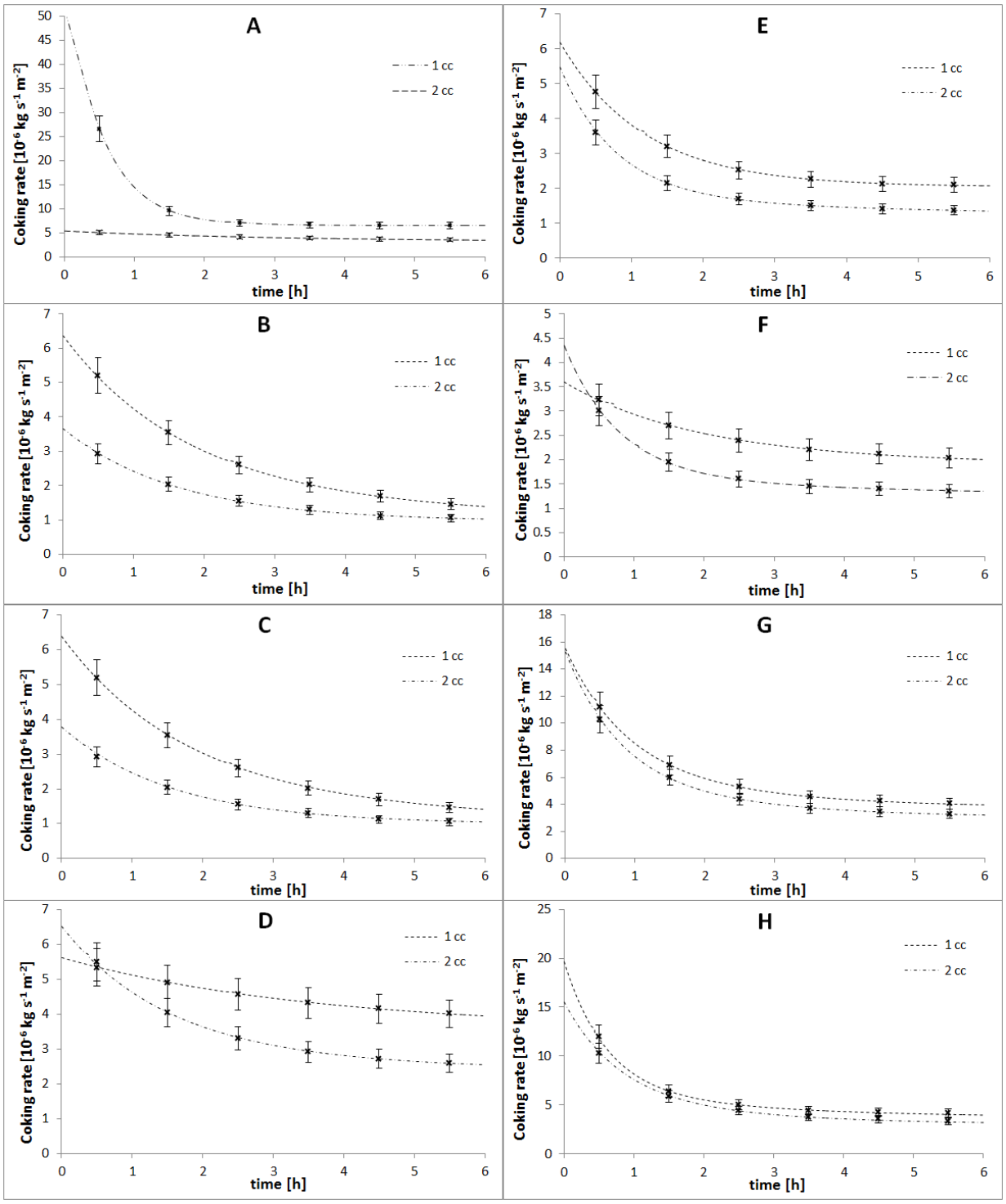

Figure 2. 5: Overview of the coking rates for the different applied conditions and over 2

coking/decoking cycles: F_{HC}= 29.18 kg s^{-1}, δ= 0.33 kg_{H2O} kg^{-1}_{HC}, $T_{reactor}$= 1160 K, P= 101.35 kPa, F_{H2O}=9.72 kg s^{-1}, 41 ppmw S/HC

Table 2. 4: Thermodynamically stable phases simulated using EkviCalc based on the fresh coupon elemental composition. Steam cracking of Ethane: F_{HC} = 29.18 10^{-6} kg s^{-1}, δ = 0.33 kg_{H2O} kg^{-1}_{HC}, Treactor = 1160 K, p = 101.35 kPa, F_{H2O} = 9.72 10^{-6} kg s^{-1}, CA of DMDS 41 ppmw S/HC.

Pretreatment		**OAN (A)**		**OAS (B & C)**		**S (D,G &H)**		**OS (E & F)**	
	acc.volt.	**10kV**	**20kV**	**10kV**	**20kV**	**10kV**	**20kV**	**10kV**	**20kV**
Stable Components	**Fe_3O_4**	-	-	-	-	21.3	22.9	20.9	22.5
	$MnCr_2O_4$	-	3.3	-	3.3	-	2.6	-	2.5
	$NiFe_2O_4$	47.6	44.7	47.6	44.7	-	-	-	-
	$NiCr_2O_4$	36.1	33.4	36.1	33.4	24.3	25.7	23.9	25.2
	Ni_2SiO_4	9.7	1.2	9.7	1.2	-	-	-	-
	NiO	5.7	-	5.7	-	-	-	-	-
	Ni_3S_2	-	-	-	-	0.9	0.9	-	-
	Ni	-	-	-	-	46.4	33.6	48.2	35.7
	Nb_2O_5	0.9	0.6	0.9	0.6	0.6	0.5	0.6	0.5
	SiO_2	-	16.8	-	16.8	6.6	13.8	6.5	13.6

Overall, pretreatments with the best coking performance B, C, E and F have less than 20 wt % of Fe and Ni on their surface, while for the other cases even a cumulative amount of 70 wt % is noted, supporting their increased catalytic behavior towards coke formation. Therefore, by application of the different pretreatments a decrease of up to 50 wt % in the amount of catalytic elements in comparison with a fresh coupon can be observed.

The opposite trend is noticed, while analyzing the results of Cr and Mn content on the pretreated coked samples. Here, the highest amounts of Cr and Mn are measured in the case of steam treated coupons, namely B, C, E and F. Especially, steam pretreatment combined with air, as in the case of B and C, increases the amount of Cr and Mn identified on the surface during the pretreatment.

From D, G and H, it is clear that presulfiding of the pretreated sample leads to a decrease of the Cr and Mn amounts on the surface, possibly indicating that sulfur damages the formed oxides during preoxidation and/or steam pretreatment.

Table 2. 5: Top-View EDX Analyses of Blank, Pretreated and coked after 2 hours samples. Steam cracking of Ethane: F_{HC} = 29.18 10^{-6} kg s^{-1}, δ = 0.33 kg_{H2O} kg^{-1}_{HC}, Treactor = 1160 K, p = 101.35 kPa, F_{H2O} = 9.72 10^{-6} kg s^{-1}, CA of DMDS 41 ppmw S/HC.

Elements	Acc. Volt.	Fresh	A		B		C		D		E		F		G		H	
			treated	2h coked	treated	2h coked	treated	2h coked	treated	2h coked	treated	2h coked	treated	2h coked	treated	2h coked	treated	2h coked
Ni	10 kV	40.3	14.8	2.0	7.0	3.7	7.0	3.7	8.7	3.6	9.1	8.5	8.7	6.8	5.3	3.1	11.2	5.6
	20 kV	33.5	22.5	27.6	9.3	10.3	9.3	10.3	12.3	13.9	9.5	9.6	10.1	10.6	6.9	7.5	15.3	16.8
Fe	10 kV	33.4	24.5	18.0	5.3	1.6	5.6	1.6	8.6	1.8	8.8	5.2	17.1	20.0	15.3	18.2	19.8	19.3
	20 kV	35.4	28.5	31.1	8.0	9.1	8.3	9.5	13.4	15.4	11.5	12.4	14.9	14.2	13.2	12.4	20.2	20.4
Cr	10 kV	23.6	42.7	50.4	63.6	65.2	63.0	64.9	64.9	70.3	63.5	62.4	52.8	43.8	58.8	50.3	46.7	42.6
	20 kV	27.0	38.0	35.0	62.5	62.1	61.6	61.1	61.2	59.6	64.3	64.6	59.5	61.9	64.8	67.2	49.6	50.8
Si	10 kV	1.7	2.2	1.8	1.8	1.4	1.7	1.4	1.0	0.6	1.7	0.7	1.6	0.8	1.4	0.7	2.9	2.0
	20 kV	1.8	2.4	2.5	2.0	2.1	2.0	2.1	1.2	1.4	2.5	2.7	2.2	2.4	2.0	2.2	3.5	3.7
Mn	10 kV	0	14.9	27.0	21.7	27.8	22.1	28.2	16.1	23.2	17.0	23.3	19.8	28.7	19.2	27.7	19.4	30.5
	20 kV	1.3	7.7	2.9	17.4	15.5	18.0	16.1	11.1	9.0	12.3	10.7	13.2	10.9	13.1	10.7	11.4	8.3
Nb	10 kV	0.9	0.8	0.7	0.6	0.4	0.7	0.4	0.8	0.7	0	0	0	0	0.0	0	0	0
	20 kV	0.8	0.9	0.9	0.8	0.9	0.9	1.0	0.8	0.8	0	0	0	0	0.1	0.1	0	0

Additionally, a certain trend is visible in the EDX analysis at 10 kV: increasing the duration of the last pretreatment step leads to a decreasing concentration of Cr, while the concentrations of Mn and Fe are increasing. Introducing air during the steam pretreatment (pretreatment B to C) leads to higher Mn contents near the surface in favor over Ni. A decrease of Cr is most of the times accompanied by an increase in Fe content on the surface. For the steam treated samples, the EDX analyses at 20 kV does not show large deviations, except for the pretreatments that include sulfur.

As a last step, using as input 10 kV compositions for coked and treated samples, the thermodynamically most stable phases are calculated with the aid of EkviCalc and summarized in Table S 3 in supporting information. Apparently, a combination of more $MnCr_2O_4$ and less Cr_2O_3 is beneficial for coke suppression. The calculated $NiCr_2O_4$ phase seems to leave the coking behavior of the alloy unaffected (pretreatment B and C). The latter phase is not present when more Ni is calculated on the surface that is always accompanied by higher pyrolytic coking rates (pretreatments D to H).

As mentioned above, in terms of coking the best pretreatments are B and C. These two exhibit significantly higher calculated amounts of $MnCr_2O_4$ and Cr_2O_3. The presence of Fe_3O_4 seems to be induced by a pure steam pretreatment, with or without DMDS, leading to elevated coking rates, which is the case for the last step of pretreatments D, E, F, G and H.

XRD patterns have been also obtained to further evaluate the crystal structure of the coupons. The crystalline phases were determined using a Siemens Diffractometer Kristalloflex D5000, with Cu Kα (λ = 0.154nm) radiation. The XRD patterns were collected in a 2θ range from 10° to 80° with a step of 0.04°. From Figures S 4 to S 8 it is obvious that these XRD patterns showed mainly three big peaks (Fe-Ni to an angle of 43.65°, 50.8° and 74.75°) for all samples which does not allow to relate this with the difference in coking behavior. The effect of the pretreatments is a

local surface effect, thus only the composition in the first few μm of the whole sample actually changes. Nevertheless, additional XRD data can be found in the Supporting information, in Annex A, by zooming in the expected compounds interesting angle areas.

2.5 Discussion

2.5.1 Air and Steam / Air pretreatment Effect (A-B-C)

For a more thorough understanding of the positive effect of the steam / air pretreatment and its duration, pretreatments A, B and C are compared in Figure 2. 6. Addition of a steam combined with Air pretreatment after a mild preoxidation in N_2 and Air, can lead to a decrease of a factor 5 of the catalytic and asymptotic coking rates during the first cracking cycle. As stated previously, by comparing pretreatments B and C, increasing the duration of the steam pretreatment does not further affect the anti-coking behavior of the alloy. This is important because industrial steam cracking furnaces are often put in so-called "hot steam stand-by" when there is a start-up or process upset. After decoking, i.e. in the second cycle, the differences become less pronounced. Nevertheless, still a factor 2 and 3 decrease was noticed for the initial and asymptotic coking rates, respectively.

In terms of surface composition, see Table A 4 in supporting information of Annex A, the steam and air treated samples showed 3 times less cumulative amount of Ni and Fe than the reference A. 30 % more Cr and Mn was measured for both B and C in comparison with A. As indicated in Figure 2. 7, the thickness and uniformity of the oxides formed after pretreatments B and C was unprecedented. Using the results of the surface composition the thermodynamically stable condensed phases expected on the coked and treated surface are calculated. For all the treated and coked samples the dominant stable phase is the chromium –manganese spinel ($MnCr_2O_4$) co-existing with chromia.

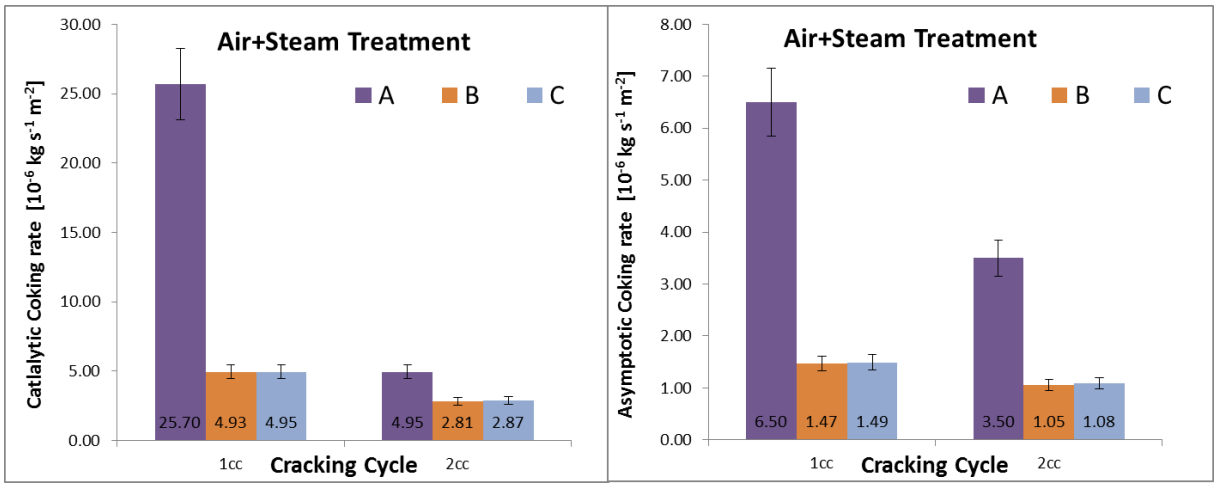

Figure 2. 6: Comparison of coking rates for the different pretreatments A, B and C to evaluate the effect of the addition of a steam combined with air pretreatment. Ethane steam cracking: F_{HC}= 29.18 kg s^{-1}, δ= 0.33 kg_{H2O} kg^{-1}_{HC}, $T_{reactor}$= 1160 K, P= 101.35 kPa, F_{H2O}=9.72 kg s^{-1}, 41 ppmw S/HC

Samples after pretreatment A show 20 % lower mole fractions of the former phase, which is in agreement with the observations in the cross-sectional elemental mappings. Pretreatments B and C lead to significantly decreased amounts of phases including Ni and Fe, such as $NiFe_2O_4$, supporting their suppressed catalytic coking behavior [47, 52, 53]. In the case of only air pretreatment the increased partial pressure of oxygen in comparison with a steam treatment, with or without air, is expected to lead to a higher oxidation rate of the surface [4, 5].

As a result, heterogeneous oxidation of the surface or further oxidation towards the bulk should be observed in comparison with a steam/air pretreatment. Additional experiments given in Supporting Information show that an air only pretreatment at 1023 K and an air only pretreatment at 1108 K leads to a factor 5 increase of the coke deposited on the surface in comparison with the optimal pretreatment B. As expected, the air pretreatments, namely A, I and J, led to increased but heterogeneous oxidation of the surface, see the Supporting Information.

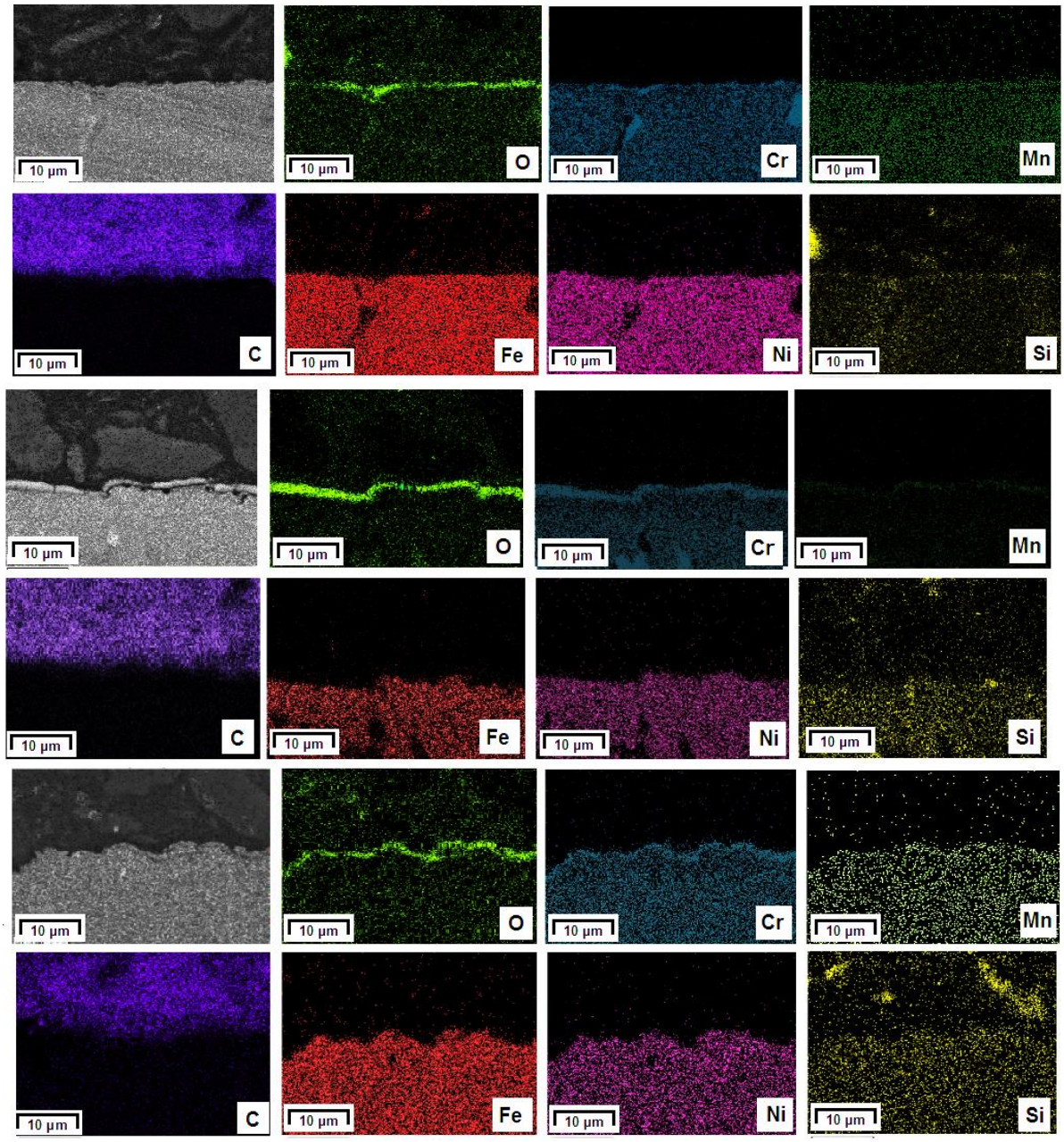

Figure 2. 7: Cross section elemental mappings of coked sample after pretreatment (from Top to the bottom): A, B and C. Magnification 3000x, Accelerating Voltage 15kV.

Note that pretreatment B cannot be applied for the entire coil surface and thus that some positions suboptimal pretreatment conditions will affect the local coking tendency. To evaluate this the effect of temperature is evaluated by adding a pretreatment similar to pretreatment B but now at a

fixed temperature of 1023 K, resulting in 30% increase of the total amount of coke. A more detailed discussion of this second order effect can be found in Supporting Information.

However, for practical purposes a good assessment of the temperature profile during pretreatment is needed to make sure that the optimal pretreatment conditions are applied where most coke is expected to be formed. This would be possible via Computational Fluid Dynamic modelling of the fire side, to mimic the pretreatment and the radial temperature profiles in the coil, as for example done by Zhang et al.[54, 55]

2.5.2 Steam Pretreatment Effect (A-E-F)

The effect of pure steam pretreatment on an oxidized surface is evaluated by comparison of sequences A, E and F. As a reference, the coupon which was treated according to pretreatment A is being considered. The catalytic coking rates are reduced with a factor 6 in comparison with the reference in the first cycle, while after the second cracking cycle the differences were less pronounced (see Figure 2. 8).

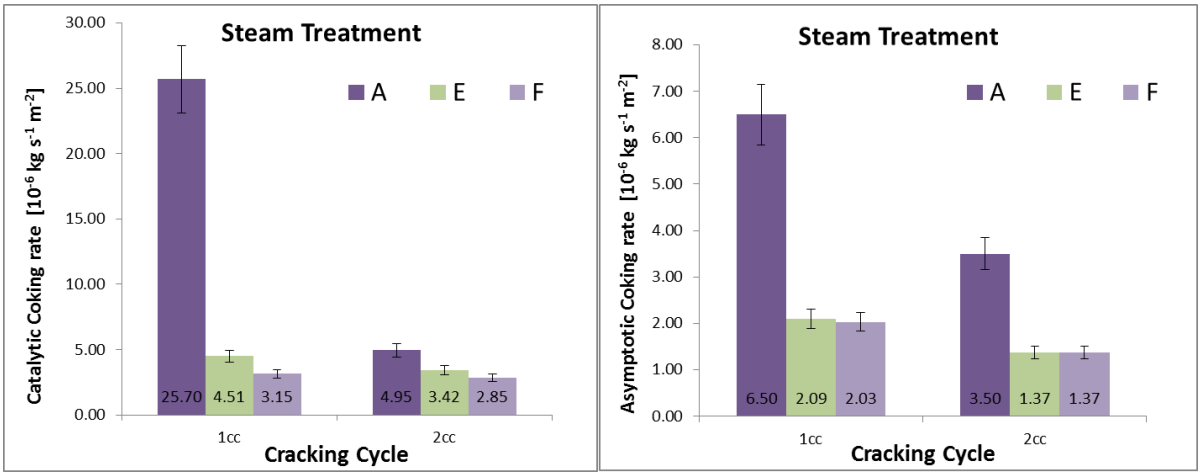

Figure 2. 8: Comparison of coking rates for the different pretreatments A, E and F to evaluate the effect of the addition of a steam pretreatment. Steam cracking of Ethane: F_{HC}= 29.18 kg s^{-1}, δ= 0.33 kg_{H2O} kg^{-1}_{HC}, $T_{reactor}$= 1160 K, P= 101.35 kPa, F_{H2O}=9.72 kg s^{-1}, 41 ppmw S/HC

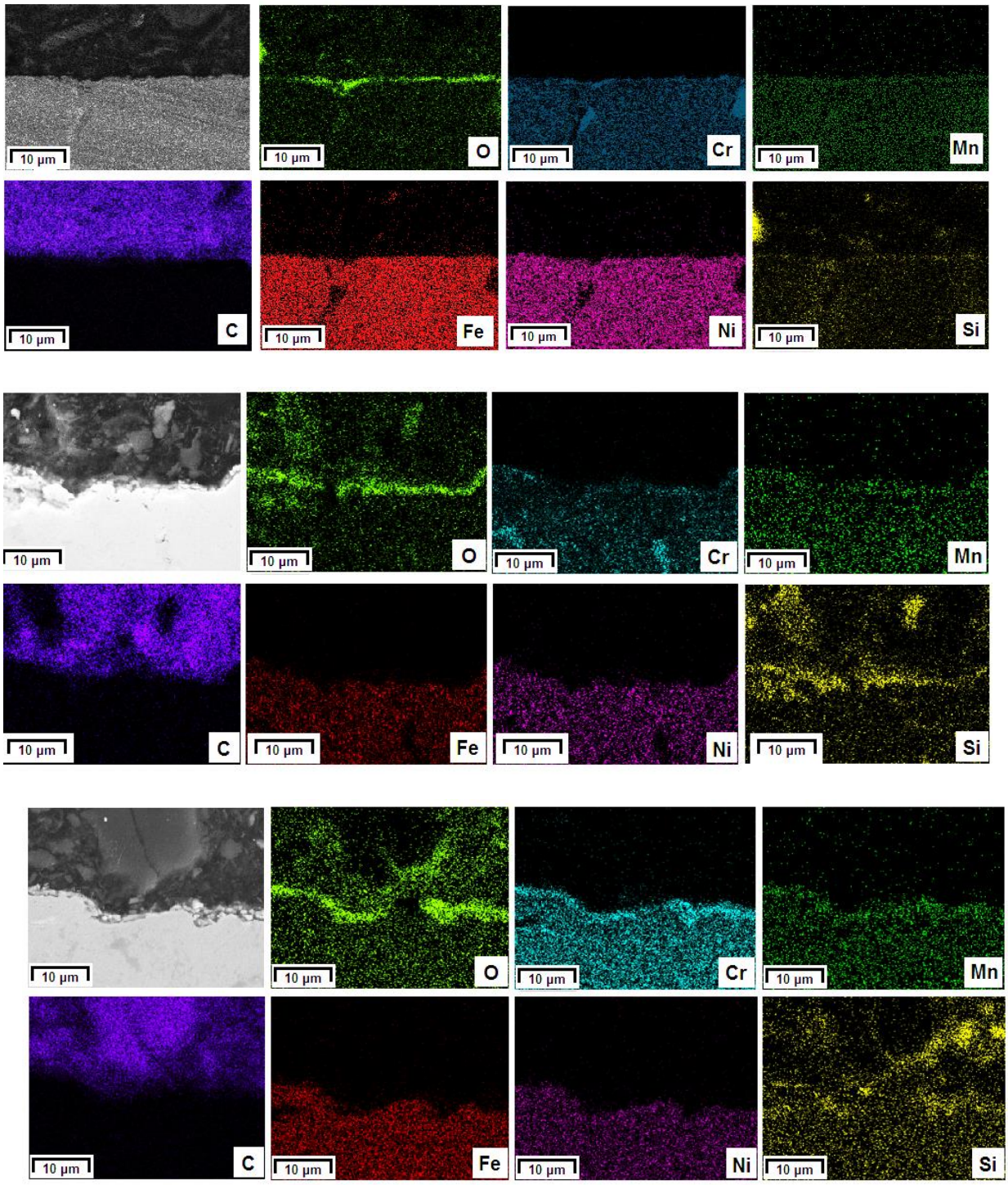

Figure 2. 9: Cross section elemental mappings of coked sample after pretreatment (from Top to the bottom): 'A', 'E' and 'F'. Magnification 3000x, Accelerating Voltage 15kV

Particularly pretreatment E leads to samples which have almost 50 % less Ni and Fe on their surface in comparison to A. Cr is clearly enriched, while the Mn content roughly increased with a factor 2. From Figure 2. 9, it is concluded that regardless the duration an increased thickness of the formed oxides is noted, followed by a developed heterogeneous structure.

Based on Table A 5 in supporting information in Annex A, the most stable phases calculated via EkviCalc for pretreatment E were $MnCr_2O_4$ and Cr_2O_3, while the amounts of Fe and Ni were slightly lower than for the reference A. Pretreatment F lead to increased amounts of phases including Fe and Ni, in line with the values observed by the surface analysis.

2.5.3 Presulfiding Effect (B-D & F-G-H)

Figure 2. 10 shows that sulfur has the most pronounced effect of all pretreatments – especially for the pyrolytic coking rates. Presulfiding after the best anti-coking pretreatment, namely B, doubled all the coking rates of the alloy, although the initial coking rate of the first cracking cycle remains almost unaffected. The samples treated according to sequence F with either an additional presulfiding step of 30 min or 1 hour of (pretreatment G and H) gave 3 and 2 times higher values for the catalytic and pyrolytic coke growth, respectively.

A sulfur pretreatment after pretreatment B gives rise to Ni and Fe, at the expense of Mn on the surface (see Table A 6 in supporting information). Consequently, an additional presulfiding step leads to a decrease of the amount of $MnCr_2O_4$ expected on the surface in favor of Cr_2O_3 for both the coked and treated samples. Additionally, for the treated samples pure Ni is formed according to the simulations in comparison with the Ni-base oxidized phases in pretreatment B. From Figure 2. 11 and Figure 2. 12, it is noted the uniformity of the oxides formed is slightly influenced.

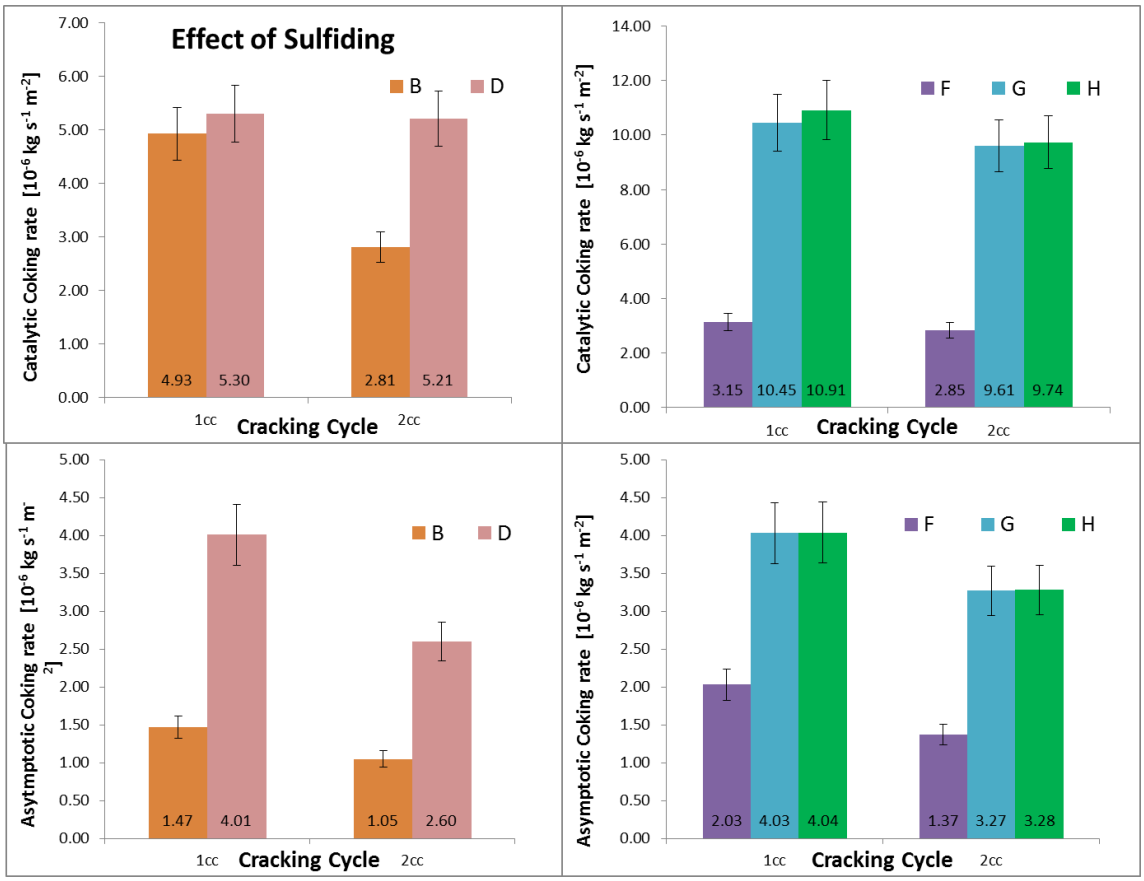

Figure 2. 10: Comparison of coking rates for the different pretreatments, B vs D and F vs G and H to evaluate the effect of Presulfiding pretreatment. Steam cracking of Ethane: F_{HC}= 29.18 kg s^{-1}, δ= 0.33 kg_{H2O} kg^{-1}_{HC}, $T_{reactor}$= 1160 K, P= 101.35 kPa, F_{H2O}=9.72 kg s^{-1}, 41 ppmw S/HC.

Finally, using the 1 hour steam treated coupon – pretreatment F - as a reference the effect of presulfiding for 30 min and 1 hour is investigated. Similar amounts of Ni and Fe are noticed after 30 min of sulfur pretreatment. After 1 hour of the same pretreatment, increased amounts of the Ni and Fe are measured at the expense of Cr. The sulfided samples show almost the same amount of $MnCr_2O_4$. The amounts of pure Ni and SiO_2 formed on the surface is rising by increasing the duration of the presulfiding pretreatment. The opposite trend is noted for Cr_2O_3 for the two sulfided samples, while no $NiCr_2O_4$ is formed in contrast with the reference F. Additionally, the SEM images show the decreased homogeneity and thickness of the oxides formed on the surface

for the sulfided samples in comparison with the reference, clearly illustrating that a DMDS pretreatment is not the best choice if low coking rates are the primary objective.

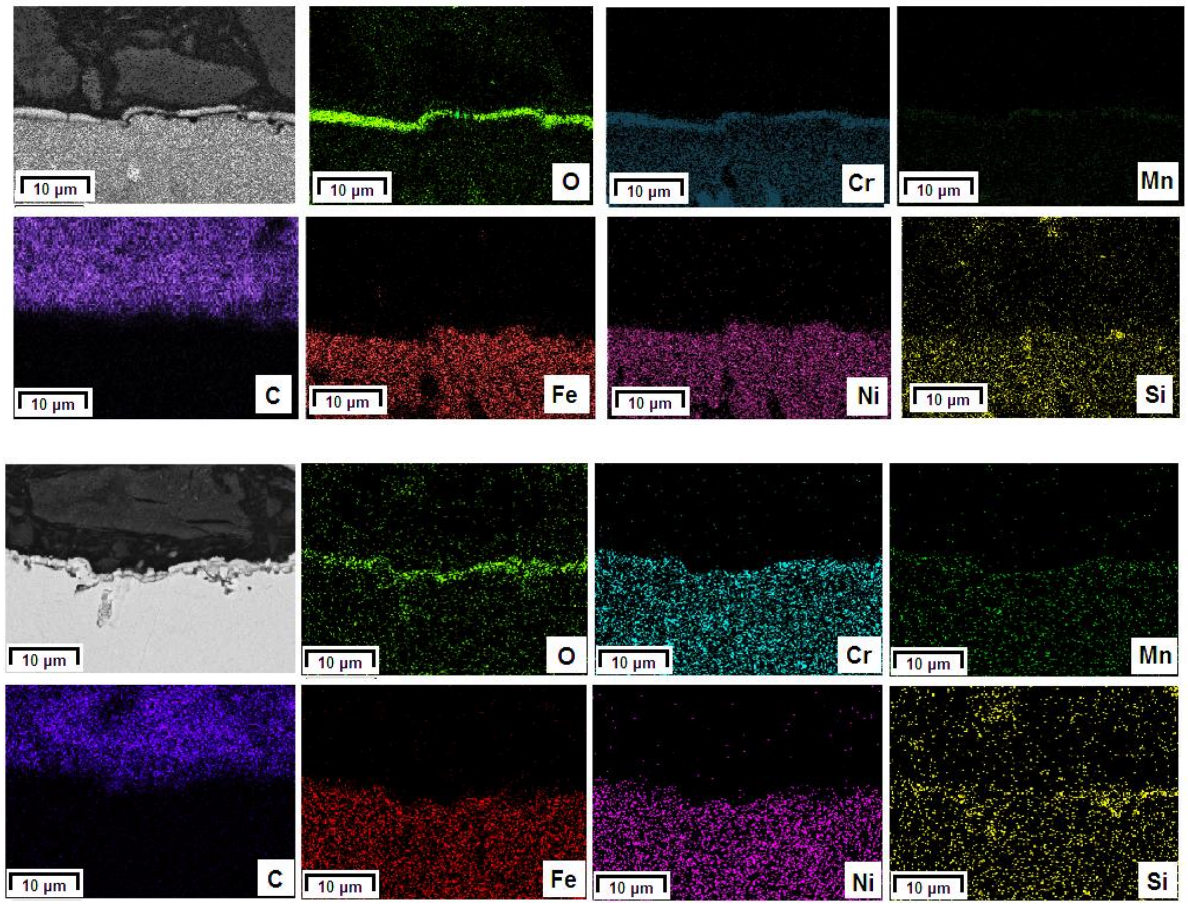

Figure 2. 11: Cross section elemental mappings of coked sample after pretreatment (from Top to the bottom): B and D. Magnification 3000x, Accelerating Voltage 15kV.

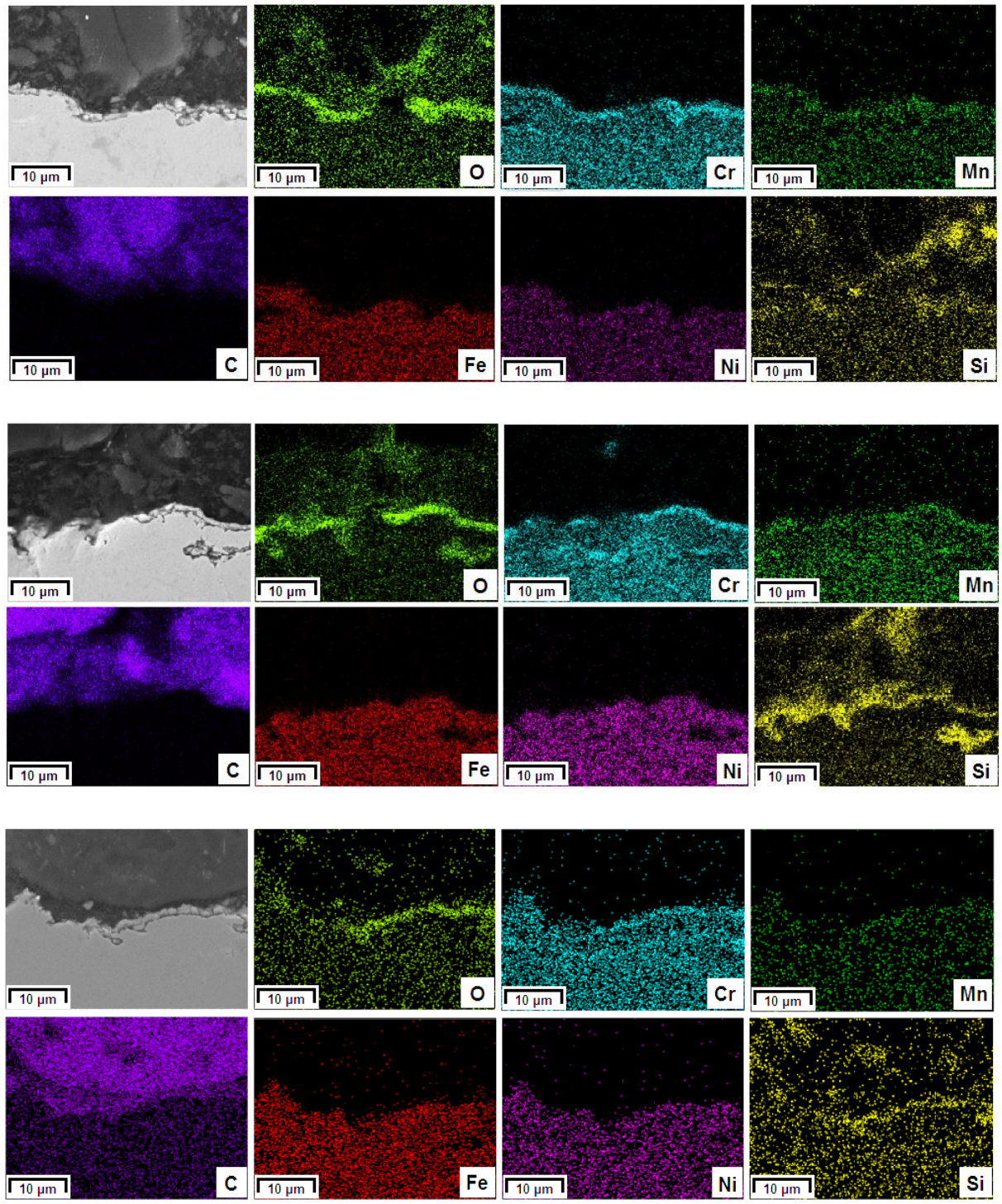

Figure 2. 12: Cross section elemental mappings of coked sample after pretreatment F (Top), G (Middle) or Pretreatment H (Bottom). Magnification 3000x, Accelerating Voltage 15kV.

2.6 Conclusion

Eight different pretreatments on a classical high temperature alloy have been evaluated in a thermogravimetric set-up in combination with SEM and EDX analyses. The experimental data show that pretreatment B, a two-step preoxidation followed by a steam/air pretreatment, is the best in reducing coke deposition for ethane steam cracking when continuously adding DMDS during cracking. The pyrolytic coking rate was at least 30% lower than the other investigated pretreatments and almost a factor 5 compared to the worst pretreatment, illustrating the importance of optimizing the surface pretreatment.

Applying a steam only pretreatment mitigates the catalytic coking by creating a very thick oxide layer which blocks catalytically active sites. However, higher pyrolytic coking rates in comparison with pretreatment B are measured. Increasing the duration of the steam pretreatment leads to even further reduction of the catalytic coking rate, but the pyrolytic coking rate remains higher than pretreatment B. Presulfiding the surface generates up to 3 times more coke. Increasing presulfiding duration did not result in lower coking rates either.

Pretreatment B leads to primarily $MnCr_2O_4$, Cr_2O_3 and $NiFe_2O_4$ on the surface, with Cr_2O_3 being more active towards coke. Increasing the duration of the steam only pretreatment leads to increased homogeneity but not when presulfiding was applied. No effect of duration was observed when the duration of the steam/air pretreatment was increased, which is very important for industrial furnaces, which are often put on the hot steam standby. Overall, mild preoxidation at elevated temperature followed by a steam/air pretreatment leads to the most homogeneous oxide layer formation consisting of mainly Cr and Mn optimizing the anti-coking performance of a high temperature Fe-Ni-Cr Alloy.

2.7 References

1. Paraskevas, P. D.; Sabbe, M. K.; Reyniers, M. F.; Papayannakos, N.; Marin, G. B., Kinetic Modeling of α-Hydrogen Abstractions from Unsaturated and Saturated Oxygenate Compounds by Carbon-Centered Radicals. *ChemPhysChem* **2014,** 15, (9), 1849-1866.
2. Paraskevas, P. D.; Sabbe, M. K.; Reyniers, M.-F.; Papayannakos, N. G.; Marin, G. B., Kinetic Modeling of α-Hydrogen Abstractions from Unsaturated and Saturated Oxygenate Compounds by Hydrogen Atoms. *The Journal of Physical Chemistry A* **2014,** 118, (40), 9296-9309.
3. Kivlen, J. A.; Koszman, I., Decoking of onstream thermal cracking tubes with h20 and h2. In Google Patents: 1971.
4. Chen, J.; Maddock, M., *Hydrocarbon Process*. 1973; Vol. 52, p 147-151.
5. Sullivan, B. K., Ethylene Cracking Heater Decoking Tutorial. In *AIChE 2014 Spring Meeting*, New Orleans, LA, 2014.
6. Heynderickx, G.; Schools, E.; Marin, G., Optimization of the decoking procedure of an ethane cracker with a steam/air mixture. *Industrial & engineering chemistry research* **2006,** 45, (22), 7520-7529.
7. Lenglet, E., Method of decoking an installation for steam cracking hydrocarbons, and a corresponding steam-cracking installation. In Google Patents: 1993.
8. HAK Decoking Technology (HDT). http://www.a-hak-is.com/en/home/what_we_do/services/furnace_services/hak_decoking_technology_hdt
9. Nunciato, D. J.; White, N. H.; Woodburn, W. A., Method for decoking fired heater tubes. In Google Patents: 1981.
10. J, D. W., Decoking and cleaning tubular heaters. In Google Patents: 1954.
11. De Saegher, J. J.; Detemmerman, T.; Froment, G. F., Three dimensional simulation of high severity internally finned cracking coils for olefins production. *Revue De L'Institut Français Du Pétrole* **1996,** 51, (2), 245-260.
12. Detemmerman, T.; Froment, G. F., Three dimensional coupled simulation of furnaces and reactor tubes for the thermal cracking of hydrocarbons. *Revue De L'Institut Français Du Pétrole* **1998,** 53, (2), 181-194.

13. Schietekat, C. M.; van Goethem, M. W. M.; Van Geem, K. M.; Marin, G. B., Swirl flow tube reactor technology: An experimental and computational fluid dynamics study. *Chemical Engineering Journal* **2014,** 238, 56-65.
14. Torigoe, T.; Hamada, K.; Furuta, M.; Sakashita, M.; Otsubo, K.; Tomita, M. In *Mixing element radiant tube (MERT) improves cracking furnace performance*, 11th Ethylene Producers' Conference, Houston, TX, 1999; Houston, TX, 1999.
15. Györffy, M.; Hineno, M.; Hashimoto, K.; Park, S.-H.; You, M.-S. In *MERT performance and technology update*, 21st Ethylene Producers' Conference, Tampa, FL, 2009; Tampa, FL, 2009.
16. Schietekat, C. M.; Van Cauwenberge, D. J.; Van Geem, K. M.; Marin, G. B., Computational fluid dynamics-based design of finned steam cracking reactors. *AIChE Journal* **2014,** 60, (2), 794-808.
17. Muñoz Gandarillas, A. E.; Van Geem, K. M.; Reyniers, M.-F.; Marin, G. B., Influence of the Reactor Material Composition on Coke Formation during Ethane Steam Cracking. *Industrial & Engineering Chemistry Research* **2014,** 53, (15), 6358-6371.
18. Muñoz Gandarillas, A. E.; Van Geem, K. M.; Reyniers, M.-F.; Marin, G. B., Coking Resistance of Specialized Coil Materials during Steam Cracking of Sulfur-Free Naphtha. *Industrial & Engineering Chemistry Research* **2014,** 53, (35), 13644-13655.
19. Petrone, S.; L.Deuis, R.; Kong, F.; Unwin , P. In *Catalyzed-assisted manufacture of olefins (CAMOL): Year-(4) update on commercial furnace installations*, Prepared for Presentation at the 2010 Spring National Meeting, March 21-25, 2010; 2010.
20. Schietekat, C. M.; Sarris, S. A.; Reyniers, P. A.; Kool, L. B.; Peng, W.; Lucas, P.; Van Geem, K. M.; Marin, G. B., Catalytic Coating for Reduced Coke Formation in Steam Cracking Reactors. *Industrial & Engineering Chemistry Research* **2015,** 54, (39), 9525-9535.
21. Petrone, S.; Chen, Y.; Deuis, R.; Benum, L.; Saunders, R.; Wong, C. In *Catalyzed-assisted manufacture of olefins (CAMOL): Realizing novel operational benefits from furnace coil surfaces*, 20th Ethylene Producers' Conference, New Orleans, LA, 2008; New Orleans, LA, 2008.

22. Wang, J.; Reyniers, M.-F.; Van Geem, K. M.; Marin, G. B., Influence of Silicon and Silicon/Sulfur-Containing Additives on Coke Formation during Steam Cracking of Hydrocarbons. *Industrial & Engineering Chemistry Research* **2008,** 47, (5), 1468-1482.
23. Reyniers, M.-F.; Froment, G. F., Influence of metal-surface and sulfur addition on coke deposition in the thermal-cracking of hydrocarbons. *Industrial & Engineering Chemistry Research* **1995,** 34, (3), 773-785.
24. Wang, J.; Reyniers, M.-F.; Marin, G. B., Influence of Dimethyl Disulfide on Coke Formation during Steam Cracking of Hydrocarbons. *Industrial & Engineering Chemistry Research* **2007,** 46, (12), 4134-4148.
25. Reyniers, M.; Froment, G. F., INFLUENCE OF METAL-SURFACE AND SULFUR ADDITION ON COKE DEPOSITION IN THE THERMAL-CRACKING OF HYDROCARBONS. *Ind. Eng. Chem. Res.* **1995,** 34, (3), 773-785.
26. Brown, D. E.; Clark, J. T. K.; Foster, A. I.; McCarroll, J. J.; Sims, M. L., Inhibition of Coke Formation in Ethylene Steam Cracking. In *Coke Formation on Metal Surfaces*, AMERICAN CHEMICAL SOCIETY: 1983; Vol. 202, pp 23-43.
27. Wang, J.; Reyniers, M.-F.; Marin, G. B., The influence of phosphorus containing compounds on steam cracking of n-hexane. *Journal of Analytical and Applied Pyrolysis* **2006,** 77, (2), 133-148.
28. Vaish, S.; Kunzru, D., Triphenyl phosphite as a coke inhibitor during naphtha pyrolysis. *Industrial & Engineering Chemistry Research* **1989,** 28, (9), 1293-1299.
29. Dhuyvetter, I.; Reyniers, M.-F.; Froment, G. F.; Marin, G. B.; Viennet, D., The influence of dimethyl disulfide on naphtha steam cracking. *Industrial & Engineering Chemistry Research* **2001,** 40, (20), 4353-4362.
30. Bajus, M.; Vesely, V.; Baxa, J.; Leclercq, P. A.; Rijks, J. A., Steam cracking of hydrocarbons: 5. Effect of thiophene on reaction-kinetics and coking. *Industrial & Engineering Chemistry Product Research and Development* **1981,** 20, (4), 741-745.
31. Bajus, M.; Vesely, V., Pyrolysis of hydrocarbons in the presence of elemental sulfur. *Collection of Czechoslovak Chemical Communications* **1980,** 45, (1), 238-254.
32. Bajus, M.; Baxa, J.; Leclercq, P. A.; Rijks, J. A., Steam cracking of hydrocarbons: 6. Effect of dibenzyl sulfide and dibenzyl disulfide on reaction-kinetics and coking.

Industrial & Engineering Chemistry Product Research and Development **1983,** 22, (2), 335-343.

33. Bajus, M.; Baxa, J., Coke formation during the pyrolysis of hydrocarbons in the presence of sulfur-compounds. *Collection of Czechoslovak Chemical Communications* **1985,** 50, (12), 2903-2909.
34. Depeyre, D.; Filcoteaux, C.; Blouri, B.; Ossebi, J. G., Pure norma-nonane steam cracking and the influence of sulfur-compounds. *Industrial & Engineering Chemistry Process Design and Development* **1985,** 24, (4), 920-924.
35. Dhuyvetter, I.; Reyniers, M. F.; Froment, G. F.; Marin, G. B.; Viennet, D., The influence of dimethyl disulfide on naphtha steam cracking. *Ind. Eng. Chem. Res.* **2001,** 40, (20), 4353-4362.
36. Towfighi, J.; Sadrameli, M.; Niaei, A., Coke formation mechanisms and coke inhibiting methods in pyrolysis furnaces. *J. Chem. Eng. Jpn.* **2002,** 35, (10), 923-937.
37. Holmen, A.; Lindvaag, O. A.; Trimm, D. L., COKE FORMATION DURING STEAM CRACKING OF HYDROCARBONS .2. EFFECT OF PREOXIDATION AND PREREDUCTION OF THE REACTOR SURFACE. *Journal of Chemical Technology and Biotechnology a-Chemical Technology* **1985,** 35, (7), 358-364.
38. Horsley, G. W.; Cairns, J. A., THE INHIBITION OF CARBON DEPOSITION ON STAINLESS-STEEL BY PRIOR SELECTIVE OXIDATION. *Appl. Surf. Sci.* **1984,** 18, (3), 273-286.
39. Luan, T. C.; Eckert, R. E.; Albright, L. F., Gaseous pretreatment of high-alloy steels used in ethylene furnaces: Pretreatment of incoloy 800. *Ind. Eng. Chem. Res.* **2003,** 42, (20), 4741-4747.
40. Jakobi, D.; Karduck, P.; Freiherr, V. R. A., The High-Temperature Corrosion Resistance of Spun-Cast Materials for Steam-Cracker Furnaces - A Comparative Study of Alumina- and Chromia-Forming Alloys. In *NACE Corrosion 2013*, 2013.
41. Jakobi, D.; van Moesdijk, C.; Karduck, P.; von Richthofen, A., Tailor-made materials for high temperature applications: New strategies for radiant coil material development. *CORROSION 2009* **2009**.

42. Asteman, H.; Hartnagel, W.; Jakobi, D., The Influence of Al Content on the High Temperature Oxidation Properties of State-of-the-Art Cast Ni-base Alloys. *Oxid. Met.* **2013,** 80, (1-2), 3-12.
43. Srinivas, V. R.; Humblot, F., Compositions to mitigate coke formation in steam cracking of hydrocarbons. In Google Patents: 2011.
44. Tong, Y.; Poindexter, M. K., Method of inhibiting coke deposition in pyrolysis furnaces. In Google Patents: 1999.
45. Gary Barone, M. H., David Smith , Restek Corporation Performance Coatings; Shawn Rowan, W. J. G., O'Brien Corporation; Phil Harris, H. L. Sulfinert® Treated Systems Preserve ppb Levels of Active Sulfur Compounds.
46. Nolang, B., Ekvicalc and Ekvibase, 4.30. In *Svensk Energi Data: Balinge*, Sweeden, 2013.
47. Reyniers, M.-F. S. G.; Froment, G. F., Influence of Metal Surface and Sulfur Addition on Coke Deposition in the Thermal Cracking of Hydrocarbons. *Industrial & Engineering Chemistry Research* **1995,** 34, (3), 773-785.
48. Van Geem, K. M.; Reyniers, M. F.; Pyl, S. P.; Marin, G. B., Effect of Operating Conditions and Feedstock Composition on Run Length of Steam Cracking Coils. In *(2009) AIChE 2009 Spring National Meeting*, Tampa, FL, 2009.
49. Snoeck, J.-W.; Froment, G.; Fowles, M., Filamentous carbon formation and gasification: thermodynamics, driving force, nucleation, and steady-state growth. *Journal of Catalysis* **1997,** 169, (1), 240-249.
50. Van Geem, K. M.; Dhuyvetter, I.; Prokopiev, S.; Reyniers, M.-F.; Viennet, D.; Marin, G. B., Coke Formation in the Transfer Line Exchanger during Steam Cracking of Hydrocarbons. *Industrial & Engineering Chemistry Research* **2009,** 48, (23), 10343-10358.
51. Rostrup-Nielsen, J.; Trimm, D. L., Mechanisms of carbon formation on nickel-containing catalysts. *Journal of Catalysis* **1977,** 48, (1-3), 155-165.
52. Baker, R. T. K.; Yates, D. J. C.; Dumesic, J. A., Filamentous Carbon Formation over Iron Surfaces. In *Coke Formation on Metal Surfaces*, AMERICAN CHEMICAL SOCIETY: 1983; Vol. 202, pp 1-21.

53. Bonnet, F.; Ropital, F.; Berthier, Y.; Marcus, P., Filamentous carbon formation caused by catalytic metal particles from iron oxide. *Materials and Corrosion* **2003,** 54, (11), 870-880.

54. Zhang, Y.; Qian, F.; Schietekat, C. M.; Van Geem, K. M.; Marin, G. B., Impact of flue gas radiative properties and burner geometry in furnace simulations. *AIChE Journal* **2015,** 61, (3), 936-954.

55. Hu, G.; Schietekat, C. M.; Zhang, Y.; Qian, F.; Heynderickx, G.; Van Geem, K. M.; Marin, G. B., Impact of radiation models in coupled simulations of steam cracking furnaces and reactors. *Industrial & Engineering Chemistry Research* **2015,** 54, (9), 2453-2465.

Chapter 3: Effect of Roughness

This chapter includes the following manuscript:

3. **Impact of initial surface roughness and aging on coke formation during Ethane Steam Cracking**

Stamatis A. Sarris[1], Steffen H. Symoens[1], Natalia Olahova[1], Kim Verbeken[2], Marie-Françoise Reyniers[1], Guy B. Marin[1], Kevin M. Van Geem[1,*]

[1]Ghent University, Laboratory for Chemical Technology, Technologiepark 914, 9052 Gent, Belgium.

[2]Ghent University, Department of Materials Science and Engineering, Technologiepark 903, 9052 Gent, Belgium

DOI: 10.1021/acs.iecr.7b02479

3.1 Abstract

Alloys composition and morphology of the inner wall of steam cracking reactors are well-known key factors that affect their coking tendency. The effect of surface roughness on the coking tendency remains uncharted so far and has been studied here for a 35/25 Ni/Cr wt % alloy in a

quartz jet stirred reactor equipped with an electro-balance, under coil outlet industrially relevant ethane steam cracking conditions: $T_{gas\ phase}$ = 1173 K, P_{tot} = 0.1 MPa and X_{C2H6} = 70 %. Up to 6 times higher initial coking rates have been observed during cyclic aging in an R_α surface roughness range of 0.15 - 7 μm and cyclic aging proved to have an effect mainly on the catalytic coking behavior. No effect was observed on the asymptotic coking rates. Scanning electron microscopy and energy diffractive X-ray surface analysis and cross-section elemental mappings suggest that the effect of surface roughness and aging on the catalytic coking rate derives mainly from changes in the metal surface composition. The amounts of metallic Ni and Fe show an increasing tendency with increasing surface roughness, explaining the pronounced coke deposition. Using EkviCalc, thermodynamic calculations were performed proposing that the amount of Cr_2O_3 gradually decreases followed by an increase of manganese chromite, $MnCr_2O_4$.

Keywords: Roughness, steam cracking, coke formation, aging, high temperature alloys, jet stirred reactor

3.2 Introduction

Steam cracking of hydrocarbons is the dominant process to manufacture light olefins[1]. Coke formation on the inner wall of the steam crackers reduces the cross-sectional area of the tubular reactor, leading to elevated pressure drop over the coil and limited heat transfer from the furnace to the reactors. Surface morphology is considered to have a major impact on the rate of coke growth. To maintain a constant cracking severity over time, the fuel flow rate to the furnace burners has to be increased. This limits the so-called run length of a furnace, since it implies that gradually the reactor tube metal temperature rises and at a certain point in time when the wall

temperature reaches values of around 1400 K – the metallurgical maximum allowed tube temperature – or at very elevated pressure drop – more than 150 kPa [2] - the reactors should be decoked on-line, typically by feeding a steam/air mixture [3-7]. This decoking procedure of roughly 48 hours reduces the yearly production capacity and hence increases the operational costs [8, 9].

To reduce coke formation several technological innovations have been proposed encompassing application of high performance alloys [10-16], coatings [17, 18] and/or in-situ or ex-situ pretreatments [19-23]. Steam cracking reactors are typically made out of heat-resistant Fe-Ni-Cr alloys which resist coke formation by a chromium oxide surface layer [13, 15]. Often aluminum and manganese are added to improve the coking resistance of the alloys aiming at the formation of a protective alumina (Al_2O_3) or manganese chromite ($MnCr_2O_4$) layer, respectively [13, 15, 16, 24]. Alternatively, a thin coating can be deposited on the reactor base alloy surface. There are two coating categories, namely barrier [25-27] coatings, that passivate the inner reactor wall, and catalytic coatings[17, 28], that aim at coke gasification.

Surface roughness is known to also have an impact on coke formation, however there is only limited quantitative information available describing its effect on coke deposition. Often, surface roughness is not measured but rather assessed qualitatively[29, 30], complicating the interpretation of experimental results. Thus, the understanding of surface phenomena involving surface roughness is very limited. Earlier studies on the effect of surface roughness on coke deposition suggest that the number of active sites for coke formation is higher for rougher surfaces at the start of a coking procedure[31]. It has also been suggested that metal particles are more easily detached from a rougher surface than a smooth one, so-called metal dusting[32], which could result in higher catalytic coking rates due to surface enrichment of metals active for

carbon filament growth. Also, filamentous coke whiskers are known to be excellent collection points for non-catalytic coke or its precursors[33]. Roughened catalytic and non-catalytic surfaces are found to promote coke formation from gas-phase and tar-droplets [34-36]. Higher coking rates on rougher surfaces have also been associated with lower tube wall temperatures since a highly polished surface could operate at temperatures that are 50-100 K below that of an unpolished surface [37]. Crynes et al. [14] reported that polishing can reduce coke deposition over Incoloy 800 coupons during pyrolysis of different light hydrocarbons at 973 K by at most 80%. Marek and Albright [38, 39] also studied coke deposition on polished and unpolished Incoloy 800 or Aluminized Incoloy 800 and, in all cases, less coke was deposited on the polished surfaces than on the rougher unpolished surfaces. However, both coking rates and elemental composition of the samples were not measured to quantitatively evaluate the effect of roughness on coke formation.

Next to the effect of the initial tube surface roughness there is also the impact of tube exposure to successive coking and decoking atmospheres, so-called cyclic aging, on the surface roughness and on the longer term coking behavior. The effective service life of steam cracking coils depends considerably on the number of cyclic cracking-decoking procedures carried out. During operation, coil materials experience coking, carburization, oxidation, creep and thermal cycling [40]. The catalytic interaction of the metal surface with the cracking gases results in a carburization process. The carbon formed and deposited on the alloy surface eventually dissolves and diffuses into the bulk. Consequently, metal carbides start forming altering the alloy mechanical properties [41]. Under oxidizing atmospheres, chromium from the metal matrix diffuses towards the tube surface and the formation of a rather stable oxide Cr_2O_3 layer protects the steel from further carburization[42]. High temperature applications such as steam cracking

rely on the alloys' precipitation hardening mechanism during aging to ensure good creep resistance. It has been shown that the deterioration of mechanical properties due to in-service lifetime is more pronounced at the surface than in the bulk of the material [41].The increased coking rate after several coking/decoking cycles leads to more frequent decoking procedures [43] and due to the repeated exposure at the high operating temperatures at the end of the run, coil materials will eventually over-age, increasing the risk of tube failure [40].

Zimmerman et al. investigated the effect of aging on coke deposition, by comparing coking rates on different steels and proposed a method for accelerated aging of the specimens consisting of 10 successive n-heptane coking/decoking cycles[44]. In this work, the initial surface roughness is systematically varied and an aging procedure similar to the one proposed by Zimmerman is applied to study the effect of initial surface roughness and aging on the coke deposition during ethane steam cracking in a jet stirred reactor (JSR) setup equipped with an electro-balance. After aging, the morphology of the coked samples and their surface metal composition were studied by means of SEM and EDX to obtain a better insight in the effect of aging.

3.3 Experimental section

3.3.1 Electrobalance set-up

Since the jet stirred reactor setup has been extensively described by Muñoz et al. [13, 15, 23], only a brief description is given here. The setup consists of three main parts: the feed section, reaction section and analysis section, see

Figure 3. **1**. The mass flow rates of the water and gases fed to the set-up are controlled by thermal mass flow controllers. First, these flows are sent to the evaporators to vaporize the water and to obtain a stable flow. Afterwards, the steam is mixed with the hydrocarbon feedstock and then

send to the pre-heaters where they are heated to 903 K before entering the reaction zone. A quartz jet stirred reactor composes the reaction section. Inside the reactor, a small coupon, 10 x 8 x 1 mm^2, cut from the inner side of an industrial coil using wire-cut Electrical Discharge Machining (EDM) with an accuracy of 1µ, is suspended from the arm of an electro-balance. The coupon mass is tracked over time giving valuable insight on the coking behavior of the tested material. In the analysis section, the reactor effluent is first quenched with an oil cooler to prevent further cracking. Afterwards, the reactor effluent composition is measured with two gas chromatographs (GC) using nitrogen as internal standard: a refinery gas analyzer dedicated to the analysis of components with less than 4 carbon atoms and a TRACE™ Ultra GC detecting hydrocarbons ranging from methane up to naphthalene.

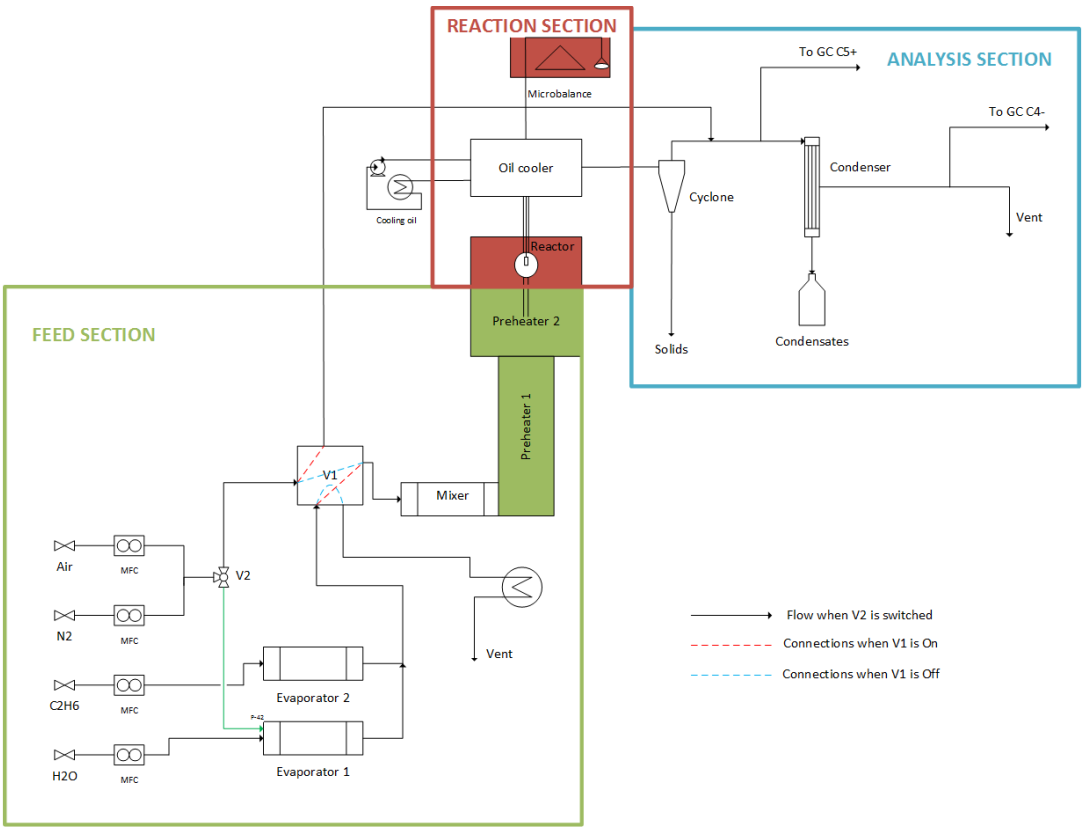

Figure 3. 1: Schematic of the JSR set-up equipped with an electro balance for the study of coke deposition on different reactor materials during steam cracking of ethane

3.3.2 Experimental procedures and conditions

Similar operating procedures and conditions were used as described in previous work. [13, 15, 23], hence only a concise description is given focusing on minor procedural differences. In principle, the aging experiments conducted in the JSR set-up consist of an in-situ pre-oxidation, that is performed prior to the first coking cycle to mimic the surface state at the start-of-run of an industrial reactor, followed by 8 successive coking and decoking cycles (see section 3.3.2.3.). A detailed overview of the experimental conditions of the different process steps is given in Table B.1. Additionally, a schematic representation of the cyclic experiments is illustrated in Figure 3. 2.

The pre-oxidation pre-treatment consists of three steps. First, a constant flow of 6.7 x 10^{-3} Nl s^{-1} flow of air is sent to the reactor at 1023 K for 14 hours. Next, a 1:1 volumetric ratio mixture of nitrogen and air is introduced to the reactor until the temperature reaches 1173 K. The last pretreatment step consists of a steam/air treatment. In the next sections, the coking and decoking steps are described in detail. After each experiment, the coupons are removed for Scanning Electron Microscope (SEM) and Energy Dispersive X-ray (EDX) analyses.

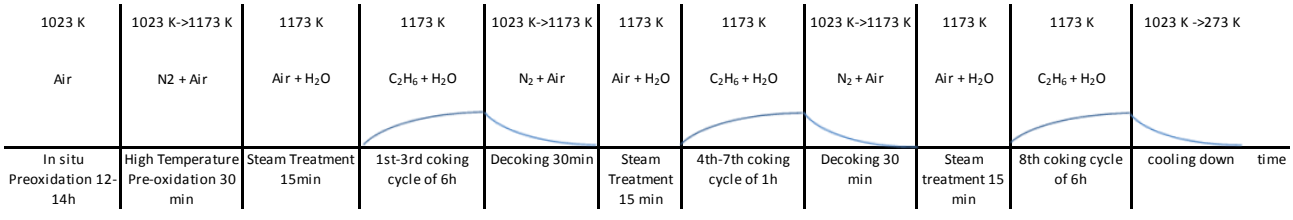

Figure 3. 2: Schematic representation of the cyclic experiments performed in JSR

3.3.2.1 Cracking

As indicated in Table B.1, to initialize a cracking run, the temperature of the reactor is raised to 1173 K under an inert flow of He of $0.14 \cdot 10^{-6}$ kg s^{-1} and the balance is tared to establish a reference state to compare the sample weight before and after cracking. The reactor is then further heated under the inert flow of He of $0.14 \cdot 10^{-6}$ kg s^{-1} to compensate for the temperature drop at the onset of the endothermic cracking reactions, e.g. to 1283 K for an ethane conversion of 70 %. Meanwhile, water and ethane are fed to the evaporators (dilution of $\delta = 0.33$ kg_{H2O}/kg_{C2H6}) and sent to the vent, aiming at a steady evaporation and mixing before sending the stream to the reactor. Once the reactor temperature is stable at 1283 K, valve V1 is switched (see Figure 3. 1), changing the process gas from an inert He atmosphere to a reactive ethane-steam atmosphere. During cracking, the furnace is kept at 1283 K to compensate for the endothermicity of the cracking reactions, which results in a reactor temperature of 1173 K. Throughout the cracking run, the gas phase composition is analyzed on-line.

3.3.2.2 Decoking and steam treatment

After cracking, the feed is again switched to the stabilizing inert He flow and the reactor is cooled to a temperature of 1023 K with a ramp of 300 K h^{-1}. When this temperature is reached, the decoking procedure is started. During decoking, the reactor is heated up from 1023 to 1173 K under a constant flow of air ($11.86\ 10^{-6}$ kg s^{-1}) and nitrogen ($9.68\ 10^{-6}$ kg s^{-1}). After this, a steam-treatment is performed for 15 minutes, feeding the reactor with a mixture of air ($11.86\ 10^{-6}$ kg s^{-1}) and steam ($6.7\ 10^{-6}$ kg s^{-1}) under isothermal conditions at 1173 K. If a next cracking cycle follows, the reactor is kept at this temperature under nitrogen He flow of of $0.14 \cdot 10^{-6}$ kg s^{-1}

overnight until the start of the next cycle. If not, the reactor is cooled down to room temperature with a ramp of 100 K per hour under an inert He atmosphere.

3.3.2.3 Cyclic Aging

To evaluate the aging behavior of the tested materials, multiple coking/decoking cycles are carried out. In between the coking cycles, decoking and steam/air treatment is performed using a procedure optimized [23] for Fe-Ni-Cr alloys.

To mimic industrial practices the cyclic aging procedure summarized in Table B.1 is used. First 3 cracking cycles of 6 hours are performed to evaluate the effect of cyclic coking-decoking on both the initial and asymptotic coking rates. After the third 6-hour cracking cycle, four short 1-hour cracking cycles are performed to rapidly age the sample. Finally, a last 6-hour cracking cycle is performed in order to assess the long term coking behavior of the sample. All coking cycles were triplicated. However, for the 8th coking cycle, the third replicate cycle was stopped after one hour and no decoking was performed in order to study the morphology and surface composition of the coked samples.

3.3.3 Determination of the surface roughness

The samples, cut from the inside of an industrial tube using wire-cut Electrical Discharge Machining (EDM) were manually polished using the UK grit papers as indicated in Table 3. 1 in order to obtain samples with a surface roughness R_α of 0.15 µm, 0.75 µm, 1.3 µm, 2.6 µm, 3.9 µm, 5.1 µm and 7.0 µm.

Many different roughness parameters are typically used in literature[45], but R_α is the most commonly used parameters by olefin producers and can be easily measured with a contact or optical profilometer. The determination of R_α is illustrated in Figure B.5 The mean value of the measured height profile is taken as Z(0) (see Figure B.5) and R_α is then defined as the arithmetic

average of the absolute values of the deviations from the mean height recorded during measurement over a distance *l* over the surface as given by equation (1):

$$R_\alpha = \frac{1}{l}\int_0^l |Z(x)|dx \quad (1)$$

Table 3. 1: UK grit papers used, corresponding expected roughness, Rα,range, and manual polishing time, t_{polish}, required to reach the obtained roughness.

UK Grit	expected R_α (μm)	t_{polish}* (s)	obtained R_α (μm)
40	6 - 8	90	7
80	4-6	60	5.1
120	2.5 - 3.5	120	3.9
180	1.5 - 2.5	120	2.6
240	1 - 2	120	1.3
320	0.5 - 1	180	0.75
500	0.3 - 0.5	360	0.3
1000	0.1 - 0.2	360	0.15

* polishing time needed to establish the targeted R_α roughness

Surface heterogeneities can often seriously affect the overall sample roughness[46]. In the present work, the surface roughness is measured along two lines parallel to the coupon sides and additionally along a line diagonally to the surface, as illustrated in Figure B.6, using a SJ210 Mutitoyo Surface Roughness Tester. It has been carefully monitored that the roughness is uniform over the complete coupon surface; only coupons with a relative error lower than 15 % on the indicated surface roughness were used in the tests.

3.3.4 Coking rate determination

A mechanistic approach of coke formation in industrial reactors is given in the supporting information. The coke deposition on each coupon is measured over time. This allows the determination of the absolute amount of coke deposited during every cracking cycle, as well as the calculation of the initial and the asymptotic coking rate. Similar to previous work [13, 15, 23] the coking rate is determined using the geometric surface area (S) of the coupon as:

$$r_c = \frac{m_{t_2} - m_{t_1}}{t_2 - t_1} \frac{1}{S} \quad (2)$$

In this work, all coking tests were triplicated and the reported values pertain to the average over the three coking runs. As mentioned above, for the 8th coking cycle the reported data pertain to an average over the two 6 hr replicate runs. The initial coking rate reported is the mean measured value between the initial 15 and 60 min and is used to characterize the catalytic activity of the sample. The initial coking rate is mainly representative of the metal-catalyzed reactions in which carbides are intermediate compounds and Fe and Ni are the main catalysts[47-49]. The asymptotic coking rate is related to the radical coking mechanism and is reported as the mean measured coking rate between the 5th and 6th hour. Obviously, the latter value is reported for the cracking run with a duration of 6 hours only.

Additionally, in some cases the effect of varying the surface roughness can be more clearly illustrated by considering the deceleration of the coking rate as a function of time determined as following:

$$a_C = \frac{r_{t_2} - r_{t_1}}{t_2 - t_1} \quad (3)$$

3.3.5 Scanning Electron Microscope (SEM) and Energy Dispersive X-ray (EDX) Analysis

SEM and EDX are used to obtain information regarding the surface morphology and elemental composition of the samples. Both top surface and cross section analyses of coked samples were performed in this work. The top surface analysis gives a qualitative idea of the coke growth and of the elemental surface composition determined at 10 kV and 20 kV. The surface compositions determined for the blank as received Fe-Ni-Cr alloy and after pre-oxidation are taken from recently published work [23] and are given in Table 3. 2 to allow comparison with the data for the coked samples obtained in this work. The cross sectional elemental mappings give a qualitative idea on the uniformity and thickness of the oxide layer formed on top of the alloy surface.

Given the broad range of coke layer thicknesses and taking into account the heterogeneity of the surface, for each sample several EDX analyses at different locations on the surface were made and the results presented in this work pertain to the mean values of multiple surface analyses at 10 kV and 20 kV. Since the penetration depth can be expected to be different for the different amounts of carbon deposited on a sample, the nominal thickness of the coke layer and the penetration depth of the electron beam for the studied coked samples have been assessed.

Table 3. 2: Surface composition of 1 hour coked samples with a roughness of R_α: R1 (0.15 µm), R2 (0.75 µm), R3 (1.3 µm), R4 (2.6 µm), R5 (3.9 µm), R6 (5.1 µm) and R7 (7.0 µm).; EDX analysis at 50x, 10 kV (top) and 20 kV (bottom); Steam cracking of Ethane: F_{HC} = 29.18 10^{-6} kg s^{-1}, δ = 0.33 kg_{H2O} kg^{-1}_{HC}, $T_{reactor}$ = 1173 K, P = 101.35 kPa, F_{H2O} = 9.72 10^{-6} kg s^{-1}, 8 cracking cycles

	kV	blank	pre-oxidized	R1	R2	R3	R4	R5	R6	R7
Ra roughness [µm]				**0.15**	**0.75**	**1.3**	**2.6**	**3.9**	**5.1**	**7**
Coke Thickness (µm)		**-**	**-**	**1.3**	**1.6**	**1.9**	**2.2**	**3.5**	**4.9**	**6.1**
Cr	10	23.6±1.1	63.6±3.3	76±3.8	80.7±4.0	80.4±4.5	61.3±3.2	48.1±2.1	47.7±2.2	47.6±2.2
	20	27.0±1.4	62.5±3.3	76±3.8	73.1±3.5	67.7±3.5	64.8±3.3	56.2±2.8	58.6±2.9	57.1±2.8
Fe	10	33.4±1.6	5.3±0.4	5.4±0.3	6.0±0.3	7.2±0.4	11.2±0.5	11.8±0.6	11.0±2	9.9±0.5
	20	35.4±1.8	8.0±0.5	6.0±0.4	6.5±0.4	7.6±0.4	8.3±0.5	13.1±0.6	11.5±2	11.1±0.6
Ni	10	40.3±2.1	7.0±0.4	7.5±0.4	3.3±0.2	3.2±0.3	1.5±0.2	9.3±0.4	0.7±2	8.1±0.4
	20	33.5±1.6	9.3±0.5	5.2±0.3	4.7±0.3	8.8±0.5	8.9±0.5	10.9±0.7	9.7±0.6	9.3±0.5
Mn	10	0.5±0.1	21.7±1.7	10.8±0.5	10.1±0.5	10.4±0.5	25.8±2.2	27.3±1.3	39.1±1.9	33.0±1.6
	20	1.3±0.1	17.4±1.5	12.2±0.6	13.5±0.7	14.6±0.6	17.2±1.5	18.3±1.2	18.1±1.1	19.9±1.1
Si	10	1.7±0.1	1.8±0.1	0.3±0.1	0.1±0.05	0.8±0.1	0.3±0.1	3.7±0.2	1.6±0.1	1.3±0.1
	20	1.8±0.1	2.0±0.1	0.8±0.1	2.3±0.1	1.5±0.1	0.8±0.1	1.7±0.1	2.2±0.1	2.6±0.1

Using the absolute amount of carbon and the surface analyses taken after 1hr of cracking in the 8th coking cycle (see section 3.3.2.3.), the penetration depth of the electron beam for the different tested surface roughness's is estimated using an empirical formula as proposed by Kanaya-Okayama[50, 51]:

$$H = \frac{0.0276 \cdot A \cdot V^{1.67}}{z^{0.89} \cdot \rho} \quad (4)$$

Where, H is the penetration depth (µm), A is the molar weight of the element (g mol^{-1}), z is the atomic number, ρ is the density of the material (g cm^{-3}), V is the energy of the electron beam

(kV). Based on this formula, the penetration depth differs for each element. An overview of the penetration depths obtained for the different elements found on the surface of the tested coupons is given in Table 3. 3.

Table 3. 3: Electron beam penetration depths for EDX-analysis, based on the Kanaya-Okayama formula[50]; the penetration depth is given for different elements in different matrices.

Element		Atomic weight (g/mol)	Atomic number	Density (g/cm^3)	Accelerating voltage kV		Penetration depth (µm) 10 kV	20 kV
Carbon	**C**	12.01	6	1.75	10	20	1.798	5.723
Oxygen	**O**	16.00	8	1.14	10	20	2.84	9.05
Nickel	**Ni**	58.69	28	8.91	10	20	0.44	1.39
Chromium	**Cr**	52.00	24	7.14	10	20	0.56	1.77
Iron	**Fe**	55.85	26	7.87	10	20	0.50	1.60
Silicon	**Si**	28.09	14	2.33	10	20	1.49	4.73
Manganese	**Mn**	54.94	25	7.47	10	20	0.54	1.72

The nominal thickness of the coke layers deposited on the studied samples is calculated using the following equation:

$$L = \frac{M_c}{\rho \cdot S} \cdot 10^{-6} \quad (5)$$

Where, L is the thickness of the coke layer (µm), M_c is the amount of coke deposited on the sample (g) after the 1 hr triplicate of the 8th coking cycle, ρ is the density of coke (1.75 g cm^{-3})[38, 46, 47], S is the surface of the coupon (196 mm^2).pretreatment.

3.3.6 Thermodynamic Calculations

To identify the thermodynamically stable compounds on the surface of the coked samples, thermodynamic calculations are performed using the elemental composition obtained by means of EDX. Similar to previous work [13, 15, 23] thermodynamic calculations are performed using Ekvicalc[52]. A summary of the gas phase composition used as input for the Ekvicalc calculations is presented in Table 3. 4. The input molar elemental composition of the coked samples given in Table 3. 4 was obtained from the EDX analysis at 10 kV and 20 kV. For the pre-oxidized surfaces, the identification of the thermodynamic stable phases using Ekvicalc is assumed not to be influenced by the surface roughness. Hence, for the pre-oxidized surfaces, possible effects of surface roughness on metal losses due to polishing of the coupons and on the coupon's surface temperature due to changes in radiative heat transfer during high temperature pre-oxidation and steam treatment are neglected. Hence, for the pre-oxidized surfaces, the surface composition is taken from recently published work[23] and is given in

Table 3. 5 to allow comparison with the data on the coked samples obtained in this work.

Table 3. 4: Input Values Used for Ekvicalc Calculations for Preoxidation and Ethane Cracking conditions

Conditions		Cracking						
Temperature [K]				1173				
Pressure [10^5 Pa]				1.03				
Gas phase composition				29.61				mol H_2
				6.16				mol CH_4
				14.09				mol C_2H_6
				24.94				mol C_2H_4
				0.25				mol C_3H_6
				0.44				mol benzene
				24.51				mol H_2O
Experiment	Acc. Volt.	R1	R2	R3	R4	R5	R6	R7
Element		Material Molar Composition (mole fraction)						
Ni	10 kV	0.07	0.03	0.03	0.01	0.08	0.01	0.07
	20 kV	0.05	0.04	0.08	0.08	0.10	0.09	0.08
Cr	10 kV	0.77	0.82	0.80	0.63	0.48	0.49	0.49
	20 kV	0.77	0.73	0.68	0.66	0.57	0.59	0.57
Fe	10 kV	0.05	0.06	0.07	0.11	0.11	0.10	0.10
	20 kV	0.06	0.06	0.07	0.08	0.12	0.11	0.10
Mn	10 kV	0.10	0.10	0.10	0.25	0.26	0.38	0.32
	20 kV	0.12	0.13	0.14	0.17	0.18	0.17	0.19
Si	10 kV	0.01	0.00	0.01	0.01	0.07	0.03	0.03
	20 kV	0.01	0.04	0.03	0.02	0.03	0.04	0.05

Table 3. 5: Normalized Ekvicalc-Calculated surface composition under Ethane Cracking conditions using the 10 and 20 kV conditions.

Component		**R1**	**R2**	**R3**	**R4**	**R5**	**R6**	**R7**
Cr2O3	10kV	0.553	0.631	0.594	0.145	-	-	-
	20kV	0.525	0.465	0.385	0.314	0.196	0.234	0.184
MnCr2O4	10kV	0.204	0.194	0.193	0.570	0.499	0.531	0.526
	20kV	0.238	0.257	0.269	0.333	0.336	0.318	0.369
Ni	10kV	0.132	0.060	0.055	0.030	0.170	0.014	0.159
	20kV	0.099	0.079	0.154	0.157	0.187	0.168	0.155
Fe	10kV	0.100	0.113	0.131	0.243	0.227	0.227	0.204
	20kV	0.119	0.119	0.135	0.157	0.224	0.206	0.194
SiO2	10kV	0.011	0.002	0.027	0.012	0.104	-	-
	20kV	0.020	0.079	0.058	0.039	0.056	0.075	0.097
MnO(s)	10kV	-	-	-	-	-	0.164	0.058
	20kV	-	-	-	-	-	-	-
Mn_2SiO_4	10kV	-	-	-	-	-	0.064	0.053
	20kV	-	-	-	-	-	-	-

3.4 Results and discussion

The data for the gas phase composition of the effluent during ethane steam cracking reported in Table B.2 pertain to average values taken over all the cracking cycles effluent analyses after 1 hr of cracking. No effect of the initial surface roughness on the gas phase composition was observed. Also, no significant differences in gas phase composition were observed for all the cracking experiments performed for a given surface roughness. From these results it is obvious that the effluent composition is not influenced by the surface roughness nor by aging. The mentioned averaged values pertain to analyses taken after 1 hour of cracking, so no conclusions can be extracted for the generated CO during the initial coking process. In the experiments, the CO yield is rather stable after 1 hour of cracking which is in line with the work of Wang et al. [21, 36]

The effect of the initial surface roughness and aging on coke formation during ethane steam cracking was evaluated using coupons with a surface roughness R_α of 0.15 µm, 0.75 µm, 1.3 µm, 2.6 µm, 3.9 µm, 5.1 µm and 7.0 µm, respectively. In this work, the surface roughness was measured immediately after polishing, i.e. before pre-oxidation pretreatment, and again after the pre-oxidation pretreatment. As shown in Figure 3. 3, pre-oxidation does not significantly influences the initial surface roughness. A newly spun-cast coil in industry has an inner surface roughness lower than 3.2 µm [53] and, hence, the investigated surface roughness range covers the inner surface of freshly manufactured steam cracking coils. Table B.2 also reports the results on coke formation during ethane steam cracking in the JSR reactor.

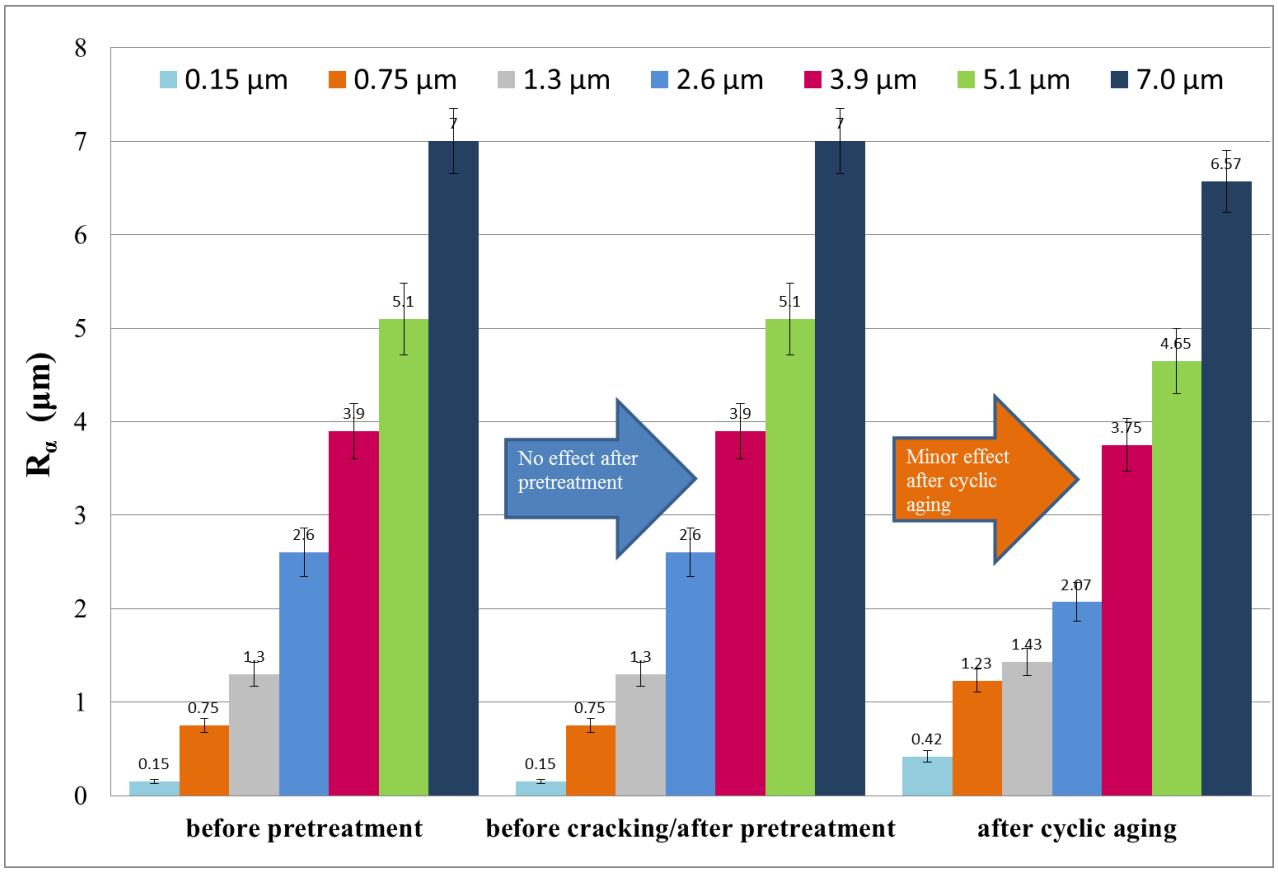

Figure 3. 3: Comparison of Rα as measured for the blank samples, the pre-oxidized samples and after decoking of the cyclically aged samples.

3.4.1 Effect of the initial surface roughness on coke formation

The results in Table B.2 indicate that when changing the initial surface roughness of 0.15 to 2.6 μm, the amount of coke deposited in the first cracking cycle remains rather stable while for the initial surface roughnesses of 3.9 to 7.0 μm, the amount of coke is 20 to 30% higher. Qualitatively, these observations are in line with earlier work by Marek and Albright [38, 39] and Crynes and Albright. [14] Although the pretreatment and operating conditions in these studies were strongly different from those in the current study, these authors also observed that polishing reduced coke deposition on Incoloy 800 [38, 39] and aluminized Incoloy 800 [14] coupons in the pyrolysis of light hydrocarbons. As stated previously, these authors did not measure the difference of roughness induced by polishing.

In the first coking cycle, the initial coking rate steadily increases with increasing initial surface roughness while there is a negligible influence on the asymptotic coking rate in the investigated roughness range, as indicated in

Figure 3. 4. For example, the initial coking rate for the sample with the highest initial roughness is 3 times larger than that measured for the lowest initial roughness.

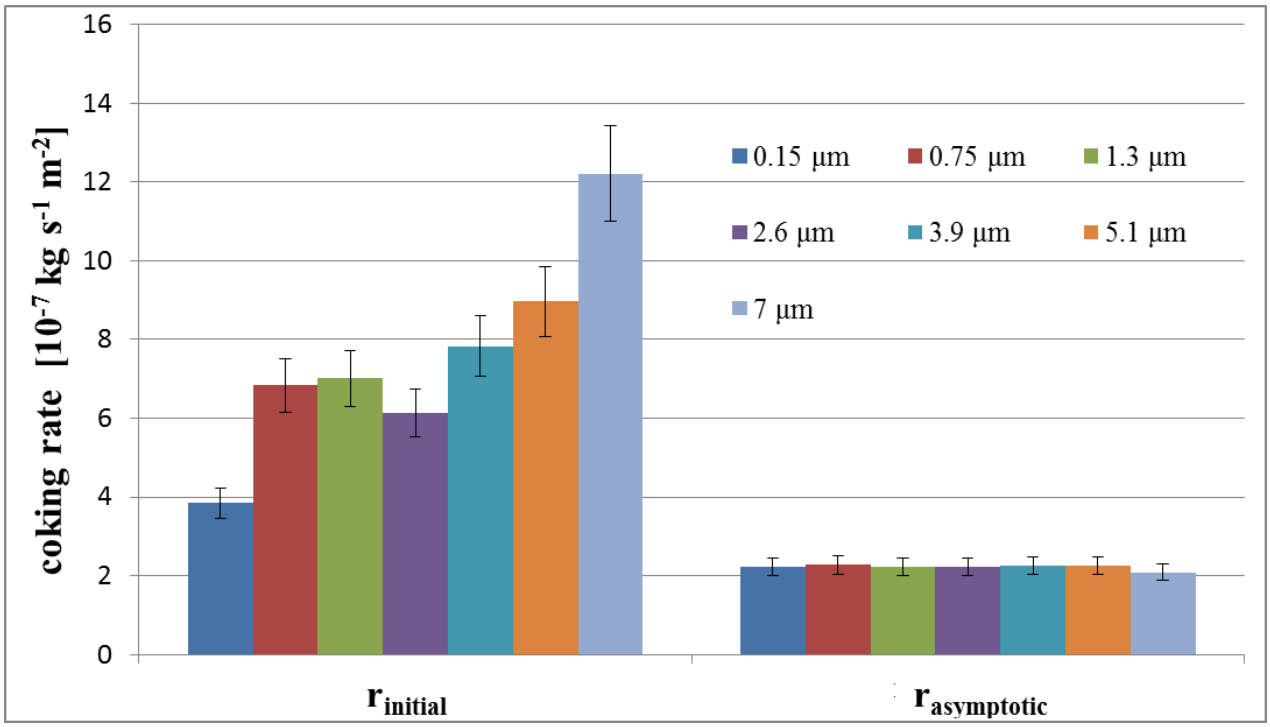

Figure 3. 4: Effect of the initial surface roughness on the initial and the asymptotic coking rate in the first cracking cycle.

Clearly, the initial surface roughness strongly affects the time required to reach the asymptotic stage. In Figure 3. 5 a), the evolution of the coking rate over different time intervals of the six hours cracking cycle is illustrated. It can be seen that for an initial surface roughness up to 3.9 µm, the asymptotic coking rate in the first coking cycle is reached after some 2-3 hrs of cracking, while this increases to some 4-5 hrs for an initial surface roughness above 5 µm. The steady increase of this effect with increasing surface roughness can be more clearly illustrated by considering the deceleration of the coking rate as a function of time, as depicted in Figure 3. 5 b). Although the coking rate decreases much faster with time with increasing surface roughness, the contribution of the catalytic coking to the coke deposition lasts longer.

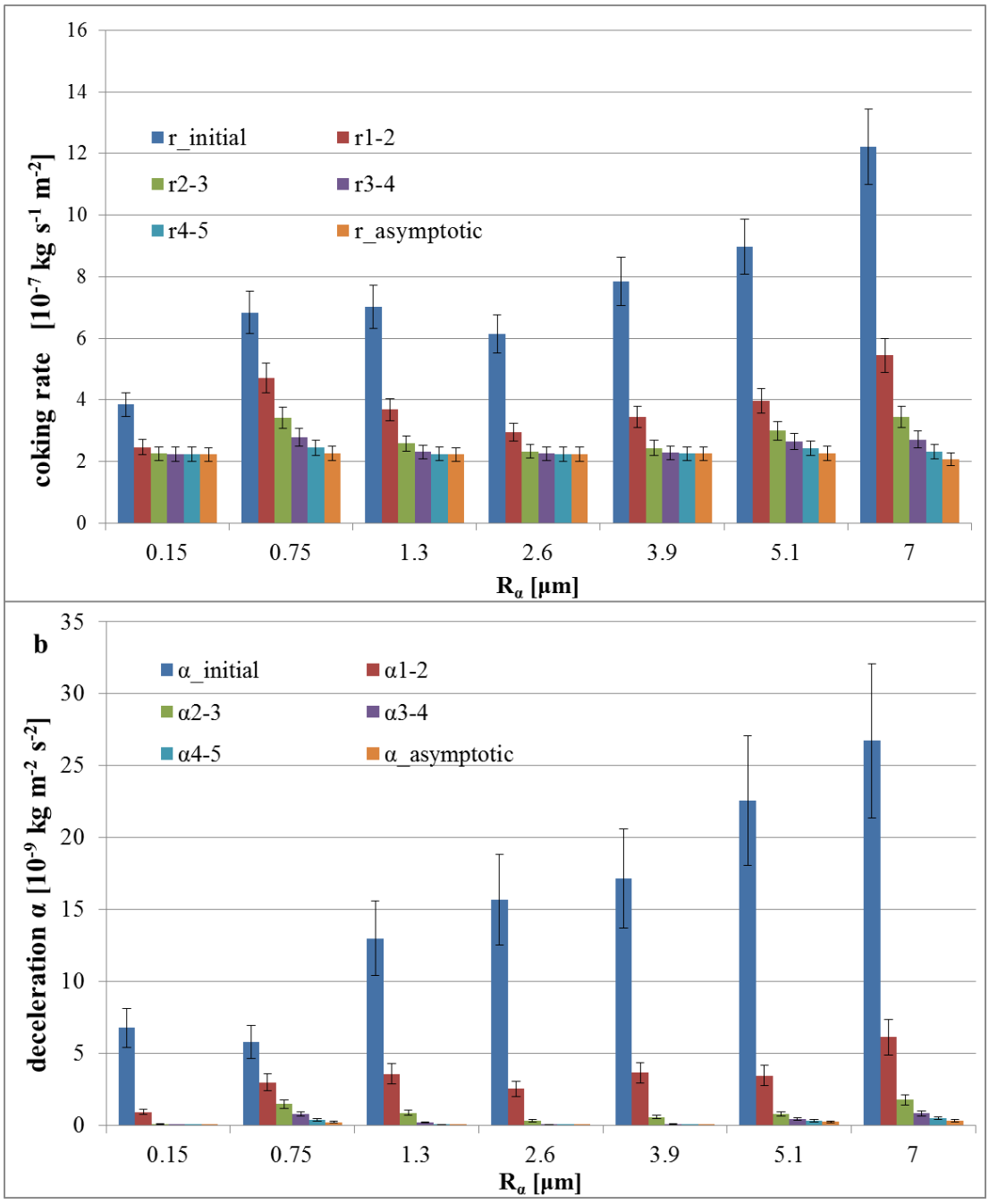

Figure 3. 5: a) Evolution of the coking rate with time in the first coking cycle as function of the initial surface roughness (rx-y: average coking rate measured in the indicated time interval in hours; e.g. r1-2: coking rate measured between the first and the second hour of cracking); b) corresponding deceleration α of the coking rate in the indicated time interval.

3.4.2 Effect of cyclic aging on coke formation

It should be highlighted that after the first cracking cycle, two uncharted phenomena play an important role in the samples' coking behavior. Since aging can affect the surface roughness, discrimination between the effect of aging and the effect of surface roughness is not straightforward.

It has been reported that due to multiple coking/decoking cycles, tube surface becomes rougher with time on stream[53]. As can be seen in Figure 3. 3, an increase by at most a factor of 3 was observed for surface roughnesses below 1.3 μm after cyclic aging while for surface roughnesses from 2.6 μm onwards, there is a slight tendency towards a decrease in roughness with aging. Hence, is can be assumed that the effect of aging on the surface roughness remains limited. From the data in Figure 3. 3, it can be concluded that differences in coking behavior observed in successive coking/decoking cycles cannot be solely attributed to an increase in surface roughness with aging.

The total amount of coke deposited in the four 6 hr coking cycles (CC1, 2, 3 and 8) remains more or less stable for the samples with an initial surface roughness up to 1.3 μm while from an initial surface roughness from 2.6 μm onwards there is a steady increase in the amount of coke deposited with aging as shown in Figure 3. 6. The effect of aging on the amount of coke deposited becomes more pronounced with increased initial surface roughness. For instance, for an initial surface roughness of 3.9 μm, the amount of coke deposited increases with some 40% from the first to the eight coking cycle while for an initial surface roughness of 7.0 μm, the amount of coke deposited doubles.

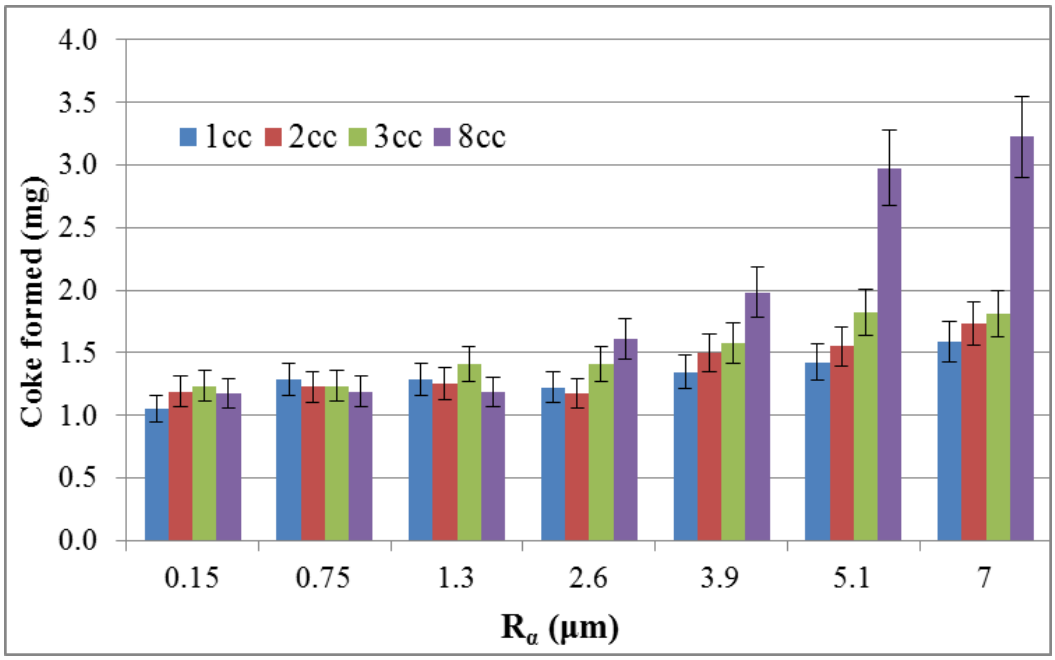

Figure 3. 6: Absolute amount of coke deposited on the samples after the 1st, 2nd, 3rd and 8th cracking cycle as function of the initial surface roughness R_α.

For all initial surface roughnesses studied, the initial coking rate steadily increases in each successive coking run (see Figure 3. 7 a), with the trend to be more clear at higher roughness values. In contrast, the asymptotic coking remains rather stable (see Figure 3. 7 b). Hence, it can be concluded that the asymptotic coking rate is not influenced by the initial surface roughness nor by aging.

From Figure 3. 8, it is clear that the time required to reach the asymptotic rate steadily increases with each successive coking cycle. The effect seems to be more pronounced with increasing initial surface roughness. For instance, for an initial surface roughness up to 2.6 µm, the asymptotic coking rate in the 8th coking cycle is reached after some 3-4 hrs of cracking, while this increases to some 5-6 hrs for an initial surface roughness above 3.9 µm. Also here, for the

samples with the higher initial surface roughness, the coking rate decreases much faster with time in the 8th coking cycle as compared to the 1st cycle.

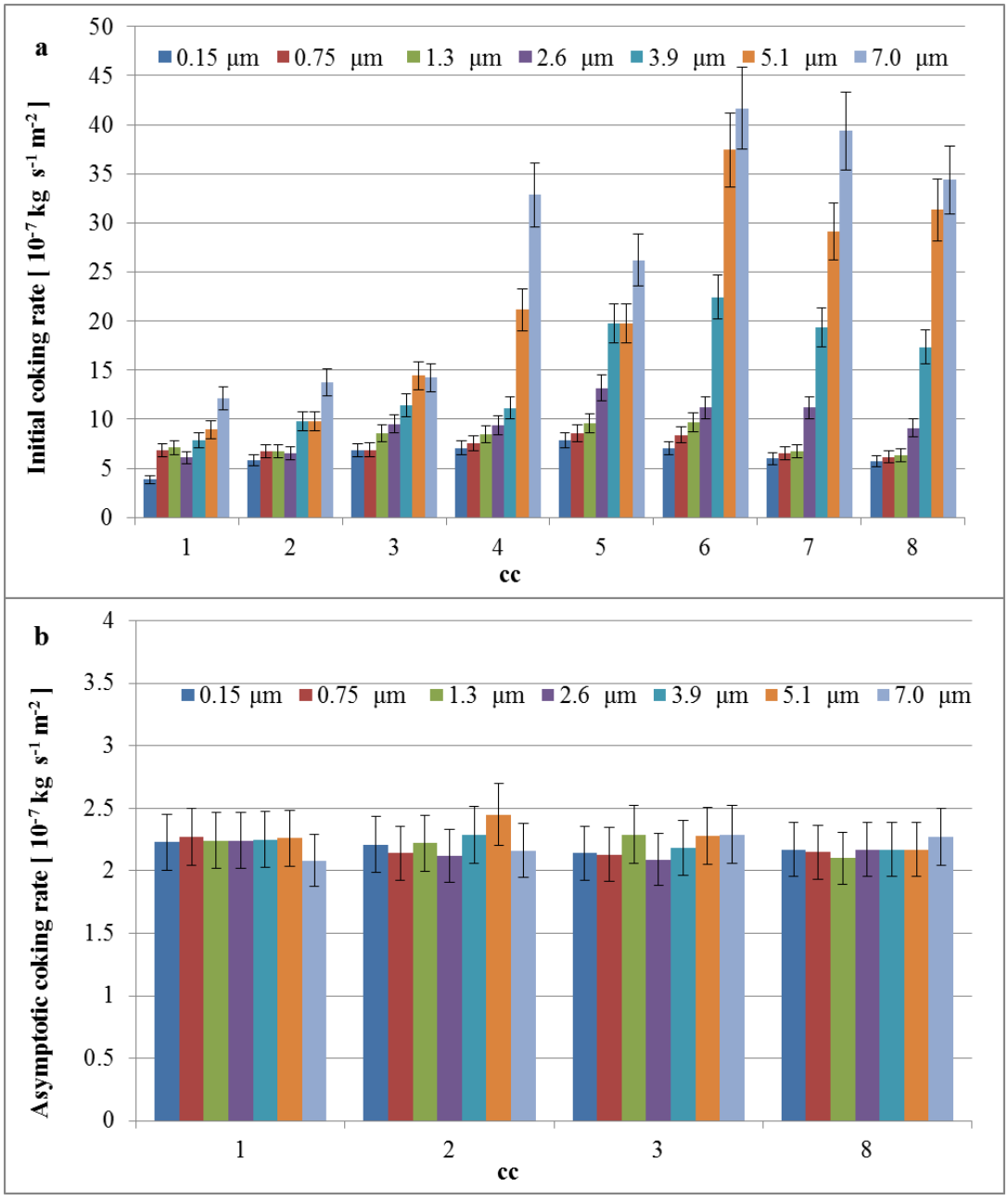

Figure 3. 7: Effect of the initial surface roughness on the initial (a) and the asymptotic (b) coking rate (b) in the 1st, 2nd, 3rd and 8th six hour cracking cycle.

As illustrated in Figure 3. 9, the fraction of the total amount of coke deposited in the first hour of the 6 hr coking cycles increases with initial surface roughness and, in particular for the higher surface roughnesses studied, steadily increases with aging. For instance, for an initial surface roughness of 7 μm, some 60% of the coke is deposited during the first hour of cracking in the first 6 hr coking cycle while this increases to more than 80% in the 8th coking cycle.

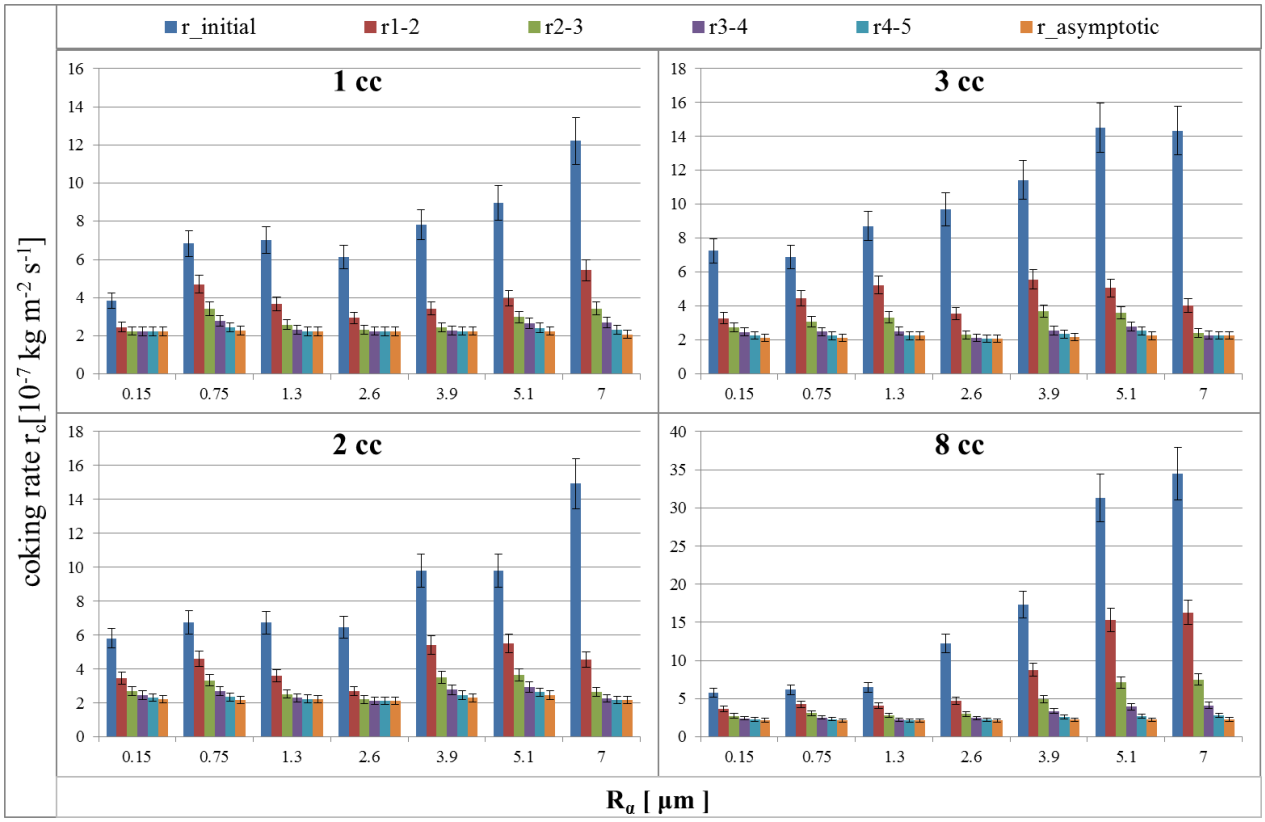

Figure 3. 8: Evolution of the coking rate with time in 1st, 2nd, 3rd and 8th six hour cracking cycle as function of the initial surface roughness (rx-y: average coking rate measured in the indicated time interval in hours; e.g. r1-2: coking rate measured between the first and the second hour of cracking).

Clearly, the initial surface roughness is a factor that influences coke formation especially in the initial stage of coke deposition. In this initial stage, coke deposition is related to the catalytic

activity of the reactor wall which is governed by the alloy's surface characteristics. It can be assumed that the initial coking rate on a fresh alloy is determined on the one hand by the number of catalytically active surface sites and on the other hand by the chemical nature, i.e. the catalytic activity, of these active sites.

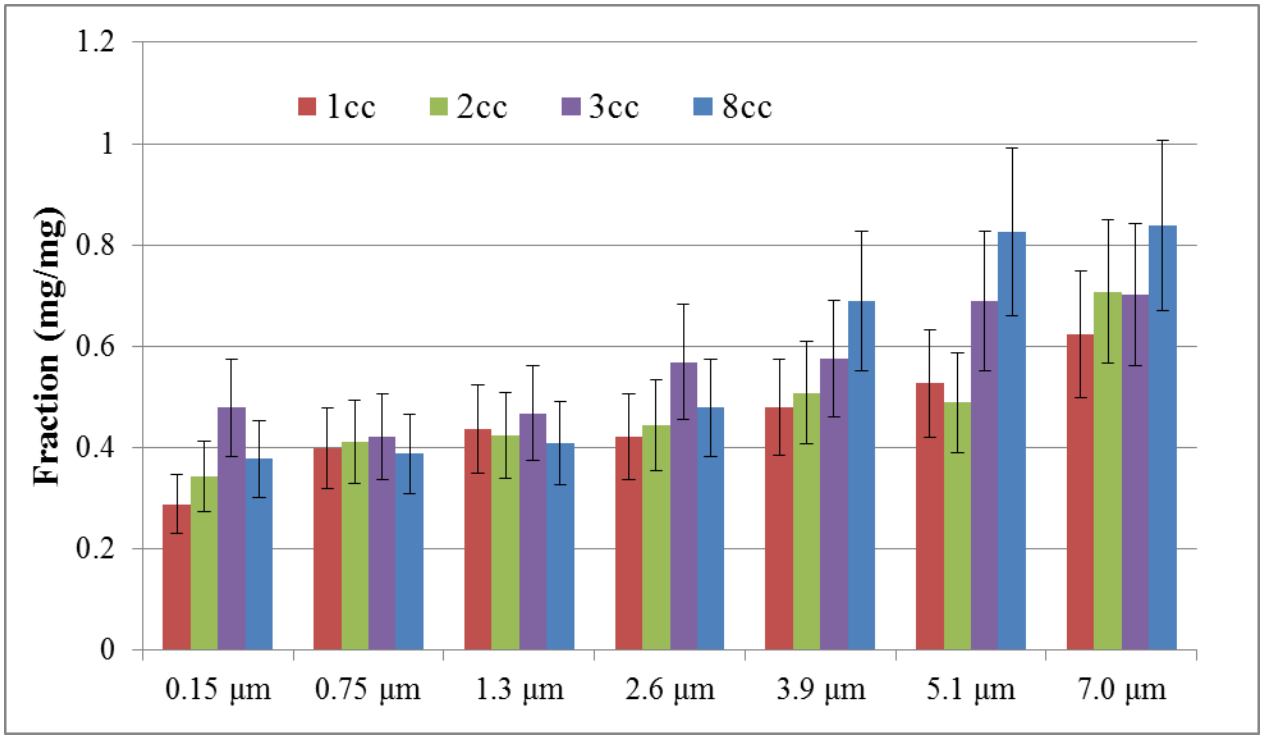

Figure 3. 9: Fraction of the total amount of coke deposited after 1 hour of cracking in the 8th cracking cycle as function of the initial R_α roughness.

The number of active surface sites can be expected to increase with surface roughness due to an increase in surface area. Since in this study the alloy and the pre-treatment of the coupons are kept the same, a more or less linear relationship between the initial coking rate and the initial surface roughness can be expected due to the increase in surface area with increasing initial surface roughness. This trend is indeed observed for the first cycle (see Figure 3. 7 a). However, in the following coking cycles this trend is also influenced by the effect of cyclic aging which is

more pronounced for higher initial surface roughness. In contrast, in the asymptotic stage, the coking rate is not affected by the initial surface roughness nor by aging. This clearly indicates that both the effect of initial surface roughness and aging gradually fade away as the surface gets covered with coke and the asymptotic coking stage is reached where coke formation is mainly driven by the gas phase composition and the cracking conditions, as illustrated graphically in Figure B.7.

As stated above, the initial surface roughness is only marginally affected by the cyclic aging procedure used in this work and, hence, the observed differences in the initial stage of coking for successive coking/decoking cycles cannot be attributed to an increase in surface roughness with aging. In other words, our results indicate that an increase in the number of catalytically active surface sites due to an increase in surface area associated with a higher surface roughness cannot be invoked to explain the effect of aging on the initial coking behavior. Therefore, it can be assumed that the cyclic aging procedure used in this study mainly influences the catalytic activity and, hence, the chemical composition of the metal surface that is in contact with the gas phase.

3.4.3 SEM and EDX analysis

To gain a better understanding on the combined effect of initial surface roughness and aging on the coking tendency of the samples, SEM and EDX analysis has been performed on the coked samples after 1hr of cracking in the 8th coking cycle (See section 3.3.2.3). SEM images are shown for the tested roughness range in Figure 3. 10. There are no signifanct differences in morphology of the coke formed after one hour of cracking in the 8th coking cycle in the different cases. Structures of 0.5 μm to 2 μm are noted for all of them.

Although the initial surface roughness seems to have no effect on the morphology of the coke, distinct differences are observed in the surface metal composition for the different coked samples, as can be seen in Table 3. 2. However, it should be noted that the thickness of the coke layer on the studied samples is different for the different surface roughnesses studied. Therefore, the nominal thickness of the coke layer (see section 3.3.5) on the studied samples was calculated and taken up in Table 3. 2. Clearly, based on the penetration depth calculated for carbon, the EDX data at 10 KV for the coked samples obtained for an initial surface roughness up to 1.3 μm can be expected to be more or less representative of the coupon's surface, while for an higher initial surface roughness it is more appropriate to consider the EDX data at 20 KV. As compared to the pre-oxidized sample prior to the first coking cycle, the EDX data at 10 kV indicate that up to an initial surface roughness of 1.3 μm, there is an important increase in the Cr content and a slight increase in the Fe content followed by an important decrease in the Mn content and a slight decrease in Ni content. At 20 kV, the EDX data indicate that from an initial surface roughness of 2.6 μm onwards, the Cr content steadily decreases, the Fe content slightly increases while the Mn content increases and the Ni content remains fairly stable.

Elemental mappings of the coked samples are presented in Figure B.8, Figure B.9 and Figure

B.10. As expected[23], a fairly homogeneous oxide layer of 2 to 3 µm thickness is observed. In all cases, the oxide layer mainly consists of Cr- and Mn-oxides.

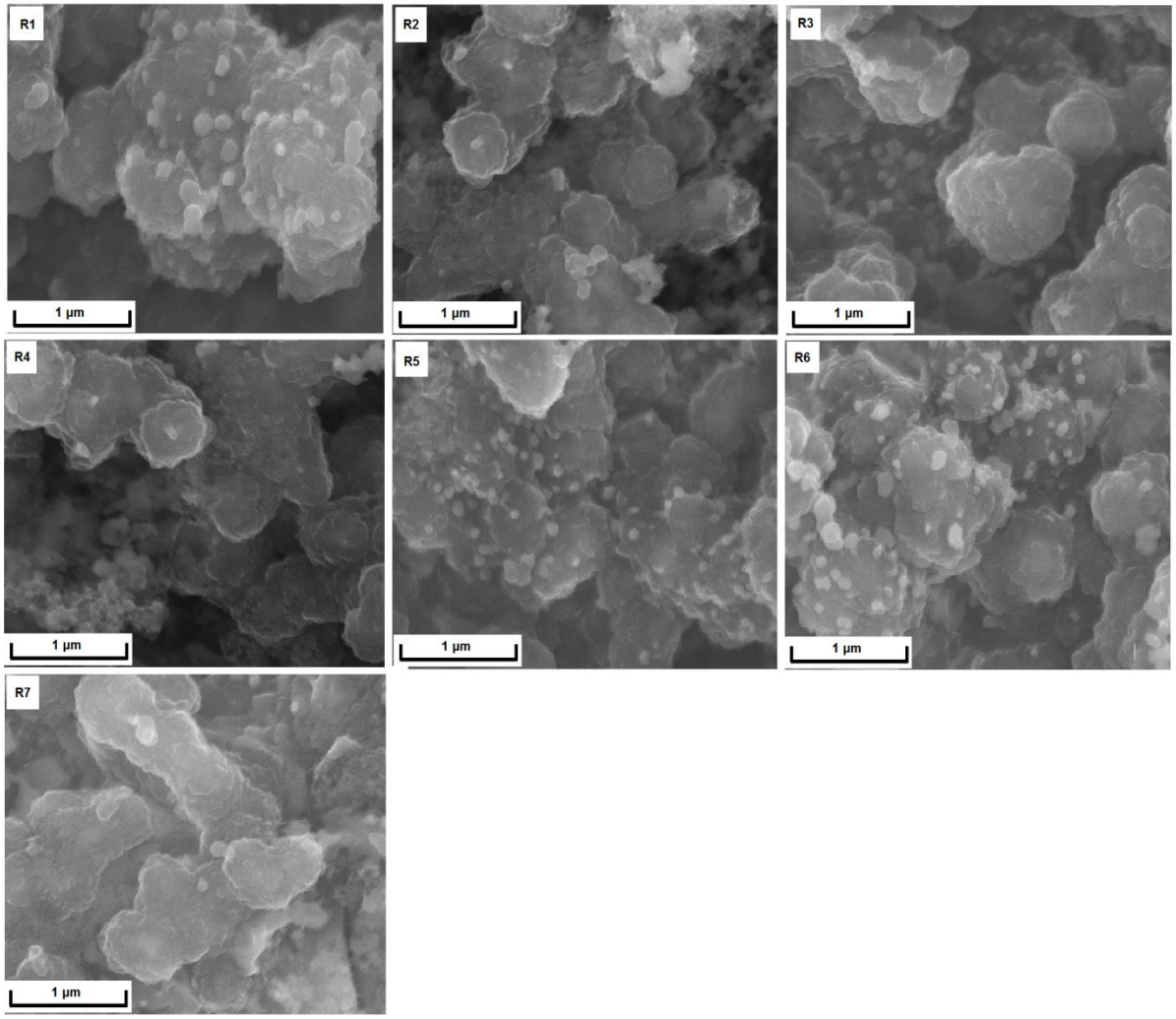

Figure 3. 10: SEM images of the coked samples obtained after 1 hour of cracking during the 8th cracking cycle for an initial surface roughness of R1 (0.15 µm), R2 (0.75 µm), R3 (1.3 µm), R4 (2.6 µm), R5 (3.9 µm), R6 (5.1 µm) and R7 (7.0 µm). 25000x, 10 kV; Steam cracking of Ethane: F_{HC} = 29.18 10^{-6} kg s^{-1}, δ = 0.33 kg_{H2O} $kg^{-1}{}_{HC}$, $T_{reactor}$ = 1173 K, P = 101.35 kPa, F_{H2O} = 9.72 10^{-6} kg s^{-1}, 8 cracking cycles

A general agreement on the exact chemical nature of the active sites involved in catalytic coke

formation is still lacking. For instance, the term "active site" has been used referring to the atomic metal, a metal carbide and/or a metal oxide. However, there are ample indications that the presence of metallic Fe and Ni at the surface promotes catalytic coke formation while the presence of a thin layer of manganese chromite, $MnCr_2O_4$, at the surface provides resistance to coking. [13, 15] Therefore, to identify thermodynamic stable phases present at the surface, EkviCalc calculations are performed, using as input the surface composition from the EDX analysis at 10 kV and 20 kV under cracking conditions.

The results presented in Table 3. 5 suggest that with increasing surface roughness, the amount of Cr_2O_3 gradually decreases with a concomitant increase of manganese chromite, $MnCr_2O_4$. The amounts of metallic Ni and Fe show a tendency to slightly increase with increasing surface roughness. As both metallic Fe and Ni are well-known catalysts for coke formation, their increased presence at the surface could offer an explanation for the observed effects on the coking in the catalytic stage[13].

To clarify to what extent the observed changes in surface metal composition with increasing initial surface roughness can be related to differences in surface temperature of the coupons due to changes in radiative heat transfer and/or to metal particle losses[14] due to increased spalling off of oxides during pre-oxidation, entrainment of coke during cracking/decoking and/or metal dusting during decoking further study is required.

3.5 Conclusions

The effect of surface roughness on the coking tendency of a classical 35/25 Ni/Cr wt % alloy was assessed in a quartz jet stirred reactor equipped with an electro-balance, under industrially relevant ethane steam cracking conditions. Changing the surface roughness, in the tested range of R_α 0.15 – 7.0 μm, has a significant influence on the initial coking tendency during steam cracking of ethane, with up to a factor 6 higher initial coking rates been observed for the worst case scenario. The effect on asymptotic coke formation and carbon oxides formation was found negligible. Conversion and selectivities are stable for the studied roughness range, suggesting that once the surface is covered by coke, there is no significant difference in the composition of the coke formed and in the available surface and, therefore, in the coking and gasification rate.

For values below the typically industrially applied 2.6 μm an increase of a factor 3 was observed in terms of roughness after several coking decoking cycles, possibly indicating that the oxide formation after decoking is rougher than an evenly polished surface.

The coking results indicate that by increasing initial surface roughness from 0.15 to 2.6 μm, the total amount of coke deposited in the first cracking cycle remains rather stable while from 3.9 to 7.0 μm, the amount of coke is some 20-30% higher. Phenomena such as metal dusting and/or spallation during coking and decoking affect the coking behavior and surface composition of the material but not its surface roughness after cyclic aging.

The increase of the roughness, leading to elevated initial coking rates, is coupled with the number of active catalytic sites and surface area in a fresh manufactured material. After SEM and EDX analysis, it is clear that up to an initial surface roughness of 1.3 μm, there is an increase in the Cr and Fe content followed by a decrease in the Mn and Ni content. The thermodynamic calculations

suggest that the amount of Cr_2O_3 gradually decreases with a concomitant increase of manganese chromite, $MnCr_2O_4$. The amounts of metallic Ni and Fe show a tendency to slightly increase with increasing surface roughness, explaining the pronounced coke formation. Nevertheless, asymptotic coke formation for a given gas phase composition and process conditions, primarily depends on the elemental composition of the material and the surface oxides homogeneity, which is dependent on the surface pretreatment but certainly not on the initial surface roughness. Therefore, industrially, the presence of Cr_2O_3 and $MnCr_2O_4$ at the surface will lead to a better long-term coking behavior for Fe-Ni-Cr alloys independently of the initial surface roughness. To elucidate to what extent the observed in this work changes in surface metal composition with increasing initial surface roughness can be related to differences in surface temperature of the coupons due to changes in radiative heat transfer and/or to metal particle losses[14] due to increased spalling off of oxides during pre-oxidation, entrainment of coke during cracking/decoking and/or metal dusting during decoking, requires further investigation.

3.6 References

1. ExxonMobil, *The Outlook for Energy: A view to 2040*. 2012.
2. Plehiers, P. M.; Reyniers, G. C.; Froment, G. F., Simulation of the run length of an ethane cracking furnace. *Ind. Eng. Chem. Res.* **1990,** 29, (4), 636-641.
3. Sullivan, B. K., Ethylene Cracking Heater Decoking Tutorial. In *AIChE Spring Natl. Meet., Conf. Proc.*, New Orleans, LA, 2014.
4. J, D. W., Decoking and cleaning tubular heaters. In Google Patents: 1954.
5. Lenglet, E., Method of decoking an installation for steam cracking hydrocarbons, and a corresponding steam-cracking installation. In Google Patents: 1993.
6. Kivlen, J. A.; Koszman, I., Decoking of onstream thermal cracking tubes with h20 and h2. In Google Patents: 1971.
7. Chen, J.; Maddock, M., *Hydrocarbon Process.* 1973; Vol. 52, p 147-151.

8. Schietekat, C. M.; Van Cauwenberge, D. J.; Van Geem, K. M.; Marin, G. B., Computational fluid dynamics-based design of finned steam cracking reactors. *AIChE J.* **2014,** 60, (2), 794-808.
9. Schietekat, C. M.; van Goethem, M. W. M.; Van Geem, K. M.; Marin, G. B., Swirl flow tube reactor technology: An experimental and computational fluid dynamics study. *Chem. Eng. J.* **2014,** 238, (0), 56-65.
10. Petrone, S. S. A.; Mandyam, R. C.; Wysiekierski, A. G., Surface alloyed high temperature alloys. In Google Patents: 2000.
11. Verdier, G.; Carpentier, F., Consider new materials for ethylene furnace applications: An innovative metallurgy solves maintenance issues. *Hydrocarbon processing* **2011,** 90, (5), 61-62.
12. Industries, M. Manaurite XM - Heat resistant alloys for hydrocarbon processing. http://www.manoir-industries.com/site/docs_wsw/fichiers_communs/docs/MI_Manaurite_XM.pdf
13. Muñoz Gandarillas, A. E.; Van Geem, K. M.; Reyniers, M.-F.; Marin, G. B., Influence of the Reactor Material Composition on Coke Formation during Ethane Steam Cracking. *Ind. Eng. Chem. Res.* **2014,** 53, (15), 6358-6371.
14. Crynes, L. L.; Crynes, B. L., Coke formation on polished and unpolished Incoloy 800 coupons during pyrolysis of light hydrocarbons. *Ind. Eng. Chem. Res.* **1987,** 26, (10), 2139-2144.
15. Muñoz Gandarillas, A. E.; Van Geem, K. M.; Reyniers, M.-F.; Marin, G. B., Coking Resistance of Specialized Coil Materials during Steam Cracking of Sulfur-Free Naphtha. *Ind. Eng. Chem. Res.* **2014,** 53, (35), 13644-13655.
16. Jakobi, D.; Karduck, P.; von Richthofen, A. F., The High-Temperature Corrosion Resistance of Spun-Cast Materials for Steam-Cracker Furnaces-A Comparative Study of Alumina-and Chromia-Forming Alloys. *CORROSION* **2013**.
17. Schietekat, C. M.; Sarris, S. A.; Reyniers, P. A.; Kool, L. B.; Peng, W.; Lucas, P.; Van Geem, K. M.; Marin, G. B., Catalytic Coating for Reduced Coke Formation in Steam Cracking Reactors. *Ind. Eng. Chem. Res.* **2015,** 54, (39), 9525-9535.
18. Chauhan, A. P. S., *Coke resistant coating technology for applications in ethylene pyrolysis heaters*. ProQuest: 2007.

19. Salari, D.; Niaei, A.; Shoja, M. R.; Nabavi, R., Coke Formation Reduction in the Steam Cracking of Naphtha on Industrial Alloy Steels Using Sulfur-Based Inhibitors. *Int. J. Chem. React. Eng.* **2010,** 8, (1).
20. Reyniers, M.-F. S. G.; Froment, G. F., Influence of Metal Surface and Sulfur Addition on Coke Deposition in the Thermal Cracking of Hydrocarbons. *Ind. Eng. Chem. Res.* **1995,** 34, (3), 773-785.
21. Wang, J.; Reyniers, M.-F.; Marin, G. B., Influence of Dimethyl Disulfide on Coke Formation during Steam Cracking of Hydrocarbons. *Ind. Eng. Chem. Res.* **2007,** 46, (12), 4134-4148.
22. Dhuyvetter, I.; Reyniers, M.-F.; Froment, G. F.; Marin, G. B.; Viennet, D., The Influence of Dimethyl Disulfide on Naphtha Steam Cracking. *Ind. Eng. Chem. Res.* **2001,** 40, (20), 4353-4362.
23. Sarris, S. A.; Olahova, N.; Verbeken, K.; Reyniers, M.-F.; Marin, G. B.; Van Geem, K. M., Optimization of the in-situ pretreatment of high temperature Ni-Cr Alloys for Ethane steam cracking. *Ind. Eng. Chem. Res.* **2017**.
24. Jakobi, D.; van Moesdijk, C.; Karduck, P.; von Richthofen, A., Tailor-made materials for high temperature applications: New strategies for radiant coil material development. *CORROSION* **2009**.
25. Zychlinski, W.; Wynns, K.; Ganser, B., Characterization of material samples for coking behavior of HP40 material both coated and uncoated using naphtha and ethane feedstock. *Mater. Corros.* **2002,** 53, (1), 30-36.
26. Ganser, B.; Wynns, K. A.; Kurlekar, Operational experience with diffusion coatings on steam cracker tubes. *Mater. Corros.* **1999,** 50, (12), 700-705.
27. Benum, L., In Achieving longer furnace runs at NOVA Chemicals. In *AIChE Spring Natl. Meet., Conf. Proc.*, New Orleans, LA, 2002.
28. Petrone, S.; L.Deuis, R.; Kong, F.; Unwin , P. In *Catalyzed-assisted manufacture of olefins (CAMOL): Year-(4) update on commercial furnace installations*, Proc. - Ethylene Prod. Conf., March 21-25, 2010; 2010.
29. Marek, J. C.; Albright, L. F., Formation and Removal of coke deposited on Stainless steeil and vycor surfaces from acetylene and ethylene. *ACS Symp. Ser.* **1982**.

30. Marek, J. C.; Albright, L. F., Surface phenomena during pyrolysis - The effects of treatments with various inorganic gases. *ACS Symp. Ser.* **1983**.
31. Kaminsky, M. P.; Hanson, J. A., *Characterization of Metal Sites Responsible for Catalytic Coking in Olefin Steam-cracking Furnaces*. Am. Inst. Chem. Eng., [Spring Natl. Meet.]: 1997.
32. Cooper, B. J.; Trimm, D. L., Carbon deposition from propylene on polycrystalline and single crystal iron. *J. Catal.* **1980,** 62, (1), 35-43.
33. Albright, L. F.; Marek, J. C., Mechanistic model for formation of coke in pyrolysis units producing ethylene. *Ind. Eng. Chem. Res.* **1988,** 27, (5), 755-759.
34. Graff, M. J.; Albright, L. F., Coke deposition from acetylene, butadiene and benzene decompositions at 500–900°C on solid surfaces. *Carbon* **1982,** 20, (4), 319-330.
35. Cai, H.; Krzywicki, A.; Oballa, M. C., Coke formation in steam crackers for ethylene production. *Chemical Engineering and Processing: Process Intensification* **2002,** 41, (3), 199-214.
36. Wang, J.; Reyniers, M.-F.; Van Geem, K. M.; Marin, G. B., Influence of Silicon and Silicon/Sulfur-Containing Additives on Coke Formation during Steam Cracking of Hydrocarbons. *Ind. Eng. Chem. Res.* **2008,** 47, (5), 1468-1482.
37. Towfighi, J.; Sadrameli, M.; Niaei, A., Coke formation mechanisms and coke inhibiting methods in pyrolysis furnaces. *J. Chem. Eng. Jpn.* **2002,** 35, (10), 923-937.
38. Marek, J. C.; Albright, L. F., Surface phenomena during pyrolysis - The effects of treatments with various inorganic gases. *ACS Symposium Series* **1983,** 202.
39. Marek, J. C.; Albright, L. F., Formation and Removal of Coke Deposited on Stainless Steel and Vycor Surfaces from Acetylene and Ethylene. *ACS Symposium Series* **1982,** 202.
40. Jasinski, W.; Zawada, P., The precipitation processes in the Manaurite XM superalloy during 1000 hours of ageing. *Int. J. Microstruct. Mater. Prop.* **2008,** 3, (4), 607-615.
41. Bennett, M. J.; Price, J. B., A physical and chemical examination of an ethylene steam cracker coke and of the underlying pyrolysis tube. *J. Mater. Sci.* **1981,** 16, (1), 170-188.
42. McKimpson, M. G.; Albright, L. F., Future coils for ethylene furnaces: reduced or no coking and increaed coil longevity. *Prepr. Pap.-Am. Chem. Soc., Div. Fuel Chem* **2004,** 49, (2), 776.

43. Bach, G.; Zimmermann, G.; Kopinke, F.-D.; Barendregt, S.; Oosterkamp, P. v. d.; Woerde, H., Transfer-Line Heat Exchanger Fouling during Pyrolysis of Hydrocarbons. *Ind. Eng. Chem. Res.* **1995**, (34), 1132-1139.
44. Zimmermann, G.; Zychlinski, W.; Woerde, H. M.; van den Oosterkamp, P., Absolute Rates of Coke Formation: A Relative Measure for the Assessment of the Chemical Behavior of High-Temperature Steels of Different Sources. *Ind. Eng. Chem. Res.* **1998,** 37, (11), 4302-4305.
45. http://www.phase2plus.com/surfaceroughnesstesters/profile-parameters.htm Surface Roughness Profile Parameters.
46. Carolus, M. D.; Bernasek, S. L.; Schwartz, J., Measuring the Surface Roughness of Sputtered Coatings by Microgravimetry. *Langmuir* **2005,** 21, (9), 4236-4239.
47. Baker, R. T. K., Electron Microscopy Studies of the Catalytic Growth of Carbon Filaments. In *Carbon Fibers Filaments and Composites*, Figueiredo, J. L.; Bernardo, C. A.; Baker, R. T. K.; Hüttinger, K. J., Eds. Springer Netherlands: Dordrecht, 1990; pp 405-439.
48. Baker, R. T. K.; Chludzinski, J. J., Filamentous carbon growth on nickel-iron surfaces: The effect of various oxide additives. *J. Catal.* **1980,** 64, (2), 464-478.
49. Baker, R. T. K., In Situ Electron Microscopy Studies of Catalyst Particle Behavior. *Catal. Rev.: Sci. Eng.* **1979,** 19, (2), 161.
50. Kanaya, K.; Okayama, S., Scanning Electron Microscopy and X-Ray Micro-analysis. In New York and London, 1992; Vol. Ed. J.J. Goldstein et al.
51. Goldstein, J.; Newbury, D. E.; Echlin, P.; Joy, D. C.; Romig Jr, A. D.; Lyman, C. E.; Fiori, C.; Lifshin, E., *Scanning electron microscopy and X-ray microanalysis: a text for biologists, materials scientists, and geologists*. Springer Science & Business Media: 2012.
52. Nolang, B., Ekvicalc and Ekvibase, 4.30. In *Svensk Energi Data: Balinge*, Sweeden, 2013.
53. Zimmermann, H.; Walzl, R., ‘‘Ethylene’’in Ullmann’s Encyclopedia of Industrial Chemistry, vol. 12. In Wiley–VCH: 2003.

Chapter 4: High temperature alloys evaluation

This chapter includes the following manuscript:

4. Experimental study of coke formation of innovative super alloys

Sarris, S. A.; Patil, M.; Reyniers, M.-F.; Marin, G. B.; Van Geem, K. M.

To be submitted

4.1 Abstract

Carbon minimization on the reactor material is one of the major research areas in the field of steam cracking. The choice of the most coking resistant material is a frequent industrial challenge, therefore a thermogravimetric study was performed in a jet stirred reactor set up (JSR) evaluating on-line the coking behavior of several Ni-Cr Fe-base super alloys at two temperatures (dilution 0.33 kg H_2O/ kg C_2H_6, T=1173 K or 1223 K, addition of DMDS, equivalent ethane conversion 70 % or 84 %). For each material first the pretreatment that led to the minimum coking rate was determined. Together with the effect of continuous addition of DMDS and the

cracking temperature increase, the effect of increasing Ni-Cr content or the effect of Al addition was evaluated. The coking results show that by increasing the Ni-Cr content the coking resistance is improved by a factor 2 during the most industrially representative conditions. As expected by increasing the temperature, the coking rate increase depending on the chosen reactor material. Off-line SEM and EDX analysis for the tested coupons filled the puzzle of the coking experimental observations.

Keywords: steam cracking, thermal cracking, presulfiding, pretreatment, jet stirred reactor, anti-coking technologies, High-Temperature Alloys

4.2 Introduction

Thermal cracking of hydrocarbons is a field full of research opportunities. Minimization of coke formation on the inner wall of tubular reactors and carbon oxide formation in steam cracking furnaces is the most frequent challenge to improve the finance of the process [1, 2].

To avoid operation above the metallurgical maximum allowable temperatures or at the maximum pressure drop, an on-line decoking procedure of about 48 hours using steam, steam and hydrogen[3] or - more commonly - a steam/air mixture[4-6] is applied. The aim of decoking is to rapidly, safely and completely remove the coke formed on the coil, creating a continuous oxide layer on the interface of the gas and coil. Alternative decoking technologies have been also developed over the past years for tubular heaters or reactors[7-16] while industrial best practices have been summarized by Sullivan[5]. The field of this work is the application of innovative surface technologies, such as high performance alloys [17, 18] and coatings [19-21]. The cost of the reactors made out of these high temperature alloys is rather pronounced and hence

maximizing their lifetime and anti-coking performance is essential. The use of additives, especially sulfur-containing ones, as pretreatment and/or continuous addition is widely applied [22-37], but its effect has been debated. Classically, an oxidative pretreatment is applied before the material is used in the steam cracker, but the different elemental composition of each alloy leads eventually to different coking behavior.

Horsley et al. [38] observed that a significant enrichment of Cr and Mn oxides at the surface of the alloy - namely $MnCr_2O_4$, MnO or Cr_2O_3, was followed by a decreased absolute coke amount. Different oxidizing gas mixtures were tested on Incoloy 800 coupons by Luan and Eckert [39] showing that temperature, duration, and composition of the pretreating gases are the predominant factors affecting the surface composition and thickness of the formed layers after pretreatment.

Jakobi and Karduck [40, 41] evaluated different spun cast alloys in industrially relevant start-up conditions. They found that a protective complex system of oxide layers with a chromium-manganese spinel on top of the chromia layer and with a thin layer of SiO_2 at the oxide-metal interface forming a total oxide layer of 1 µm is formed on top of chromia forming alloys. Alumina-forming alloys displayed a thin protecting Al_2O_3 layer with a thickness of 100 nm showing increased corrosion and carburization resistance, especially if the temperature exceeds 1173 K. Similarly, Asteman and Hartnagel [42] investigated the impact of the Al and Cr content in alloys and concluded that the Al_2O_3 forming alloy, containing 4 wt % Al (NiCr25Al4), has the best preoxidation properties with minimal spallation, compared to the Cr_2O_3 former (NiCr28), even after 500 h isothermal exposure. Adding more Al to the alloy (10 wt % Al: NiCr25Al10) results not only in an extremely poor machinability (hard and brittle) but it also results in a reduced carburization resistance.

Typically, very limited information is available about the link between pretreatment and coke formation, not even in patents, where only vague claims about the combination of sulfur and other compounds were mentioned [43, 44]. Pretreatment times vary between 30 minutes and 4 hours at temperatures in the range of 873 to 1223 K. Recently, Sarris et.al [45], optimized the pretreatment for Fe-Ni-Cr alloys, stating that a similar optimization procedure should be always performed for different elemental composition alloys. Therefore, the aim of this study is the comparison of 4 optimized high temperature alloys under industrially relevant cracking conditions. Their coking resistance is thermo gravimetrically analyzed. Detailed experimental coking rates and gas phase composition are provided, supported by surface and cross-sectional SEM and EDX observations to assist the interpretation of the experimental results.

4.3 Experimental section

4.3.1 Electrobalance set-up

The jet stirred reactor set-up has been extensively described in previous work [17, 18, 45], therefore, only a brief description is given here. The set-up consists out of three parts: a feed section, a reactor section and an analysis section as shown in Figure 4. 1. The mass flow rates of gasses and water are controlled by thermal mass flow controllers. All the lines in contact with sulfur are Sulfinert®-treated[46]. The water is vaporized to steam in an evaporator, mixed with the heated hydrocarbon feedstock and further heated before entering the reactor inlet at a temperature of 903 K. A jet stirred reactor made out of quartz is used, with a flat coupon in the center of the JSR suspended from the arm of an electrobalance. The coupon dimensions are 10 mm × 8 mm × 1 mm. The mass changes are tracked over time with a frequency of 1 Hz. Subsequently, the reactor effluent is quenched to prevent further cracking and its composition is

measured with two gas chromatographs (GC) using nitrogen as internal standard i.e. a refinery gas analyzer dedicated to the analysis of components with less than 5 carbon atoms and a TRACE™ Ultra GC detecting hydrocarbons ranging from methane to naphthalene. For ethane cracking no heavier products are measured than naphthalene. In detail, from the peak areas of the TCD-channel, experimentally determined calibration factors and the known amount of nitrogen, the flows of hydrogen, methane, carbon oxides and C2 hydrocarbons are calculated. The calculated methane flow is subsequently used as internal standard for the flow determination of higher hydrocarbons in the FID-channels. A schematic representation of the use of internal standards is given in Annex C.

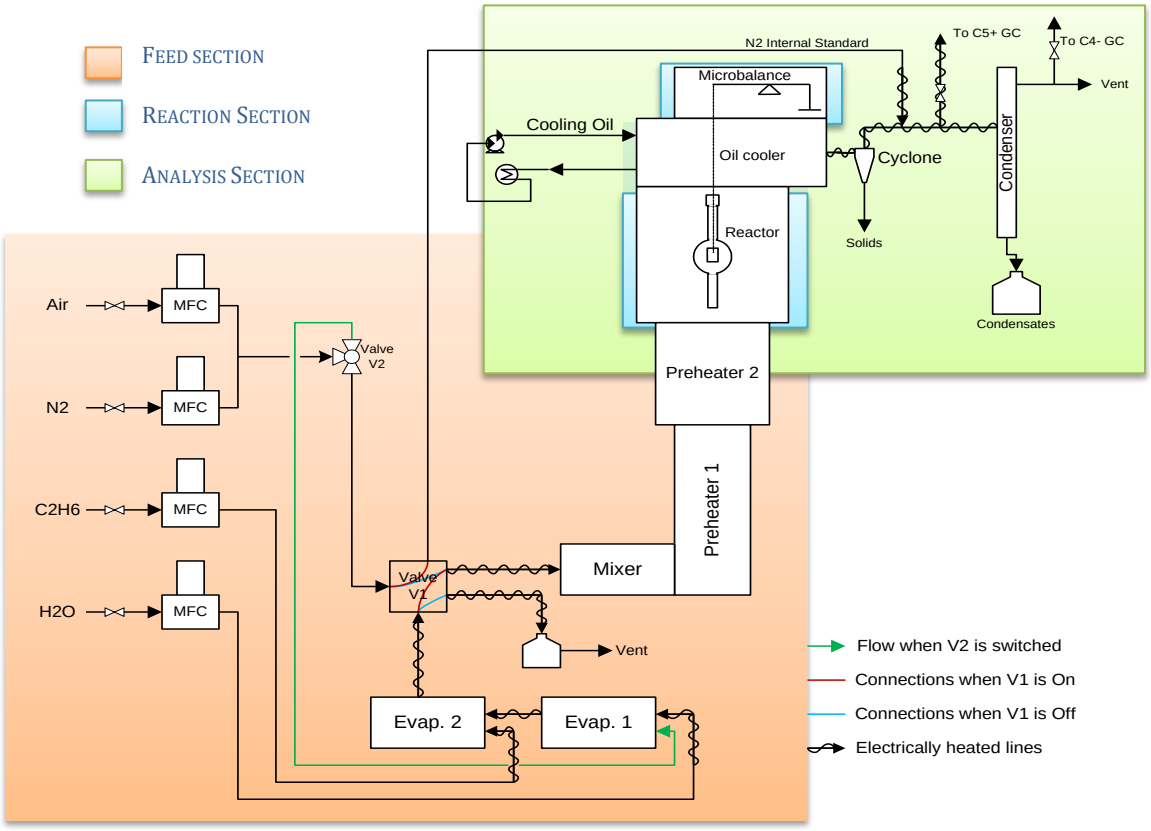

Figure 4. 1: Diagram of the thermogravimetric set-up for the study of coke deposition during steam cracking of ethane

4.3.2 Experimental procedures and conditions

Four different alloys are evaluated under a broad range of industrially relevant conditions. Operating procedures and conditions used in this work are summarized in Table 4. 1. The experiments consisted of eight cracking cycles, three of 6 h cracking and decoking, four short of 1 h and a last one of 6 hours. The heating ramp used during stabilization, heating and cooling of the set-up is 300 $K \cdot h^{-1}$. For all the performed experiments before the first cycle, an initial preoxidation step, oxidation for 14 hours in the presense of Air at 1023 K, is performed to mimic the state of the alloy in an industrial steam cracker at start of run conditions. As next steps, the

pretreatment procedure consists of a "decoking" step followed by a last steam or steam/air treatment. In case that presulfiding is applied, then it is performed after these pretreatment steps, exactly before cracking. The experiments with a presulfiding step before the cracking cycle are labeled with "PreS". After cracking, the pretreatment is again performed to both burn the coke formed on the sample and regenerate the oxides formed on the sample surface.

Table 4. 1: Operational procedures and conditions during pretreatment, decoking and cracking

	Process step	Alloy	Duration	Temperature (K)	Gas feed flow (Nl/s)			Water flow (10^{-6} kg s^{-1})
					N_2	Ethane	Air	
	Initial preoxidation	**Common**	12-14 hours	1023	-	-	0.0067	-
Pretreatment	**Pretreatment (or Decoking)**	**Optimal Fe-Ni-Cr**	30 minutes	from 1023 to 1173 K	0.0083	-	0.0083	-
		Optimal Al-content	15 minutes	1023 K	-	-	0.0083	-
	Steam Treatment	**Optimal Fe-Ni-Cr**	15 minutes	1173 K	-	-	0.0083	6.7
		Optimal Al-content	45 minutes	from 1023 to 1173 K	-	-	-	6.7
PreS*	**Presulfiding**	**Common**	30 minutes	1100	-	-	-	5.6
Cracking	**1st cracking cycle**	**Common**	6 hours	1173 or 1223	-	0.0241	-	9.7
Decoking	**Pretreatment (or Decoking)**	**Optimal Fe-Ni-Cr**	30 minutes	from 1023 to 1173 K	0.0083	-	0.0083	-
		Optimal Al-content	15 minutes	1023 K	-	-	0.0083	-
	Steam Treatment	**Optimal Fe-Ni-Cr**	15 minutes	1173 K	-	-	0.0083	6.7
		Optimal Al-content	45 minutes	from 1023 to 1173 K	-	-	-	6.7
PreS*	**Presulfiding**	**Common**	30 minutes	1100	-	-	-	5.6
Cracking	**next cracking cycle**	**Common**	6 hours	1173 or 1223	-	0.0241	-	9.7

* PreS : presulfiding is applied after the pretreatment only for the presulfided experiments

During experiments with continuous addition of DMDS, labeled with “CA”, 41 ppmw S/HC diluted in the water is fed; this value corresponds to typical amounts used in industrial ethane cracking furnaces to limit the formation of carbon oxides. The reactor temperature is set throughout the cracking runs at 1173 or 1223 K, the latter labeled with “HT”, a value that is reached within 5 minutes after introducing the cracking mixture in the reactor. The standard experiment, without any addition of DMDS before or during cracking and at the typical temperature of 1173 K is noted as “Blank”. Table 4. 2 summarizes the labelling of the experiments performed throughout this work. After cracking for 6 hours, the reactor temperature is set to 1023 K and the flow rate of ethane and steam is set to zero, leaving only helium to purge the reactor.

Table 4. 2: Experimental labels based on the conditions

Label	Experimental conditions
Blank	No addition of DMDS before or during cracking
PreS	Presulfiding is performed before cracking
CA	DMDS is added continuously diluted in the water
CA + PreS	A presulfiding step is performed, while DMDS is also fed during cracking
CA HT	DMDS is added continuously diluted in the water; the cracking temperature is increased at 1223 K

Surface characteristics were determined by analyzing the tested samples by means of SEM and EDX. While cooling down to room temperature, a He flow of $0.6 \cdot 10^{-6}$ kg $\cdot$ s^{-1} is used as inert gas while the ramp is set to 100 K per hour. For the Fe-Ni-Cr alloys the recently published[45] optimized pretreatment is used, while for the Al-content alloy a similarly optimized pretreatment is performed. . Both are summarized in Figure 4. 2.

ID	Treatment			Cracking	Treatment			Cracking	Cooling down or pretreatment followed by next cycle
	Preoxidation	Pretreatment		Presulfiding		Pretreatment		Presulfiding		
Optimal Fe-Ni-Cr	1023 K Air	1023 K -> 1173 K N_2 + Air	1173 K Steam/Air	1100 K Steam with 500 ppmw DMDS/H_2O	1173 K or 1223 K $C_2H_6 + H_2O$	1023 K -> 1173 K N_2 + Air	1173 K Steam/Air	1100 K Steam with 500 ppmw DMDS/H_2O	1173 K or 1223 K $C_2H_6 + H_2O$	time
	OA - 14 h	Air Treatment	Steam/Air Treatment	PreS*	1st coking cycle - 6h	Air Treatment	Steam/Air Treatment	PreS*	2nd coking cycle - 6h	
Optimal Al-content	1023 K Air	1023 K Air	1023 K -> 1173 K Steam	1100 K Steam with 500 ppmw DMDS/H_2O	1173 K or 1223 K $C_2H_6+H_2O$	1023 K Air	1023 K -> 1173 K Steam	1100 K Steam with 500 ppmw DMDS/H_2O	1173 K or 1223 K $C_2H_6 + H_2O$	time
	OA - 14 h	Air Treatment	Steam Treatment	PreS*	1st coking cycle - 6h	Air Treatment	Steam Treatment	PreS*	2nd coking cycle - 6h	

* PreS step only for presulfiding experiments

Figure 4. 2: Schematic representation of the cyclic experiments and pretreatment conditions performed in JSR for the different alloys

4.3.3 Coking rate calculation

The coke deposition on each sample is measured over time by continuously weighing the mass of the sample. This allows the determination of the total amount of coke after every cracking cycle, as well as the calculation of the initial catalytic coking rate and the asymptotic pyrolytic coking rate. Similarly with previous work [17, 18, 45], the coking rate is determined as:

$$R_c = \frac{m_{t_2} - m_{t_1}}{t_2 - t_1} \frac{1}{S} \quad (4.1)$$

where R_c is the coking rate in $kg \cdot s^{-1} \cdot m^{-2}$, mt_j the mass of coke at time j in kg, t_j the experimental time at instant j in s and S the surface area of the coupon in m^2.

The mean value of the coking rate between 15 minutes and 60 minutes is defined as the initial or catalytic coking rate, i.e. characterizing the catalytic coking behavior of the sample. The asymptotic coking rate is related to the pyrolytic coking mechanism and is reported as the mean measured coking rate between the 5^{th} and 6^{th} hour of cracking (see Figure 4. 3).

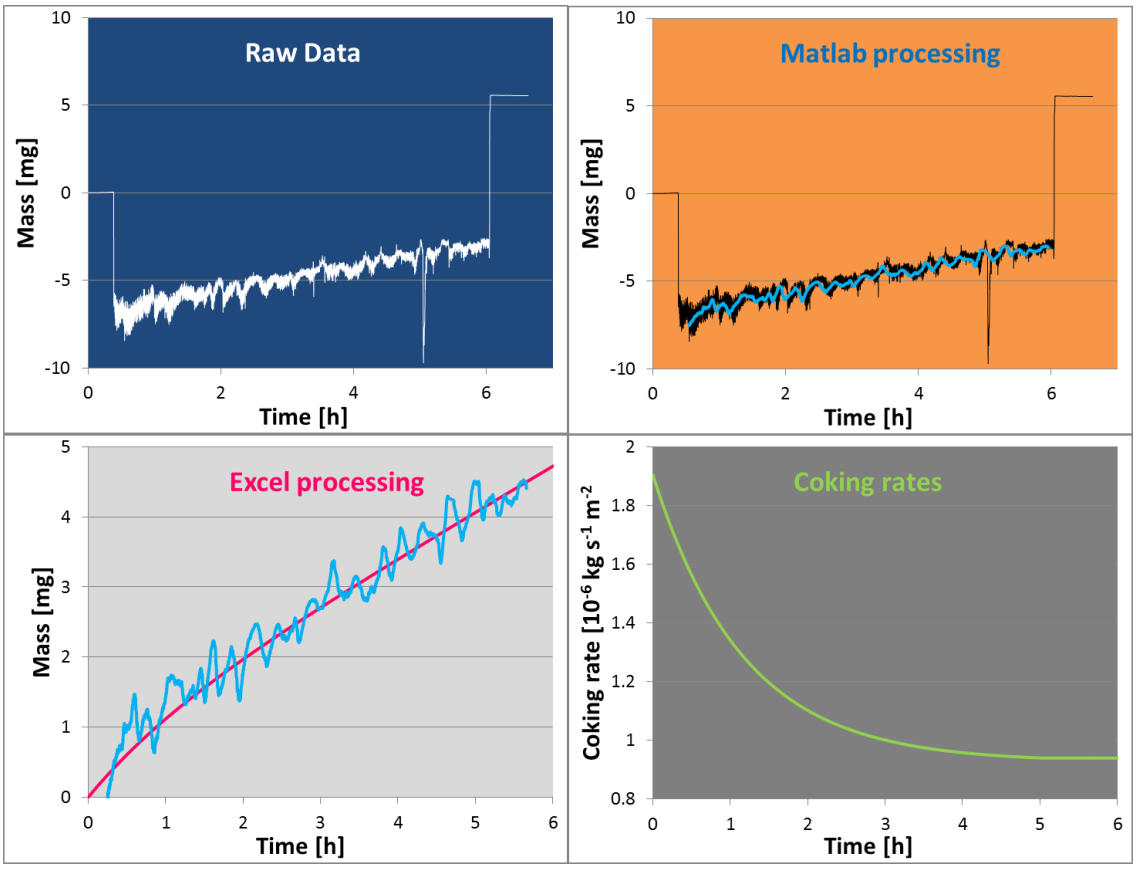

Figure 4. 3: Processing sequence for the coking rates determination

4.3.4 Scanning Electron Microscope and Energy Dispersive X-ray Analysis

Scanning Electron Microscopy (SEM) and Energy Dispersive X-ray Spectroscopy (EDX) are used to obtain information regarding the surface morphology and to perform chemical analysis. Top surface analyses are performed in both 10 and 20 kV, giving insight for the top surface and mid-range surface of the coupon, respectively. As shown in Figure 4. 4, the top surface analyses gave a qualitative idea of the elemental composition of the surface, and was performed at 10 kV and 20 kV, while the cross sectional mappings evaluated the uniformity of the oxides generated during each applied pretreatment. The surface composition is an average of EDX analyses on two

different locations of the examined coupons. Analyses are performed for coked and pretreated samples.

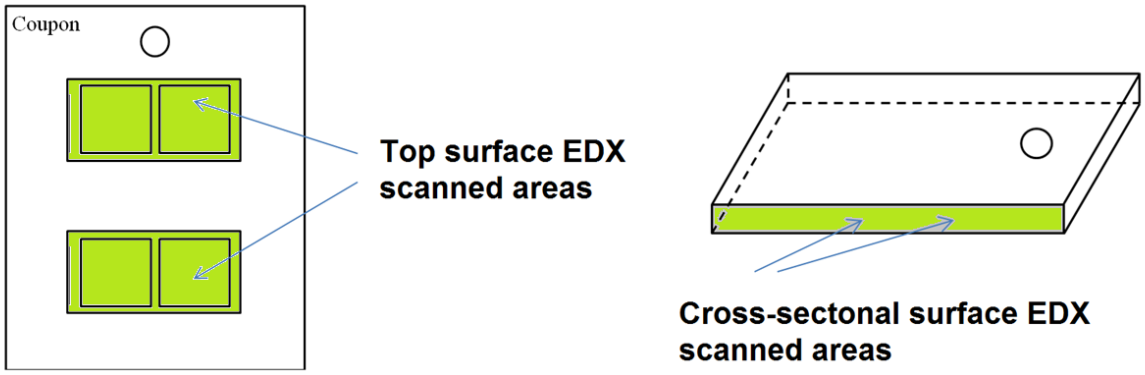

Figure 4. 4: Representation of the top surface analysis (left) and cross-sectional (right) analysis of the examined coupons

4.4 Experimental results and discussion

An overview of the coking and gas effluent analysis of the experiments performed is given in the supporting information in Appendix C. In general, by adding DMDS during cracking an increase of the coking rates is noted followed by a decrease in the formation of the carbon oxides. As expected, by increasing the temperature the coking rates increase, however the quantitative trend is different for all the alloys. By enriching the alloy composition in Cr and Ni the observed coking rates drop significantly. Most of the alloys indicated a quite pronounced stability during the cyclic aging in terms of coking rates, except for the high temperature experiments at 1223 K. Overall, minor differences can be observed for the gas effluent by changing the alloy under the same conditions, while no differences are observed during the cyclic aging and during each cracking cycle per material, therefore only the average gas phase composition is reported. A more

detailed analysis of the experimental observation is done by splitting the investigated phenomena into sections, below.

4.4.1 Blank experiments

In Figure 4. 5, the coking behavior of the four different alloys in the absence of DMDS at 1173 K, is highlighted. It should be first underlined that industrially the use of DMDS is necessary to suppress the pronounced carbon oxides formation, however to thoroughly and fundamentally evaluate the effect of the addition of DMDS before or during cracking this type of experiment is necessary. Under the tested conditions, the 40/48 Cr/Ni alloy outperforms in coke inhibition the rest of the alloys, during the initial catalytic coking step. Similar anti-coking performance is noted by the 35/45 Cr/Ni alloy. Close to these two, the 25/35 Cr/Ni alloy shows from 20 to 30 % worse coking behavior. The worst performance is noted by the Al-content alloy, having overall from 2 to 3 times more pronounced coking rates than the rest of the samples. However, given the fact that DMDS is always used in industry, this negative experimental observation should not be considered discouraging for industrial use.

The coking trends remain the same for the asymptotic coking rate, with suppressed values in comparison with the catalytic phase for all the samples. It is known that Ni and Fe are coke formation precursors, while a pronounced Cr, Mn and Al content, evidence mainly of dense passivating oxides, can be responsible for a positive anti-coking behavior of an alloy[17]. The elemental composition of the coked samples is in line with the coking observations, with the Al-content alloy having the most pronounced content of Fe and Ni on its surface, as shown in Table 4. 3. Also, the sum of Cr and Mn in the non-Al alloys is more than 85 wt % in any case, while for the Al-content alloy the sum of Cr and Al is less than 80 wt %, implying its deficiency in anti-coking behavior. In Annex C, an additional comparison of the cross section analyses is made.

Table 4. 3: Top surface elemental composition of the coked samples for the Blank runs.

Magnification: 50 X; accelerating Voltages 10 and 20 kV.

Blank run		**25/35 Cr/Ni**	**35/45 Cr/Ni**	**Al-content**	**40/48 Cr/Ni**
Elements	acc. volt.	coked samples (wt %)			
Ni	10 kV	9.1	7.7	15.3	8
	20 kV	3.6	1.7	16.4	2.3
Fe	10 kV	6.6	0.8	11.4	1.3
	20 kV	4.5	1.9	9.7	0.6
Cr	10 kV	80.4	49.2	17.3	72.4
	20 kV	77.5	64	20.6	80.9
Si	10 kV	0.2	1.6	2.2	1.2
	20 kV	0.5	1.3	2	1
Mn	10 kV	3.6	46.7	-	16.9
	20 kV	13.3	30.5	-	14.8
Nb	10 kV	0.1		0.6	0.2
	20 kV	0.5	0.5	1	0.4
Al	10 kV	-	-	53.2	-
	20 kV	-	-	50.3	-

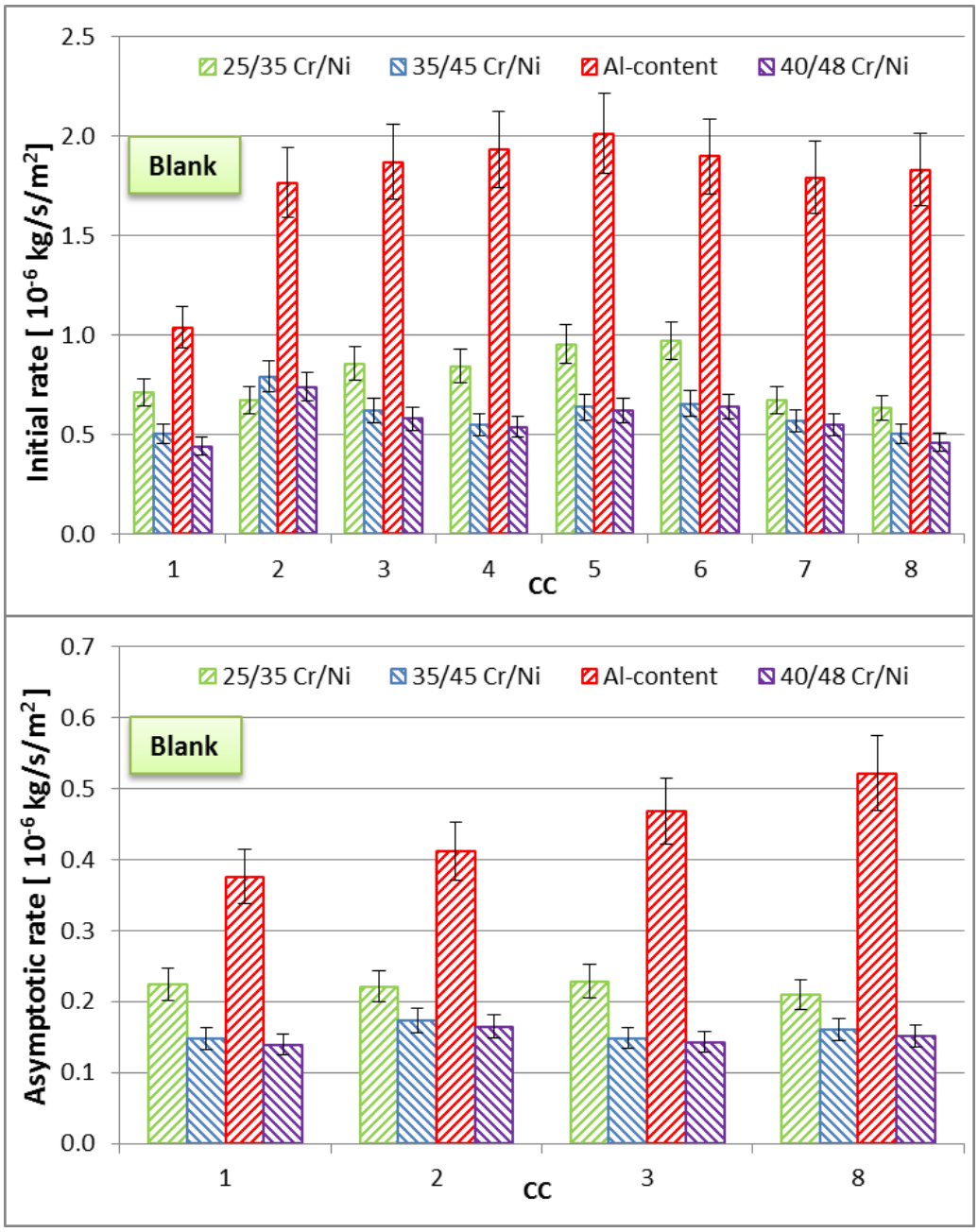

Figure 4. 5: Initial (top) and asymptotic (bottom) coking rates for the Blank runs for the four different alloys tested. Ethane steam cracking: F_{HC}= 29.18 x 10^{-6} kg s^{-1}, δ= 0.33 kg_{H2O} $kg^{-1}{}_{HC}$, $T_{reactor}$= 1173 K, P= 101.35 kPa, F_{H2O}=9.72 x 10^{-6} kg s^{-1}.

4.4.2 Continuous addition experiments

By comparing the catalytic coking behavior of the four different alloys under CA conditions, see Figure 4. 6 top, the Al-content material is in this case the only one that cokes less when DMDS is continuously added than in its absence. The Al-content alloy is outperformed only by the 40/48 Cr/Ni material, that cokes from 20 % to 50 % less depending on the cycle. Overall, the ranking among the rest Fe-Ni-Cr alloys remains the same with the Blank runs, but with more pronounced differences. By continuously feeding DMDS all the non Al-content alloys indicate roughly 7 times higher coking rates in comparison with the Blank runs, while the carbon oxides formation is suppressed by a factor 5.

Table 4. 4: Top surface elemental composition of the coked samples for the CA runs.

Magnification: 50 X; accelerating Voltages 10 and 20 kV

CA		**25/35 Cr/Ni**	**35/45 Cr/Ni**	**Al-content**	**40/48 Cr/Ni**
Elements	acc. volt.	coked samples (wt %)			
Ni	10 kV	3.7	7.6	13.8	7.8
	20 kV	10.3	2.1	20.2	2.3
Fe	10 kV	1.6	2	7.5	1.5
	20 kV	9.1	2.6	11.2	0.6
Cr	10 kV	65.2	47.9	9.8	72.2
	20 kV	62.1	63	18.9	80.9
Si	10 kV	1.4	2.1	2.1	1.2
	20 kV	2.1	1.3	1.2	1
Mn	10 kV	27.8	40.4	-	16.9
	20 kV	15.5	30.7	-	15.2
Nb	10 kV	0.4	-	0.4	0.4
	20 kV	0.9	-	0.4	0.4
Al	10 kV	-	-	66.5	-
	20 kV	-	-	48	-

As mentioned above, the best performance is noted again by the 40/48 Cr/Ni alloy, that cokes almost 2 times less than the 35/45 Cr/Ni one, and that is from 3 to 5 times better than the 25/35 Cr/Ni. Similar trends, but more suppressed are noted for the asymptotic coking rates of all the alloys.

The elemental composition of the tested coked samples – see Table 4. 4 – remains similar with the ones of the Blank runs, verifying that the elemental composition of a well pretreated surface is affected mainly by the decoking and pretreatment procedure. In Annex C, an additional comparison of the cross section analyses is made.

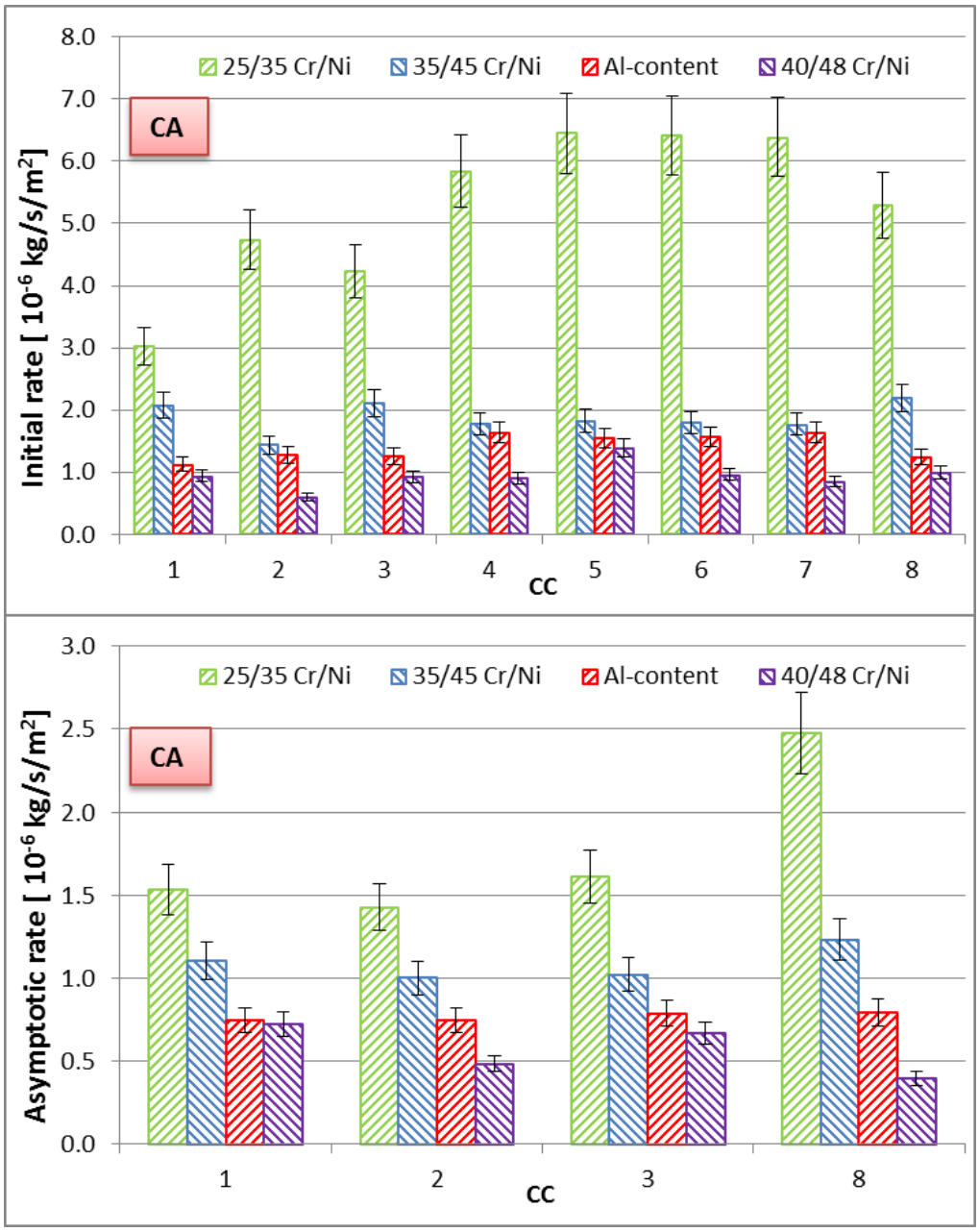

Figure 4. 6: Initial (top) and asymptotic (bottom) coking rates for the CA runs for the four different alloys tested. Ethane steam cracking: F_{HC}= 29.18 x 10^{-6} kg s^{-1}, δ= 0.33 kg_{H2O} kg^{-1}_{HC}, $T_{reactor}$= 1173 K, P= 101.35 kPa, F_{H2O}=9.72 x 10^{-6} kg s^{-1}.

4.4.3 Presulfiding effect

The presulfiding effect is evaluated for both the Blank and CA runs. Initially, by comparison of Figure 4. 5 and Figure 4. 7, the presulfiding treatment step seems to have a negligible effect towards the coking behavior of the Al-content alloy, for both its catalytic and pyrolytic coking behavior. For the non Al-content alloys, a 2 to 3 times increase is observed after the addition of the presulfiding step before cracking. Nevertheless, the Al-content alloy performs worser in terms of pyrolytic coking. The order of coking remains the same with the above mentioned observations; the 25/35 Cr/Ni material performs worst, while the 40/48 Cr/Ni best. No positive effect can be observed towards the carbon oxides suppression.

Table 4. 5: Top surface elemental composition of the coked samples for the PreS runs.

Magnification: 50 X; accelerating Voltages 10 and 20 kV.

PreS		**25/35 Cr/Ni**	**35/45 Cr/Ni**	**Al-content**	**40/48 Cr/Ni**
Elements	acc. volt.	coked samples (wt %)			
Ni	10 kV	7.8	4.2	15.4	18.2
	20 kV	16.2	13	10	10.2
Fe	10 kV	7.5	2.8	9.2	3.1
	20 kV	15.7	15.5	9.6	2.3
Cr	10 kV	57.8	68.9	8.9	64.1
	20 kV	51.5	60.5	13.9	62.9
Si	10 kV	3.2	0.8	1.6	1.1
	20 kV	4.1	1.5	5.5	2.3
Mn	10 kV	22.9	22.4	-	12.5
	20 kV	11.3	8.7	3.6	19.6
Nb	10 kV	0.8	0.9	0.6	1.2
	20 kV	1.2	0.8	3.1	2.8
Al	10 kV	-	-	64.2	-
	20 kV	-	-	54.4	-

From Table 4. 5, comparing with the values of the Blank runs, it is obvious that the presulfided samples have pronounced content of Ni and Fe on their top surface, justifying their pronounced

coking rates. That is not the case for the Al-content alloy that shows increased amounts of Al. However, this material is the only one that does show a negligible effect of presulfiding on its coking behavior, in agreement with its elemental composition.

While comparing Figure 4. 6 and Figure 4. 8, it is clear that when presulfiding is combined with the continuous addition of DMDS, it has a light effect in terms of coking rates causing in most of the cases an increase of roughly 10 to 20 %. Overall, it seems that under these conditions, the 25/35 Cr/Ni alloy cokes at least 2 times more than the rest. The best anti-coking performance is attributed to the 40/48 Cr/Ni alloy being even two times better than the second best Al-content material that is performing roughly 10 % better than the third 35/45 Cr/Ni.

The elemental composition of the CA + PreS samples is almost the same with PreS ones, see Table 4. 5 and Table 4. 6, verifying once more that the elemental composition of a surface is a strong function of the pretreatment. In Annex C, an additional comparison of the cross section analyses of the tested samples is provided.

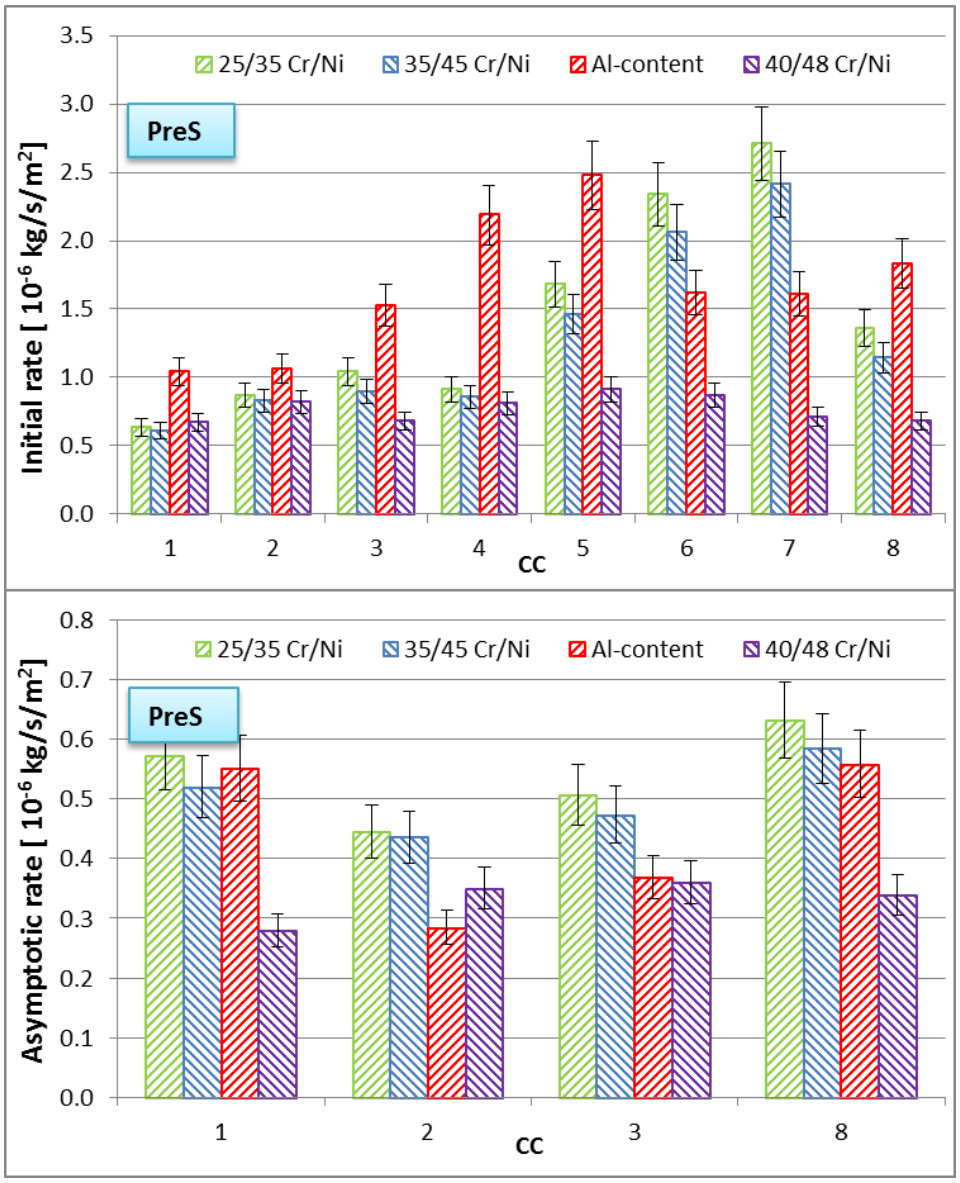

Figure 4. 7: Initial (top) and asymptotic (bottom) coking rates for the PreS runs for the four different alloys tested. Ethane steam cracking: F_{HC}= 29.18 x 10^{-6} kg s^{-1}, δ= 0.33 kg_{H2O} kg^{-1}_{HC}, $T_{reactor}$= 1173 K, P= 101.35 kPa, F_{H2O}=9.72 x 10^{-6} kg s^{-1}.

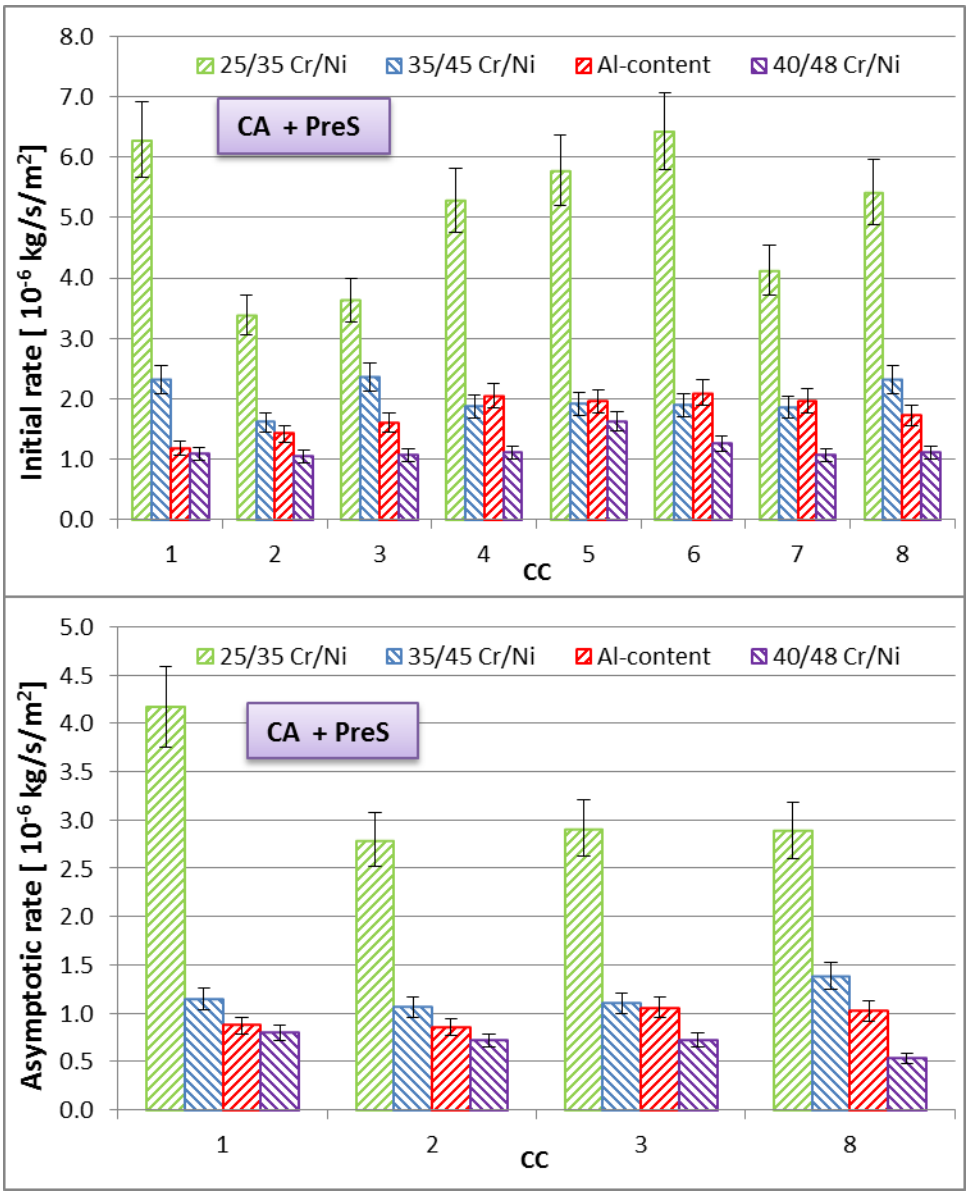

Figure 4. 8: Initial (top) and asymptotic (bottom) coking rates for the CA + PreS runs for the four different alloys tested. Ethane steam cracking: F_{HC}= 29.18 x 10^{-6} kg s^{-1}, δ= 0.33 kg_{H2O} $kg^{-1}{}_{HC}$, $T_{reactor}$= 1173 K, P= 101.35 kPa, F_{H2O}=9.72 x 10^{-6} kg s^{-1}.

Table 4. 6: Top surface elemental composition of the coked samples for the CA + PreS runs.

Magnification: 50 X; accelerating Voltages 10 and 20 kV.

CA + PreS		**25/35 Cr/Ni**	**35/45 Cr/Ni**	**Al-content**	**40/48 Cr/Ni**
Elements	acc. volt.	coked samples (wt %)			
Ni	10 kV	12.3	3.4	15.7	18.5
	20 kV	21.7	13.1	10.1	10.6
Fe	10 kV	12	2.1	9.2	3.5
	20 kV	24.1	15.4	9.6	2.3
Cr	10 kV	47.8	69.6	8.7	64
	20 kV	40	60.3	13.7	62.5
Si	10 kV	3.3	0.7	1.6	0.8
	20 kV	4.1	1.4	5.9	2.5
Mn	10 kV	23.9	23.6	-	12.1
	20 kV	9.1	9	3.2	19.4
Nb	10 kV	0.7	0.6	0.4	1.1
	20 kV	1	0.8	3.5	2.7
Al	10 kV	-	-	64.4	-
	20 kV	-	-	54	-

4.4.4 Temperature effect

Evaluation of the performance of the four tested alloys under 50 K higher temperature corresponds to the possibility of hot spots close to the outlet of the reactor, where locally a temperature rise can be observed. The experiment used for that test is the one of continuous addition of DMDS at 1223 K. To evaluate the effect of the higher temperature, the CA at standard temperature is used as reference. Based on Figure 4. 6 and Figure 4. 9, by increasing temperature by 50 K, the coking rates are doubled to tripled for the 25/35 and 35/45 Cr/Ni alloys. For the Al-content the catalytic coking rate rises significantly depending on the cracking cycle, while the asymptotic coking rate increases even by a factor 2. The 40/48 Cr/Ni alloy outperforms again all the tested materials, by increasing its coking rates by less than 15 % in comparison with the lower

temperature experiments, remaining in any case at least 10 % better than any other material in the high temperature experiments.

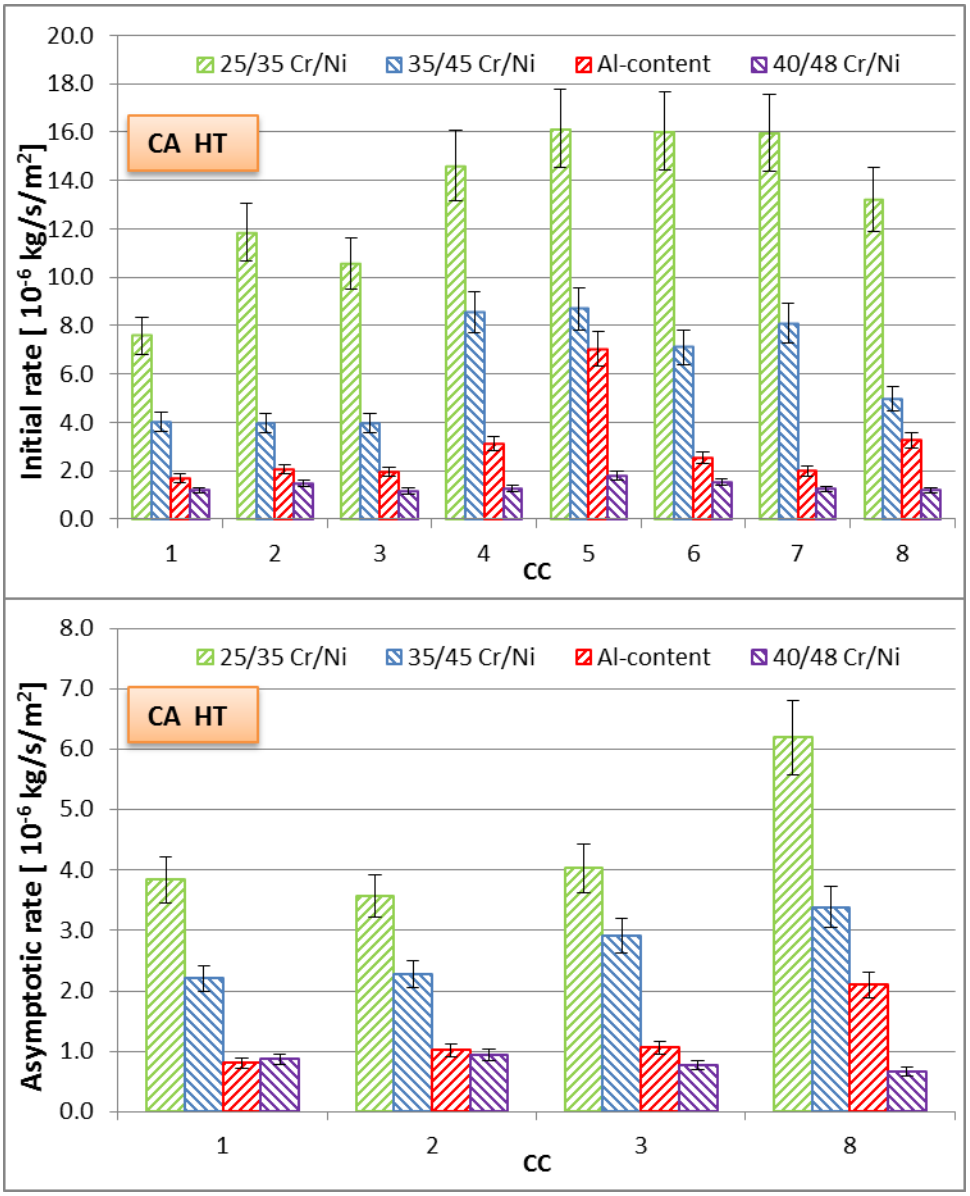

Figure 4. 9: Initial (top) and asymptotic (bottom) coking rates for the CA HT runs for the four different alloys tested. Ethane steam cracking: F_{HC}= 29.18 x 10^{-6} kg s^{-1}, δ= 0.33 kg_{H2O} $kg^{-1}{}_{HC}$, $T_{reactor}$= 1173 K, P= 101.35 kPa, F_{H2O}=9.72 x 10^{-6} kg s^{-1}.

Judging by Table 4. 4 and Table 4. 7, the 40/48 alloy has a rather pronounced amount of Ni on its surface and the least amount of Fe. Nevertheless it outperforms the rest of the alloys in terms of anti-coking performance. The existence of Cr, Mn and Al on top of the surface are known to improve the anti-coking behavior of an alloy, but their relative anti-coking performance has not been evaluated yet. Based on Table 4. 7 and Figure 4. 9, the relative reactivity of Fe is expected to be higher than the one of Ni. Also, the existence of Mn on top of the surface seems to improve the anti-coking behavior of an alloy at cracking temperatures higher than 1173 K. In Annex C, an additional comparison of the cross section analyses is made for all the tested coupons.

Table 4. 7: Top surface elemental composition of the coked samples for the CA HT runs.

Magnification: 50 X; accelerating Voltages 10 and 20 kV.

CA HT		**25/35 Cr/Ni**	**35/45 Cr/Ni**	**Al-content**	**40/48 Cr/Ni**
Elements	acc. volt.	coked samples (wt %)			
Ni	10 kV	43.4	8.2	7.1	22.2
	20 kV	45.4	5.7	8.1	10
Fe	10 kV	20.3	7.3	7.1	1.6
	20 kV	21.4	12	6.2	0.1
Cr	10 kV	27.7	78.2	66.8	58.3
	20 kV	26.7	75.3	52.4	60.8
Si	10 kV	0.7	0.1	1	0.8
	20 kV	0.9	0.3	1	1.1
Mn	10 kV	7.4	6	-	15.7
	20 kV	4.8	6.6	-	23.6
Nb	10 kV	0.5	0.2	1.5	1.3
	20 kV	0.8	0.1	0.5	1.4
Al	10 kV	-	-	16.4	-
	20 kV	-	-	31.9	-

4.5 Conclusions

Four different super alloys were experimentally evaluated under 5 different conditions in terms of anti-coking performance. Overall, the worst performance was noticed for the 25/35 Cr/Ni alloy. In the absence of DMDS, the Al-content material performed from 2 to 3 times worse than the competition, while the non Al alloys performed rather similarly. When DMDS was added continuously in the feed the best performance was noted by the higher Cr/Ni content alloy, while the worst from the 25/35 Cr/Ni one. The Al-containing alloy performed similarly to slightly better than the 35/45 Cr/Ni alloy, showing the Al anti-coking performance. The effect of presulfiding is more pronounced in the case that it is applied on a Blank run than on a CA run. The Al-content alloy had the most stable behavior after application of presulfiding, being slightly better than the 35/45 Cr/Ni alloy, yet worse than the 40/48 Cr/Ni one. The existence of Cr, Mn and Al on top of the surface are already known to improve the anti-coking behavior of an alloy, but their relative anti-coking performance has not been evaluated yet. Adding Al is not sufficient to create a super alloy with strong anti-coking capabilities. The relative coking reactivity of Fe is higher than the one of Ni. Also, the existence of Mn on top of the surface seems to improve the anti-coking behavior of an alloy at cracking temperatures higher than 1173 K in comparison with the ones of Cr or Al.

4.6 References

1. Paraskevas, P. D.; Sabbe, M. K.; Reyniers, M. F.; Papayannakos, N.; Marin, G. B., Kinetic Modeling of α-Hydrogen Abstractions from Unsaturated and Saturated Oxygenate Compounds by Carbon-Centered Radicals. *ChemPhysChem* **2014,** 15, (9), 1849-1866.

2. Paraskevas, P. D.; Sabbe, M. K.; Reyniers, M.-F.; Papayannakos, N. G.; Marin, G. B., Kinetic Modeling of α-Hydrogen Abstractions from Unsaturated and Saturated Oxygenate Compounds by Hydrogen Atoms. *The Journal of Physical Chemistry A* **2014,** 118, (40), 9296-9309.
3. Kivlen, J. A.; Koszman, I., Decoking of onstream thermal cracking tubes with h20 and h2. In Google Patents: 1971.
4. Chen, J.; Maddock, M., *Hydrocarbon Process*. 1973; Vol. 52, p 147-151.
5. Sullivan, B. K., Ethylene Cracking Heater Decoking Tutorial. In *AIChE Spring Natl. Meet., Conf. Proc.*, New Orleans, LA, 2014.
6. Heynderickx, G.; Schools, E.; Marin, G., Optimization of the decoking procedure of an ethane cracker with a steam/air mixture. *Industrial & engineering chemistry research* **2006,** 45, (22), 7520-7529.
7. Lenglet, E., Method of decoking an installation for steam cracking hydrocarbons, and a corresponding steam-cracking installation. In Google Patents: 1993.
8. HAK Decoking Technology (HDT). http://www.a-hak-is.com/en/home/what_we_do/services/furnace_services/hak_decoking_technology_hdt
9. Nunciato, D. J.; White, N. H.; Woodburn, W. A., Method for decoking fired heater tubes. In Google Patents: 1981.
10. J, D. W., Decoking and cleaning tubular heaters. In Google Patents: 1954.
11. De Saegher, J. J.; Detemmerman, T.; Froment, G. F., Three dimensional simulation of high severity internally finned cracking coils for olefins production. *Revue De L'Institut Français Du Pétrole* **1996,** 51, (2), 245-260.
12. Detemmerman, T.; Froment, G. F., Three dimensional coupled simulation of furnaces and reactor tubes for the thermal cracking of hydrocarbons. *Revue De L'Institut Français Du Pétrole* **1998,** 53, (2), 181-194.
13. Schietekat, C. M.; van Goethem, M. W. M.; Van Geem, K. M.; Marin, G. B., Swirl flow tube reactor technology: An experimental and computational fluid dynamics study. *Chemical Engineering Journal* **2014,** 238, 56-65.
14. Torigoe, T.; Hamada, K.; Furuta, M.; Sakashita, M.; Otsubo, K.; Tomita, M. In *Mixing element radiant tube (MERT) improves cracking furnace performance*, 11th Ethylene Producers' Conference, Houston, TX, 1999; Houston, TX, 1999.

15. Györffy, M.; Hineno, M.; Hashimoto, K.; Park, S.-H.; You, M.-S. In *MERT performance and technology update*, 21st Ethylene Producers' Conference, Tampa, FL, 2009; Tampa, FL, 2009.
16. Schietekat, C. M.; Van Cauwenberge, D. J.; Van Geem, K. M.; Marin, G. B., Computational fluid dynamics-based design of finned steam cracking reactors. *AIChE J.* **2014,** 60, (2), 794-808.
17. Muñoz Gandarillas, A. E.; Van Geem, K. M.; Reyniers, M.-F.; Marin, G. B., Influence of the Reactor Material Composition on Coke Formation during Ethane Steam Cracking. *Ind. Eng. Chem. Res.* **2014,** 53, (15), 6358-6371.
18. Muñoz Gandarillas, A. E.; Van Geem, K. M.; Reyniers, M.-F.; Marin, G. B., Coking Resistance of Specialized Coil Materials during Steam Cracking of Sulfur-Free Naphtha. *Ind. Eng. Chem. Res.* **2014,** 53, (35), 13644-13655.
19. Petrone, S.; L.Deuis, R.; Kong, F.; Unwin , P. In *Catalyzed-assisted manufacture of olefins (CAMOL): Year-(4) update on commercial furnace installations*, Proc. - Ethylene Prod. Conf., March 21-25, 2010; 2010.
20. Schietekat, C. M.; Sarris, S. A.; Reyniers, P. A.; Kool, L. B.; Peng, W.; Lucas, P.; Van Geem, K. M.; Marin, G. B., Catalytic Coating for Reduced Coke Formation in Steam Cracking Reactors. *Ind. Eng. Chem. Res.* **2015,** 54, (39), 9525-9535.
21. Petrone, S.; Chen, Y.; Deuis, R.; Benum, L.; Saunders, R.; Wong, C. In *Catalyzed-assisted manufacture of olefins (CAMOL): Realizing novel operational benefits from furnace coil surfaces*, 20th Ethylene Producers' Conference, New Orleans, LA, 2008; New Orleans, LA, 2008.
22. Wang, J.; Reyniers, M.-F.; Van Geem, K. M.; Marin, G. B., Influence of Silicon and Silicon/Sulfur-Containing Additives on Coke Formation during Steam Cracking of Hydrocarbons. *Ind. Eng. Chem. Res.* **2008,** 47, (5), 1468-1482.
23. Reyniers, M.-F.; Froment, G. F., Influence of metal-surface and sulfur addition on coke deposition in the thermal-cracking of hydrocarbons. *Industrial & Engineering Chemistry Research* **1995,** 34, (3), 773-785.
24. Wang, J.; Reyniers, M.-F.; Marin, G. B., Influence of Dimethyl Disulfide on Coke Formation during Steam Cracking of Hydrocarbons. *Ind. Eng. Chem. Res.* **2007,** 46, (12), 4134-4148.

25. Reyniers, M.; Froment, G. F., INFLUENCE OF METAL-SURFACE AND SULFUR ADDITION ON COKE DEPOSITION IN THE THERMAL-CRACKING OF HYDROCARBONS. *Ind. Eng. Chem. Res.* **1995,** 34, (3), 773-785.
26. Brown, D. E.; Clark, J. T. K.; Foster, A. I.; McCarroll, J. J.; Sims, M. L., Inhibition of Coke Formation in Ethylene Steam Cracking. In *Coke Formation on Metal Surfaces*, AMERICAN CHEMICAL SOCIETY: 1983; Vol. 202, pp 23-43.
27. Wang, J.; Reyniers, M.-F.; Marin, G. B., The influence of phosphorus containing compounds on steam cracking of n-hexane. *Journal of Analytical and Applied Pyrolysis* **2006,** 77, (2), 133-148.
28. Vaish, S.; Kunzru, D., Triphenyl phosphite as a coke inhibitor during naphtha pyrolysis. *Industrial & Engineering Chemistry Research* **1989,** 28, (9), 1293-1299.
29. Dhuyvetter, I.; Reyniers, M.-F.; Froment, G. F.; Marin, G. B.; Viennet, D., The influence of dimethyl disulfide on naphtha steam cracking. *Industrial & Engineering Chemistry Research* **2001,** 40, (20), 4353-4362.
30. Bajus, M.; Vesely, V.; Baxa, J.; Leclercq, P. A.; Rijks, J. A., Steam cracking of hydrocarbons: 5. Effect of thiophene on reaction-kinetics and coking. *Industrial & Engineering Chemistry Product Research and Development* **1981,** 20, (4), 741-745.
31. Bajus, M.; Vesely, V., Pyrolysis of hydrocarbons in the presence of elemental sulfur. *Collection of Czechoslovak Chemical Communications* **1980,** 45, (1), 238-254.
32. Bajus, M.; Baxa, J.; Leclercq, P. A.; Rijks, J. A., Steam cracking of hydrocarbons: 6. Effect of dibenzyl sulfide and dibenzyl disulfide on reaction-kinetics and coking. *Industrial & Engineering Chemistry Product Research and Development* **1983,** 22, (2), 335-343.
33. Bajus, M.; Baxa, J., Coke formation during the pyrolysis of hydrocarbons in the presence of sulfur-compounds. *Collection of Czechoslovak Chemical Communications* **1985,** 50, (12), 2903-2909.
34. Depeyre, D.; Filcoteaux, C.; Blouri, B.; Ossebi, J. G., Pure norma-nonane steam cracking and the influence of sulfur-compounds. *Industrial & Engineering Chemistry Process Design and Development* **1985,** 24, (4), 920-924.

35. Dhuyvetter, I.; Reyniers, M. F.; Froment, G. F.; Marin, G. B.; Viennet, D., The influence of dimethyl disulfide on naphtha steam cracking. *Ind. Eng. Chem. Res.* **2001,** 40, (20), 4353-4362.

36. Towfighi, J.; Sadrameli, M.; Niaei, A., Coke formation mechanisms and coke inhibiting methods in pyrolysis furnaces. *J. Chem. Eng. Jpn.* **2002,** 35, (10), 923-937.

37. Holmen, A.; Lindvaag, O. A.; Trimm, D. L., COKE FORMATION DURING STEAM CRACKING OF HYDROCARBONS .2. EFFECT OF PREOXIDATION AND PREREDUCTION OF THE REACTOR SURFACE. *Journal of Chemical Technology and Biotechnology a-Chemical Technology* **1985,** 35, (7), 358-364.

38. Horsley, G. W.; Cairns, J. A., The Inhibition of Carbon Deposition on Stainless Steel by Prior Selective Oxidation. *Appl. Surf. Sci.* **1984,** 18, 273.

39. Luan, T. C.; Eckert, R. E.; Albright, L. F., Gaseous pretreatment of high-alloy steels used in ethylene furnaces: Pretreatment of incoloy 800. *Ind. Eng. Chem. Res.* **2003,** 42, (20), 4741-4747.

40. Jakobi, D.; Karduck, P.; Freiherr, V. R. A., The High-Temperature Corrosion Resistance of Spun-Cast Materials for Steam-Cracker Furnaces - A Comparative Study of Alumina- and Chromia-Forming Alloys. In *NACE Corrosion 2013*, 2013.

41. Jakobi, D.; van Moesdijk, C.; Karduck, P.; von Richthofen, A., Tailor-made materials for high temperature applications: New strategies for radiant coil material development. *CORROSION* **2009**.

42. Asteman, H.; Hartnagel, W.; Jakobi, D., The Influence of Al Content on the High Temperature Oxidation Properties of State-of-the-Art Cast Ni-base Alloys. *Oxid. Met.* **2013,** 80, (1-2), 3-12.

43. Srinivas, V. R.; Humblot, F., Compositions to mitigate coke formation in steam cracking of hydrocarbons. In Google Patents: 2011.

44. Tong, Y.; Poindexter, M. K., Method of inhibiting coke deposition in pyrolysis furnaces. In Google Patents: 1999.

45. Sarris, S. A.; Olahova, N.; Verbeken, K.; Reyniers, M.-F.; Marin, G. B.; Van Geem, K. M., Optimization of the in-situ pretreatment of high temperature Ni-Cr Alloys for Ethane steam cracking. *Ind. Eng. Chem. Res.* **2017**.

46. Gary Barone, M. H., David Smith , Restek Corporation Performance Coatings; Shawn Rowan, W. J. G., O'Brien Corporation; Phil Harris, H. L. Sulfinert® Treated Systems Preserve ppb Levels of Active Sulfur Compounds.

Chapter 5: Ti-base alloy evaluation

This chapter includes the following manuscript:

5. Ti-base alloy coking behavior during steam cracking of ethane

Sarris, S. A.; Reyniers, M.-F.; Marin, G. B.; Van Geem, K. M.

To be submitted

5.1 Abstract

Reactor material technologies are in the core of the research around anti-coking technologies. In an effort to evaluate the coking performance of a Ti-base alloy under ethane steam cracking conditions, a thermogravimetric experimental study was performed in a jet stirred reactor under industrially relevant conditions ($T_{gasphase}$ = 1173 K, P_{tot} = 0.1 MPa, X_{C2H6} = 70 %, dilution δ= 0.33 kg_{H2O}/kg_{HC}). As a first step, the optimal pretreatment for Fe-Ni-Cr Alloys was applied and compared with a pretreatment at increased temperature, aiming at a better oxidation of the surface and thus coking behavior of the material. The results indicated decreased coking rates of the Ti-Alloy at the expense of the pronounced formation of carbon oxides. Additionally, the tested coupons showed crack propagation after application of cyclic aging and cooling down back to

ambient conditions. Therefore, the tested Ti-Alloy cannot be considered an industrially interesting steam cracking reactor alloy. Additionally, scanning electron microscopy combined with energy-dispersive X-ray spectroscopy was used to characterize the metal surface and cross section morphology of the studied samples and the coke morphology. Thus suggested that the rapid and disorderly oxidation of the surface and bulk made the alloy brittle leading to observable crack initiation and propagation.

Keywords: Ti-base alloy, carburization, steam cracking, pretreatment, cracking, thermal cracking, oxidation, ethane, coke formation, aging, jet stirred reactor, cyclic aging

5.2 Introduction

The predominant process to manufacture light olefins is steam cracking of hydrocarbons. The major problem occurring during this process is the coke deposition on the inner wall of the tubular crackers. The formed coke layer reduces the available reactant cross-sectional area causing elevated pressure drop along the reactor. These promote bimolecular over monomolecular reactions, decreasing the olefin selectivity. As a result, more energy is required to maintain the cracking severity and the desired selectivity[1, 2]. When the metallurgic limits are reached or the pressure drop over the reactor is excessive, the operation is ceased and decoking of the reactor is necessary, typically lasting 48 h. The latter affects negatively the process finance[3]. In an effort to mitigate coke formation several anti-coking technologies have been evolved, namely 3-D reactor technologies[4-6], application of additives[7-10] and use of advanced surface technologies[11-17]. Innovative high temperature alloys belong in the last category.

The present work, testing the cracking behavior of a Ti-base alloy, belongs clearly in the latter category. Titanium and titanium alloys are excellent candidates for aerospace applications owing to their high strength to weight ratio and excellent corrosion resistance.[18] The effect of titanium additions on the microstructure and precipitation properties of Fe-Bi-Al-Cr ferritic alloys has been evaluated by Rawlings et al[19]. In general, addition of Titanium in the alloys is found to improve the tensile, toughness, creep properties and corrosion resistance[20]. Most of the times enriches the composition of a high temperature alloy in concentrations of 0 to 10 wt %[21], aiming at an increased rigidity. However, to the best of the knowledge of the authors, it has not been used as base material for crackers, therefore no quantitative or qualitative coking behavior observations are available. In order to evaluate the coking performance of this alloy under ethane steam cracking conditions, an experimental study was performed in a jet-stirred reactor thermogravimetric set-up. As a first step, the optimum pretreatment of Fe-Ni-Cr alloys was applied and compared with a pretreatment increased by 100 K temperature. This, based on the available literature[22-25], aimed at a better oxidation of the surface, thus at an improved coking behavior of the material. According to that a factor 8 increase in the absolute weight of oxides is expected by increasing the temperature from 1173 K to 1273 K.

Coking results were obtained proving the concept, allowing comparison of the standard treatment used for Fe-Ni-Cr alloys with the one at higher oxidation temperature. Additionally, a comparison with a well-known 25/35 Cr/Ni alloy allowed evaluation of the coking behavior of the new alloy. SEM and EDX results helped with the interpretation of the experimental results justifying the potentials of the new alloy.

5.3 Experimental section

5.3.1 Electrobalance set-up

Similary to previous work, the jet stirred reactor set-up is used for the performed experiments [11, 12, 26], therefore, only a brief description is given here. The set-up consists out of three parts: a feed section, a reactor section and an analysis section as shown in Figure 5. 1. The mass flow rates of gasses and water are controlled by thermal mass flow controllers. All the lines in contact with sulfur are Sulfinert®-treated[27]. The water is vaporized to steam in an evaporator, mixed with the heated hydrocarbon feedstock and further heated before entering the reactor inlet at a temperature of 903 K. A jet stirred reactor made out of quartz is used, with a flat coupon in the center of the JSR suspended from the arm of an electrobalance. The coupon dimensions are 10 mm × 8 mm × 1 mm. The mass changes are tracked over time with a frequency of 1 Hz. Subsequently, the reactor effluent is quenched to prevent further cracking and its composition is measured with two gas chromatographs (GC) using nitrogen as internal standard i.e. a refinery gas analyzer dedicated to the analysis of components with less than 5 carbon atoms and a TRACE^{TM} Ultra GC detecting hydrocarbons ranging from methane to naphthalene. For ethane cracking no heavier products are measured than naphthalene. In detail, from the peak areas of the TCD-channel, experimentally determined calibration factors and the known amount of nitrogen, the flows of hydrogen, methane, carbon oxides and C2 hydrocarbons are calculated. The calculated methane flow is subsequently used as internal standard for the flow determination of higher hydrocarbons in the FID-channels. A schematic representation of the use of internal standards is given in supporting information.

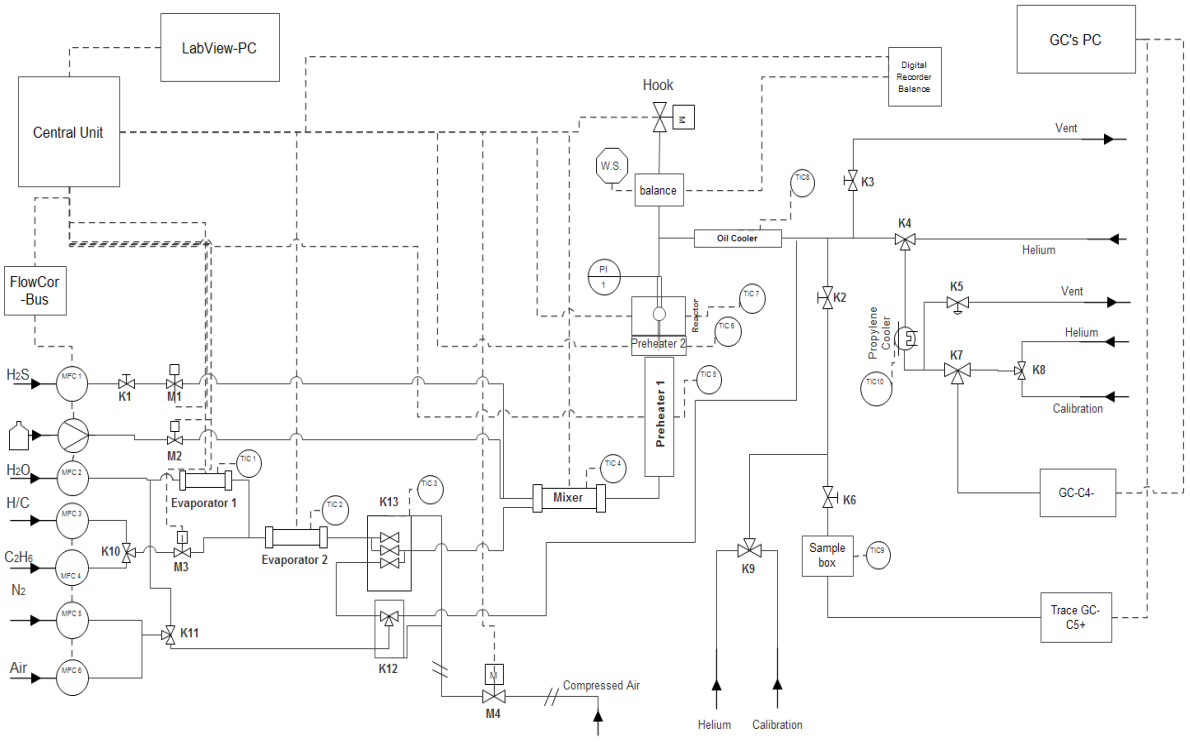

Figure 5. 1: Process Flow Diagram of the thermogravimetric set-up for the study of coke deposition during steam cracking of ethane

5.3.2 Experimental procedures and conditions

Four The coking performance of the new Ti-base alloy under ethane steam cracking conditions was evaluated in the JSR set-up. Initially, the effect of the in-situ pretreatment was evaluated under blank ethane steam cracking conditions.

As mentioned above, a higher temperature pre-oxidation - 1273 K instead of 1173 K - than the optimized for Fe-Ni-Cr alloys should increase significantly the absolute weight of oxides formed on Titanium[23, 24]. Based on previous work the formation of a uniform and thick oxide layer can improve the anti-coking behavior of a material[11, 12, 26]. However, to the best of the knowledge of the authors, no coking rates results are available for Ti-base alloys. Therefore, the

Ti-base alloy was tested under industrially relevant conditions for two different pretreatments, the optimized for Fe-Ni-Cr alloys and one at higher oxidation temperature.

Table 5. 1 and Table 5. 2 summarize the experimental conditions and sequences under the two different pretreatments.

Table 5. 1: Conditions of the two different applied pretreatments

Pretreatment		**Steps**		
	Id	**1**	**2**	**3**
Optimized Fe-Ni-Cr pretreatment	***A***	$6.7 \cdot 10^{-3}$ Nl s^{-1} of Air; 14h; T=1023 K	1:1 $8.15 \cdot 10^{-3}$ Nl s^{-1} of Air:N_2; 30 min; T=from 1023 K to 1173 K	$8.15 \cdot 10^{-3}$ Nl s-1 of Air and $6.67 \cdot 10^{-6}$ kg s^{-1} Steam; 15min ; T=1173 K
High Temperature Preoxidation + Steam Treatment at higher temperature	***B***	$6.7 \cdot 10^{-3}$ Nl s^{-1} of Air; 14h; T=1023 K	1:1 $8.15 \cdot 10^{-3}$ Nl s^{-1} of Air:N_2; 30 min; T=from 1023 K to 1273 K	$8.15 \cdot 10^{-3}$ Nl s^{-1} of Air and $6.67 \cdot 10^{-6}$ kg s^{-1} Steam; 15min ; T=1273 K

Table 5. 2: Experimental sequence during the two performed pretreatments

	1023 K Air	1023-> 1173 K N_2+Air	1173 K Air+H_2O	1173 K C_2H_6 +H_2O	1023-> 1173 K N_2+Air	1173 K Air +H_2O	1173 K C_2H_6 +H_2O	1023-> 1173 K N_2+Air	1173 K Air +H_2O	1173-> 273 K He	
A	In situ Pre-oxidation 14 h	mild Pre-oxidation 30 min	Steam Treatment 15 min	1st coking cycle of 6 h	Decoking 30 min	Steam Treatment 15 min	2^{nd}-8^{th} coking cycle of [2^{nd}, 3^{rd} and 8^{th} of 6 h, 4-7^{th} of 1 h]	Decoking 30 min	Steam Treatment 15 min	cooling down	time
	1023 K Air	1023-> 1273 K N_2+Air	1273 K Air+H_2O	1173 °C C_2H_6 +H_2O	1023-> 1273 K N_2+Air	1273 K Air +H_2O	1173 K C_2H_6 +H_2O	1023-> 1273 K N_2+Air	1273 K Air +H_2O	1273-> 273 K He	
B	In situ Pre-oxidation 14 h	High T Pre-oxidation 50 min	Steam Treatment 15 min	1st coking cycle of 6 h	Decoking at higher T 50 min	Steam Treatment 15 min	2nd-8th coking cycle of [2^{nd}, 3^{rd} and 8^{th} of 6 h, 4-7^{th} of 1 h]	Decoking at higher T 50 min	Steam Treatment 15 min	cooling down	time

5.3.3 Coking rate calculation

The coke deposition is measured over time by continuously weighing the mass of the hanged sample. This allows the determination of the total amount of coke after every cracking cycle, as well as the calculation of the initial catalytic coking rate and the asymptotic pyrolytic coking rate. Similarly with previous work [11, 12, 26], the coking rate is determined as:

$$R_c = \frac{m_{t_2} - m_{t_1}}{t_2 - t_1} \frac{1}{S} \quad (5.1)$$

where R_c is the coking rate in $kg \cdot s^{-1} \cdot m^{-2}$, mt_j the mass of coke at time j in kg, t_j the experimental time at instant j in s and S the surface area of the coupon in m^2.

The mean value of the coking rate between 15 minutes and 60 minutes is defined as the initial or catalytic coking rate, i.e. characterizing the catalytic coking behavior of the sample. The asymptotic coking rate is related to the pyrolytic coking mechanism and is reported as the mean measured coking rate between the 5^{th} and 6^{th} hour of cracking.

5.3.4 Scanning Electron Microscope and Energy Dispersive X-ray Analysis

Scanning Electron Microscopy (SEM) and Energy Dispersive X-ray Spectroscopy (EDX) are used to obtain information regarding the surface morphology and to perform chemical analysis. Top surface analyses are performed in both 10 and 20 kV, giving insight for the top surface and mid-range surface of the coupon, respectively. As shown in Figure 5. 2, the top surface analyses gave a qualitative idea of the elemental composition of the surface, and was performed at 10 kV and 20 kV, while the cross sectional mappings evaluated the uniformity of the oxides generated during each applied pretreatment. The surface composition is an average of EDX analyses on two

different locations of the examined coupons. Analyses are performed for coked and pretreated samples.

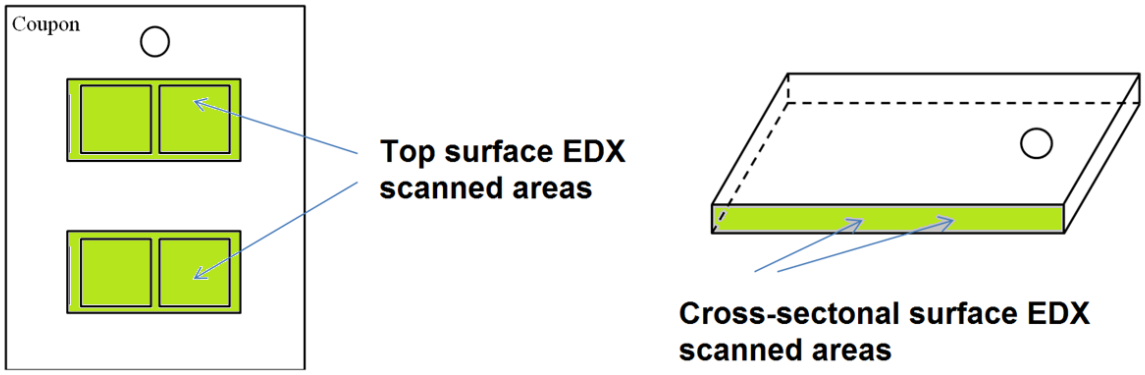

Figure 5. 2: Representation of the top surface analysis (left) and cross-sectional (right) analysis of the examined coupons

5.4 Experimental results

Table 5. 3 illustrates the most important mass yields during ethane cracking. For a better comparison the effluent results of a typically used material are also included. A factor 10 and 300 increased values of CO, for the optimized for Fe-Ni-Cr alloys and higher temperature pretreatment respectively, were measured over the 8 cracking cycles in comparison with the Fe-Ni-Cr alloy. For CO_2, the effect was less pronounced; only after application of the high temperature pre-oxidation (B) an increase of a factor 3 was observed. In addition, the increase of Carbon oxides is followed by an increase of H_2. A minor decrease of CH_4 is also noticed, however it is still within the error margin of measured values. The observations support the idea that Ti and/or Ti-oxides present on the surface have a catalytic effect towards coke gasification. These results prove that the Ti-base alloy is significantly worse than the reference material.

Table 5. 3: Averaged (over the 8 cracking cycles) mass product yields. Ethane steam cracking: F_{HC}= 29.18 x 10^{-6} kg s^{-1}, δ= 0.33 kg_{H2O} kg^{-1}_{HC}, $T_{reactor}$= 1173.15 K, P= 101.35 kPa, F_{H2O}=9.72 x 10^{-6} kg s^{-1}

Components [wt%]	Fe-Ni-Cr alloy A	Ti-base alloy A	Ti-base alloy B
H_2 [±0.07]	4.24	4.39	4.45
CO_2 [±0.003]	0.006	0.005	0.019
CO	0.05 [1]	0.56 [2]	1.87 [3]
CH_4 [±0.21]	6.99	6.97	6.91
C_2H_6 [±0.52]	30.13	30.19	30.06
C_2H_4 [±0.25]	49.86	49.61	49.57
C_3H_8 [±0.03]	0.11	0.11	0.11
C_3H_6 [±0.02]	0.74	0.70	0.69
C_2H_2 [±0.05]	1.38	1.46	1.41
1,3-C_4H_6 [±0.07]	2.00	1.93	1.89
Benzene [±0.13]	2.46	2.53	2.53

[1] [±0.008], [2] [±0.07], [3] [±0.35]

Nevertheless, coking rates results are also processed and summarized in Table 5. 4. For a qualitative comparison of the coking performance, the results of the reference material during continuous addition of 41 ppmw S/HC of DMDS are presented as well. As it is observed in Figure 5. 3 and Figure 5. 4, independently on the cracking cycle the Ti-base alloy performs significantly worse than the reference material. The increased temperature pretreatment improves the coking rates of the Ti-base alloy. However, this improved coking behavior still keeps the Ti-base alloy out of competition against the blank reference coking behavior. In terms of anti-coking performance, the Ti-base alloy is placed between the reference during steam cracking with continuous addition of DMDS and the reference with no DMDS addition.

Additionally, the reference material maintains a rather stable coking behavior over cyclic aging, while the sample of the Ti-base alloy shows increased coking after several cycles.

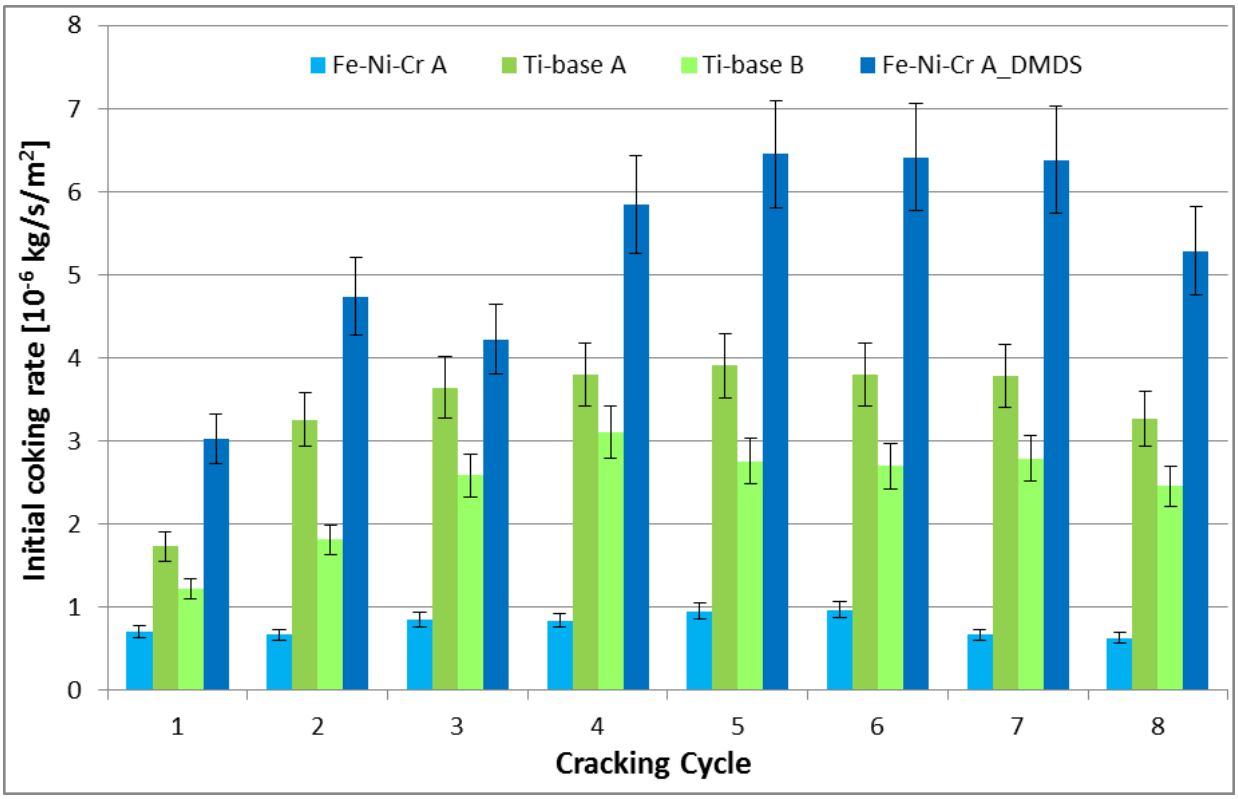

Figure 5. 3: Calculated initial coking rates for the reference 25/35 Cr/Ni and Ti-base alloy

The most problematic result obtained for the Ti-base Alloy coupons was their behavior after cooling down to ambient conditions. More specifically, the coupons broke either in slices or in smaller pieces. In Figure 5. 5, an indication of the thickness decrease after cracking and of the thickness of the slices is given. Clearly, thick oxides are formed during oxidation of Ti, making the coupon more brittle as material towards mechanical stresses. The latter leads to the formation of cracks due to the mechanical stresses evolved during cooling down at temperatures lower than 1023 K. An additional example of a cracked coupon is given in Figure 5. 6. To illustrate more

accurately the crack formed on the coupons and for a better understanding of the phenomenon, SEM and EDX analyses are performed.

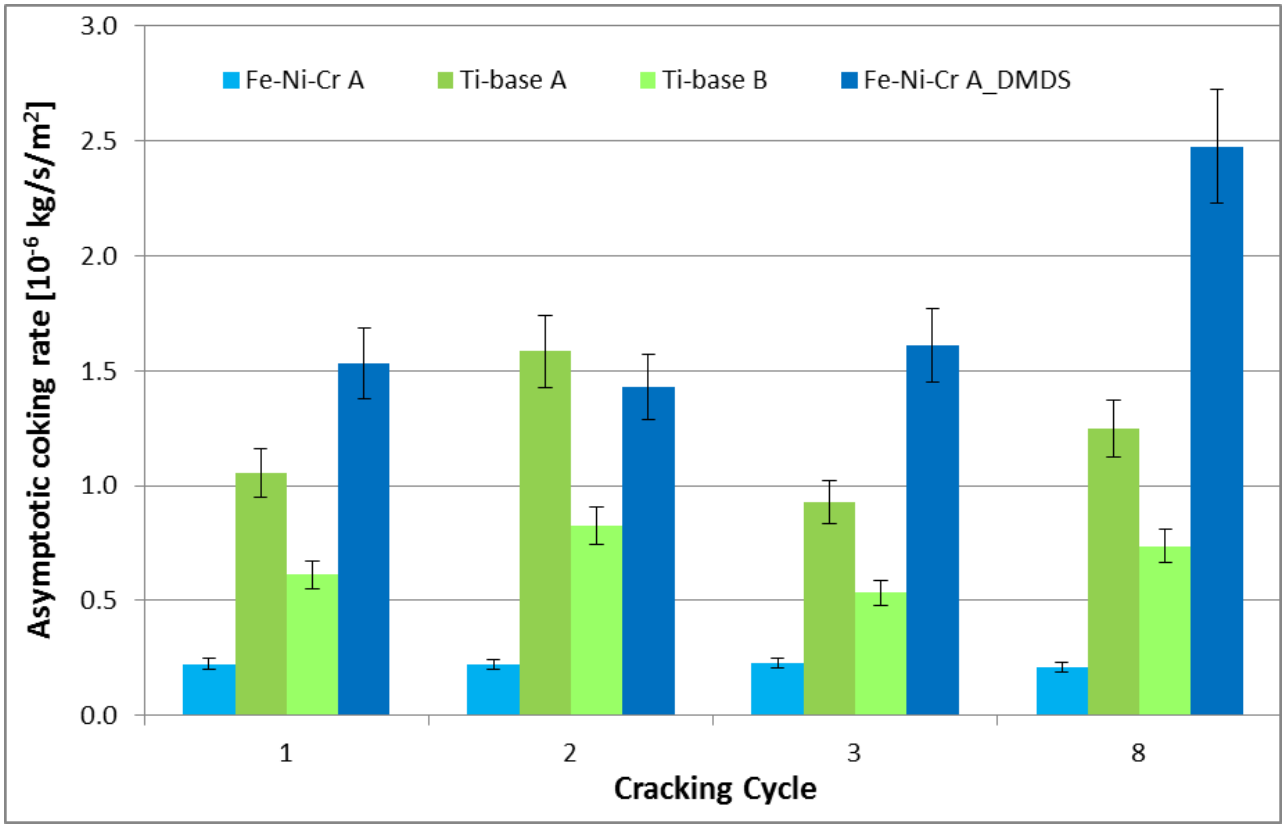

Figure 5. 4: Calculated asymptotic coking rates for the reference 25/35 Cr/Ni and Ti-base alloy

Table 5. 4: Calculated initial (average 15min-60min) and asymptotic (average 5h-6h) coking rates. Ethane steam cracking: F_{HC}= 29.18 x 10^{-6} kg s^{-1}, δ= 0.33 kg_{H2O} kg^{-1}_{HC}, $T_{reactor}$= 1173.15 K, P= 101.35 kPa, F_{H2O}=9.72 x 10^{-6} kg s^{-1}.

Alloy Conditions	Fe-Ni-Cr alloy Blank	Ti-base alloy Blank	Ti-base alloy Blank	Fe-Ni-Cr alloy CA
Pretreatment	A	A	B	A
Cracking Temperature (K)	1173	1173	1173	1173
dilution	0.33	0.33	0.33	0.33
CA DMDS (ppmw S per HC)	0	0	0	41
Cc	Coke formed (mg)			
1	1.29	5.48	3.66	7.55
2	1.26	9.01	4.99	8.38
3	1.41	7.43	4.82	8.66
4	0.60	3.57	2.93	4.12
5	0.67	3.03	2.17	4.55
6	0.69	2.97	2.13	4.53
7	0.47	2.95	2.32	4.51
8	1.19	7.69	5.35	12.46
Cc	Initial coking rate [10^{-6} kg/s/m^2]			
1	0.71	1.73	1.23	3.03
2	0.67	3.26	1.81	4.74
3	0.86	3.65	2.59	4.23
4	0.85	3.80	3.11	5.85
5	0.96	3.91	2.76	6.45
6	0.97	3.80	2.70	6.42
7	0.67	3.79	2.79	6.39
8	0.63	3.27	2.46	5.29
Cc	Asymptotic coking rate [10^{-6} kg/s/m^2]			
1	0.22	1.06	0.61	1.53
2	0.22	1.58	0.83	1.43
3	0.23	0.93	0.53	1.61
8	0.21	1.25	0.74	2.47

Figure 5. 5: Thickness values of the Ti-base alloy before cracking (left), after cracking (middle) and of a broken slice (right), pretreated at 1173 K

Figure 5. 6: Broken Ti-base alloy coupon after cracking pretreated at 1273 K

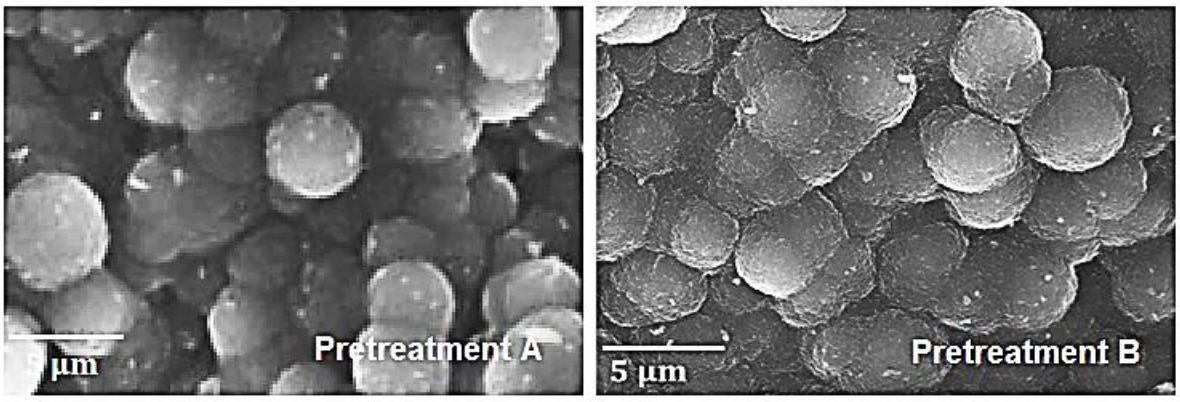

Figure 5. 7: Coke formed on top of the surface of the Ti-base alloy after application of the optimized pretreatment of Fe-Ni-Cr alloys.

In Figure 5. 7, the coke structure after the pretreatment A and pretreatment B is illustrated, during pyrolytic coke formation. The observed structure seems rather similar, implying that the mechanism of coke formation was not different in the two pretreatments, however the available surface due to the crack formation and the oxides coverage of the surface were probably more pronounced. The cross sectional analyses of the two samples treated at the two different temperatures reveal part of the phenomenon occurring in this study (Figure 5. 8 and Figure 5. 9). At the standard temperature, 1173 K, 0.1 to 0.2 μm thick oxides are formed and spalling off the coupon from both sides leaving no oxide covering the surface. At 1273 K, thick oxides are formed leading to oxidation of almost the whole coupon volume. Clearly the oxides that are formed are quite brittle. Thus, they are separating from the core of the coupon. In the case of the increased temperature oxidation, the core is too thin, therefore the crack is propagating causing breakage of the coupon in smaller pieces. Based on Figure 5. 10, a comparison of the Ti-base alloy with the reference alloy can be done. It is obvious that the uniformity of the oxides formed on top of this alloy allows a sufficient coverage of the catalytic active sites.

Combining the above experimental results with the formation of cracks on the samples' surface can give a fruitful insight on the phenomenon. Based on the increased values of carbon oxides and H_2 differences of the yields, an increased catalytic surface of the Ti-base alloy samples can be assumed, which is most probably derived from the presence of the surface cracks. As a result both coke formation and coke gasification were catalyzed.

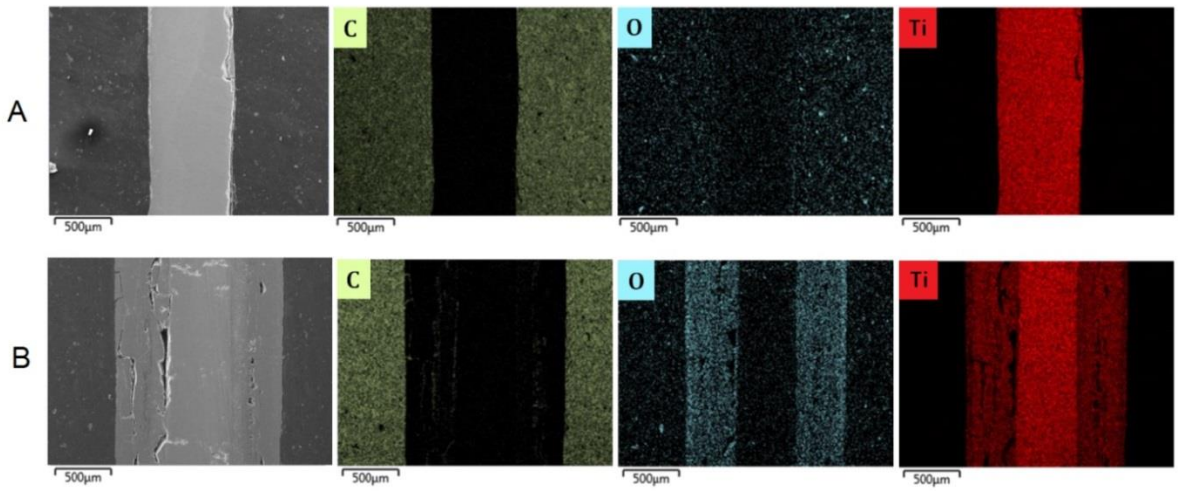

Figure 5. 8: SEM and EDX cross sectional analysis of the two pretreatments. A is referring to temperature of 1173 K and B to 1273 K.

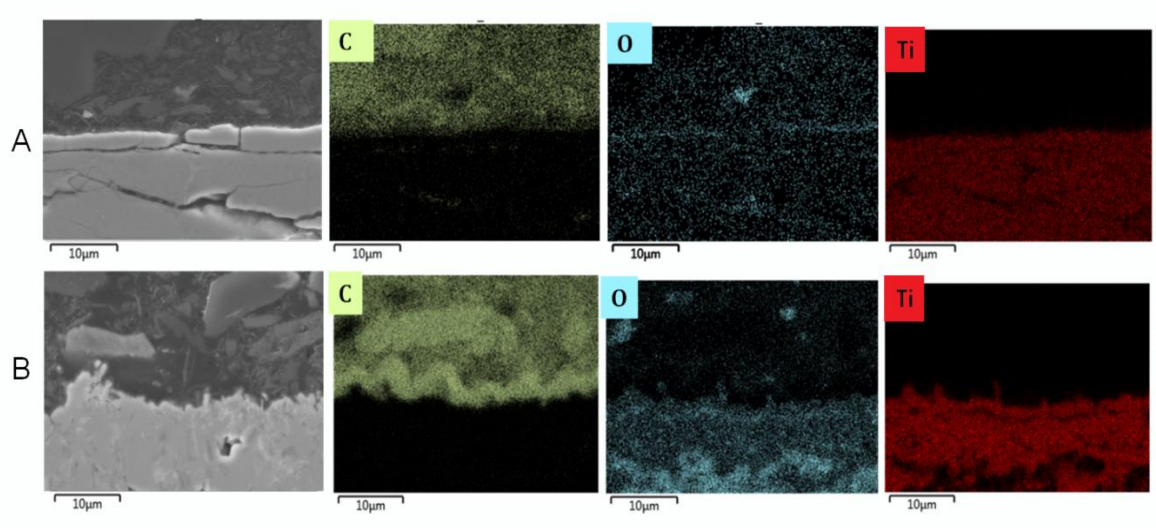

Figure 5. 9: SEM and EDX cross sectional analysis of the two pretreatments. A is referring to temperature of 1173 K and B to 1273 K.

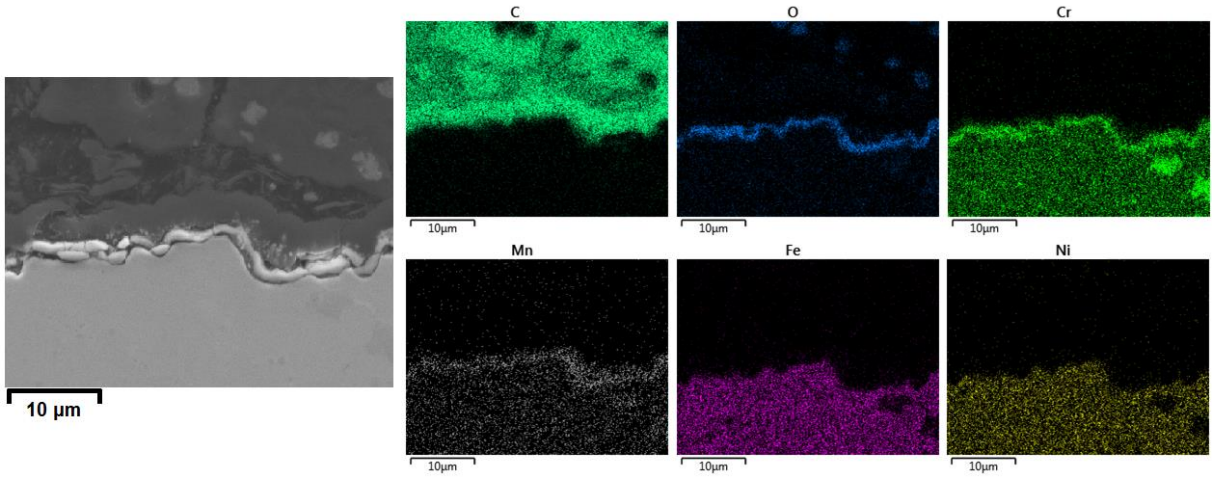

Figure 5. 10: SEM and EDX cross sectional elemental mappings for the reference 25/35 Cr/Ni alloy.

5.5 Conclusions

Four different super alloys were experimentally evaluated under 5 different conditions in terms of anti-coking performance. Overall, the worst performance was noticed for the 25/35 Cr/Ni alloy. In the absence of DMDS, the Al-content material performed from 2 to 3 times worse than the competition, while the non Al alloys performed rather similarly. When DMDS was added continuously in the feed the best performance was noted by the higher Cr/Ni content alloy, while the worst from the 25/35 Cr/Ni one. The Al-containing alloy performed similarly to slightly better than the 35/45 Cr/Ni alloy, showing the Al anti-coking performance. The effect of presulfiding is more pronounced in the case that it is applied on a Blank run than on a CA run. The Al-content alloy had the most stable behavior after application of presulfiding, being slightly better than the 35/45 Cr/Ni alloy, yet worse than the 40/48 Cr/Ni one. The existence of Cr, Mn and Al on top of the surface are already known to improve the anti-coking behavior of an alloy, but their relative anti-coking performance has not been evaluated yet. Adding Al is not sufficient

to create a super alloy with strong anti-coking capabilities. The relative coking reactivity of Fe is higher than the one of Ni. Also, the existence of Mn on top of the surface seems to improve the anti-coking behavior of an alloy at cracking temperatures higher than 1173 K in comparison with the ones of Cr or Al.

5.6 References

1. Rao, M. R.; Plehiers, P. M.; Froment, G. F., The coupled simulation of heat transfer and reaction in a pyrolysis furnace. *Chemical engineering science* **1988,** 43, (6), 1223-1229.
2. Stefanidis, G.; Merci, B.; Heynderickx, G. J.; Marin, G. B., CFD simulations of steam cracking furnaces using detailed combustion mechanisms. *Computers & chemical engineering* **2006,** 30, (4), 635-649.
3. Heynderickx, G.; Schools, E.; Marin, G., Optimization of the decoking procedure of an ethane cracker with a steam/air mixture. *Industrial & engineering chemistry research* **2006,** 45, (22), 7520-7529.
4. Brown, D. J., Internally finned radiant coils: A valuable tool for improving ethylene plant economics. In *6th EMEA Petrochemicals Technology Conference*, London, UK, 2004.
5. Albano, J.; Sundaram, K.; Maddock, M. *Application of extended surfaces in pyrolysis coils*; New York, NY; American Institute of Chemical Engineers: 1988.
6. Schietekat, C. M.; van Goethem, M. W. M.; Van Geem, K. M.; Marin, G. B., Swirl flow tube reactor technology: An experimental and computational fluid dynamics study. *Chem. Eng. J.* **2014,** 238, (0), 56-65.
7. Reyniers, M.-F. S. G.; Froment, G. F., Influence of Metal Surface and Sulfur Addition on Coke Deposition in the Thermal Cracking of Hydrocarbons. *Ind. Eng. Chem. Res.* **1995,** 34, (3), 773-785.
8. Wang, J.; Reyniers, M.-F.; Marin, G. B., Influence of Dimethyl Disulfide on Coke Formation during Steam Cracking of Hydrocarbons. *Ind. Eng. Chem. Res.* **2007,** 46, (12), 4134-4148.

9. Wang, J.; Reyniers, M.-F.; Marin, G. B., The influence of phosphorus containing compounds on steam cracking of n-hexane. *Journal of Analytical and Applied Pyrolysis* **2006,** 77, (2), 133-148.
10. Wang, J.; Reyniers, M.-F.; Van Geem, K. M.; Marin, G. B., Influence of Silicon and Silicon/Sulfur-Containing Additives on Coke Formation during Steam Cracking of Hydrocarbons. *Ind. Eng. Chem. Res.* **2008,** 47, (5), 1468-1482.
11. Muñoz Gandarillas, A. E.; Van Geem, K. M.; Reyniers, M.-F.; Marin, G. B., Influence of the Reactor Material Composition on Coke Formation during Ethane Steam Cracking. *Ind. Eng. Chem. Res.* **2014,** 53, (15), 6358-6371.
12. Muñoz Gandarillas, A. E.; Van Geem, K. M.; Reyniers, M.-F.; Marin, G. B., Coking Resistance of Specialized Coil Materials during Steam Cracking of Sulfur-Free Naphtha. *Ind. Eng. Chem. Res.* **2014,** 53, (35), 13644-13655.
13. Verdier, G.; Carpentier, F., Consider new materials for ethylene furnace applications: An innovative metallurgy solves maintenance issues. *Hydrocarbon processing* **2011,** 90, (5), 61-62.
14. Wolpert, P.; Ganser, B.; Jakobi, D.; Kirchheiner, R., Using steam; tube with uniform cross-section; pyrolysis; antideposit agents; interior fins; swirling gas flow. In Google Patents: 2005.
15. Jakobi, D.; van Moesdijk, C.; Karduck, P.; von Richthofen, A., Tailor-made materials for high temperature applications: New strategies for radiant coil material development. *CORROSION* **2009**.
16. Jakobi, D.; Karduck, P.; von Richthofen, A. F., The High-Temperature Corrosion Resistance of Spun-Cast Materials for Steam-Cracker Furnaces-A Comparative Study of Alumina-and Chromia-Forming Alloys. *CORROSION* **2013**.
17. Asteman, H.; Hartnagel, W.; Jakobi, D., The Influence of Al Content on the High Temperature Oxidation Properties of State-of-the-Art Cast Ni-base Alloys. *Oxidation of Metals* **2013,** 80, (1-2), 3-12.
18. Zhang, S.; Zeng, W.; Gao, X.; Zhou, D.; Lai, Y., Role of titanium carbides on microstructural evolution of Ti-35V-15Cr-0.3Si-0.1C alloy during hot working. *Journal of Alloys and Compounds* **2016,** 684, 201-210.

19. Rawlings, M. J. S.; Liebscher, C. H.; Asta, M.; Dunand, D. C., Effect of titanium additions upon microstructure and properties of precipitation-strengthened Fe-Ni-Al-Cr ferritic alloys. *Acta Materialia* **2017,** 128, 103-112.
20. Polmear, I.; StJohn, D.; Nie, J.-F.; Qian, M., 7 - Titanium Alloys. In *Light Alloys (Fifth Edition)*, Butterworth-Heinemann: Boston, 2017; pp 369-460.
21. Petrone, S. S. A.; Mandyam, R. C.; Wysiekierski, A. G., Surface alloyed high temperature alloys. In Google Patents: 2000.
22. Kumar, S.; Sankara Narayanan, T. S. N.; Ganesh Sundara Raman, S.; Seshadri, S. K., Thermal oxidation of Ti6Al4V alloy: Microstructural and electrochemical characterization. *Materials Chemistry and Physics* **2010,** 119, (1–2), 337-346.
23. Kofstad, P.; Anderson, P. B.; Krudtaa, O. J., Oxidation of titanium in the temperature range 800–1200°C. *Journal of the Less Common Metals* **1961,** 3, (2), 89-97.
24. Kofstad, P., High-temperature oxidation of titanium. *Journal of the Less Common Metals* **1967,** 12, (6), 449-464.
25. Kumar, S.; Narayanan, T. S. N. S.; Raman, S. G. S.; Seshadri, S. K., Thermal oxidation of CP-Ti: Evaluation of characteristics and corrosion resistance as a function of treatment time. *Materials Science and Engineering: C* **2009,** 29, (6), 1942-1949.
26. Sarris, S. A.; Olahova, N.; Verbeken, K.; Reyniers, M.-F.; Marin, G. B.; Van Geem, K. M., Optimization of the in-situ pretreatment of high temperature Ni-Cr Alloys for Ethane steam cracking. *Ind. Eng. Chem. Res.* **2017**.
27. Gary Barone, M. H., David Smith , Restek Corporation Performance Coatings; Shawn Rowan, W. J. G., O'Brien Corporation; Phil Harris, H. L. Sulfinert® Treated Systems Preserve ppb Levels of Active Sulfur Compounds.

Chapter 6: Application of coatings

This chapter includes the following manuscripts:

6. Al-based barrier coating for coke reduction in Steam Crackers

Stamatis A. Sarris, Steffen H. Symoens, Natalia Olahova, Reyniers, M.-F.; Marin, G. B.; Van Geem, K. M.

To be submitted

6.1 Abstract

Alumina containing coatings have been claimed as being a major step forwards to improve furnace run lengths used in the ethylene industry. Therefore, in this work a commercial coating CoatAlloy has been compared to the uncoated base material. First, the effect of the coating pretreatment was evaluated in an electro balance set-up during ethane steam cracking under industrially relevant conditions ($T_{gasphase}$ = 1173 K, P_{tot} = 0.1 MPa, X_{C2H6} = 70 %, dilution δ= 0.33 kg_{H2O}/kg_{HC}). Additionally, the effects of presulfiding with 500 ppmw DMDS/H_2O, continuous addition of 41 ppmw S/HC of DMDS, and a combination thereof were evaluated. The tested samples were examined using online thermogravimetry, scanning electron microscopy and

energy diffractive X-ray for surface and cross-section analysis together with X-ray photoelectron spectroscopy and wavelength-dispersive X-ray spectroscopy for surface analysis. The passivating coating was found to perform better than the reference Ni-Cr Fe-base alloy after application of the optimized pretreatment while no effect on the product distribution was observed. Presulfiding of the coating affects negatively the observed coking rates in comparison with the reference alloy. The presence of steam proved to be detrimental for the anti-coking performance of the coating.

Keywords: CoatAlloy, passivating coating, steam cracking, thermal cracking, ethane, coke formation, Ni-Cr alloy, aging, jet stirred reactor

6.2 Introduction

Carbon deposition on the inner wall of industrial steam crackers affects negatively the process economics. During coke formation, the reactor cross-sectional area is reduced, leading to build up of pressure drop over its length. The latter phenomenon results in a change in ethylene selectivity[1, 2], while the highly isolative coke layer decreases the heat transfer coefficient from the furnace to the reactors. To keep the cracking severity stable over time and compensate the additional conductive heat resistance, the fuel flow rate to the furnace burners has to be increased, while the reactor tube metal temperature rises over time. When the coke is exceeding the maximum allowed quantity per set-up, a decoking procedure of typically steam/air mixture is necessary[3-6]. This cyclic cracking-decoking operation borders the annual production capacity having high operating costs. To date, several anti-coking technologies have been introduced and tested in the field of steam cracking, such as three-dimensional (3D) reactor technologies [7-13], feed additives [14-22] and surface technologies [23-26] or combination of them.

Distinction should be made between barrier coatings that passivate the inner wall and catalytic coatings, that convert coke to carbon oxides. A barrier coating passivates the base alloy by covering the active sites responsible for the catalytic coke formation. However, the non-catalytic coke formation through a free-radical mechanism - often termed pyrolytic coke formation - is not prevented. In contrast, catalytic coatings aim not only to eliminate catalytic coke formation by covering the active sites but also to provide catalytic sites for converting radically formed coke to carbon oxides and hydrogen by reaction with steam via gasification reactions.

Several authors have investigated the application of barrier coatings in steam cracking reactors. Zychlinski et al. [27] tested the performance of the AlcroPlex® coating, an Al/Si barrier coating that is applied in a two-step chemical vapor deposition process. The coating managed to suppress the total coke deposition up to 90 % for ethane cracking and up to 80 % for naphtha cracking compared to a reference HP 40 material. Ganser et al. [28] tested also AlcroPlex® in an industrial ethane cracker observing double run length followed by lower CO formation. In addition, decoking was accomplished in less than half the normal time followed by no tube carburization, while the coating seemed essentially unchanged after a year.

NOVA Chemicals and Kubota have developed ANK 400, an inert micron-sized manganese chromium oxide spinel, to reduce both catalytic and pyrolytic coke [29, 30]. Application of fresh ANK400 tubes in two ethane cracking furnaces resulted in a run length increase of more than a factor 10, while subsequent runs had a duration of around 175 days.

Besides the inert barrier coatings, several catalytic coatings have also been developed. The so-called Catalyzed-Assisted Manufacture of Olefins (CAMOL) coating was developed by Quantiam Technologies and Nova Chemicals and it has been commercialized by BASF Qtech since 2011 [25, 31-33]. SK-corporation developed a method of online coating the reactor inner

walls with a catalytic film, called PY-COAT [34]. The method comprises three steps of vapor depositing: a solution of a metal alkoxide and a chromic compound to form a buffer layer on the inner walls; a metal alkoxide as a barrier on the buffer layer and finally an alkali metal/alkaline earth metal compound alone or mixed with metal alkoxides as a decoking layer on the barrier. Application in a Millisecond naphtha cracking furnace more than doubled the run length. Recently, a novel catalytic coating by GE, called 'YieldUp', was evaluated under ethane steam cracking conditions both in a pilot plant and a laboratory scale reactor by Schietekat et al [26]. Although the run length increased even by a factor 6, a quite increased formation of carbon oxides was observed.

Westaim Surface Engineered Products developed another barrier coating, called CoatAlloy [35-37], consisting of an engineered surface, an enrichment pool and diffusion barriers coated on the bulk alloy. In the original patent [38], the intermediary diffusion barrier is an aluminum-containing coating deposited directly onto the bulk alloy substrate prior to deposition of the enrichment pool. The enrichment pool is a MCrAlX material in which M can be nickel, cobalt, iron or an alloy and X is yttrium, hafnium, zirconium, lanthanum or a combination thereof. This enrichment pool and the bulk alloy are heat-treated to metallurgical bond the coating and to form a multiphasic microstructure. The overlay coating is then aluminized by depositing a layer of aluminum and oxidizing the resulting coating to form an alumina surface layer. Between 1995 and 2001 several improvements have been made to the technology resulting in an increased operating limit from 1293 K (Original CoatAlloy^{TM}) to 1333 K (CoatAlloy^{TM} - 1060) and 1373 K (CoatAlloy^{TM} - 1100) [37]. By 2001, CoatAlloy coatings were installed in 25 furnaces globally and typically resulted in a decrease in coking rate by about 90 % [37]. However, no information are available on the exact process conditions used in these furnaces.

In all the anti-coking technologies no exact details are provided on decoking, pretreatment or cracking conditions, therefore the positive impact on the results is not straightforward. For this reason, these technologies have not been used extensively industrially. In the following work, the commercially applied passivating coating CoatAlloy is tested under several industrially relevant conditions in a jet stirred reactor (JSR) set-up after evaluating two different pretreatments. Online coking rates and ex-situ analysis of the surface, by means of SEM and EDX, XPS and WDS of the tested coupons are providing an insight on the occurring phenomena, leading to selection of the optimal conditions for minimizing coking with this passivating technology.

6.3 Experimental section

6.3.1 Electro balance set-up

The coking experiments were performed in a jet stirred reactor set-up equipped with an electro balance [24, 39, 40]. The JSR is designed to carry out thermogravimetric analyses on different reactor materials. Coke formed during the experiments is measured as a function of time under a broad range of conditions covering most of the industrial cases. Therefore, the set-up is capable of evaluating the effect of different pretreatment conditions (e.g. application of additives, temperature and duration of the pretreatment) as well as varying cracking conditions (e.g. use of the feed additives, steam dilution and cracking temperature) on coke formation, product distribution together with surface composition and morphology.

During an experiment, the coke deposited on the metal sample is accurately monitored online and processed afterwards to obtain coking rates. The reactor effluent is online analyzed via gas chromatography to evaluate the cracking conditions. The surface morphology and chemical

composition of the coupons are analyzed by means of SEM and EDX. The combination of the mentioned set-up together with the experimental procedure gives valuable information on the coke formation phenomenon occurring during steam cracking of hydrocarbons and leads to a rather global explanation of the influence of the studied material and conditions.

The experimental set-up with its sequences is described in detail previous work [5, 41] and in Annex D. In the feed section, the hydrocarbon feedstock and water (or water with DMDS) are fed, evaporated, mixed and preheated before sent to the reaction section. There, the steam cracking process is conducted leading to coke formation on the sample. The reactor effluent is quenched using an oil cooler and a fraction of the effluent is withdrawn for online C_{4-} and C_{5+} gas chromatography analysis, while the rest is sent directly to the vent.

6.3.2 Experimental procedures and conditions

The experiments conducted in the JSR set-up consist of three 6 hours coking and decoking cycles, followed by four short cycles of 1 hour and a last cycle of 6 hours to evaluate the effect of cyclic aging on each applied set of conditions. An overview of the experimental sequence followed in the aging experiments together with detailed information on the conditions for each process step is given in Table 6. 1. In case of presulfiding of the reactor, the same sequence of pretreatment and decoking was followed. After oxidation in air at 1023 K and decoking procedure the samples were presulfided at 1100 K introduced to a diluted mixture of DMDS (500 ppmw DMDS per water). Cracking of ethane was performed at similar conditions with previous work[5, 26] (see Table 6. 1). Table 6. 2 summarizes the steps of the followed treatment when the presulfiding step is executed.

Because of the negative noticed effect of nitrogen on the formation and preservation of the Al-oxides[42-45], in the case of the Al-based coating, an alternative treatment is suggested where no

nitrogen was fed during pretreatment or decoking; hence only steam and air was fed to the reactor for 45 min, as summarized in Figure 6. 1.

Table 6. 1: Schematic overview of the coking-decoking experiments with cyclic aging

Process step	Duration	Temperature (K)	Gas feed flow (Nl/s)			Water flow (10^{-6} kg/s)
			N_2	Ethane	Air	
Preoxidation	12-14 hours	1023	-	-	0.0067	-
High-temperature preoxidation	30-40 minutes	Heating up from 1023 to 1173	0.0083[a]	-	0.0083	6.7[a]
Steam treatment	15 minutes	1173	-	-	0.0083	6.7
1st cracking cycle	6 hours	1173	-	0.0241	-	9.7
Decoking	30-40 minutes	Heating up from 1023 to 1173	0.0083[a]	-	0.0083	6.7[a]
Steam treatment	15 minutes	1173	-	-	0.0083	6.7
2nd cracking cycle	6 hours	1173	-	0.0241	-	9.7
Decoking	30-40 minutes	Heating up from 1023 to 1173	0.0083[a]	-	0.0083	6.7[a]
Steam treatment	15 minutes	1173	-	-	0.0083	6.7
3rd cracking cycle	6 hours	1173	-	0.0241	-	9.7
Decoking	30-40 minutes	Heating up from 1023 to 1173	0.0083[a]	-	0.0083	6.7[a]
Steam treatment	15 minutes	1173	-	-	0.0083	6.7
Cyclic aging		Consists of 4 cycles of: · Heating up from 1023 to 1173 K · Cracking at 1173 K (1 hour) · Decoking from 1023 to 1173 K · Steam treatment at 1173 K (15 minutes)				
8th cracking cycle	6 hours	1173	-	0.0241	-	9.7
Decoking	30minutes	Heating up from 1023 to 1173	0.0083[a]	-	0.0083	6.7[a]
Steam treatment	15 minutes	1173	-	-	0.0083	6.7
Cooling down	Not specified	To ambient temperature	-	-	-	-

a: during pretreatment or decoking of the optimized treatment of the experiments of the CoatAlloy material no N_2 was fed and instead a steam/air treatment was performed continuously during decoking

Table 6. 2: Overview of the presulfiding treatment procedure

Process step	Duration	Temperature (K)	Gas feed flow (Nl/s)			Water flow (10^{-6} kg/s)
			N_2	Ethane	Air	
Preoxidation	12-14 hours	1023	-	-	0.0067	-
High-temperature preoxidation	30minutes	Heating up from 1023 to 1173	0.0083[a]	-	0.0083	6.7[a]
Steam treatment	15 minutes	1173	-	-	0.0083	6.7
Cooling down	15 minutes	to 1110	0.0067	-	-	-
Presulfiding	30 minutes	1100	-	-	-	5.6
Cooling down or next cycle	Not specified	To cracking temperature	-	-	-	-

a: during pretreatment or decoking of the CoatAlloy material no N_2 was fed and instead a steam/air treatment was performed continuously during decoking

ID	Treatment				Cracking	Treatment			Cracking	Cooling down or next cycle
Optimal Fe-Ni-Cr	1023 K Air	1023 K -> 1173 K N_2 + Air	1173 K Steam/Air	1100 K Steam with 500 ppmw DMDS/H_2O	1173 K $C_2H_6 + H_2O$	1023 K -> 1173 K N_2 + Air	1173 K Steam/Air	1100 K Steam with 500 ppmw DMDS/H_2O	1173 K $C_2H_6 + H_2O$	time
	OA - 14 h	DEC - 30 min	Steam/Air Treatment	PreS*	1st coking cycle - 6h	DEC - 30 min	Steam/Air Treatment	PreS*	2nd coking cycle - 6h	
Al-content pretreatment	1023 K Air	1023 K -> 1173 K Steam/Air	1173 K Steam/Air	1100 K Steam with 500 ppmw DMDS/H_2O	1173 K $C_2H_6+H_2O$	1023 K -> 1173 K Steam/Air	1173 K Steam/Air	1100 K Steam with 500 ppmw DMDS/H_2O	1173 K $C_2H_6 + H_2O$	time
	OA - 14 h	DEC - 30 min	Steam/Air Treatment	PreS*	1st coking cycle - 6h	DEC - 30 min	Steam/Air Treatment	PreS*	2nd coking cycle - 6h	

* PreS step only for presulfiding experiments

Figure 6. 1: Applied pretreatment sequence per material

6.3.3 Samples: Materials and preparation

The metal coupons made out of 25/35 Cr/Ni on which coke will be deposited are cut as close as possible to the internal surface of industrial tubes in dimensions 10 × 8 × 1 mm³ (total surface area S = 1.96 × 10^{-4} m^2). A schematic drawing of these coupons and a picture of the industrial tubes with a cut coupon are depicted in Figure 6. 2 and Figure 6. 3, respectively.

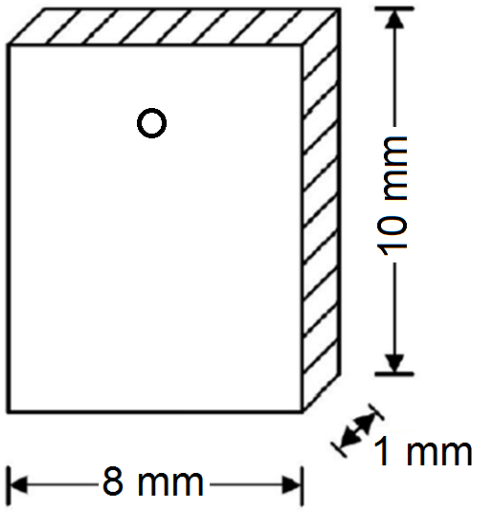

Figure 6. 2: Schematic drawing of coupons dimensions.

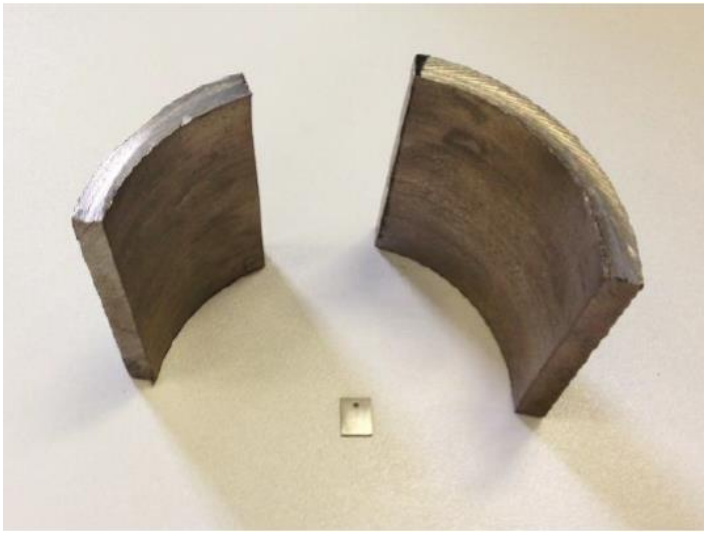

Figure 6. 3: Part of an industrial coil and a JSR coupon.

The composition of the reference alloy is given in Table 6. 3. The detailed composition of CoatAlloy is not commercialized, however its expected cross section build is illustrated on Figure 6. 4.

Table 6. 3: Composition of the reference 25/35 Cr/Ni alloy[46]

C	Mn	Si	Ni	Cr	Mo	Nb	Cu	Fe	Ti, Zr, W
0.45-0.5	< 1.5	1.5 - 2	33 - 36	24 - 27	< 0.5	0.5 - 1	< 0.25	>31.18	add

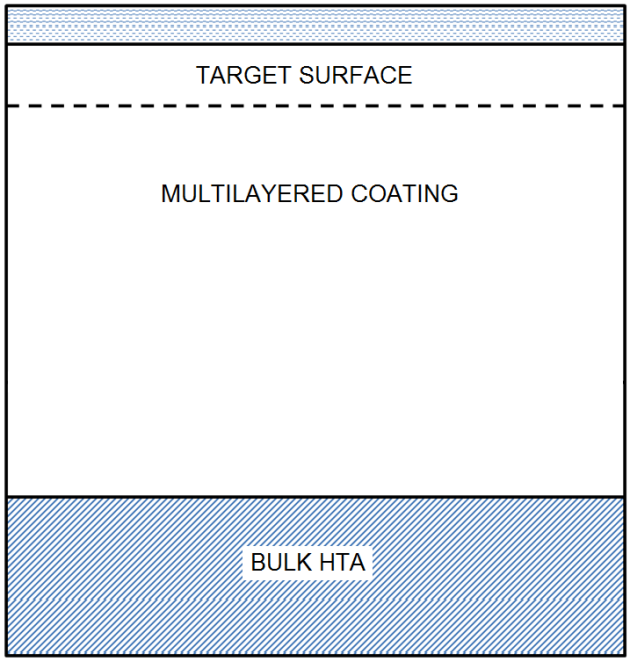

Figure 6. 4: Cross section build-up of the CoatAlloy^{TM} passivating coating according to the manufacturer[47].

6.3.4 Coking rate determination

Similar to previous work [24, 39, 40], during the cracking experiment, various data is logged, such as temperatures, mass flows and the mass of the deposited coke. Due to the movement of the coupon during cracking, the raw balance output contains high frequency noise, which is removed by a low-pass filter in Matlab, resulting in a filtered weight curve.

From 15-60 minutes, the calculated coking rate is considered as representative of the catalytic behavior of the material, while the one calculated from 5th to 6th hour is referring to the long-term

behavior of the material, corresponding to the pyrolytic coking occurring when all the surface of the coupon is covered by coke. In this work, the former is referred as initial coking rate while the latter as asymptotic.

6.3.5 Surface characterization

SEM and EDX are used to obtain information regarding the surface morphology and elemental composition of the samples. The top surface analysis gives a qualitative idea of the coke growth together with elemental quantitative data of the surface, performed in 10 kV and 20 kV. the uniformity of the oxides formed on the surface is evaluated with the cross section elemental mappings.

Additionally, in this work, wavelength-dispersive spectroscopy (WDS) and X-ray photoelectron spectroscopy (XPS) are used for some of the samples to gain improved insight on the effect of N_2 and sulfur on their surface. For WDS, the detection of sulphur is performed using a PET (Penta-Erythritol) crystal, which allows a sulphur detection of even 0.1 wt% sulphur or even below. In Table 6. 4, the location of the XPS peaks of the most common elements for the JSR coupons is given.

Table 6. 4: Location of the XPS peaks for the most relevant elements for the JSR-coupons

Element + orbital	Location peak [eV]
Si_{2p} + Al_{2s}	95-130
S_{2p}	155-175
C_{1s}	275-295
N_{1s}	390-410
O_{1s}	520-540
Cr_{2p}	565-605
Mn_{2p}	635-660
Fe_{2p}	700-740
Ni_{2p}	845-900

6.4 Results and discussion

6.4.1 Products and coke formation

Averaged yields of the main products, initial and asymptotic coking rates for the performed cracking experiments on the reference and CoatAlloy for the two pretreatments and the sulfur addition during the cyclic aging procedure are summarized in Table D.1.

For all the different conditions cyclic aging was applied. Practically, the coking results after aging are the most representative of the coking behavior of an industrial cracker under similar conditions. Overall, the gas phase composition is not affected apart from the carbon oxides yields. In principle, the addition of sulfur during cracking or as pretreatment step led to carbon oxides decrease. Significant differences were noted between the reference material and the passivating formulation under the different conditions – except from the case of the blank runs. In detail,

during blank runs almost 2 times more CO was noted for the passivating coating compared to the reference. Application of an additional presulfiding step before every cracking cycle of the blank lead to 20 % decrement of carbon oxides formation for both the reference and the coated sample. Comparing the blank run with the one that sulfur was continuously added the reduction was more elaborated; a factor 5 and 2 mitigation of CO and CO_2, respectively, was observed for the reference alloy, while the diminution for CoatAlloy was 8 and 2, correspondingly. After combination of presulfiding and continuous sulfur addition, no evident substantial effect was noticed from the case of only continuous addition.

As noted in Figure 6. 5, in terms of coking, under blank run conditions, CoatAlloy cokes from 2 to 5 times more than the reference, when the same treatment was used. In the case that the treatment for CoatAlloy did not include N_2 and only steam/air mixture was applied, the asymptotic coking rate observed was comparable with the one of the reference material, decreased even by a factor 3 in comparison with the normal treatment.

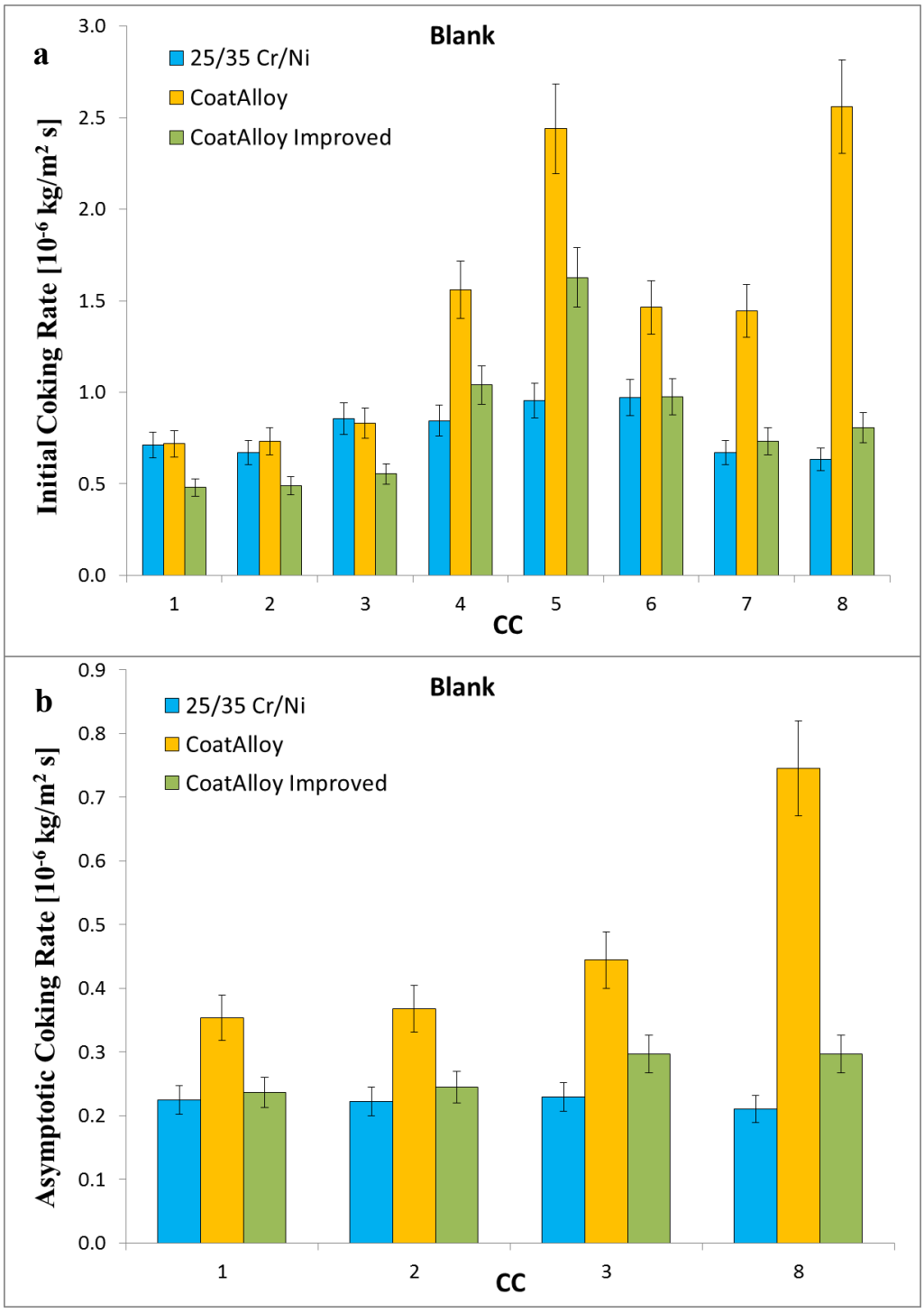

Figure 6. 5: Initial and asymptotic coking rates of Blank runs

If only presulfiding is added to the blank experiments, namely PreS experiments, then both samples show an average increase of a factor 2 in the asymptotic coking rate compared to the

blank conditions, see Figure 6. 6. Additionally, after cyclic aging the asymptotic coking rate of CoatAlloy decreases by 15 %, while for the reference remains rather stable. Overall, it can be concluded that under presulfiding conditions the two samples perform similarly.

When DMDS is continuously added, as observed in Figure 6. 7, initially the reference performs almost 2 times better than CoatAlloy. However, by application of cyclic aging the performance of the barrier coating improves significantly, while the reference material seems to remain rather stable. In that way, the coating leads from 10 to 50 % lower coking rates for the initial and asymptotic respectively.

If presulfiding is implemented to the above conditions – the case of the PreS + CA experiments - then during the first cycles, the reference performs significantly better than CoatAlloy, as illustrated in Figure 6. 8. Nevertheless, again the coating seems to perform a lot better after cyclic aging giving the impression that with one more cycle would even outrun the reference material in anti-coking performance. It is overall suggested that the presulfiding is avoided when the passivating coating is applied on the coil.

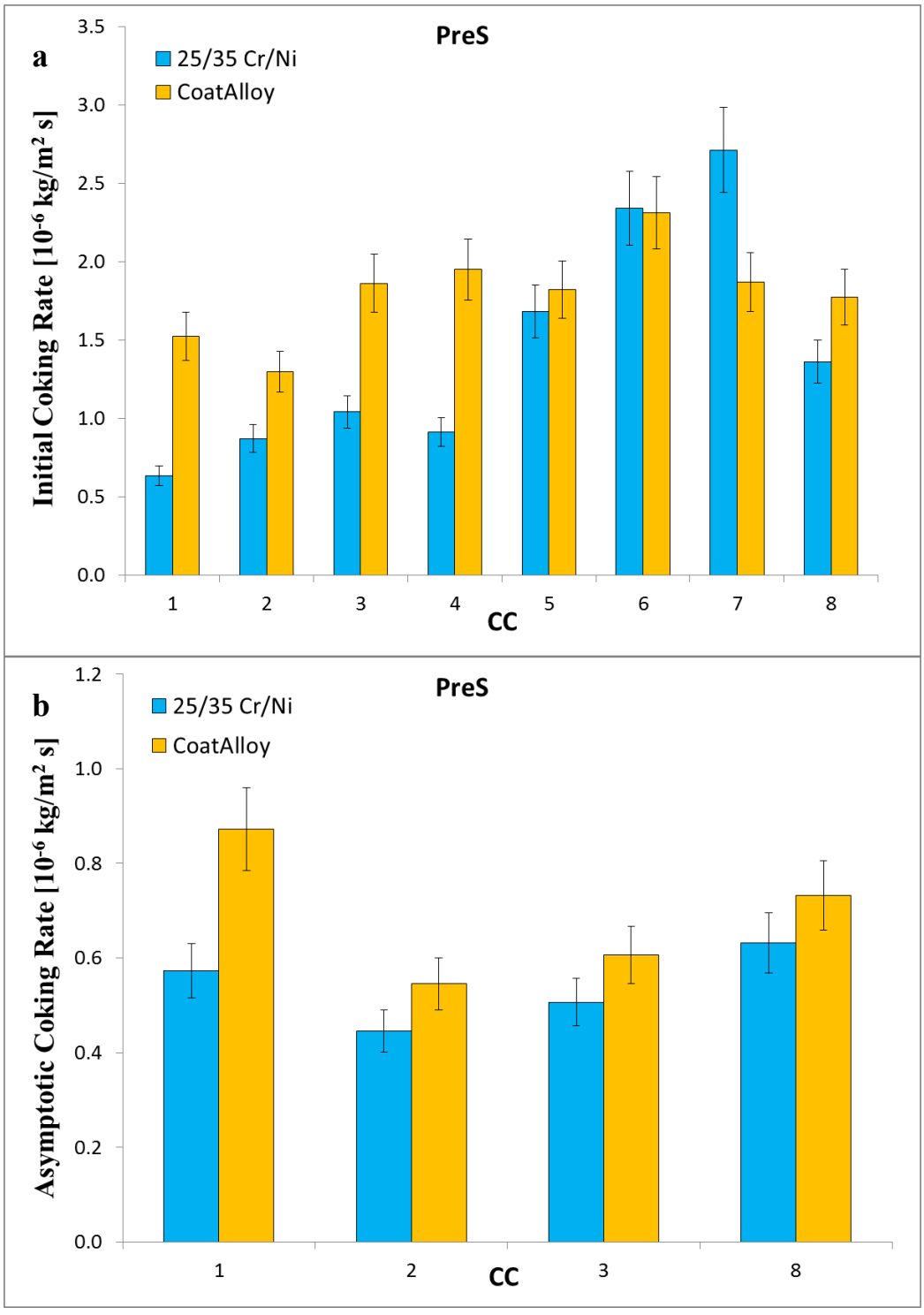

Figure 6. 6: Initial and asymptotic coking rates of Presulfiding runs

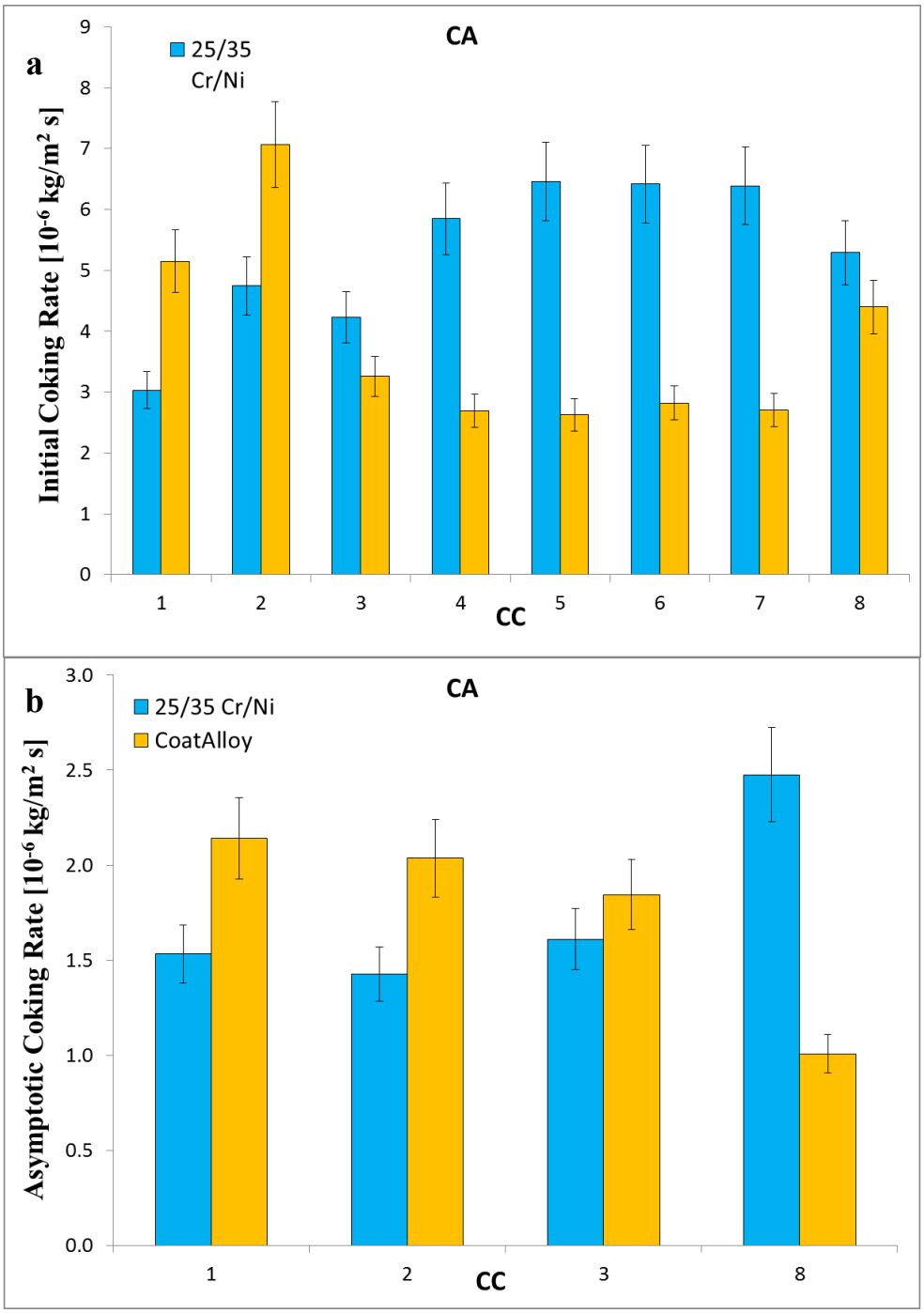

Figure 6. 7: Initial and asymptotic coking rates of CA experiments

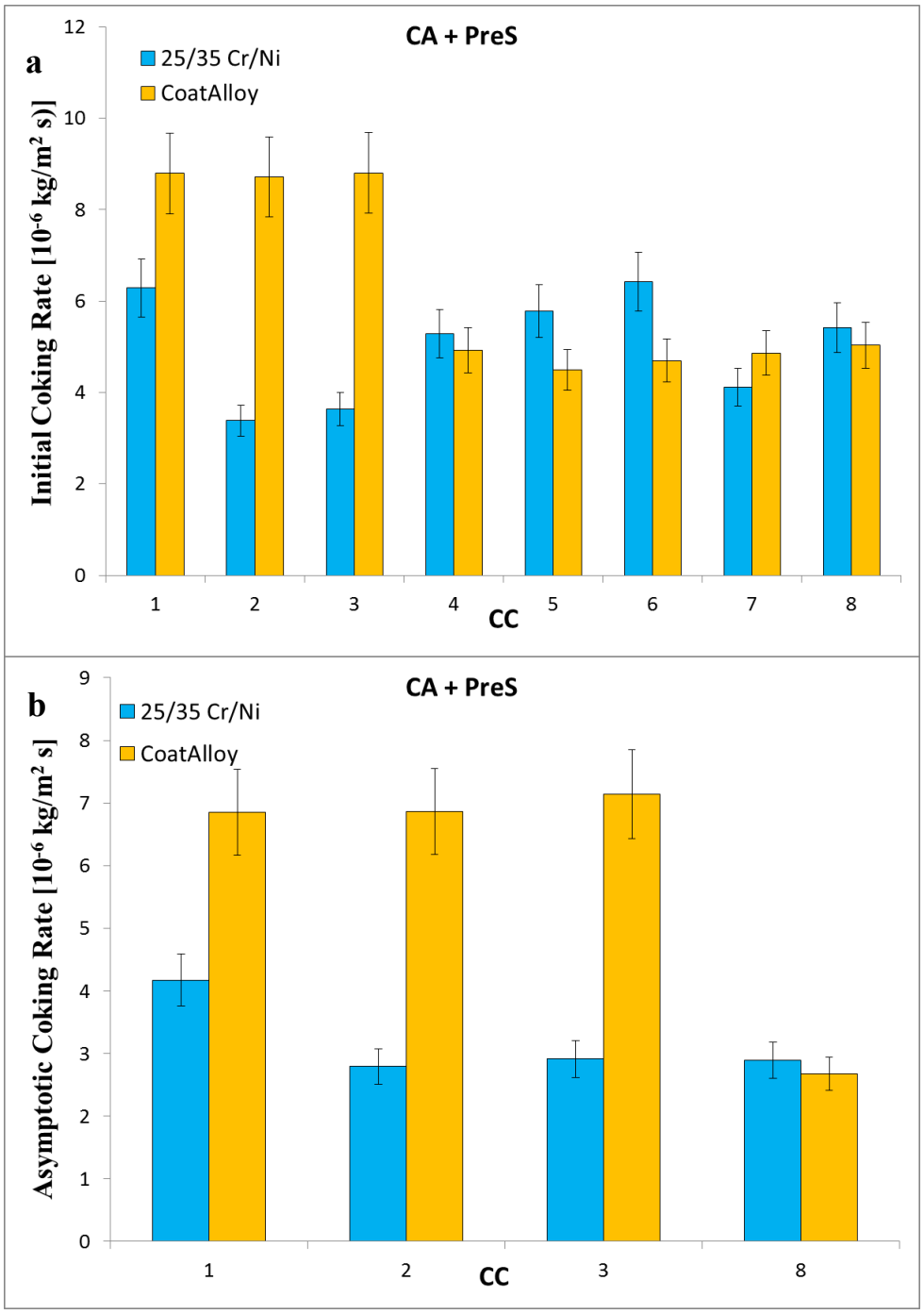

Figure 6. 8: Initial and asymptotic coking rates of PreS+CA experiments.

6.4.2 Surface Analysis

All the samples were examined for both top surface and cross section analysis. The idea is to observe structural and composition differences by the top surface analysis. Using the latter, clear conclusions can be already made. As a last step, the cross-section elemental analyses evaluating the homogeneity, thickness and qualitative composition of the layers formed on the surface. Last step, in an attempt to obtain insight on the effect of N_2 and sulfur on the surface of the coating, additional analysis on XPS and WDS were also performed.

In Figure 6. 9, a first evaluation of the effect of the improved pretreatment on the coke structure can be done. A more porous and complicated coke structure can be easily observed on the CoatAlloy pretreated with the standard pretreatment for Fe-Ni-Cr Alloys. When no N_2, but only steam with air is fed during pretreatment and decoking, the structures noted are more similar with the reference material, certainly less porous too. This difference can be linked with the less available surface and therefore less active sites promoting coke formation, justifying the improved performance of CoatAlloy after pure steam treatment.

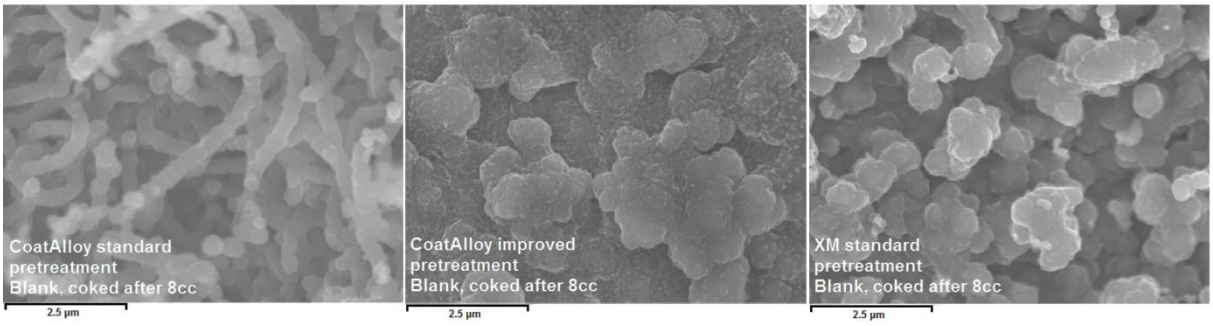

Figure 6. 9:Coked CoatAlloy after the typical treatment(left), coked CoatAlloy after the improved treatment (middle) and coked 25/35 Cr/Ni after standard treatment.

Magnification: 15000x, Accelerating Voltage: 10kV

From Figure D.2 to Figure D.6, the cross sectional analyses of the CoatAlloy over the different applied conditions are illustrated. The untreated coating is consisted of Al and O, having a thickness of 5-8 μm. In Figure D.3, a coupon exposed to N_2 for 14 h at 1023 K is shown. A uniform layer of Cr beneath the coating can be observed, together with a decreased thickness coating layer. The latter is also more heterogeneous. The same Cr layer can be seen also in Figure D.4, here overlaying with Mn and O, implying the formation of a Cr and Mn oxide layer under the coating. When N_2 is excluded from the pretreatment, a thin layer of Cr is again observed under the coating, however the oxygen is not present. The thickness of the coating remains to the fresh levels. By comparing Figure D.4 and Figure D.5, it can be observed that the improved pretreatment keeps the coating thickness unaffected, leaving the Cr layer isolated underneath the alumina layer. In agreement with similar work done[42], this can support the idea of a more stable alumina α layer for the steam/air treatment in comparison with a mix of alumina γ and α layer formed after application of the optimal pretreatment for Fe-Ni-Cr alloys[5].

Similarly with the above, Figure D.6 presents the coating after the improved pretreatment combined with presulfiding of the surface. No significant effect is noted, while the thin Cr layer beneath the coating being absent and the thickness of the alumina layer unaffected.

To further evaluate the effect of the N_2 on the surface of the coating, XPS (Figure D.7) analyses are performed, too. The results show no nitrogen found on the surface. For the conducted analysis the detection limit is 0.1 to 1 at%, so if nitrogen is present on the surface then should be less than that amount or it simply reacts with the surface oxides by removing active oxygen atoms from the surface. The latter cannot be identified by the analytical section of the used set-up in the gas effluent.

The same effect is noted from the XPS analysis (Figure D.8) of the presulfided coated coupons. Insignificant amounts of sulfur are identified, thus the assumption of the sulfides formation on the surface of the coating is not valid.

As a last step, an analysis with WDX is carried out in the following section, which allows penetrating deeper into the sample at detection limits of 0.01 wt%. It should be kept in mind that if sulfur can be detected, it will be in very low amounts, which most probably would make no difference in terms of kinetic behavior.

Only three measurements have been carried out to detect nitrogen. In all three cases either no weight percentage is obtained or the error margin is larger than the peak of nitrogen itself. This is an effect of the overlap of the peak of nitrogen with the peaks of oxygen. Even WDS cannot distinguish sufficiently well between these peaks and a quantification of the nitrogen content in the samples is thus not possible. In practice this leads to a background peak on the left of the nitrogen peak that is larger than the peak itself.

However, the lack of a larger nitrogen peak already suggests that there is insignificant amount of nitrogen on the surface of the coupons. This theory is supported by the fact that the background peak on the right, which does not display any overlap with other peaks, is only as high as the nitrogen peak itself. As the background is always subtracted from the peak, this means that practically no nitrogen can be present in the sample. The WDS measurements therefore indicate that no nitrites are formed on the surface of the coupon after prenitration, in accordance with the observations of the XPS analyses. Figure D.9 shows a WDS image of a prenitrated coated sample.

6.5 Conclusions

A different pretreatment on the commercially used CoatAlloy coating was evaluated under ethane steam cracking conditions and compared with a reference Fe-Ni-Cr alloy. Overall, the addition of sulfur on-stream or as pretreatment leads to decreased carbon oxidesformation. Apart from the blank experiments, no significant observable differences were noted between the reference material and the passivating formulation under the different conditions. The coating generated almost 2 times more CO compared to the reference material for the blank runs. An additional presulfiding step before cracking, when no sulfur was added during cracking, lead to 20 % decrement of carbon oxides formation for both the reference and the coated sample.

Comparing the blank run with the one that sulfur was continuously added the reduction was more elaborated; a factor 5 and 2 mitigation of CO and CO_2 respectively was observed for 25/35 Cr/Ni, while the diminution for CoatAlloy was 8 and 2 correspondingly. After combination of continuous addition of sulfur and presulfiding, no evident substantial effect was noticed from the case of only continuous addition.

In terms of coking, under blank run conditions CoatAlloy cokes from 2 to 5 times more than 25/35 Cr/Ni, when the same treatment was used. In the case that the treatment for CoatAlloy did not include nitrogen and only steam/air mixture was applied, the asymptotic coking rate observed was comparable with the one of the reference material, decreased even by a factor 3 in comparison with the normal treatment.

If presulfiding is added to the blank experiments, then CoatAlloy shows an average increase of 20% in the asymptotic coking rate compared to the reference material. Presulfiding increases the coking rate by a factor 2 in the case of 25/35 Cr/Ni, but for CoatAlloy the effect is less pronounced, especially after cyclic aging; only 30% increase is observed for the pyrolytic coking rate.

When DMDS was continuously added, initially 25/35 Cr/Ni performs almost 2 times better than CoatAlloy. However, by application of cyclic aging the performance of the barrier coating improves significantly, while the reference material seems to remain rather stable. In that way, the coating leads from 10 to 50 % lower coking rates for catalytic and pyrolytic respectively.

The coating seems to perform a lot better after cyclic aging and in the presence of DMDS during cracking giving the impression that with additional cracking cycles would even outrun the reference material.

6.6 References

1. Paraskevas, P. D.; Sabbe, M. K.; Reyniers, M.-F.; Papayannakos, N. G.; Marin, G. B., Kinetic Modeling of α-Hydrogen Abstractions from Unsaturated and Saturated Oxygenate Compounds by Hydrogen Atoms. *The Journal of Physical Chemistry A* **2014,** 118, (40), 9296-9309.
2. Paraskevas, P. D.; Sabbe, M. K.; Reyniers, M. F.; Papayannakos, N.; Marin, G. B., Kinetic Modeling of α-Hydrogen Abstractions from Unsaturated and Saturated Oxygenate Compounds by Carbon-Centered Radicals. *ChemPhysChem* **2014,** 15, (9), 1849-1866.
3. Kivlen, J. A.; Koszman, I., Decoking of onstream thermal cracking tubes with h20 and h2. In Google Patents: 1971.

4. Sullivan, B. K., Ethylene Cracking Heater Decoking Tutorial. In *AIChE Spring Natl. Meet., Conf. Proc.*, New Orleans, LA, 2014.
5. Sarris, S. A.; Olahova, N.; Verbeken, K.; Reyniers, M.-F.; Marin, G. B.; Van Geem, K. M., Optimization of the in-situ pretreatment of high temperature Ni-Cr Alloys for Ethane steam cracking. *Ind. Eng. Chem. Res.* **2017**.
6. Diaby, A. L.; Miklavcic, S. J.; Addai-Mensah, J., Optimization of scheduled cleaning of fouled heat exchanger network under ageing using genetic algorithm. *Chemical Engineering Research and Design* **2016,** 113, (Supplement C), 223-240.
7. De Saegher, J. J.; Detemmerman, T.; Froment, G. F., Three dimensional simulation of high severity internally finned cracking coils for olefins production. *Revue De L'Institut Français Du Pétrole* **1996,** 51, (2), 245-260.
8. Detemmerman, T.; Froment, G. F., Three dimensional coupled simulation of furnaces and reactor tubes for the thermal cracking of hydrocarbons. *Revue De L'Institut Français Du Pétrole* **1998,** 53, (2), 181-194.
9. Schietekat, C. M.; van Goethem, M. W. M.; Van Geem, K. M.; Marin, G. B., Swirl flow tube reactor technology: An experimental and computational fluid dynamics study. *Chemical Engineering Journal* **2014,** 238, 56-65.
10. Torigoe, T.; Hamada, K.; Furuta, M.; Sakashita, M.; Otsubo, K.; Tomita, M. In *Mixing element radiant tube (MERT) improves cracking furnace performance*, 11th Ethylene Producers' Conference, Houston, TX, 1999; Houston, TX, 1999.
11. Györffy, M.; Hineno, M.; Hashimoto, K.; Park, S.-H.; You, M.-S. In *MERT performance and technology update*, 21st Ethylene Producers' Conference, Tampa, FL, 2009; Tampa, FL, 2009.
12. Schietekat, C. M.; Van Cauwenberge, D. J.; Van Geem, K. M.; Marin, G. B., Computational fluid dynamics-based design of finned steam cracking reactors. *AIChE J.* **2014,** 60, (2), 794-808.
13. Barazandeh, K.; Dehghani, O.; Hamidi, M.; Aryafard, E.; Rahimpour, M. R., Investigation of coil outlet temperature effect on the performance of naphtha cracking furnace. *Chemical Engineering Research and Design* **2015,** 94, (Supplement C), 307-316.
14. Wang, J.; Reyniers, M.-F.; Van Geem, K. M.; Marin, G. B., Influence of Silicon and Silicon/Sulfur-Containing Additives on Coke Formation during Steam Cracking of Hydrocarbons. *Ind. Eng. Chem. Res.* **2008,** 47, (5), 1468-1482.
15. Wang, J.; Reyniers, M.-F.; Marin, G. B., Influence of Dimethyl Disulfide on Coke Formation during Steam Cracking of Hydrocarbons. *Ind. Eng. Chem. Res.* **2007,** 46, (12), 4134-4148.
16. Reyniers, M.-F.; Froment, G. F., Influence of metal-surface and sulfur addition on coke deposition in the thermal-cracking of hydrocarbons. *Industrial & Engineering Chemistry Research* **1995,** 34, (3), 773-785.
17. Dhuyvetter, I.; Reyniers, M.-F.; Froment, G. F.; Marin, G. B.; Viennet, D., The influence of dimethyl disulfide on naphtha steam cracking. *Industrial & Engineering Chemistry Research* **2001,** 40, (20), 4353-4362.
18. Bajus, M.; Vesely, V.; Baxa, J.; Leclercq, P. A.; Rijks, J. A., Steam cracking of hydrocarbons: 5. Effect of thiophene on reaction-kinetics and coking. *Industrial & Engineering Chemistry Product Research and Development* **1981,** 20, (4), 741-745.
19. Bajus, M.; Vesely, V., Pyrolysis of hydrocarbons in the presence of elemental sulfur. *Collection of Czechoslovak Chemical Communications* **1980,** 45, (1), 238-254.

20. Bajus, M.; Baxa, J.; Leclercq, P. A.; Rijks, J. A., Steam cracking of hydrocarbons: 6. Effect of dibenzyl sulfide and dibenzyl disulfide on reaction-kinetics and coking. *Industrial & Engineering Chemistry Product Research and Development* **1983,** 22, (2), 335-343.
21. Bajus, M.; Baxa, J., Coke formation during the pyrolysis of hydrocarbons in the presence of sulfur-compounds. *Collection of Czechoslovak Chemical Communications* **1985,** 50, (12), 2903-2909.
22. Depeyre, D.; Filcoteaux, C.; Blouri, B.; Ossebi, J. G., Pure norma-nonane steam cracking and the influence of sulfur-compounds. *Industrial & Engineering Chemistry Process Design and Development* **1985,** 24, (4), 920-924.
23. Munoz Gandarillas, A. E.; Van Geem, K. M.; Reyniers, M.-F.; Marin, G. B., Influence of the Reactor Material Composition on Coke Formation during Ethane Steam Cracking. *Industrial & Engineering Chemistry Research* **2014,** 53, (15), 6358-6371.
24. Muñoz Gandarillas, A. E.; Van Geem, K. M.; Reyniers, M.-F.; Marin, G. B., Coking Resistance of Specialized Coil Materials during Steam Cracking of Sulfur-Free Naphtha. *Ind. Eng. Chem. Res.* **2014,** 53, (35), 13644-13655.
25. Petrone, S.; Chen, Y.; Deuis, R.; Benum, L.; Saunders, R.; Wong, C. In *Catalyzed-assisted manufacture of olefins (CAMOL): Realizing novel operational benefits from furnace coil surfaces*, 20th Ethylene Producers' Conference, New Orleans, LA, 2008; New Orleans, LA, 2008.
26. Schietekat, C. M.; Sarris, S. A.; Reyniers, P. A.; Kool, L. B.; Peng, W.; Lucas, P.; Van Geem, K. M.; Marin, G. B., Catalytic Coating for Reduced Coke Formation in Steam Cracking Reactors. *Ind. Eng. Chem. Res.* **2015,** 54, (39), 9525-9535.
27. Zychlinski, W.; Wynns, K. A.; Ganser, B., Characterization of material samples for coking behavior of HP40 material both coated and uncoated using naphtha and ethane feedstock. *Materials and Corrosion-Werkstoffe Und Korrosion* **2002,** 53, (1), 30-36.
28. Ganser, B.; Wynns, K. A.; Kurlekar, A., Operational experience with diffusion coatings on steam cracker tubes. *Mater. Corros.* **1999,** 50, (12), 700-705.
29. Benum, L. In *Achieving longer furnace runs at NOVA Chemicals*, 2002 AIChE Spring Meeting, New Orleans, LA, 2002; New Orleans, LA, 2002.
30. Györffy, M.; Benum, L.; Sakamoto, L. In *Increased run length and furnace performance with Kubota and NOVA Chemicals' ANK 400 anticoking technology; data from current installations as well as technologyimprovements for higher thermal stability and decoking robustness*, 2006 AIChE National Meeting, Orlando, FL, 2006; Orlando, FL, 2006.
31. Petrone, S.; Deuis, R.; Unwin, P. In *Catalyzed-assisted manufactur of olefins (CAMOL): Year-(4) update on commercial furnace installations*, 22th Ethylene Producers's Conference San Antonio, TX, 2010; San Antonio, TX, 2010.
32. Petrone, S.; Deuis, R.; Kong, F.; Chen, Y. Catalytic surfaces and coatings for the manufacture of petrochemicals. US 2013/0337999 A1, 2013.
33. Rech, S. Catalyzed-Assisted Manufacture of Olefins (CAMOL™): Updated for Use in Naphtha Service. (August 21, 2014),
34. SK-Corporation In *Coke Inhibition Technologies - Commercial Experience: F. SK Corporation - PY-COAT*, 13th Ethylene Producers' Conference, Houston, TX, 2001; Houston, TX, 2001.

35. Petrone, S.; Manyam, R.; Wysiekierski, A.; Tzatzov, K.; Chen, Y. In *A "carbon-like" coating to improved coking resistance in pyrolysis furnaces*, 10th Annual Ethylene Producers' Conference, New Orleans, LA, 1998; New Orleans, LA, 1998.
36. Bergeron, M.; Maharajh, E.; McCall, T. In *A low coking environment for pyrolysis furnace - CoatAlloy*, 11th Annual Ethylene Producers' Conference, Houston, TX, 1999; Houston, TX, 1999.
37. Redmond, T.; Bailey, A.; Chen, Y.; Fisher, G.; Miller, R. In *Performance of Coatalloy coating systems in ethylene pyrolysis furnaces using different feedstocks*, 12th Annual Ethylene Producers' Conference, Atlanta, GA, 2000; Atlanta, GA, 2000.
38. Petrone, S.; Mandyam, R.; Wysiekierski, A. Surface alloyed high temperature alloys. US6093260, 1997.
39. Sarris, S. A.; Olahova, N.; Verbeken, K.; Reyniers, M.-F.; Marin, G. B.; Van Geem, K. M., Optimization of the in-situ pretreatment of high temperature Ni-Cr Alloys for Ethane steam cracking. *Industrial & Engineering Chemistry Research* **2017**.
40. Muñoz Gandarillas, A. E.; Van Geem, K. M.; Reyniers, M.-F.; Marin, G. B., Influence of the Reactor Material Composition on Coke Formation during Ethane Steam Cracking. *Ind. Eng. Chem. Res.* **2014,** 53, (15), 6358-6371.
41. Muñoz, A. E.; Van Geem, K. M.; Reyniers, M.-F.; Marin, G. B., Influence of the Reactor Material Composition on Coke Formation During Ethane Steam Cracking. *Industrial & Engineering Chemistry Research* **2014**.
42. Asteman, H.; Hartnagel, W.; Jakobi, D., The Influence of Al Content on the High Temperature Oxidation Properties of State-of-the-Art Cast Ni-base Alloys. *Oxidation of Metals* **2013,** 80, (1-2), 3-12.
43. Jakobi, D.; Gommans, R., 15 - Typical failures in pyrolysis coils for ethylene cracking. In *Corrosion by Carbon and Nitrogen*, Woodhead Publishing: 2007; pp 259-270.
44. Grabke, H. J.; Spiegel, M., 6 - Occurrence of metal dusting – referring to failure cases. In *Corrosion by Carbon and Nitrogen*, Woodhead Publishing: 2007; pp 90-102.
45. Lin, R. Q.; Fu, C.; Liu, M.; Jiang, H.; Li, X.; Ren, Z. M.; Russell, A. M.; Cao, G. H., Microstructure and oxidation behavior of Al + Cr co-deposited coatings on nickel-based superalloys. *Surface and Coatings Technology* **2017,** 310, 273-277.
46. Industries, M. Manaurite XM - Heat resistant alloys for hydrocarbon processing. http://www.manoir-industries.com/site/docs_wsw/fichiers_communs/docs/MI_Manaurite_XM.pdf
47. Paradigm, Petrochemical: CoatAlloy™. In Paradigm Shift Technologies Inc.: Toronto, Canada, 2015.

Chapter 7: Metallurgic Aging

This chapter includes the following manuscript:

7. **Effect of long-term high temperature oxidation on coking behavior and microstructure of Ni-Cr alloys**

   Stamatis A. Sarris, Manjunath Patil, Reyniers, M.-F.; Marin, G. B.; Van Geem, K. M.

   To be submitted

7.1 Abstract

The service time of an industrial cracker is strongly dependent on the long-term coking behavior and microstructure stability of the reactor coil alloy. Super alloys are known to withstand temperatures up to even 1400 K. In this work, several commercially available alloys have been first exposed to a long term oxidation at 1423 K for 500 h, so-called metallurgic aging. Subsequently, their coking behavior was evaluated in-situ in a thermogravimetric setup under ethane steam cracking conditions ($T_{gasphase}$ = 1173 K, P_{tot} = 0.1 MPa, X_{C2H6} = 70 %, continuous addition of 41 ppmw S/HC of DMDS, dilution δ= 0.33 kg_{H2O}/kg_{HC}) and compared with their

unaged coking behavior. The tested samples were also examined using scanning electron microscopy and energy diffractive X-ray for surface and cross-section analysis. The alloys with increased Cr-Ni content or with the addition of Al showed improved stability against bulk oxidation and anti-coking behavior after application of metallurgic aging.

Keywords: Ni-Cr alloys, steam cracking, metallurgic aging, thermal cracking, ethane, coke formation, jet stirred reactor

7.2 Introduction

Surface technologies to reduce carbon deposition on the inner wall of industrial steam crackers are in the foreground of research because of their potential for improving the process economics . Due to coke deposition, the reactor cross-sectional area is reduced, leading to excessive pressure drop over its length. The latter results in a change in ethylene selectivity[1, 2], while the highly isolative coke layer decreases the heat transfer from the furnace to the reactors. To keep the cracking severity stable over time and compensate the additional conductive heat resistance, the fuel flow rate to the furnace burners has to be increased, which makes that the reactor tube metal temperature rises over time. When the coke or the temperature of the coil is approaching the maximum allowable value, a decoking procedure with a steam/air mixture is necessary[3-5]. This cyclic cracking-decoking operation affects the annual production capacity if the plant is furnace limited, resulting in a higher operating costs. Many authors have investigated the relation between the elemental composition and microstructure of several alloys and coatings under oxidizing or carburizing environments[6-12]. To date, several anti-coking technologies have been introduced

and tested in the field of steam cracking, such as three-dimensional (3D) reactor technologies [13-18] including application of coatings[19-32], feed additives [33-41] and surface technologies [21, 29, 42, 43] or combination of them. The focus of most of them is on the coking behavior of the alloy, but not on its long-term behavior. Further scientific studies evaluated the coking performance of different alloys and coatings under industrially relevant conditions[21, 43-48]. However, the coking behavior is not experimentally correlated with the microstructure of the samples in any of the studies.

In literature typically only the effect on the microstructure and on the mechanical properties of the alloys is evaluated in the long-term oxidation studies. Nevertheless, the coking behavior of an alloy when the temperature is close its metallurgic limits is obviously of great importance and therefore it is studied in this work. The coking experimental results are compared both with not aged and cyclically aged ones. SEM and EDX observations on both the surface and the cross sectional oxidation of the alloys as well as the microstructure of them allow a better understanding of the studied phenomena.

7.3 Experimental section

7.3.1 Electro balance set-up

The coking experiments were performed at the jet stirred reactor set-up of the Laboratory for Chemical Technology (LCT) of Ghent University. The JSR is designed in order to carry out thermogravimetric analyses on different reactor materials. Coke formed during the experiments is measured as a function of time under a broad range of conditions covering most of the industrial cases. The set-up is capable of evaluating the effect of different pretreatment conditions (e.g.

application of additives, temperature and duration of the pretreatment) as well as varying cracking conditions (e.g. use of the feed additives, steam dilution and cracking temperature) on coke formation, product distribution together with surface composition and morphology.

During an experiment, the coke deposited on the metal sample, see Figure 7. 1, is accurately monitored online with resolution up to 0,1 μg per second. The weight signal is off-line processed afterwards in order to obtain coking rates. The reactor effluent is online analyzed via gas chromatography to evaluate the stability and reproducibility of the cracking conditions. The surface morphology and chemical composition of the coupons are typically analyzed off-line by means of SEM and EDX. The combination of the mentioned set-up together with the experimental procedure gives valuable information on the coke formation phenomenon occurring during steam cracking of hydrocarbons and leads to a rather global explanation of the influence of the studied material and conditions.

The experimental set-up with its sequences is described in detail in similar work [5, 49], however, for practical reasons a short description with the adaptation of some minor parts is given here as well. Figure 7. 2 gives a simplified diagram of the feed section of the experimental set-up.

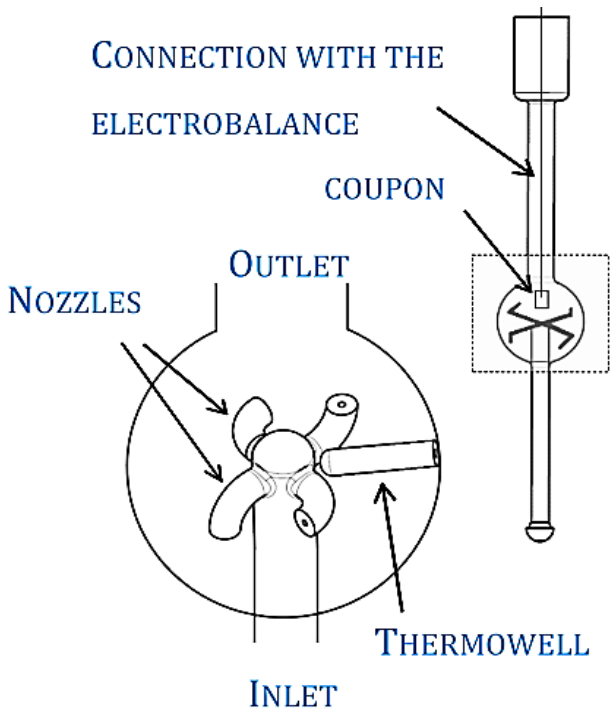

Figure 7. 1: Representation of the JSR reactor

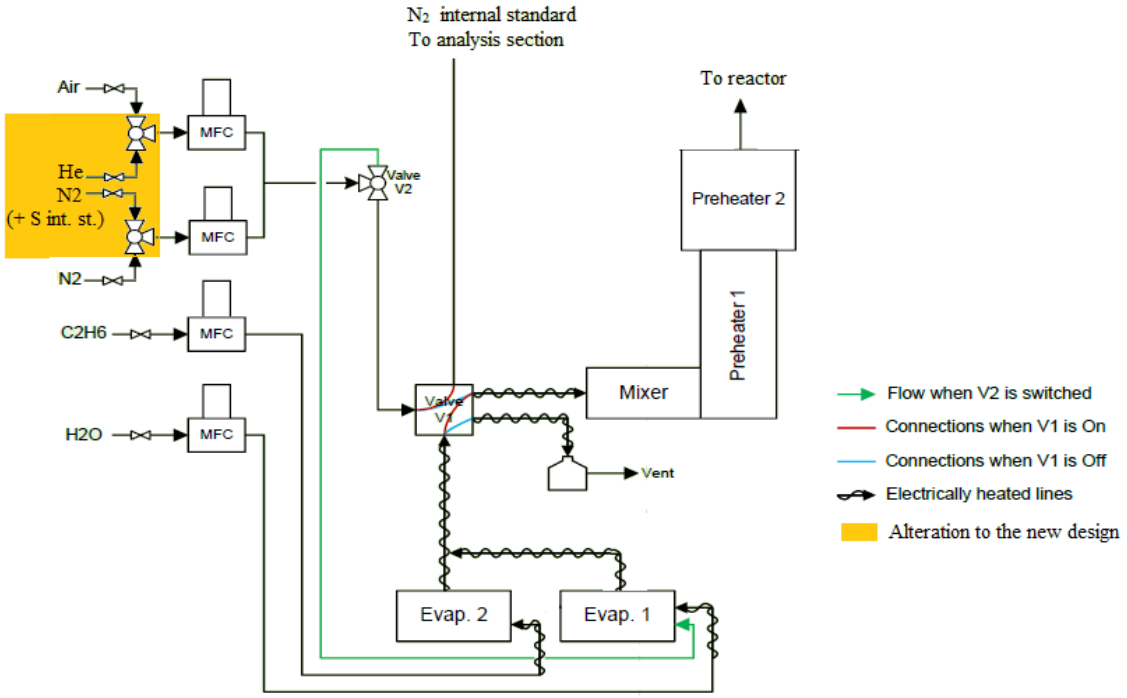

Figure 7. 2: Diagram of the JSR feed and preheating section for the study of coke deposition on different reactor materials and pretreatments during steam cracking of ethane.

In the feed section, the hydrocarbon feedstock and water (or water with DMDS) are fed, evaporated, mixed and preheated before sent to the reaction section. There, the steam cracking process is conducted leading to coke formation on the sample. The reactor effluent is quenched using an oil cooler and a fraction of the effluent is withdrawn for online C_4^- and C_{5+} gas chromatography analysis, while the rest is sent directly to the vent.

7.3.2 Metallurgic aging oven

In this work, an additional oven was used to off-line pretreat the coupons that subsequently were tested in the JSR. In this oven, high temperature oxidation and/or nitration can be performed. The oven is capable of withstanding temperatures up to 1600 K for more than 500 h.

7.3.3 Experimental conditions and procedures

Typically, the experiments conducted on the JSR set-up consist of 3 cracking cycles of 6 hours coking and decoking cycles, followed by four short cycles of 1 hour and a last cycle of 6 hours to evaluate the effect of cyclic aging on each applied set of conditions. This procedure is called cyclic aging and it is performed in order to evaluate the effect of the several cyclic cracking and decoking runs on the coking behavior of the tested material. An overview of the order kept in the aging experiments is given in Figure 7. 3. In Table 7. 1 and Table 7. 2, detailed process conditions of the cyclic and metallurgic aging procedures are summarized.

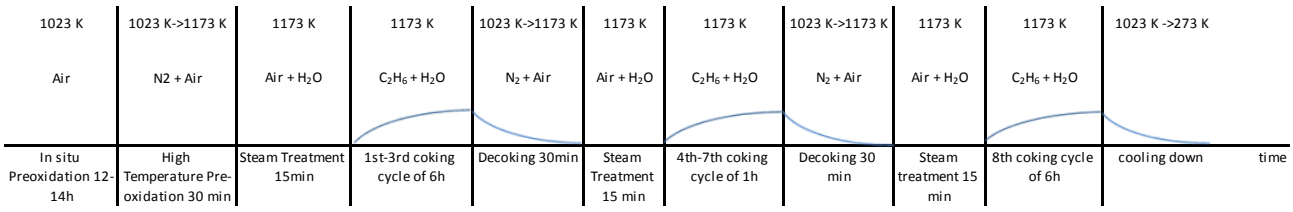

Figure 7. 3: Typical timeline of the cyclic aging experiments

Table 7. 1: Schematic overview of the coking-decoking experiment with the cyclic aging procedure, with detailed process conditions

Process step	Duration	Temperature (K)	Gas feed flow (10^{-6} kg s^{-1})			Water flow (10^{6} kg s^{-1})
			N_2	Ethane	Air	
Preoxidation	12-14 hours	1023	-	-	9.575	-
Decoking	30-40 minutes	Heating up from 1023 to 1173	9.683	-	11.862	-
Steam treatment	15 minutes	1173	-	-	11.862	6.7
1st cracking cycle	6 hours	1173	-	29.167	-	9.7
Decoking	30-40 minutes	Heating up from 1023 to 1173	9.683	-	11.862	-
Steam treatment	15 minutes	1173	-	-	11.862	6.7
2nd cracking cycle	6 hours	1173	-	29.167	-	9.7
Decoking	30-40 minutes	Heating up from 1023 to 1173	9.683	-	11.862	-
Steam treatment	15 minutes	1173	-	-	11.862	6.7
3rd cracking cycle	6 hours	1173	-	29.167	-	9.7
Decoking	30-40 minutes	Heating up from 1023 to 1173	9.683	-	11.862	-
Steam treatment	15 minutes	1173	-	-	11.862	6.7
Cyclic aging	Consists of 4 cycles of: o Heating up from 1023 to 1173 K o Cracking at 1173 K (1 hour) o Decoking from 1023 to 1173 K o Steam treatment at 1173 K (15 minutes)					
8th cracking cycle	6 hours	1173	-	29.167	-	9.7
Decoking	30-40 minutes	Heating up from 1023 to 1173	9.683	-	11.862	-
Steam treatment	15 minutes	1173	-	-	11.862	6.7
Cooling down	Not specified	To ambient temperature	-	-	-	-

Table 7. 2: Schematic overview of the metallurgic aging procedure with one coking-decoking cycle

Process step	Duration	Temperature (K)	Gas feed flow (10^{-6} kg s^{-1})			Water flow (10^{-6} kg s^{-1})
			N_2	Ethane	Air	
Metallurgic aging	500 hours	1423	-	-	9.575	-
High-temperature preoxidation	30-40 minutes	Heating up from 1023 to 1173	9.683	-	11.862	-
Steam treatment	15 minutes	1173	-	-	11.862	6.7
1st cracking cycle	6 hours	1148	-	29.167	-	9.7
Decoking	30-40 minutes	Heating up from 1023 to 1173	9.683	-	11.862	-
Steam treatment	15 minutes	1173	-	-	11.862	6.7
Cooling down	Not specified	To ambient temperature	-	-	-	-

7.3.4 Samples: Materials and preparation

The metal coupons were made out 25/35 Cr/Ni, 35/45 Cr/Ni and 40/48 Cr/Ni alloys. Additionally, an Al-content alloy is evaluated. These coupons are exposed to cyclic and metallurgic aging experiments. The coupons on which the coke will be deposited are cut as close as possible to the internal surface of industrial tubes in dimensions 10 × 8 × 1 mm³ (total surface area S = 1.96×10^{-4} m^2). Schematic drawings of these coupons and of the point that they are cut from the industrial tubes are depicted in Figure 7. 4 and Figure 7. 5 respectively.

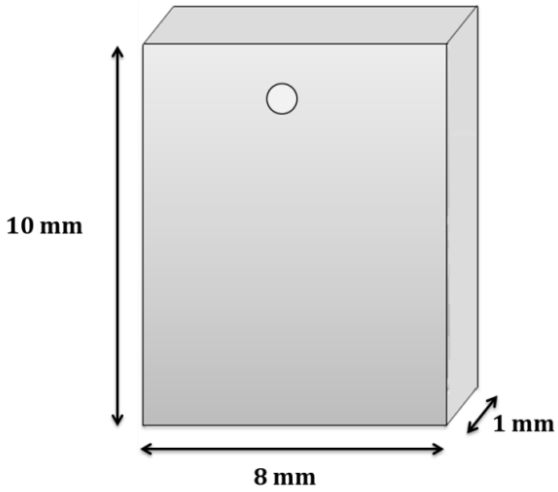

Figure 7. 4: Schematic representation of the JSR samples

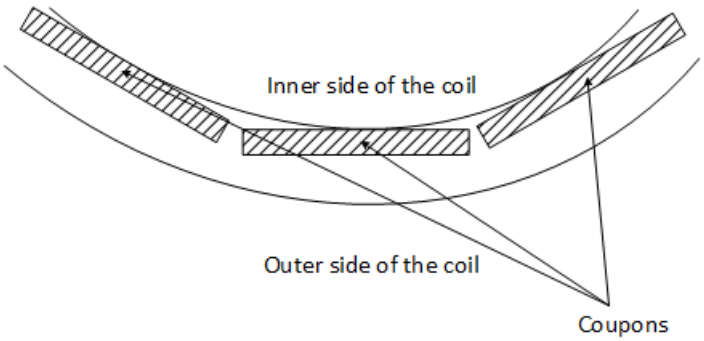

Figure 7. 5: Coupon extraction point

7.3.5 Coking rate determination

During the cracking experiment, various data is logged, such as temperatures, mass flows and the mass of the deposited coke. Due to the movement of the coupon during cracking, the raw balance output contains high frequency noise, which is removed by a low-pass filter in Matlab, resulting in a filtered weight curve. Since the raw balance output in the first 15 minutes of cracking is very unreliable due to the transient start-of-run effects after an abrupt change in the environment and volumetric flow, the coking data is processed after these first 15 minutes. The filtering step also

serves to withhold large disturbances from the raw coking data and to reduce the amount of data points. Next, the filtered weight curve is regressed by minimizing the total sum of squares to the following equation with parameters A, B, C and D:

$$W = At + B\left(1 - \frac{1}{2}(e^{-Ct} + e^{-Dt})\right)$$

Equation 1 is called the fitted weight curve, with W the amount of coke (10^{-6} kg) on the surface at time t (s). Via the fitted weight curve, data points for the first 15 minutes are calculated. The corresponding coking rate curve can be obtained by differentiating Equation 1:

$$r_{c,coupon} = \frac{dW}{dt} = A + \frac{B}{2}(Ce^{-Ct} + De^{-Dt}) \quad \left(\frac{10^{-6}kg}{s}\right)$$

The reported coking rate is then easily obtained by converting to the desired units:

$$r_c = \frac{1000}{3600 \cdot S_{coupon}} \cdot r_{c,coupon} \quad \left(\frac{10^{-6}kg}{s \cdot m^2}\right)$$

With S_{coupon} the surface area of the coupon in m^2. The coking rate can also be calculated as a discrete derivative from the fitted weight curve as:

$$r_c = \frac{1000}{3600 \cdot S_{coupon}} \cdot \left(\frac{W_{t_i} - W_{t_{i-1}}}{t_i - t_{i-1}}\right) \quad \left(\frac{10^{-6}kg}{s \cdot m^2}\right)$$

The processing of the coking data is visualized in Figure 7. 6.

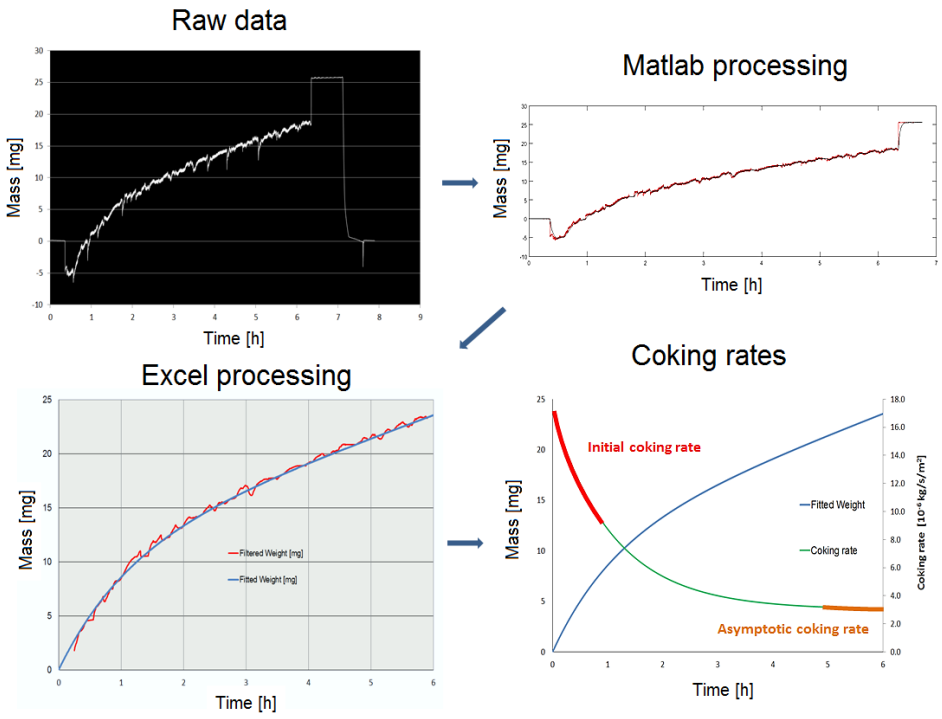

Figure 7. 6: The processing of coking data: from raw balance output to coking rate curve

From 15-60 minutes, the calculated coking rate is considered as representative of the catalytic behavior of the material, while the one calculated from 5th to 6th hour is referring to the long-term behavior of the material, corresponding to pyrolytic coking occurring when the complete surface of the coupon is covered by coke. In this work, the former is referred as initial coking rate while the latter as asymptotic.

7.3.6 Surface characterization

SEM and EDX are used to obtain information regarding the surface morphology and elemental composition of the samples. Both top surface and cross section analyses of coked samples were performed in this work. The top surface analysis gives a qualitative idea of the coke growth together with elemental quantitative data of the surface, performed in 10 kV and 20 kV. On the other hand the cross section mappings explain the uniformity of the oxides generated due to exposure to an oxidative or carburizing environment. In this work, during the cross sectional analyses also the microstructure of the metallurgically aged alloys is evaluated. In the EDX analysis, the detected oxygen and carbon are omitted in the results both not to block viable results for other elements such as Cr, Mn and Fe, but also because their quantitative determination is not possible via EDX.

7.4 Experimental results

In Table 7. 3 an overview of the calculated initial and asymptotic coking rates for all the different experiments is given. The results can be interpreted in many different ways. Initially the effect of the different aging procedures on the coking rates, keeping as reference the 1 cc and as fixed variable the elemental composition. Subsequently, the effect of the different elemental composition of the coupon on the coking rates for all the different applied conditions. Additionally, the effect of the different applied conditions on the elemental composition can be discussed using the SEM and EDX top and cross sectional analyses. Therefore, in the next sections, a more detailed discussion of the results is provided.

Table 7. 3: Coking results of the performed experiments

	Experiment	Cyclic Aging Al-content	25/35 Cr/Ni	35/45 Cr/Ni	40/48 Cr/Ni
Conditions	**Ethane Flow [10^{-6} kg s^{-1}]**		29.17		
	Steam Flow [10^{-6} kg s^{-1}]		9.72		
	CA DMDS amount (ppmw S/HC)		41		
	Temperature (K)		1173		
	Pressure		1.02		
	dillution		0.33		
Initial Coking Rate [10^{-6} kg/s/m^2]	**cc**				
	1st cc	1.18	3.03	1.13	0.94
	After 8 cc	2.14	5.29	1.24	0.99
	Metallurgicly Aged	2.03	11.38	2.67	0.97
Asymptotic Coking Rate [10^{-6} kg/s/m^2]	**cc**				
	1st cc	0.97	1.53	0.74	0.72
	After 8 cc	1.21	2.47	0.79	0.40
	Metallurgicly Aged	1.46	2.52	1.00	0.51

7.4.1 Coke formation

In Figure 7. 7, a schematic comparison of the coking behavior for the different alloys under all the range of the applied conditions is shown. Judging by that, the worst anti-coking performance is observed for the 25/35 Cr/Ni alloy, showing in any case at least a factor 3 higher coking rates than the other materials. The best coking behavior is observed for the 40/48 Cr/Ni alloy that is at least 10 % better than the competition. For the catalytic coking rate, during the 1st cc, the differences are significant only for the 25/35 Cr/Ni alloy, coking almost a factor 3 more than the rest. For the remaining alloys the differences are negligible for the catalytic coking rates, however the ascending ranking in order of anti-coking performance is the following:

25/35 Cr/Ni < Al-content < 35/45 Cr/Ni < 40/48 Cr/Ni

Similar quantitative trends can be noted for the asymptotic coking rate, implying that the catalytic and pyrolytic coke formation are coupled phenomena. After application of cyclic aging even though the order of magnitude of the coking rates increases for all the alloys except from the 40/48 Cr/Ni one, the ranking of the materials remains the same. Here, the 25/35 Cr/Ni alloy cokes almost a factor 6 more than the best alloy, for both the catalytic and pyrolytic coking. Nevertheless, the differences remain similar among the rest alloys. Application of cyclic aging leads to an increase of about double for the catalytic coking rates of the Al-content and the 25/35 Cr/Ni alloy. For the asymptotic coking rate a less pronounced increase of almost 30 % is noted for these two alloys. For the remaining alloys – namely 35/45 and 40/48 Cr/Ni - the cyclic aging effect is negligible, implying their better anti-coking performance and stability during aging.

The metallurgic aging, having as target to evaluate the materials after extreme oxidation conditions, similar to the end of run conditions of an industrial coil, is noted with orange in

Figure 7. 7. The anti-coking performance ranking of the alloys changes slightly when only considering the catalytic coking rate:

$$25/35\ Cr/Ni\ <\ 35/45\ Cr/Ni\ <\ Al\text{-}content\ <\ 40/48\ Cr/Ni$$

The Al-content alloy cokes 2 times more than the high concentration of Cr/Ni alloys, while the 35/45 Cr/Ni one performs almost 15 % worse than the former. The 25/35 Cr/Ni material remains the worst having almost a factor 10 higher coking rates. Unfortunately, the improved performance of the Al-content alloy is not maintained during the pyrolytic coking stage. Here, the ranking is equal to the original one, with most of the alloys performing similarly with the cyclic aged ones, supporting the idea that the strongest factors influencing the radical pyrolytic coke formation are the cracking conditions, the applied pretreatment and the elemental composition, in agreement with previous observations.[5]

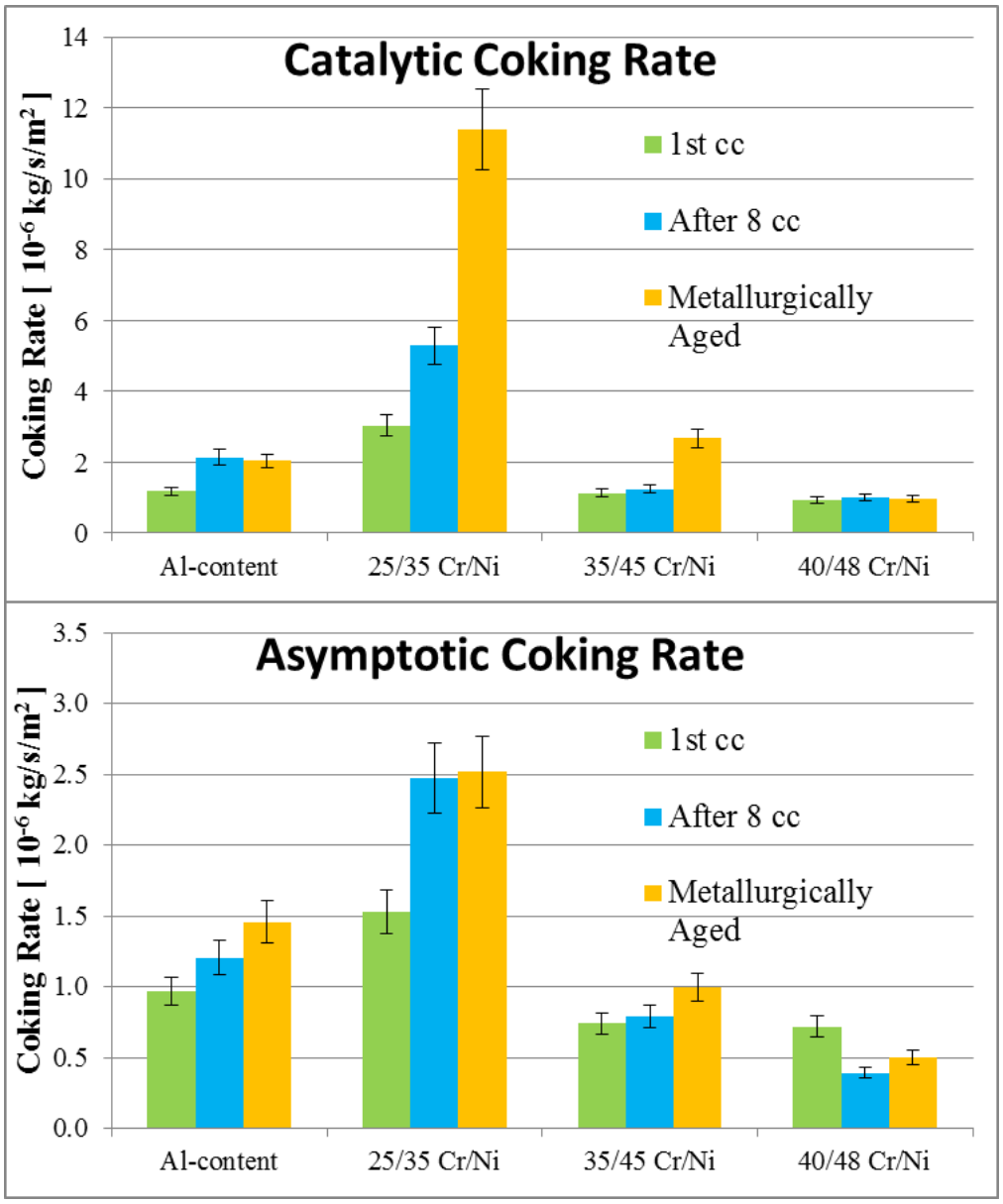

Figure 7. 7: Coking rates for the 1st cracking cycle (green), the one after the cyclic aging (blue) and the one after metallurgic aging (orange).

7.4.2 Surface Analysis

The coke formation observations are in line with the top surface elemental compositions measured by means of EDX, see Table 7. 4. In Figure 7. 8, Ni and Fe are chosen as the representative catalytic coking elements, while in Figure 7. 9, Cr is picked for all the alloys and Al is picked for the Al-content, as representatives for the passivating behavior[5, 43, 46]. In detail, the best anti-coking performance is noticed for the 40/48 Cr/Ni alloy that has the lowest cumulative concentration of Fe and Ni on its surface, but also the highest amounts of Cr. The ranking of the tested alloys under the different conditions is fully aligned with the cumulative Fe and Ni content. It is clear that the existence of Cr in excess on the top surface of an alloy, gives rise to the formation of Cr oxides having a good anti-coking performance. However, for the Al-content no clear conclusions can be extracted. Certainly, in line with previous work, the absence of Fe and Ni in combination with the excess of elements responsible for the formation of oxides plays a significant role for the anti-coking performance of an alloy.

Table 7. 4: Top surface elemental composition for the coked samples after cyclic and metallurgic aging. Magnification: 50 x, Accelerating voltage: 10 and 20 kV

Alloy		**25/35 Cr/Ni**		**35/45 Cr/Ni**		**Al-content**		**40/48 Cr/Ni**	
Elements	acc. volt.	cyclic	metallurgic	cyclic	metallurgic	cyclic	metallurgic	cyclic	metallurgic
Ni	10 kV	3.7	13.9	7.6	20.9	13.8	54.2	8	16.1
	20 kV	10.3	11.9	2.1	27	20.2	31.2	2.3	6
Fe	10 kV	1.6	19.1	2	8.2	7.5	22.8	1.3	0
	20 kV	9.1	19.2	2.6	9.2	11.2	16.1	0.6	0.8
Cr	10 kV	65.2	43.6	47.9	34.3	9.8	17.6	72.4	71.2
	20 kV	62.1	45.8	63	29.6	18.9	17.7	80.9	75.4
Si	10 kV	1.4	4.3	2.1	20.9	2.1	1.1	1.2	1.2
	20 kV	2.1	4.6	1.3	31.2	1.2	1.7	1	13.5
Mn	10 kV	27.8	17.7	40.4	1.1	-	-	16.9	11.6
	20 kV	15.5	17.1	30.7	0.7	-	1.9	14.8	4.1
Nb	10 kV	0.4	1.4	-	5.1	0.4	1.7	0.2	0
	20 kV	0.9	1.5	-	2.3	0.4	-	0.4	0.2
Al	10 kV	-	-	-	-	66.5	2.6	-	-
	20 kV	-	-	-	-	48	30.8	-	-

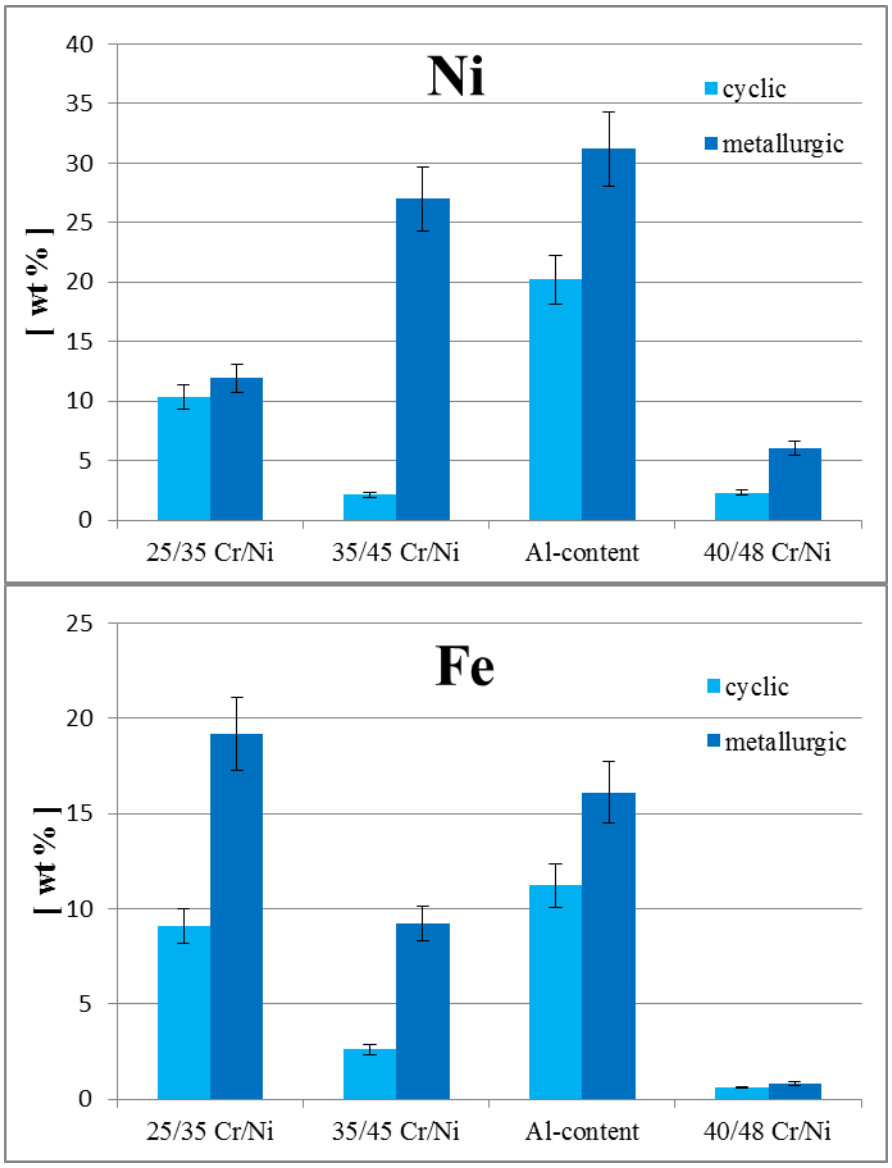

Figure 7. 8: Ni content (top) and Fe content of the tested coked samples. Magnification: 50 x, Accelerating voltage: 20 kV

The ranking of the tested alloys under the different conditions is fully aligned with the cumulative Fe and Ni content. It is clear that the existence of Cr in excess on the top surface of an alloy, gives

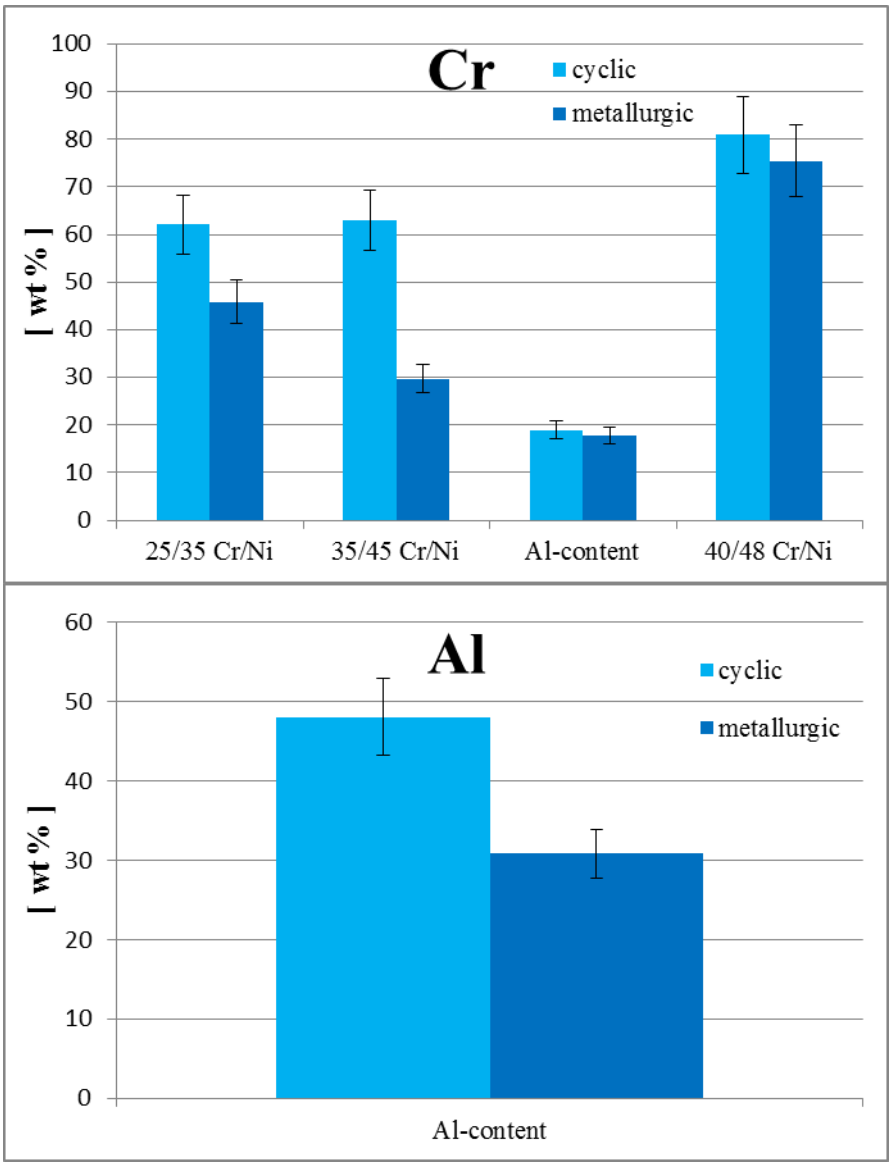

Figure 7. 9: Cr content and Al-content of the coked samples. Magnification: 50 x, Accelerating voltage: 20 kV

7.4.3 Cross sectional Analysis

Except from the top surface elemental composition of the tested alloys, the cross sectional elemental composition is evaluated. It is found that the homogeneity of the oxides formed on a surface is also responsible for its subsequent anti-coking performance[5]. From Figure 7. 10, it is clear that the Al-content alloy has a very nicely oxidized surface after application of cyclic aging, forming mainly a Al oxide of roughly 2 to 3 μm thickness. After application of the metallurgic aging, the oxide remains quite homogeneous, however in some points it is replaced or overlaps with Cr oxides. The thickness is also decreased by almost 1 μm. This is in agreement with the coking observations. Probably the overlaying of Cr and Al improves the initial catalytic coking behavior of the alloy after metallurgic aging, however it does not affect significantly the pyrolytic coking rate to influence the ranking of the alloys.

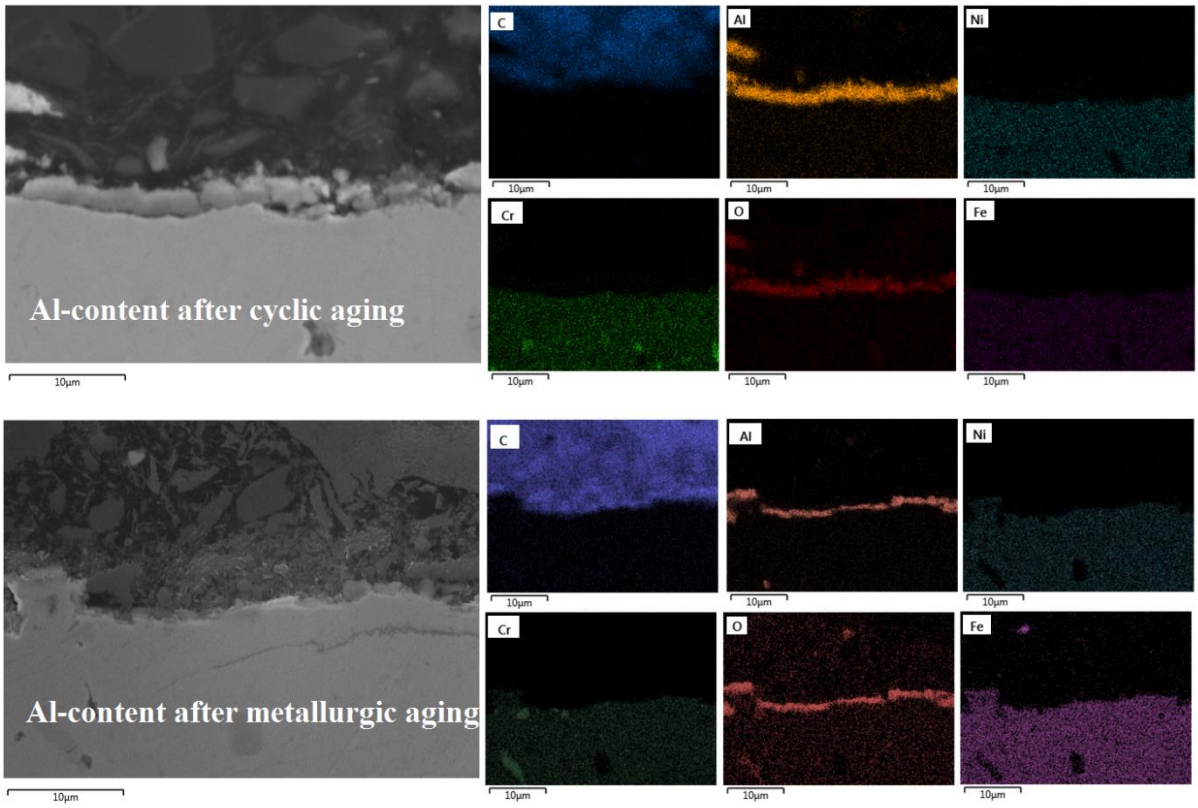

Figure 7. 10: Al-content after cyclic aging and after metallurgic aging. Magnification: 3000 x, Accelerating Voltage: 15 kV

In Figure 7. 11

Figure 7. 11, Figure 7. 12 and Figure 7. 13, the superiority of the optimized pretreatment is vociferous. At the standard cyclic aging the alloys are forming a perfectly homogeneous Cr – Mn oxide layer of 2 to 3 µm thickness. Clearly the minor compositional differences imply that the Cr is less catalytic than Mn towards coke formation, while the increase in Ni is not enough to affect the coking performance of a material negatively if the latter is properly pretreated. A significant differences among the non Al and Al-content alloys is the thickness of the oxides formed after the metallurgic aging. Evidently, the addition of Al in the composition of an alloy halts its oxidation at higher temperatures[47, 50]. Oxygen cannot move towards the bulk as easily as in the case of

the non Al ones. This phenomenon seems to be more pronounced in the 25/35 Cr/Ni alloy and less in the 35/45 Cr/Ni one, while in the 40/48 is almost absent. Additionally, for the 25/35 Cr/Ni alloy, Ni and Fe overlay with the passivating oxides for metallurgically aged sample, obviously catalyzing coke formation in line with the measured coking rates.

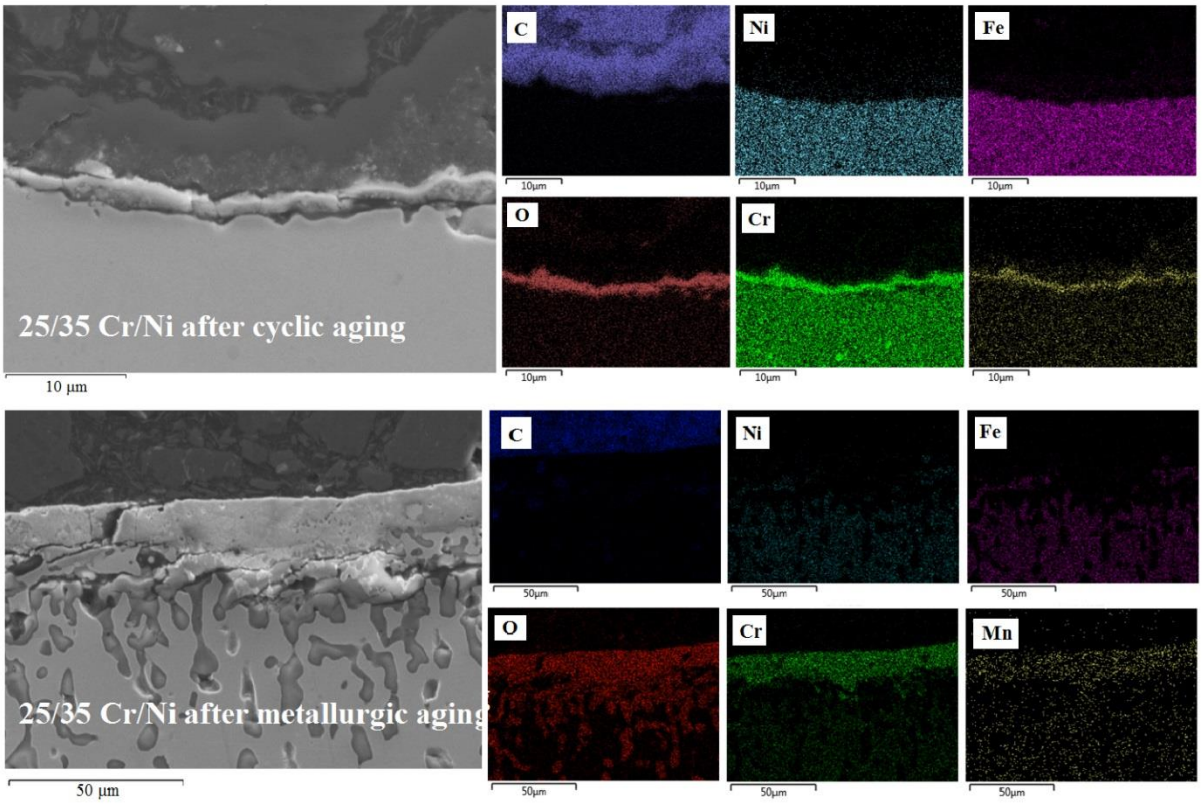

Figure 7. 11: 25/35 Cr/Ni alloy after cyclic aging and after metallurgic aging. Magnification: 3000 x (top) and 1000 x (bottom), Accelerating Voltage: 15 kV

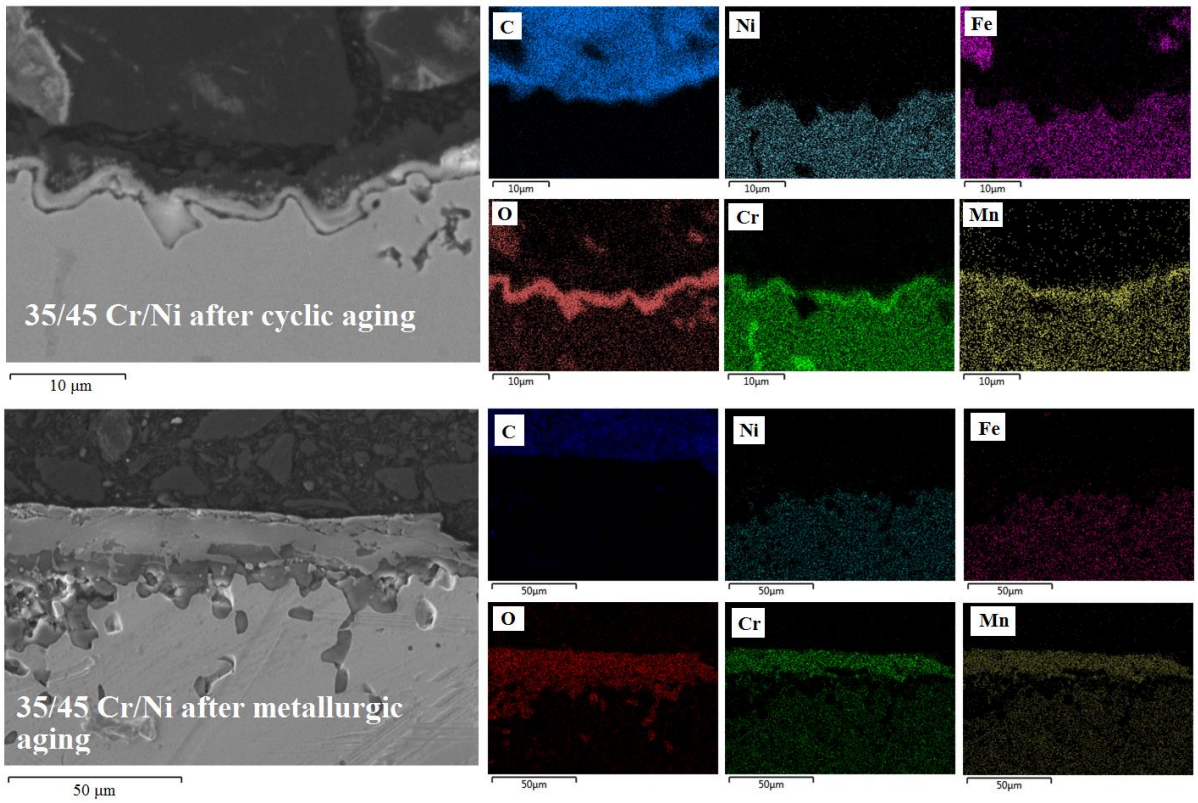

Figure 7. 12: 35/45 Cr/Ni alloy after cyclic aging and after metallurgic aging. Magnification: 3000 x (top) and 1000 x (bottom), Accelerating Voltage: 15 kV

The differences noted in the bulk of the alloys, in these cross sectional analyses led to the next section, that identifies possible microstructure patterns in the bulk of the metallurgically aged alloys.

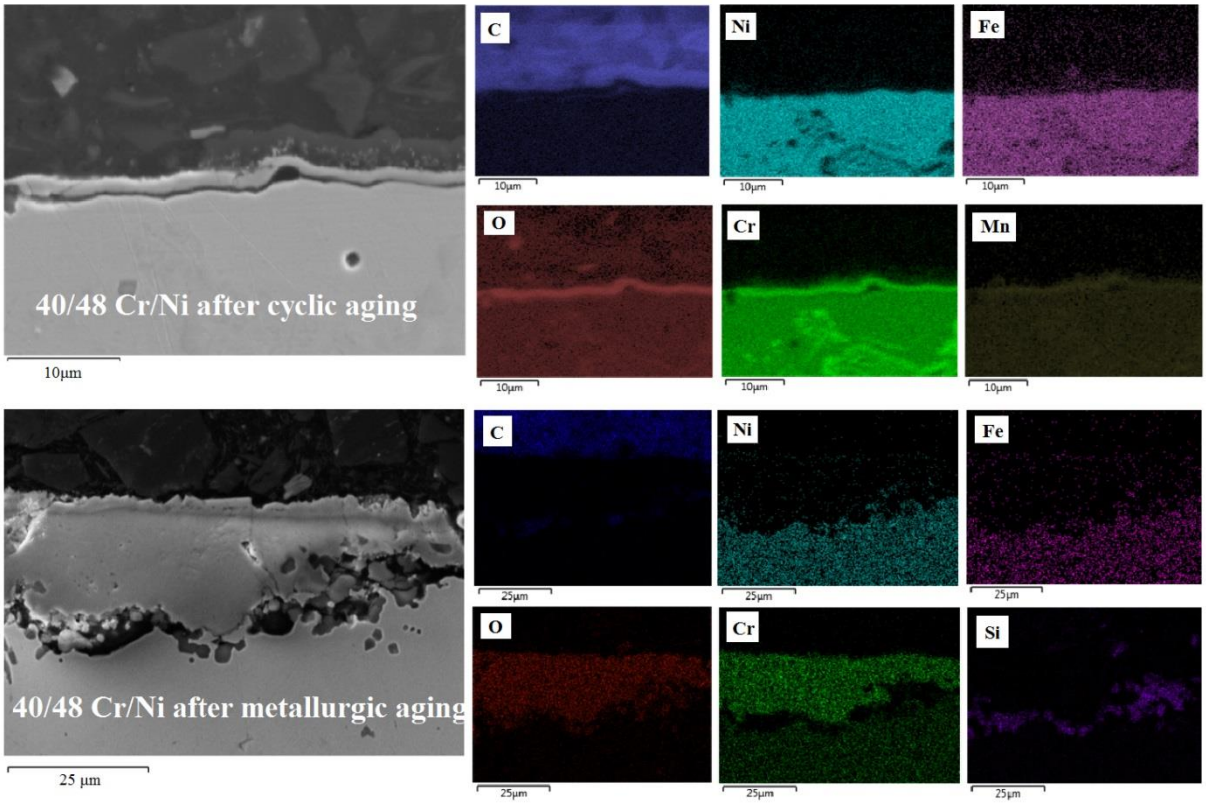

Figure 7. 13: 35/45 Cr/Ni alloy after cyclic aging and after metallurgic aging. Magnification: 3000 x (top) and 1500 x (bottom), Accelerating Voltage: 15 kV

7.4.4 Microstructure Analysis

In Figure 7. 14, the microstructure of the four alloys after exposure to the long-term oxidation is shown. In the figure the black spots identified are spots with increased concentration in Si, Al and C, implying the existence of SiC or AlC. The dark grey areas indicate a precipitation of Cr and C while the white ones increase concentration of Nb and C. It is known that metallurgic crack initiation after high temperature oxidation happens mainly in Chromium carbides rich zones. Also, when the microstructure of an alloy is not significantly elaborated, the alloy is not significantly aged[51, 52]. The most pronounced microstructure is noted for the Fe-Ni-Cr alloys,

justifying that the microstructure of an alloy is independent of its coking behavior. The 25/35 and 40/48 Cr/Ni alloys have almost identical microstructure pattern, but totally different coking behavior after metallurgic aging, while the 35/45 is most pronounced affected, even though its coking behavior is better than the former and worse than the latter. The Al-content alloy shows no elaborated microstructure, but its coking behavior is still not the best. Therefore, no clear conclusions can be made towards coke formation if the microstructure of an alloy is evaluated.

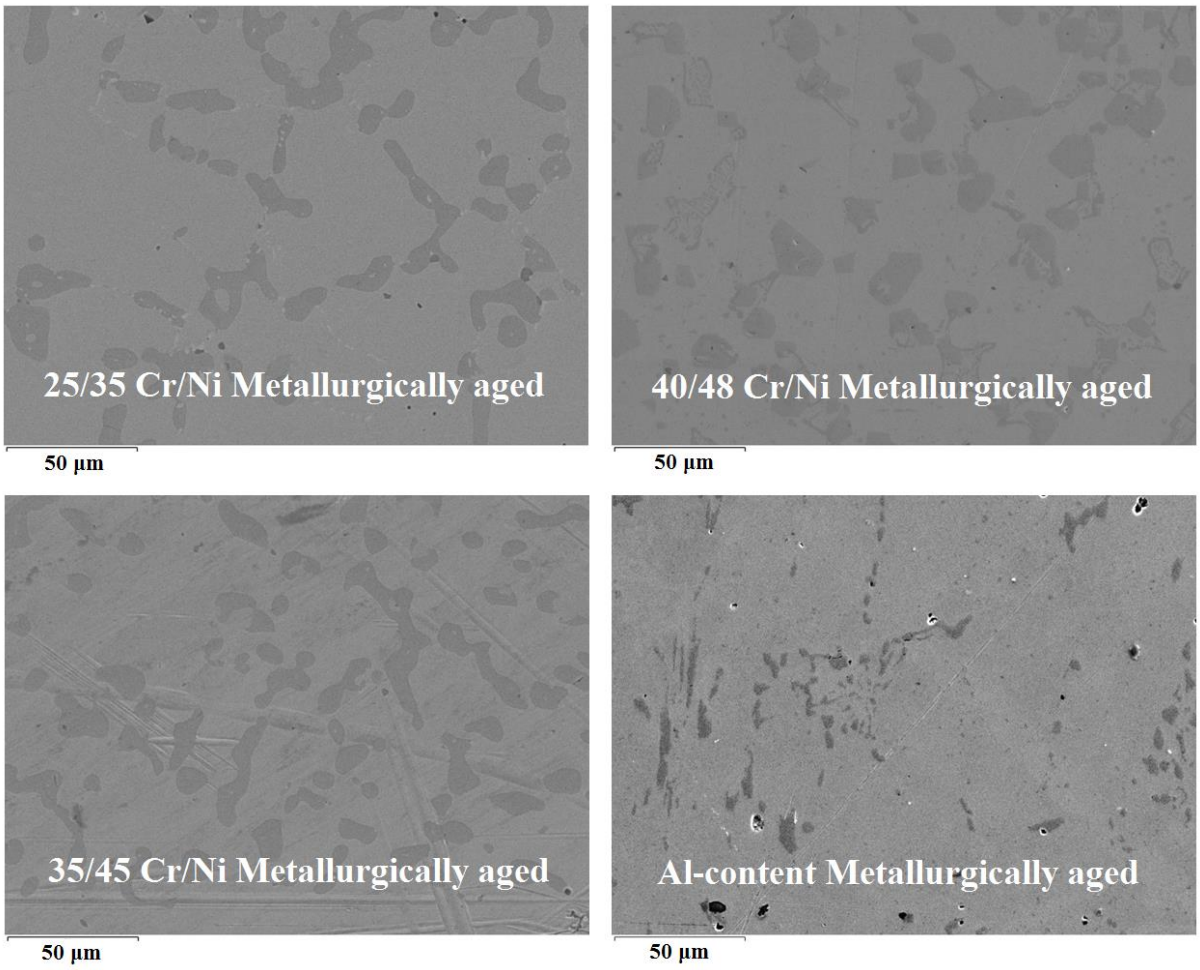

Figure 7. 14: Microstructure SEM pictures after metallurgic aging. Magnification : 550 x, Accelerating Voltage: 15 kV. Dark grey

7.5 Conclusions

The coking behavior of four different alloys was evaluated in a thermogravimetric set-up after their exposure to a long-term high temperature oxidation for 500 h. The results indicated that for the same conditions the coking resistance is improved by increasing the content of Cr and Ni of a high temperature alloy. Cyclic aging, the effect of 8 cracking/decoking cycles on coke formation had a minor effect on the tested alloys. Mainly the 25/35 Cr/Ni alloy showed pronounced coking rates after cyclic aging. The worse the anti-coking behavior of the material is more pronounced after the metallurgic aging. For the best tested material, a negligible effect was noticed after the long-term oxidation. The catalytic and pyrolytic coking behavior of the materials is quite aligned, implying that the two phenomena are interconnected. In line with previous work and literature, the absence of Fe and Ni helps the anti-coking performance of an alloy. Most of the alloys indicated a rather homogeneous coverage of their surface by oxides - mainly of Cr nature for the non Al-content alloys. For the Al-containing alloy, the thickness of the oxides covering typically the surface after cyclic aging is reduced by almost 1 μm, in contrast with the other alloys for which the oxides' thickness was significantly increased. In line with the available literature, the addition of Al in the content of a high temperature alloy, forms Al oxides that protect the bulk from further oxidation. No elaborated microstructure was found in any alloy, therefore the alloys all are quite resistant in terms of aging, however the non Al-containing alloys showed increased concentration of Carbides of Si and Nb in comparison with the Al-containing one. No correlation between the microstructure and the coking behavior of an alloy was found.

7.6 References

1. Paraskevas, P. D.; Sabbe, M. K.; Reyniers, M.-F.; Papayannakos, N. G.; Marin, G. B., Kinetic Modeling of α-Hydrogen Abstractions from Unsaturated and Saturated Oxygenate Compounds by Hydrogen Atoms. *The Journal of Physical Chemistry A* **2014,** 118, (40), 9296-9309.
2. Paraskevas, P. D.; Sabbe, M. K.; Reyniers, M. F.; Papayannakos, N.; Marin, G. B., Kinetic Modeling of α- Hydrogen Abstractions from Unsaturated and Saturated Oxygenate Compounds by Carbon- Centered Radicals. *ChemPhysChem* **2014,** 15, (9), 1849-1866.
3. Kivlen, J. A.; Koszman, I., Decoking of onstream thermal cracking tubes with h20 and h2. In Google Patents: 1971.
4. Sullivan, B. K., Ethylene Cracking Heater Decoking Tutorial. In *AIChE 2014 Spring Meeting*, New Orleans, LA, 2014.
5. Sarris, S. A.; Olahova, N.; Verbeken, K.; Reyniers, M.-F.; Marin, G. B.; Van Geem, K. M., Optimization of the in-situ pretreatment of high temperature Ni-Cr Alloys for Ethane steam cracking. *Industrial & Engineering Chemistry Research* **2017**.
6. Pascal, C.; Braccini, M.; Parry, V.; Fedorova, E.; Mantel, M.; Oquab, D.; Monceau, D., Relation between microstructure induced by oxidation and room-temperature mechanical properties of the thermally grown oxide scales on austenitic stainless steels. *Materials Characterization* **2017,** 127, 161-170.
7. Li, Y.; Chen, C.; Han, T.; Ranabhat, J.; Feng, X.; Shen, Y., Microstructures and oxidation behavior of NiCrAlCoY-Al composite coatings on Ti-6Al-4V alloy substrate via high-energy mechanical alloying method. *Journal of Alloys and Compounds* **2017,** 697, 268-281.
8. Lin, R. Q.; Fu, C.; Liu, M.; Jiang, H.; Li, X.; Ren, Z. M.; Russell, A. M.; Cao, G. H., Microstructure and oxidation behavior of Al + Cr co-deposited coatings on nickel-based superalloys. *Surface and Coatings Technology* **2017,** 310, 273-277.

9. Song, B.; Pala, Z.; Voisey, K. T.; Hussain, T., Gas and liquid-fuelled HVOF spraying of Ni50Cr coating: Microstructure and high temperature oxidation. *Surface and Coatings Technology*.
10. Voicu, R.; Andrieu, E.; Poquillon, D.; Furtado, J.; Lacaze, J., Microstructure evolution of HP40-Nb alloys during aging under air at 1000 °C. *Materials Characterization* **2009,** 60, (9), 1020-1027.
11. de Almeida, L. H.; Ribeiro, A. F.; Le May, I., Microstructural characterization of modified 25Cr–35Ni centrifugally cast steel furnace tubes. *Materials Characterization* **2002,** 49, (3), 219-229.
12. Jakobi, D.; Karduck, P.; von Richthofen, A. F., The High-Temperature Corrosion Resistance of Spun-Cast Materials for Steam-Cracker Furnaces-A Comparative Study of Alumina-and Chromia-Forming Alloys. *CORROSION 2013* **2013**.
13. De Saegher, J. J.; Detemmerman, T.; Froment, G. F., Three dimensional simulation of high severity internally finned cracking coils for olefins production. *Revue De L'Institut Français Du Pétrole* **1996,** 51, (2), 245-260.
14. Detemmerman, T.; Froment, G. F., Three dimensional coupled simulation of furnaces and reactor tubes for the thermal cracking of hydrocarbons. *Revue De L'Institut Français Du Pétrole* **1998,** 53, (2), 181-194.
15. Schietekat, C. M.; van Goethem, M. W. M.; Van Geem, K. M.; Marin, G. B., Swirl flow tube reactor technology: An experimental and computational fluid dynamics study. *Chemical Engineering Journal* **2014,** 238, 56-65.
16. Torigoe, T.; Hamada, K.; Furuta, M.; Sakashita, M.; Otsubo, K.; Tomita, M. In *Mixing element radiant tube (MERT) improves cracking furnace performance*, 11th Ethylene Producers' Conference, Houston, TX, 1999; Houston, TX, 1999.
17. Györffy, M.; Hineno, M.; Hashimoto, K.; Park, S.-H.; You, M.-S. In *MERT performance and technology update*, 21st Ethylene Producers' Conference, Tampa, FL, 2009; Tampa, FL, 2009.
18. Schietekat, C. M.; Van Cauwenberge, D. J.; Van Geem, K. M.; Marin, G. B., Computational fluid dynamics-based design of finned steam cracking reactors. *AIChE Journal* **2014,** 60, (2), 794-808.

19. Petrone, S.; Mandyam, R.; Wysiekierski, A. Surface alloyed high temperature alloys. US6093260, 1997.
20. SK-Corporation In *Coke Inhibition Technologies - Commercial Experience: F. SK Corporation - PY-COAT*, 13th Ethylene Producers' Conference, Houston, TX, 2001; Houston, TX, 2001.
21. Schietekat, C. M.; Sarris, S. A.; Reyniers, P. A.; Kool, L. B.; Peng, W.; Lucas, P.; Van Geem, K. M.; Marin, G. B., Catalytic Coating for Reduced Coke Formation in Steam Cracking Reactors. *Industrial & Engineering Chemistry Research* **2015,** 54, (39), 9525-9535.
22. Zychlinski, W.; Wynns, K. A.; Ganser, B., Characterization of material samples for coking behavior of HP40 material both coated and uncoated using naphtha and ethane feedstock. *Materials and Corrosion-Werkstoffe Und Korrosion* **2002,** 53, (1), 30-36.
23. Ganser, B.; Wynns, K. A.; Kurlekar, A., Operational experience with diffusion coatings on steam cracker tubes. *Materials and Corrosion* **1999,** 50, (12), 700-705.
24. Benum, L. In *Achieving longer furnace runs at NOVA Chemicals*, 2002 AIChE Spring Meeting, New Orleans, LA, 2002; New Orleans, LA, 2002.
25. Györffy, M.; Benum, L.; Sakamoto, L. In *Increased run length and furnace performance with Kubota and NOVA Chemicals' ANK 400 anticoking technology; data from current installations as well as technologyimprovements for higher thermal stability and decoking robustness*, 2006 AIChE National Meeting, Orlando, FL, 2006; Orlando, FL, 2006.
26. Petrone, S.; Manyam, R.; Wysiekierski, A.; Tzatzov, K.; Chen, Y. In *A "carbon-like" coating to improved coking resistance in pyrolysis furnaces*, 10th Annual Ethylene Producers' Conference, New Orleans, LA, 1998; New Orleans, LA, 1998.
27. Bergeron, M.; Maharajh, E.; McCall, T. In *A low coking environment for pyrolysis furnace - CoatAlloy*, 11th Annual Ethylene Producers' Conference, Houston, TX, 1999; Houston, TX, 1999.
28. Redmond, T.; Bailey, A.; Chen, Y.; Fisher, G.; Miller, R. In *Performance of Coatalloy coating systems in ethylene pyrolysis furnaces using different feedstocks*, 12th Annual Ethylene Producers' Conference, Atlanta, GA, 2000; Atlanta, GA, 2000.
29. Petrone, S.; Chen, Y.; Deuis, R.; Benum, L.; Saunders, R.; Wong, C. In *Catalyzed-assisted manufacture of olefins (CAMOL): Realizing novel operational benefits from*

furnace coil surfaces, 20th Ethylene Producers' Conference, New Orleans, LA, 2008; New Orleans, LA, 2008.

30. Petrone, S.; Deuis, R.; Unwin, P. In *Catalyzed-assisted manufactur of olefins (CAMOL): Year-(4) update on commercial furnace installations*, 22th Ethylene Producers's Conference San Antonio, TX, 2010; San Antonio, TX, 2010.
31. Petrone, S.; Deuis, R.; Kong, F.; Chen, Y. Catalytic surfaces and coatings for the manufacture of petrochemicals. US 2013/0337999 A1, 2013.
32. Rech, S. Catalyzed-Assisted Manufacture of Olefins (CAMOL™): Updated for Use in Naphtha Service. (August 21, 2014),
33. Wang, J.; Reyniers, M.-F.; Van Geem, K. M.; Marin, G. B., Influence of Silicon and Silicon/Sulfur-Containing Additives on Coke Formation during Steam Cracking of Hydrocarbons. *Industrial & Engineering Chemistry Research* **2008,** 47, (5), 1468-1482.
34. Wang, J.; Reyniers, M.-F.; Marin, G. B., Influence of Dimethyl Disulfide on Coke Formation during Steam Cracking of Hydrocarbons. *Industrial & Engineering Chemistry Research* **2007,** 46, (12), 4134-4148.
35. Reyniers, M.-F.; Froment, G. F., Influence of metal-surface and sulfur addition on coke deposition in the thermal-cracking of hydrocarbons. *Industrial & Engineering Chemistry Research* **1995,** 34, (3), 773-785.
36. Dhuyvetter, I.; Reyniers, M.-F.; Froment, G. F.; Marin, G. B.; Viennet, D., The influence of dimethyl disulfide on naphtha steam cracking. *Industrial & Engineering Chemistry Research* **2001,** 40, (20), 4353-4362.
37. Bajus, M.; Vesely, V.; Baxa, J.; Leclercq, P. A.; Rijks, J. A., Steam cracking of hydrocarbons: 5. Effect of thiophene on reaction-kinetics and coking. *Industrial & Engineering Chemistry Product Research and Development* **1981,** 20, (4), 741-745.
38. Bajus, M.; Vesely, V., Pyrolysis of hydrocarbons in the presence of elemental sulfur. *Collection of Czechoslovak Chemical Communications* **1980,** 45, (1), 238-254.
39. Bajus, M.; Baxa, J.; Leclercq, P. A.; Rijks, J. A., Steam cracking of hydrocarbons: 6. Effect of dibenzyl sulfide and dibenzyl disulfide on reaction-kinetics and coking. *Industrial & Engineering Chemistry Product Research and Development* **1983,** 22, (2), 335-343.

40. Bajus, M.; Baxa, J., Coke formation during the pyrolysis of hydrocarbons in the presence of sulfur-compounds. *Collection of Czechoslovak Chemical Communications* **1985,** 50, (12), 2903-2909.

41. Depeyre, D.; Filcoteaux, C.; Blouri, B.; Ossebi, J. G., Pure norma-nonane steam cracking and the influence of sulfur-compounds. *Industrial & Engineering Chemistry Process Design and Development* **1985,** 24, (4), 920-924.

42. Munoz Gandarillas, A. E.; Van Geem, K. M.; Reyniers, M.-F.; Marin, G. B., Influence of the Reactor Material Composition on Coke Formation during Ethane Steam Cracking. *Industrial & Engineering Chemistry Research* **2014,** 53, (15), 6358-6371.

43. Muñoz Gandarillas, A. E.; Van Geem, K. M.; Reyniers, M.-F.; Marin, G. B., Coking Resistance of Specialized Coil Materials during Steam Cracking of Sulfur-Free Naphtha. *Industrial & Engineering Chemistry Research* **2014,** 53, (35), 13644-13655.

44. Wang, J.; Reyniers, M.-F.; Marin, G. B., The influence of phosphorus containing compounds on steam cracking of n-hexane. *Journal of Analytical and Applied Pyrolysis* **2006,** 77, (2), 133-148.

45. Van Geem, K. M.; Reyniers, M. F.; Pyl, S. P.; Marin, G. B., Effect of Operating Conditions and Feedstock Composition on Run Length of Steam Cracking Coils. In *(2009) AIChE 2009 Spring National Meeting*, Tampa, FL, 2009.

46. Muñoz Gandarillas, A. E.; Van Geem, K. M.; Reyniers, M.-F.; Marin, G. B., Influence of the Reactor Material Composition on Coke Formation during Ethane Steam Cracking. *Industrial & Engineering Chemistry Research* **2014,** 53, (15), 6358-6371.

47. Asteman, H.; Hartnagel, W.; Jakobi, D., The Influence of Al Content on the High Temperature Oxidation Properties of State-of-the-Art Cast Ni-base Alloys. *Oxidation of Metals* **2013,** 80, (1-2), 3-12.

48. Lyle, F. A.; Baker, R. T. K., *Coke Formation on Metal Surfaces*. AMERICAN CHEMICAL SOCIETY: 1983; Vol. 202, p 332.

49. Muñoz, A. E.; Van Geem, K. M.; Reyniers, M.-F.; Marin, G. B., Influence of the Reactor Material Composition on Coke Formation During Ethane Steam Cracking. *Industrial & Engineering Chemistry Research* **2014**.

50. Jasinski, W.; Zawada, P., The precipitation processes in the Manaurite XM superalloy during 1000 hours of ageing. *International Journal of Microstructure and Materials Properties* **2008,** 3, (4-5), 607-615.

51. Jasinski, W.; Zawada, P., The precipitation processes of Manaurite XM superalloy after 2000 hours of aging. *Archives of Foundry Engineering* **2008**.

Chapter 8. Conclusions and Perspectives

8.1. Conclusions

The use of experimental results of laboratory, bench and pilot scale nature is inevitable to perform scale up studies of the observed trends. Improvements in the reactive and analytical sections will bring better accuracy of effluent analysis and coking rates measurements. Also, the development of set-ups with industrially more representative conditions throughout the reactant volume, but also more accurate measurements of the pressure, temperature and fed flows will allow more realistic experimental observations.

The aim of this PhD thesis was the study different parameters influencing coke formation during ethane steam cracking always in an attempt to minimize coke formation on the reactor coil. Clearly, as highlighted during this thesis, there is plenty of space for scientific research in the field of steam cracking and carbon minimization both from the materials perspective and process conditions one.

In the second chapter of this work, the importance of the pretreatment optimization for the different used materials was highlighted. Eight different pretreatments were tested on a classical high temperature alloy in a thermogravimetric set-up in combination with SEM & EDX and XRD analyses. A two-step preoxidation followed by a steam/air pretreatment, was found to be the best in reducing coke deposition for ethane steam cracking when continuously adding DMDS during the run. At least 30% lower pyrolytic coking rates than the other investigated pretreatments were obtained and almost a factor 5 compared to the worst

pretreatment, illustrating the importance of optimizing the surface pretreatment. Applying a steam only pretreatment mitigates the catalytic coking by creating a very thick oxide layer which blocks catalytically active sites. However, higher pyrolytic coking rates in comparison with the optimal pretreatment B are measured. Increasing the duration of the steam pretreatment led to further reduction of the catalytic coking rate, however the pyrolytic coking rate remained higher than pretreatment B. After presulfiding in different durations the surface generated up to 3 times more coke. Pretreatment B leads to primarily $MnCr_2O_4$, Cr_2O_3 and $NiFe_2O_4$ on the surface. Increasing the duration of the steam only pretreatment leads to increased homogeneity but not for presulfiding. The duration of the steam/air pretreatment played no role - very important for industrial furnaces - which are often put on the hot steam standby. Overall, mild preoxidation at elevated temperature followed by a steam/air pretreatment leads to the most homogeneous oxide layer formation consisting of mainly Cr and Mn optimizing the anti-coking performance of a high temperature Fe-Ni-Cr Alloy.

In the third chapter, the surface roughness effect was evaluated in a range of R_α 0.15 – 7.0 µm, showing a significant influence on the catalytic coking rates during steam cracking of ethane at 1173 K and leading to an increase of a factor 6 at the worst case. In terms of pyrolytic coke formation and reactor effluent, the influence of roughness faded away. Conversion and selectivity together with CO and CO_2 values are stable for all the different values, suggesting that once the first coke layer is formed and the catalytic active sites are covered, there is no significant difference in the coking and gasification rate. By increasing the roughness, the available bare metal surface is increased which makes that the catalytic coking rate is a strong function of the roughness. If this additional area is properly pretreated then the pyrolytic coking rate remains unaffected. After SEM and EDX analysis, the measured surface composition indicates that the amount of Cr and Fe is increasing with increased cracking/decoking cycles, while the amount of Ni and Mn is decreased. In general

an Increase of the roughness leads to elevated catalytic coking rate due to the additional catalytic sites and area in a fresh manufactured material. However, pyrolytic coke formation is, besides the gas phase composition, a strong function of the material elemental composition and surface oxides homogeneity. The latter is mainly a function of the pretreatment of the surface. Industrially, the presence of Cr_2O_3 and $MnCr_2O_4$ at the surface will lead to a quite better coking behavior for Fe-Ni-Cr alloys independently of the surface roughness.

In Chapter 4, four innovative alloys were experimentally evaluated in JSR. Overall, the worst performance was measured for the 25/35 Cr/Ni alloy. In the absence of DMDS, the Al-content material performed from 2 to 3 times worse than the competition, that coked rather similarly. When DMDS was added continuously in the feed the best performance was found for the higher Cr/Ni content alloy, with the worst belonging to the 25/35 Cr/Ni one. The Al-content alloy showed similar to slightly better than the 35/45 Cr/Ni alloy behavior, underlining the Al anti-coking performance. The effect of presulfiding is more pronounced in the case that it is applied on a Blank run than on a continuous addition run. The Al-content alloy had the most stable behavior after application of presulfiding, being slightly better than the 35/45 Cr/Ni alloy, yet worse than the 40/48 Cr/Ni one. The presence of Cr, Mn and Al on top of the surface improve the anti-coking behavior of an alloy, however their relative anti-coking performance has not been evaluated yet. The relative coking reactivity of Fe appeared to be higher than the one of Ni. Also, the existence of Mn on top of the surface seems to improve the anti-coking behavior of an alloy at cracking temperatures higher than 1173 K in comparison with the ones of Cr or Al.

In the field of super alloys, in Chapter 5, the JSR experimental set-up was proven capable of evaluating the coking performance of a Ti-base alloy under industrially relevant ethane steam cracking conditions. The results were disappointing with a factor 10 and 300 increased values of CO, for the typical and higher temperature pretreatment respectively, measured over the 8

cracking cycles in comparison with the reference 25/35 Cr/Ni alloy. A factor 3 increase of the CO2 was observed in between the higher temperature preoxidation and the optimized preoxidation used for Fe-Ni-Cr when applied to the Ti-base alloy. No significant difference was observed for the CO2 values of Ti-Alloy in comparison with the reference 25/35 Cr/Ni alloy. The increase of Carbon oxides is followed by an increase of H2, supporting the idea that Ti and Ti-oxides are catalytic towards coke gasification. The pronounced differences in terms of gas phase composition are supported by the increased surface. Clearly at the points of cracks formation coke gasification catalyzed, affecting the gas phase product distribution. The use of the Ti-base alloy in an industrial cracker is considered highly risky and certainly not beneficial in terms of coking or carbon oxides formation.

In Chapter 6, a barrier passivating commercially known coating, namely "CoatAlloy". Overall, the addition of sulfur on-stream or as pretreatment lead to decreased carbon oxides formation. Apart from the blank experiments, no significant observable differences were noted between the reference material and the passivating formulation under the different conditions. The coating generated almost 2 times more CO compared to the reference for the blank runs. Presulfiding before cracking, led to 20 % reduction of carbon oxides formation for both the reference and the coated sample. In terms of coking, under blank run conditions CoatAlloy cokes from 2 to 5 times more than the reference, when the same treatment was used. In the case that the treatment for CoatAlloy did not include nitrogen and only steam/air mixture was applied, the asymptotic coking rate observed was comparable with the one of the reference material, decreased even by a factor 3 in comparison with the normal treatment. By application of cyclic aging the performance of the barrier coating improves significantly, while the reference material seems to remain rather stable. In that way, the coating leads from 10 to 50 % lower coking rates for catalytic and pyrolytic respectively. The coating seems to perform a lot better after cyclic aging and in the presence of DMDS during cracking giving

the impression that after several cracking cycles would even outperform the reference material. At higher operating temperatures this is definitely expected .

In Chapter 7, the effect of metallurgic aging on the coking rates of four different alloys was for first time evaluated in a thermogravimetric set-up. This, after their exposure to a long-term high temperature oxidation for 500 h. Based on the results the coking resistance is improved by increasing the content of Cr and Ni of a high temperature alloy. Cyclic aging after metallurgical aging had a minor effect on the tested alloys. Mainly the 25/35 Cr/Ni alloy showed pronounced coking rates after cyclic aging. The worse the intrinsic anti-coking behavior of the material is, the more pronounced the effect the metallurgic aging is. For the best tested material, a negligible effect was noticed after the long-term oxidation. Overall, the catalytic and pyrolytic coking behavior of the materials is quite aligned, implying that the two phenomena are interconnected. In agreement, with previous work and literature, the absence of Fe and Ni helps the anti-coking performance of an alloy. Most of the alloys indicated a rather uniform coverage of their surface by oxides - mainly of Cr nature for the non Al-content alloys. For the Al-content alloy, the thickness of the oxides covering typically the surface after cyclic aging is reduced by almost 1 μm, in contrast with the rest alloys that the oxides' thickness was dramatically increased. , the addition of Al to a high temperature alloy, forms Al oxides that protect the bulk from further oxidation. No elaborated microstructure was found in any alloy while no correlation between the microstructure and the coking behavior of an alloy was found.

8.2. Perspectives

Finding the optimal material, process conditions, pretreatments to mitigate coke formation in industrial steam crackers is not an easy task. With the present work several different aspects

of the carbon minimization are investigated. However, there are still many things to be experimentally tested.

The main point of improvement is the too low temperatures at the coupon gas interface compared to industrial conditions. New reactor designs can be used in order to overcome this problem. Different heating methods, such as inductive heating of the coupon, will allow a more representative concept. Additionally, an improved analysis section similar to the bench scale or pilot plant set-up will add quality to the obtained gas effluent results. Adaptation can be made in the downstream lines, by reducing the residence time of the outlet gas before its introduction to the analytics. Also, automation of the set-up will add up to its reproducibility capability.

Experimentally, the effect of the pretreatment should be ideally evaluated for all the different available materials. In this thesis, this is done for a single material, showing the complexity of the phenomena occurring. The effect of Steam and Air are certainly in the core of research, together with the applied temperature in each case. Surface analysis of the samples after pretreatment will always have a significant role in the fundamental understanding of the different conditions applied. For the used coatings the pretreatment should be also affected by the bulk properties, for example oxidation and carburization resistance.

It would be certainly interesting if the effect of roughness would be evaluated in different alloys as well and under different cracking conditions. Additionally, to accurately represent the surface before and after, the measurement of the surface roughness can be always optimized by 3-D measurement equipment. The effect can be scaled-up by additional pilot-plant experiments and CFD simulations.

The market will always generate promising innovative high temperature alloys, illustrating resistance against carburization, oxidation and aging. Nevertheless, in combination with the pretreatment, the optimal cracking conditions, namely temperature, dilution, concentration of

additives, per alloy should be always investigated and optimized. Different additives and several impurities found in the steam or hydrocarbon feedstock can always cause a nightmare in the observed coking trends.

Application of coatings in steam cracking remains a challenge, since they sometimes introduce additional problems in practice. The increase of carbon oxides can cause significant issues in the separation section. deactivating or poisoning the catalysts downstream of the steam cracker towards the dehydrogenation units. In some cases, if the experimental observations are combined with Computational Fluid Dynamics (CFD) then the coil coating can be wisely applied to only improve the run length of the process.

Metallurgists are often only looking into the effect of carburization, oxidation and aging, while the process engineering research focuses on the coking rates, effluent and run length observations. Surface characterization of both the alloy and the coke formed with several different techniques will help to elucidate on the effect of process conditions, elemental composition, surface morphology on both catalytic and pyrolytic mechanisms of coke formation. It is clear that the expertise from both fields needs to be combined. The oxidation states found on the surface and the relative coke formation kinetics of these should be in the core of interest in order to chart the carbon growth phenomenon.

To develop the best anti-coking technology all factors should be accounted. In other words, the above mentioned experimental process observations, must be always combined with CFD analysis and deep knowledge of the metallurgy should all contribute to targeted research towards coke minimization and improved run length.

The distillate of all the above can eventually lead to an accurate mathematical prediction of carbon formation and deposition in the industrial crackers, taking into account the surface elemental composition and morphology, the feedstock characteristics, the reactor design, the

cyclic cracking and decoking effect and the process conditions. Certainly, in this thesis a first - to the maximum possible in four years - thorough experimental attempt has been done.

Appendix A. Supplementary information to Chapter 2.

This Appendix contains data published as supporting information of the manuscript in chapter 2:

Optimization of the in-situ pretreatment of high temperature Ni-Cr Alloys for Ethane steam cracking

Stamatis A. Sarris[1], Natalia Olahova[1], Kim Verbeken[2], Marie-Françoise Reyniers[1], Guy B. Marin[1], Kevin M. Van Geem[1,*]

[1]Ghent University, Laboratory for Chemical Technology, Technologiepark 914, 9052 Gent, Belgium.

[2]Ghent University, Department of Materials Science and Engineering, Technologiepark 903, 9052 Gent, Belgium

Effect of Temperature and Air Pretreatment

The effect of an air treatment at higher temperature (1108 K) for the initial step, followed by the OAS.1 pretreatment, namely pretreatment I, has also been evaluated, see Figure A. 1. The total amount of coke deposited after this pretreatment was significantly higher than the rest pretreatments - even by a factor 8. Thus, among pretreatments A, I and J, the former was finally chosen as the base case for the pretreatment study.

Pretreatment K is the same pretreatment with optimal pretreatment B but at a stable temperature of 1023 K. The coking results show an increase of 30 % in the total amount of coke formed on the coupon in comparison with the optimal pretreatment B. Figure A. 2 shows the decreased homogeneity of the oxides formed on the surface when the temperature of the steam/air pretreatment is increased by 150 K.

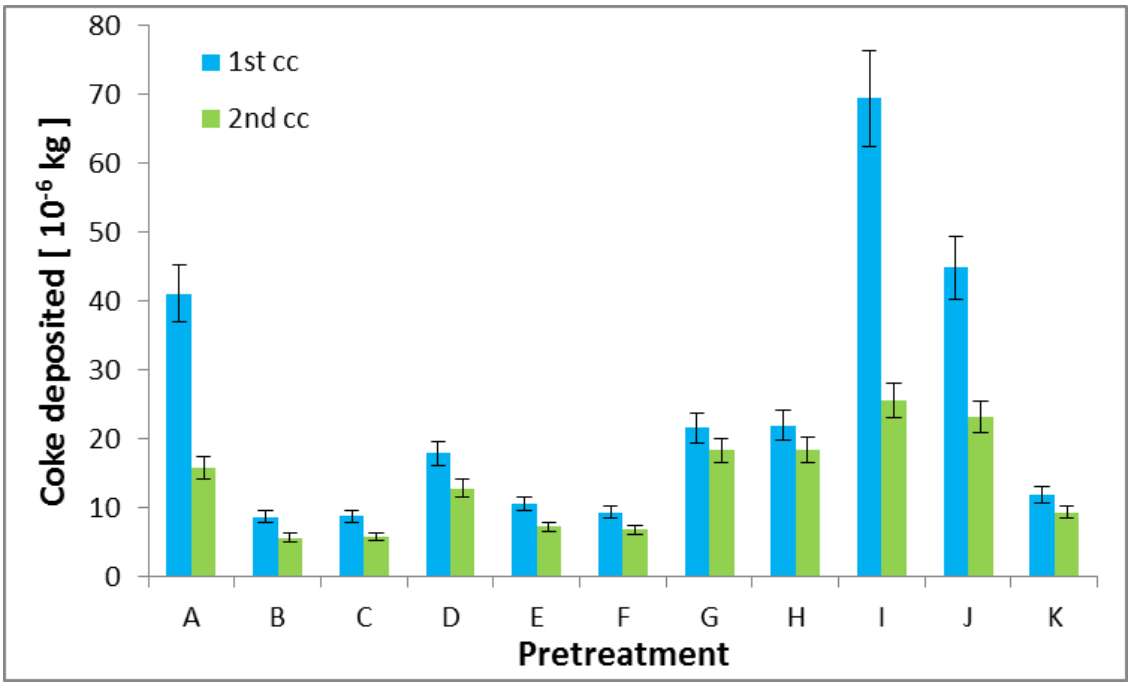

Figure A. 1: Total coke deposited on the samples after the 1st or the 2nd cracking cycle

Table A. 1: Conditions of the pretreatments investigated.

Id	Steps			
	1	**2**	**3**	**4**
A	6.7 · 10-3 Nl s^{-1} of Air; 14h; T=1023 K	1:1 8.15 · 10^{-3} Nl s^{-1} of Air:N_2; 30 min; T=from 1023 K to 1173 K	-	-
B	6.7 · 10^{-3} Nl s^{-1} of Air; 14h; T=1023 K	1:1 8.15 · 10^{-3} Nl s^{-1} of Air:N_2; 30 min; T=from 1023 K to 1173 K	8.15 · 10^{-3} Nl s^{-1} of Air and 6.67 · 10^{-6} kg s^{-1} Steam; 15min ; T=1173 K	-
C	6.7 · 10^{-3} Nl s^{-1} of Air; 14h; T=1023 K	1:1 8.15 · 10^{-3} Nl s^{-1} of Air:N_2; 30 min; T=from 1023 K to 1173 K	8.15 · 10^{-3} Nl s-1 of Air and 6.67 · 10^{-6} kg s^{-1} Steam; 1min ; T=1173 K	-
D	6.7 · 10^{-3} Nl s^{-1} of Air; 14h; T=1023 K	1:1 8.15 · 10^{-3} Nl s^{-1} of Air:N_2; 30 min; T=from 1023 K to 1173 K	8.15 · 10^{-3} Nl s^{-1} of Air and 6.67 · 10^{-6} kg s^{-1} Steam; 15min ; T=1173 K	5.55 · 10^{-6} kg s^{-1} of Steam with DMDS 500 ppmw DMDS/H2O; 1 hour; T=1100 K
E	6.7 · 10^{-3} Nl s^{-1} of Air; 14h; T=1023 K	1:1 8.15 · 10^{-3} Nl s^{-1} of Air:N_2; 30 min; T=from 1023 K to 1173 K	6.67 · 10^{-6} kg s^{-1} Steam; 15min; T=1173 K	-
F	6.7 · 10^{-3} Nl s^{-1} of Air; 14h; T=1023 K	1:1 8.15 · 10^{-3} Nl s^{-1} of Air:N_2; 30 min; T=from 1023 K to 1173 K	6.67 · 10^{-6} kg s^{-1} Steam; 1 hour; T=1173 K	-
G	6.7 · 10^{-3} Nl s^{-1} of Air; 14h; T=1023 K	1:1 8.15 · 10^{-3} Nl s^{-1} of Air:N_2; 30 min; T=from 1023 K to 1173 K	6.67 · 10^{-6} kg s^{-1} Steam; 1 hour; T=1173 K	5.55 · 10^{-6} kg s^{-1} of Steam with DMDS 500 ppmw DMDS/H2O; 1 hour; T=1100 K
H	6.7 · 10^{-3} Nl s^{-1} of Air; 14h; T=1023 K	1:1 8.15 · 10^{-3} Nl s^{-1} of Air:N_2; 30 min; T=from 1023 K to 1173 K	6.67 · 10^{-6} kg s^{-1} Steam; 1 hour; T=1173 K	5.55 · 10^{-6} kg s^{-1} of Steam with DMDS 500 ppmw DMDS/H2O; 1 hour; T=1100 K
I	6.7 · 10^{-3} Nl s^{-1} of Air; 14h; T=1108 K	8.15 · 10^{-3} Nl s^{-1} of Air and 6.67 · 10^{-6} kg s^{-1} Steam; 15 min ; T=1173 K	-	-
J	6.7 · 10^{-3} Nl s^{-1} of Air; 14h; T=1023 K	-	-	-
K	6.7 · 10^{-3} Nl s-1 of Air; 14h; T=1023 K	8.15 · 10^{-3} Nl s^{-1} of Air and 8.15 · 10^{-3} Nl s^{-1} of N_2 ; 30 min; T=1023 K	8.15 · 10^{-3} Nl s^{-1} of Air and 6.67 · 10^{-6} kg s^{-1} Steam; 15 min ; T=1023 K	-

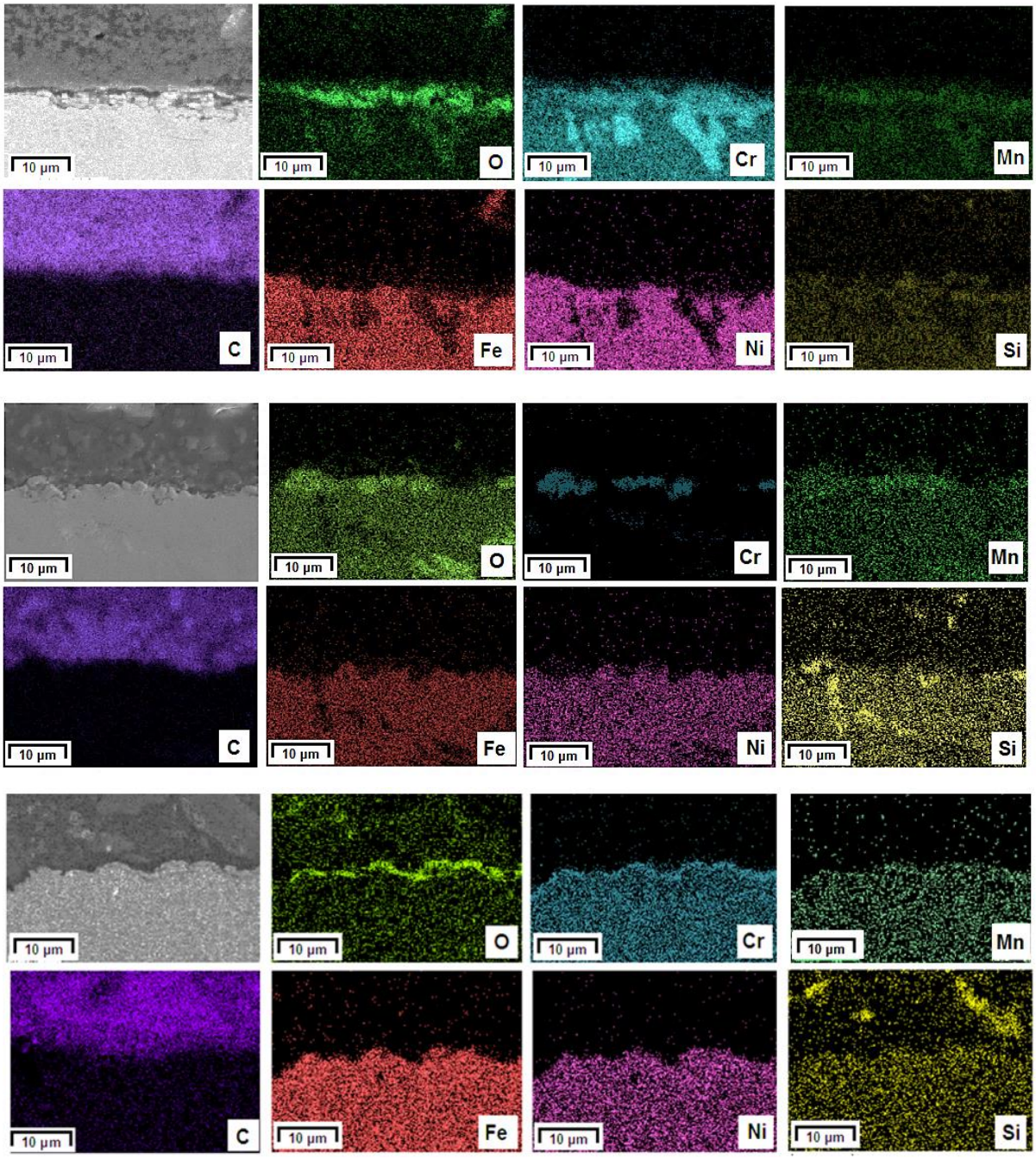

Figure A. 2: Cross section elemental mappings of coked sample after pretreatment I (top), pretreatment J (middle) and pretreatment K (bottom).

Table A. 2: EkviCalc input molar values for the surface and gas phase composition

ID		Fresh	A	B	C	D	E	F	G	H	Surface composition		
T (K)		298	1173	1173	1173	1100	1173	1173	1100	1100	Elements	Acc. Volt.	Fresh
Pressure [10^5 atm]						1						kV	molar %
mol	N_2	79	89.50	34.16	34.16						Ni	10	40.3
	O_2	21	10.50	9.08	9.08							20	33.5
	H_2O			56.76	56.76	99.99	100	100	99.99	99.99	Fe	10	33.4
	DMDS					0.01			0.01	0.01		20	35.4
Cracking conditions											Cr	10	23.6
Temperature (K)		1160										20	27.0
Pressure [10^5 atm]		1.03									Si	10	1.7
gas phase		31 mol H_2										20	1.8
		6.16 mol CH_4									Mn	10	0.0
		8.68 mol C_2H_6										20	1.3
		26.45 mol C_2H_4									Nb	10	0.9
		27.71 mol H_2O										20	0.8

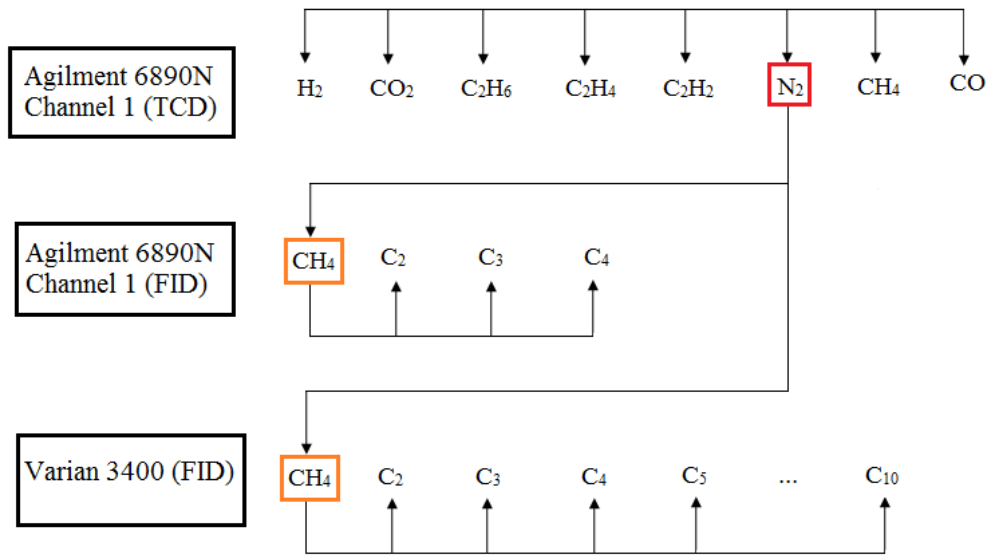

Figure A. 3: Schematic overview of the use of internal standards for quantitative composition analysis

XRD analysis

To further evaluate the crystal structure of the coupons XRD analysis was performed. The crystalline phases were determined using a Siemens Diffractometer Kristalloflex D5000, with Cu Kα (λ = 0.154nm) radiation. The XRD patterns were collected in a 2θ range from 10° to 80° with a step of 0.04°. Since the patterns of the pretreated samples showed mainly three big peaks (Fe-Ni to an angle of 43.65°, 50.8° and 74.75°), in all of them zoomed figures are added per angle regions showing possibly identified oxidized phases.

In Figure A. 4, the effect of steam/air pretreatment is evaluated. As mentioned above, the first thing noted should be that the peaks of the Fe-Ni and Ni-Cr-Fe spinels are significantly more intense than the ones of the oxides identified in the sample. It is clear that by adding a step of steam/air pretreatment in the sequence, the peaks of Fe-Ni to an angle in the region of 43.5° to 44.5° (Figure A. 4 e) are relatively more intense and clear, while without it there is also a shoulder of Ni-Cr-Fe observed in the pattern. The opposite is observed to an angle of 50.5° to 51.5° (Figure A. 4 g). A small shift in the positioning of most of the peaks occurs, deriving from small differences between the crystal sizes measured and the ones that are available in the database of the machine. As far as the oxides are concerned, the peaks of Cr_2O_3 (to an angle of 24.4° to 24.8° and 35.5° to 36.5° - see Figure A. 4 a and c) are easily observed in the steam/air pretreated samples, while by increasing the duration of the pretreatment the peak of $MnFe_2O_4$ also occurs (C vs B) to an angle of 18.0° to 18.4°(Figure A. 4 a). In some peaks the possibility of the Magnetite, NbO, Fe_2O_3 or Fe-$2Cr_2O_4$ spinel could be also valid but the peaks are not that intense to make clear conclusions.

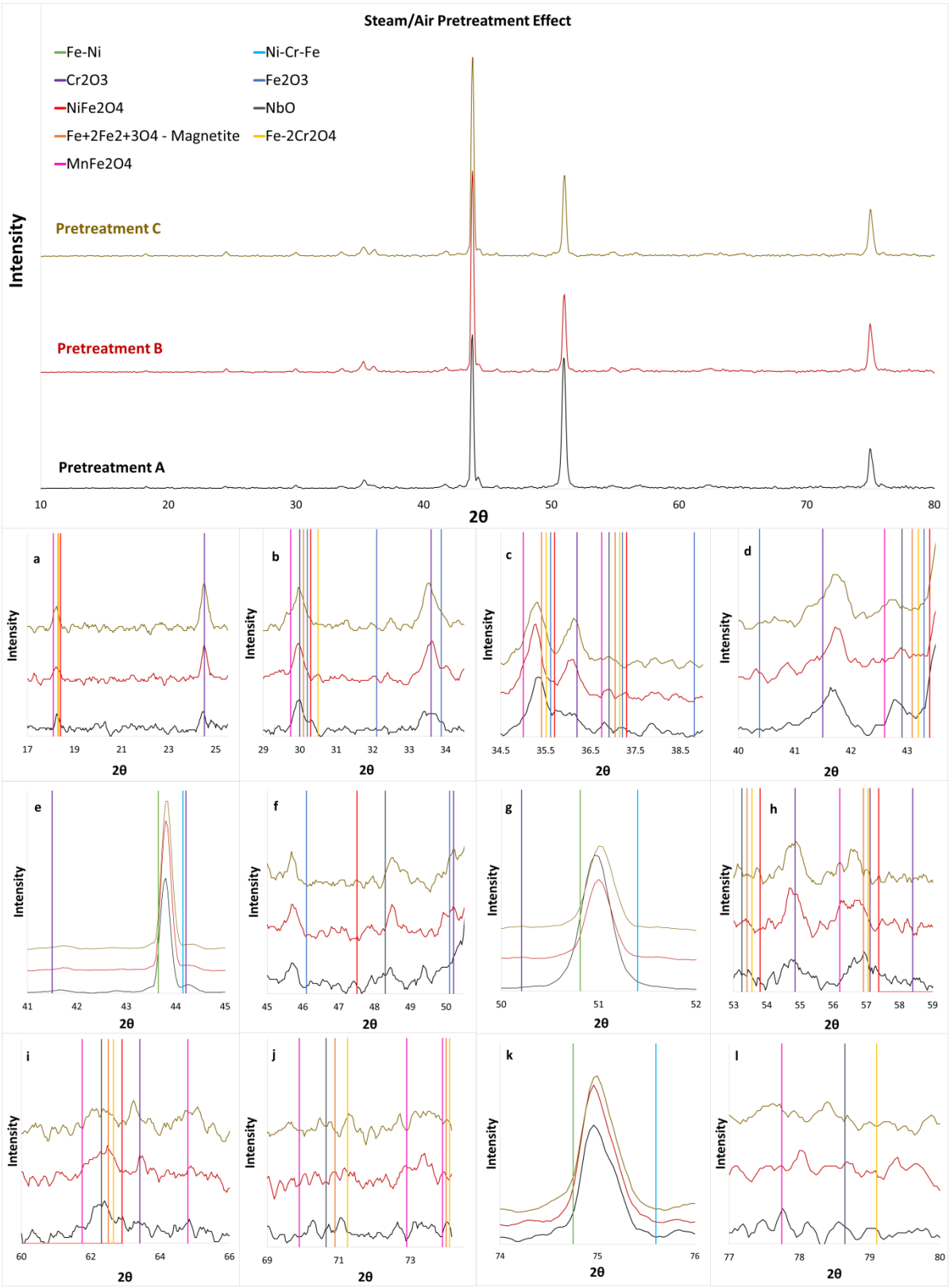

Figure A. 4: XRD patterns of pretreatment A, B and C. Top: overview of the full XRD pattern, From a to l: 'zoomed in' patterns for the identification of possible additional compounds.

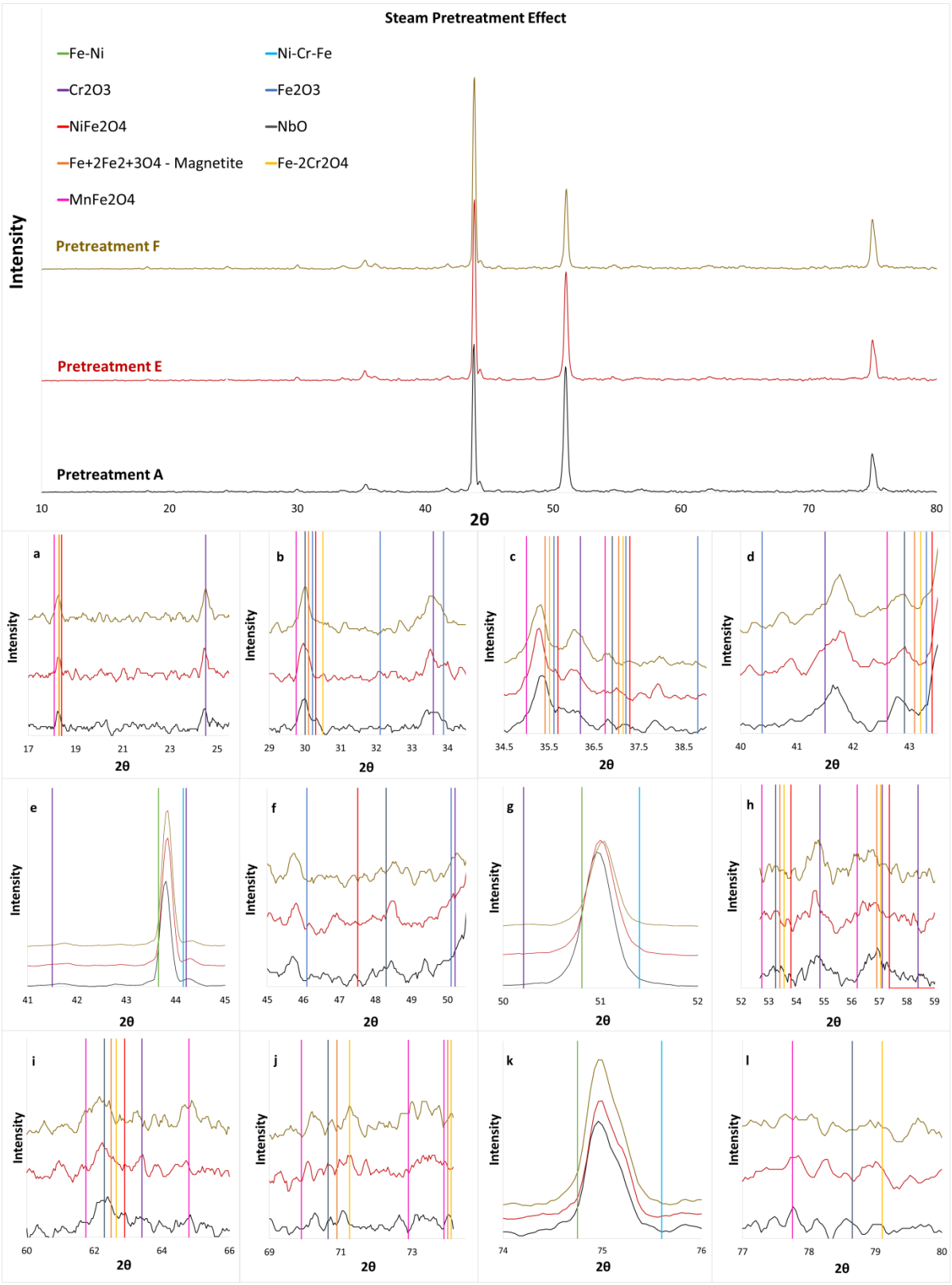

Figure A. 5: XRD patterns of pretreatment A, E and F (from bottom to top). Top: overview of the full XRD pattern, From a to l: 'zoomed in' patterns for the identification of possible additional compounds.

In Figure A. 5, the effect of steam pretreatment is analyzed based on XRD patterns. Again, the three main peaks of the patterns are the ones of Fe-Ni and the shoulders next to them of Ni-Cr-Fe. From Figure A. 5 a to d it is noted that $MnFe_2O_4$ and Cr_2O_3 phases are increased by increasing the duration of the steam pretreatment.

In Figure A. 6, the XRD patterns of the effect of a presulfiding step on a steam/air pretreated sample are shown. Besides minor differences on the intensity of the peaks of Cr_2O_3 and NbO, as it observed in Figure A. 6 f and i, and the more clear peak of Fe-Ni of the pretreatment B in comparison with pretreatment D, nothing additional can be highlighted.

The effect of two different presulfiding steps applied on a steam pretreated sample is discussed in Figure A. 7. By increasing the duration of the presulfiding step, the second Fe-Ni peak becomes more intense. NbO peak is clear in all the samples (see Figure A. 7 f and i), while $MnFe_2O_4$ is more intense in the area of 34.5° to 35.5° (see Figure A. 7 c and d). Finally, Figure A. 7 a and c point out that Cr_2O_3 is decreasing by increasing the time of presulfiding.

The superiority of the best anticoking pretreatment can be noted in Figure A. 8. In all the pretreatments that were not included in the main manuscript the Fe-Ni peaks in the angle region of 50.5° to 51.5° are more intense. Additionally, the optimal pretreatment B has the most intense Cr_2O_3 peaks for most of the crystal phases occurring – namely 24.5°, 33.6°, 36.2° and 54.8° (Figure A. 8 a, b, c and h).

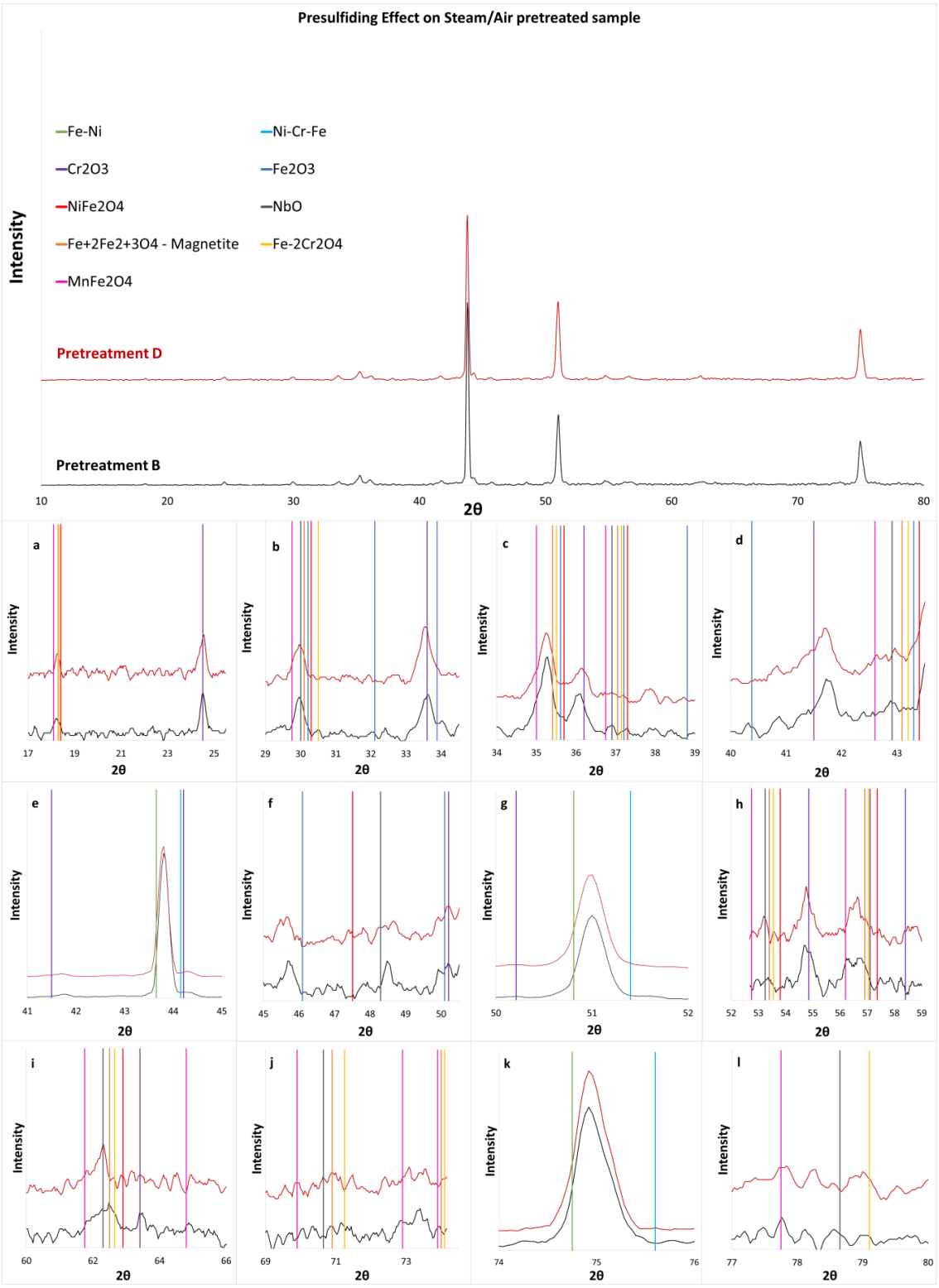

Figure A. 6: XRD patterns of pretreatment B and D . Top: overview of the full XRD pattern, From a to l: 'zoomed in' patterns for the identification of possible additional compounds.

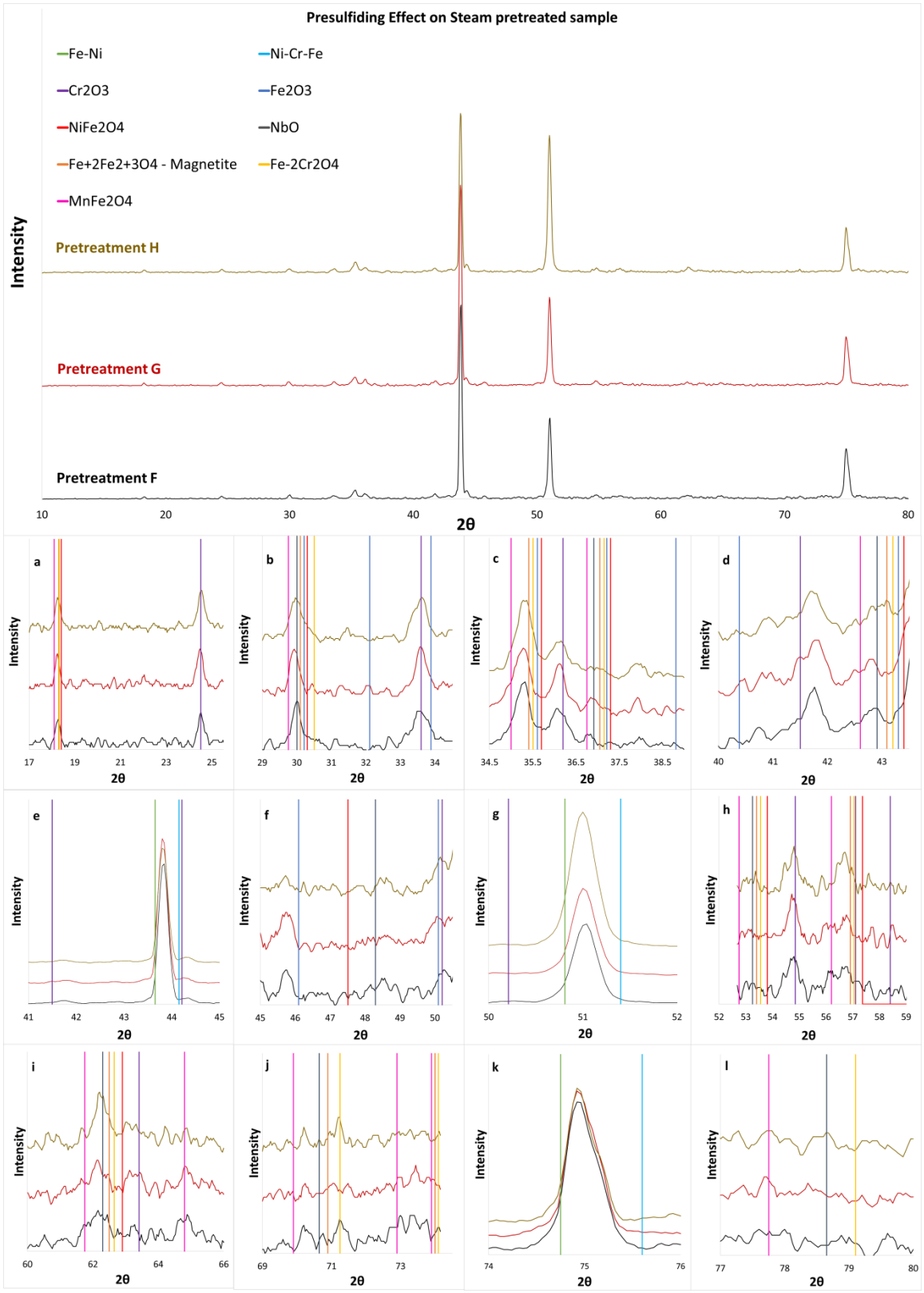

Figure A. 7: XRD patterns of pretreatment F, G and H. Top: overview of the full XRD pattern, From a to l: 'zoomed in' patterns for the identification of possible additional compounds.

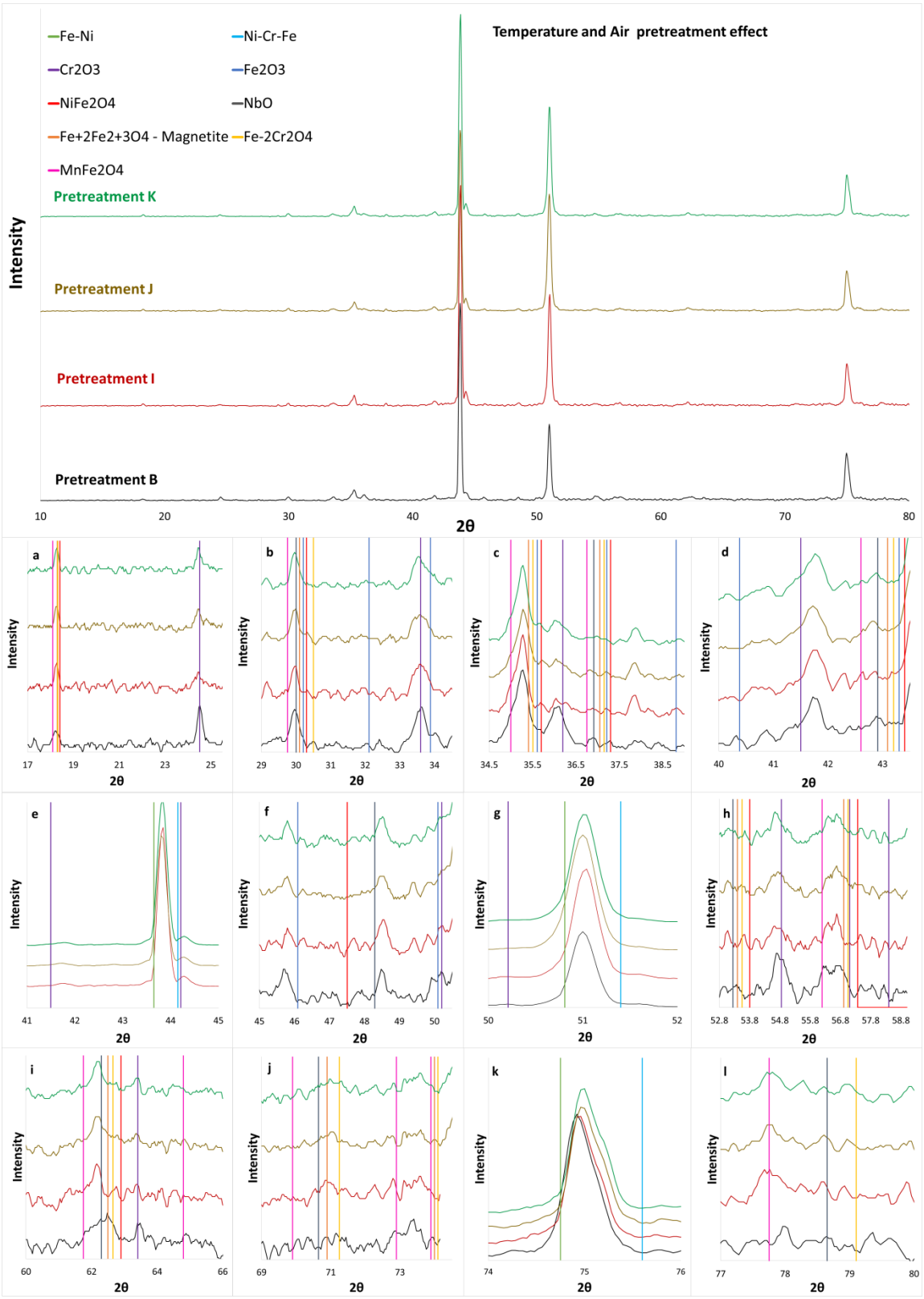

Figure A. 8: XRD patterns of pretreatment B, I, J and K. Top: overview of the full XRD pattern, From a to l: 'zoomed in' patterns for the identification of possible additional compounds.

Table A. 3: Thermodynamically stable phases calculated via EkviCalc by the EDX analysis of the pretreated (up) and coked (down) samples at 10kV. Steam cracking of Ethane: F_{HC} = 29.18 10^{-6} kg s^{-1}, δ = 0.33 kg_{H2O} kg^{-1}_{HC}, Treactor = 1160 K, p = 101.35 kPa, F_{H2O} = 9.72 10^{-6} kg s^{-1}, CA of DMDS 41 ppmw S/HC.

	Stable components	Fresh	A	B	C	D	E	F	G	H
Treated	$MnCr_2O_4$(s)	-	38.4	54.3	55.9	34.6	40.9	54.0	44.7	41.9
	Cr_2O_3(s)	-	15.0	20.2	18.5	39.3	23.8	-	27.7	11.3
	SiO_2(highquartz)	-	10.9	8.7	8.6	4.0	8.0	8.6	6.5	12.2
	$NiCr_2O_4$(s)	-	4.7	9.8	9.6	-	15.9	22.1	-	-
	$NiFe_2O_4$(beta)	27.6	31.0	6.6	6.9	-	-	-	-	-
	Fe_3O_4(s)	-	-	-	-	6.1	6.9	15.3	11.7	14.0
	Nb_2O_5(s)	0.5	0.2	0.5	0.5	0.5	-	-	0.0	-
	Ni(alpha)	-	-	-	-	14.6	4.4	0.1	8.4	19.6
	Ni_3S_2(l)	-	-	-	-	1.0	-	-	1.1	1.0
	CrO_2(s)	41.9	-	-	-	-	-	-	-	-
	NiO(s)	24.3	-	-	-	-	-	-	-	-
	Ni_2SiO_4(s)	5.7	-	-	-	-	-	-	-	-
	Stable components		**A**	**B**	**C**	**D**	**E**	**F**	**G**	**H**
Coked	$MnCr_2O_4$(s)		53.7	66.0	67.2	53.6	49.3	43.7	53.0	44.4
	MnO(s)		-	-	-	-	-	4.4	-	0.2
	Mn_2SiO_4(s)		-	-	-	-	-	3.1	-	7.8
	$MnSiO_3$(s)		0.7	-	-	-	-	-	2.3	-
	Cr_2O_3(s)		-	15.6	14.6	32.2	20.5	-	-	-
	SiO_2(highquartz)		6.4	6.5	6.2	2.4	2.6	-	3.3	-
	Fe(alpha)		35.5	3.7	3.8	4.1	10.7	36.9	35.7	37.4
	Ni(alpha)		3.8	8.2	8.2	7.7	16.9	12.0	5.8	10.22

Table A. 4: Top-View EDX Analyses of Pretreated and coked after 2 hours samples (up). Thermodynamically stable phases calculated via EkviCalc by the EDX analysis of the respective samples at 10kV (down). Steam cracking of Ethane: F_{HC} = 29.18 10^{-6} kg s^{-1}, δ = 0.33 kg_{H2O} kg^{-1}_{HC}, $T_{reactor}$ = 1160 K, p = 101.35 kPa, F_{H2O} = 9.72 10^{-6} kg s^{-1}, CA of DMDS 41 ppmw S/HC.

Elements	Acc. Volt.	A		B		C	
		treated	2h coked	treated	2h coked	treated	2h coked
Ni	10 kV	14.8	2.0	7.0	3.7	7.0	3.7
	20 kV	22.5	27.6	9.3	10.3	9.3	10.3
Fe	10 kV	24.5	18.0	5.3	1.6	5.6	1.6
	20 kV	28.5	31.1	8.0	9.1	8.3	9.54
Cr	10 kV	42.7	50.4	63.6	65.2	63.0	64.9
	20 kV	38.0	35.0	62.5	62.1	61.6	61.1
Si	10 kV	2.2	1.8	1.8	1.4	1.7	1.4
	20 kV	2.4	2.50	2.0	2.1	2	2.1
Mn	10 kV	14.9	27.0	21.7	27.8	22.1	28.2
	20 kV	7.7	2.9	17.4	15.5	17.9	16.1
Nb	10 kV	0.8	0.7	0.6	0.4	0.7	0.4
	20 kV	0.9	0.9	0.8	0.9	0.9	1.0
Stable components	$MnCr_2O_4$(s)	38.4	53.7	54.3	66	55.9	67.2
	$MnSiO_3$(s)	-	0.7	-	-	-	-
	Cr_2O_3(s)	15.0	-	20.2	15.6	18.5	14.6
	SiO_2(highquartz)	10.9	6.4	8.7	6.5	8.6	6.2
	$NiCr_2O_4$(s)	4.7	-	9.8	-	9.6	-
	$NiFe_2O_4$(beta)	31.0	-	6.6	-	6.9	-
	Fe_3O_4(s)	-	-	-	-	-	-
	Fe(alpha)	-	35.5		3.7	-	3.8
	Nb_2O_5(s)	0.2	-	0.5	-	0.5	-
	Ni(alpha)	-	3.8	-	8.2	-	8.2

Table A. 5: Top-View EDX Analyses of Pretreated and coked after 2 hours samples (up). Thermodynamically stable phases calculated via EkviCalc by the EDX analysis of the respective samples at 10kV (down). Steam cracking of Ethane: F_{HC} = 29.18 10^{-6} kg s^{-1}, δ = 0.33 kg_{H2O} kg^{-1}_{HC}, Treactor = 1160 K, p = 101.35 kPa, F_{H2O} = 9.72 10^{-6} kg s^{-1}, CA of DMDS 41 ppmw S/HC.

Elements	Acc. Volt.	A		E		F	
		treated	2h coked	treated	2h coked	treated	2h coked
Ni	10 kV	14.8	2.0	9.1	8.5	8.7	6.8
	20 kV	22.5	27.6	9.5	9.6	10.1	10.6
Fe	10 kV	24.5	18.0	8.8	5.2	17.1	210.0
	20 kV	28.5	31.0	11.5	12.4	14.9	14.2
Cr	10 kV	42.7	50.4	63.5	62.4	52.8	43.8
	20 kV	38.0	35.0	64.3	64.6	59.5	61.9
Si	10 kV	2.2	1.8	1.7	0.7	1.6	0.8
	20 kV	2.4	2.5	2.5	2.7	2.2	2.4
Mn	10 kV	14.9	27.0	17.0	23.3	19.8	28.7
	20 kV	7.7	2.9	12.3	10.7	13.2	10.9
Nb	10 kV	0.8	0.7	0	0	0	0
	20 kV	0.9	0.9	0	0	0	0
Stable components	$MnCr_2O_4$(s)	38.4	53.7	40.9	49.3	54.0	43.7
	Mn_2SiO_4(s)						3.1
	MnO(s)						4.4
	$MnSiO_3$(s)		0.7				
	Cr_2O_3(s)	15.0		23.8	20.5	-	
	SiO_2(highquartz)	10.9	6.4	8.0	2.6	8.6	
	$NiCr_2O_4$(s)	4.7		15.9		22.1	
	$NiFe_2O_4$(beta)	31.0		-		-	
	Fe_3O_4(s)	-		6.9		15.3	
	Fe(alpha)		35.5		10.7		36.9
	Nb_2O_5(s)	0.2		-		-	
	Ni(alpha)	-	3.8	4.4	16.9	0.1	12.0

Table A. 6: : Top-View EDX Analyses of Pretreated and coked after 2 hours samples (up). Thermodynamically stable phases calculated via EkviCalc by the EDX analysis of the respective samples at 10kV (down). Steam cracking of Ethane: F_{HC} = 29.18 10^{-6} kg s^{-1}, δ = 0.33 kg_{H2O} $kg^{-1}{}_{HC}$, Treactor = 1160 K, p = 101.35 kPa, F_{H2O} = 9.72 10^{-6} kg s^{-1}, CA of DMDS 41 ppmw S/HC.

Elements	Acc. Volt.	B		D		F		G		H	
		treated	2h coked	treated	2h coked	treated	2h coked	treated	2h coked	treated	2h coked
Ni	10 kV	7.0	3.7	8.7	3.6	8.7	6.8	5.3	3.1	11.2	5.6
	20 kV	9.3	10.3	12.3	13.9	10.1	10.6	6.9	7.5	15.3	16.8
Fe	10 kV	5.3	1.6	8.6	1.8	17.1	20.00	153	18.2	19.8	19.3
	20 kV	8.0	9.1	13.4	15.4	14.9	14.2	13.2	12.4	20.2	20.4
Cr	10 kV	63.6	65.2	64.9	70.3	52.8	43.8	58.8	50.3	46.7	42.6
	20 kV	62.5	62.1	61.2	59.6	59.5	61.9	64.8	67.2	49.6	50.8
Si	10 kV	1.8	1.4	1.0	0.6	1.6	0.8	1.4	0.7	2.9	2.0
	20 kV	2.0	2.1	1.2	1.4	2.2	2.4	2.0	2.2	3.5	3.7
Mn	10 kV	21.7	27.8	16.1	23.2	19.8	28.7	19.2	27.7	19.4	30.5
	20 kV	17.4	15.5	11.1	9.0	13.2	10.9	13.1	10.7	11.4	8.3
Nb	10 kV	0.6	0.4	0.8	0.7	0	0	0.0	0	0	0
	20 kV	0.8	0.9	0.8	0.8	0	0	0.1	0.1	0	0
Stable components	$MnCr_2O_4$(s)	54.3	66.0	34.6	536	54.0	43.7	44.7	53.0	41.9	44.4
	MnO(s)	-	-	-	-	-	4.4	-	-	-	0.2
	Mn_2SiO_4(s)	-	-	-	-	-	3.1	-	-	-	7.8
	$MnSiO_3$(s)	-	-	-	-	-	-	-	2.3	-	-
	Cr_2O_3(s)	20.2	15.6	39.3	32.2	-	-	27.7	-	11.3	-
	SiO_2(highquartz)	8.7	6.5	4.0	2.4	8.6	-	6.5	3.3	12.2	-
	$NiCr_2O_4$(s)	9.8	-	-	-	22.1	-	-	-	-	-
	$NiFe_2O_4$(beta)	6.6	-	-	-	-	-	-	-	-	-
	Fe_3O_4(s)	-	-	6.1	-	15.3	-	11.7	-	14.0	-
	Fe(alpha)	-	3.7		4.1	-	36.9	-	35.7	-	37.4
	Nb_2O_5(s)	0.5	-	0.5	-	-	-	0.0	-	-	-
	Ni(alpha)	-	8.2	14.6	7.7	0.1	12.0	8.4	5.8	19.6	10.2
	Ni_3S_2(l)		-	1.0	-			1.1		1.0	

Appendix B. Supplementary information to Chapter 3.

This Appendix contains data published as supporting information of the manuscript in chapter 3:

Impact of initial surface roughness and aging on coke formation during Ethane Steam Cracking

Stamatis A. Sarris[1], Steffen H. Symoens[1], Natalia Olahova[1], Kim Verbeken[2], Marie-Françoise Reyniers[1], Guy B. Marin[1], Kevin M. Van Geem[1,*]

[1]Ghent University, Laboratory for Chemical Technology, Technologiepark 914, 9052 Gent, Belgium.

[2]Ghent University, Department of Materials Science and Engineering, Technologiepark 903, 9052 Gent, Belgium

Coke formation mechanisms

The carbon deposition process during thermal cracking in the presence, or not, of steam, is a quite complex phenomenon. It has been extensively described in literature[1-4] that it mainly consists of three mechanisms; catalytic coke formation, coke growth from existing carbon layers onwards and gas phase coking, as illustrated in Figure B. 1.

The initial phase of carbon deposition is the formation of a porous network of carbon filaments, catalyzed typically by Ni and Fe present at the surface of the reactor walls. It is widely accepted that catalytic carbon formation[5-9] on metallic surfaces involves surface reactions, diffusion and precipitation of carbon. As a first step, a hydrocarbon molecule is chemisorbed on a metal crystallite of the surface. Dehydrogenation of the R-CH groups takes place with the hydrogen atoms recombining and desorb into the gas phase. As a result, the carbon atoms are formed at the surface, dissolve in and diffuse through the metal particle. The carbon accumulation in the particle causes a pressure build up at the dislocations and the grain boundaries, which may exceed the tensile strength of the metal.

Potentially, the metal particle is then lifted from the surface and carbon crystallizes at the rear end of the particle. Growing stems are developed that carry crystallites on their top. The precipitation of the carbon can give rise to structural deficiencies in the carbon lattice, thereby creating reactive carbon sites along this layer. Additional hydrocarbon molecules from the gas phase are incorporated at these sites causing addable filamentous coke growth. In that way, a porous layer of interwoven filaments is developed. The metal particles at the top of the whiskers are becoming more accessible from the gas phase. Therefore the deposition rate increases, while the diffusion rate through the metal remains stable. Carbon migration over the metal surface occurs, surrounding the carbon stems. At this point, surface carbon can occur, encapsulating the metal and terminating any further coke growth.

Dissociative chemisorption of water molecules on the metal particles produces highly reactive oxygen atoms that react with surface carbon to from carbon monoxide, which desorbs in the gas phase. This reaction prevents the fast encapsulation of the metal tip of the filament and therefore the termination of this reaction, in other words the "deactivation of the metallic active site". How quickly these phenomena are occurring is a matter of relative kinetics of carbon growth, gasification, dissolution and diffusion. Certainly, the properties of the alloy are very important in all the mechanisms, however in this study the composition was kept stable to isolate the effect of roughness.

The heterogeneous non-catalytic mechanism is the major source of coke in an industrial cracker, since it takes place over the complete run length. The coke in contact with the gas phase looks like a succession of several discrete layers, deriving from the coke-gas interface[10, 11]. Coke formation is described by the reaction of gas phase precursors with active centers of the surface. Kopinke et al[1] have provided a general scale for the coking tendency of several precursors. For example, acetylene, anthracenes, cyclic naphthenes and aromatics possess a high tendency for coke formation. Ethylene is not the most reactive one, however due to its high concentration is very important. No significant differences of the relative constants of a particular hydrocarbon were found for different materials[1], supporting that the active centers are radical in nature and positioned in the coke matrix. The radicals can be generated by hydrogen abstraction from the partially dehydrogenated carbon layer being determined by the gas phase composition and the available coked reactor surface[12]. The coke radicals react by addition with unsaturated molecules and radicals from the gas phase. After dehydrogenation, graphitic layers are formed[13].

The last mechanism, also known as homogeneous non-catalytic coking results from a sequence of molecular and/or radical reactions in the gas phase. These lead to high molecular weight polynuclear aromatic compounds which remain solid even at high temperatures. As a

result, they collide at the wall and integrate in the coke layer[14]. In this work, the latter mechanism contributes very little, since there are not a lot heavy compounds generated in the gas phase due the light feedstock (ethane).

Jet stirred reactor

A small coupon of dimensions 10 mm x 8 mm x 1 mm is hanged by the arm of the electro balance in the center of a spherical jet stirred reactor, right above the jets, as illustrated in Figure B. 2. As recently published by our research group and is represented in Figure B. 3 [15], the mixing is quite ideal, with negligible changes of the gas phase concentrations and temperature around the coupon. Therefore, the set-up is suitable for the study of coke formation on high temperature alloys.

Coking rates

The coking rates presented in this paper, see Table B. 2, have been calculated using the geometric surface of the samples. In order to calculate the coking rates based on the real sample surface, parameters such as the sampling length of the equipment used and the mean spacing (S) of the local peaks measured – see Figure B. 4 - should be recorded. The equipment used, a SJ210 Mutitoyo Surface Roughness Tester, does not provide logging of the above mentioned values that would allow the calculation of the real surface of the samples tested. A general idea of the arithmetical range of the mean spacing per surface roughness values, which is summarized in Table B. 3 can be given by the operational manual of the equipment[16]. The mean spacing *S*, for *n* number of spaces is calculated by the following formula (B.1):

$$S = \frac{1}{n}\sum_{1}^{n} S_i \qquad \text{(B.1)}$$

From Table B. 3, the S_{min} corresponds to the minimum theoretically expected mean spacing, while the S_{max} is representative of the maximum value of the theoretically expected mean spacing for the measured R_{α} roughness value in each case. The theoretical range of the mean spacing increases by increasing surface roughness.

SEM & EDX results

The analyzed samples are covered by a carbon layer of a different thickness for the different roughness values. However, clearly, based on the penetration depth calculated for carbon, see Table 3.3 of the manuscript, the EDX data at 10 KV for the coked samples obtained for an initial surface roughness up to 1.3 μm can be expected to be more or less representative of the coupon's oxidized surface. For a higher initial surface roughness it is more appropriate to consider the EDX data at 20 KV. Therefore, it is theoretically possible to extract fruitful observations based on these results. Regarding the impact of the different base metal composition for the different surface roughness values, this is typically the expected result from the EDX analysis.

As compared to the not coked only pre-oxidized sample, the EDX data at 10 kV show that up to an initial surface roughness of 1.3 μm, there is an important increase in the Cr content and a slight increase in the Fe content followed by an pronounced decrease in the Mn content and a slight decrease in Ni content. At 20 kV, the EDX data indicate that for an initial surface roughness of 2.6 μm onwards, the Cr content steadily decreases, the Fe content slightly increases while the Mn content increases and the Ni content remains fairly stable. The amounts of metallic Ni and Fe show a tendency to slightly increase with increasing surface roughness. As both metallic Fe and Ni are well-known catalysts for coke formation, their increased presence at the surface further explain the observed effects on the coking in the catalytic stage[13].

Carbon and Oxygen are excluded by the analysis since their detection is not quantitative by means of EDX. The results obtained are normalized and not "absolute" values, however they are representative of the oxidized layer existing under the coked surface. For lighter elements, such as Carbon and Oxygen, other techniques could be used.

However, no differences are expected on the elemental composition of the coke layer, since no differences are observed experimentally in terms of asymptotic coking, while the coke structure remains rather stable for all the different surface roughness values. The latter are confirmed by Table B. 2 and Figure 3. 10. As a result, no additional analysis is suggested regarding the Carbon and Oxygen content.

Catalytic coking fraction in steam cracking

Analogously to the studied cracker or set-up, different observations regarding the fraction of the initial coke deposited on the tube surface versus the coke formed during the asymptotic period can be made. Typically in the models describing the coking behavior of industrial crackers presented in the literature[13, 17, 18], only the contribution of heterogeneous non-catalytic coke formation is taken into account. Homogeneous non-catalytic coking only contributes significantly at temperatures higher than $1170\ K$ or during the cracking of heavy feedstocks, e.g. atmospheric gas oil or vacuum gas oil. In order to justify neglecting the catalytic mechanism, the following theory is developed based on observations on coke deposits formed during industrial operation as shown in the work of Reyniers [19].

Based on literature data [20], the average height of the catalytic coking layer in an industrial cracker tube is determined. Combined with the average density of catalytic coke, the amount of catalytic coke deposited on the cracker tube is determined.

$$m_{coke} = h_{coke}\,\rho_{coke} = 100\ 10^{-6}\ [m] * 1.6\ 10^{3}\ \left[\frac{kg}{m^3}\right] = 0.160\left[\frac{kg}{m^2}\right] \qquad (2)$$

Based on that, an average coking rate is determined by interpolating exponentially between the maximum coking rate and asymptotic coking rate obtained by experiments in a micro-reactor setup. This average catalytic coking rate is determined to be $2.083\ 10^{-6}\ \frac{kg}{m^2\ s}$ at $1083\ K$. Combined with an activation energy of $167.36\ 10^3\ \frac{J}{mol}$, a rate expression for catalytic coke formation is determined.

$$r_{coke,av}(catalytic) = 2.45\ 10^2 \exp\left(-\frac{167.36\ 10^3}{R\ T}\right)\left[\frac{kg}{m^2\ s}\right] \quad (3)$$

Based on these calculations, Reyniers [19] concludes that for temperatures higher than $1070\ K$, the catalytic coking mechanism is only important for about $10\ hrs$ which is in the order of magnitude of 1 % of the total run length of an industrial cracker. The error made by not considering the catalytic coking mechanism is limited to less than 3 % which was deemed acceptable by the author.

In the presented work, it is clear that the time needed to reach the asymptotic coking depends on the initial surface roughness. However, overall the asymptotic coking is reached after the first 2-3 hours. Judging by the previous work done in coke formation during steam cracking[13, 17, 21-24], definitely the most important step for the simulation of the run length of an industrial cracker is the representation and prediction of the asymptotic coking, where no significant differences are observed for the – quite broad- studied roughness range.

However, to fundamentally model coke formation the study of all the parameters has equivalent importance. An industrial run length can last from 30 to 150 days[25] , depending on the applied process conditions, feedstock and reactor material and geometry. Industrially the initial coking is not expected to be more than the 5 % of the total coke formed on the reactor walls, therefore the roughness will not have a significant effect on the overall run length but it will certainly affect the initial coking behavior of a cracker.

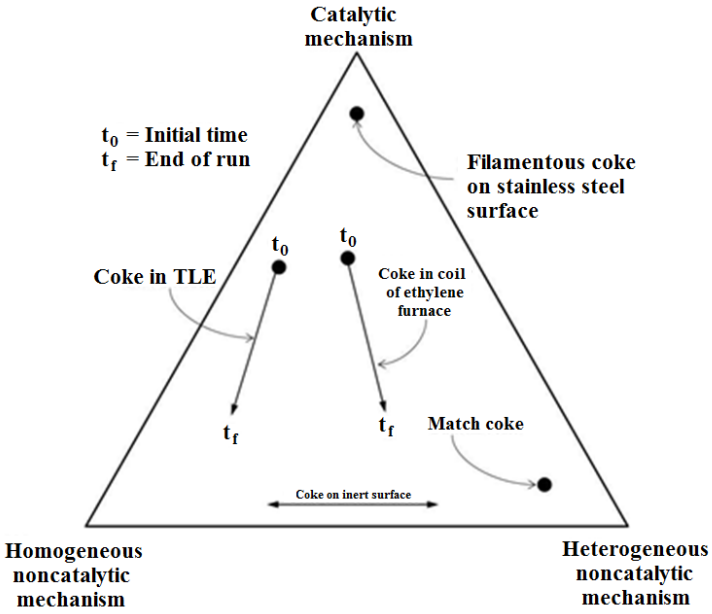

Figure B. 1: Comparison of the relative importance of the three main coking mechanisms[26]

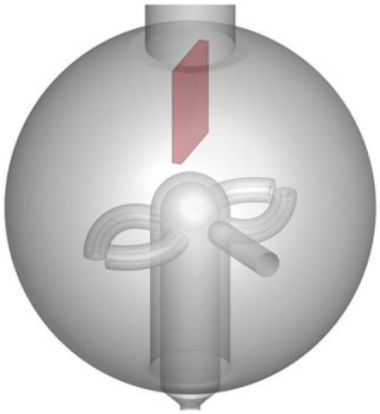

Figure B. 2: Coupon position in the reactor

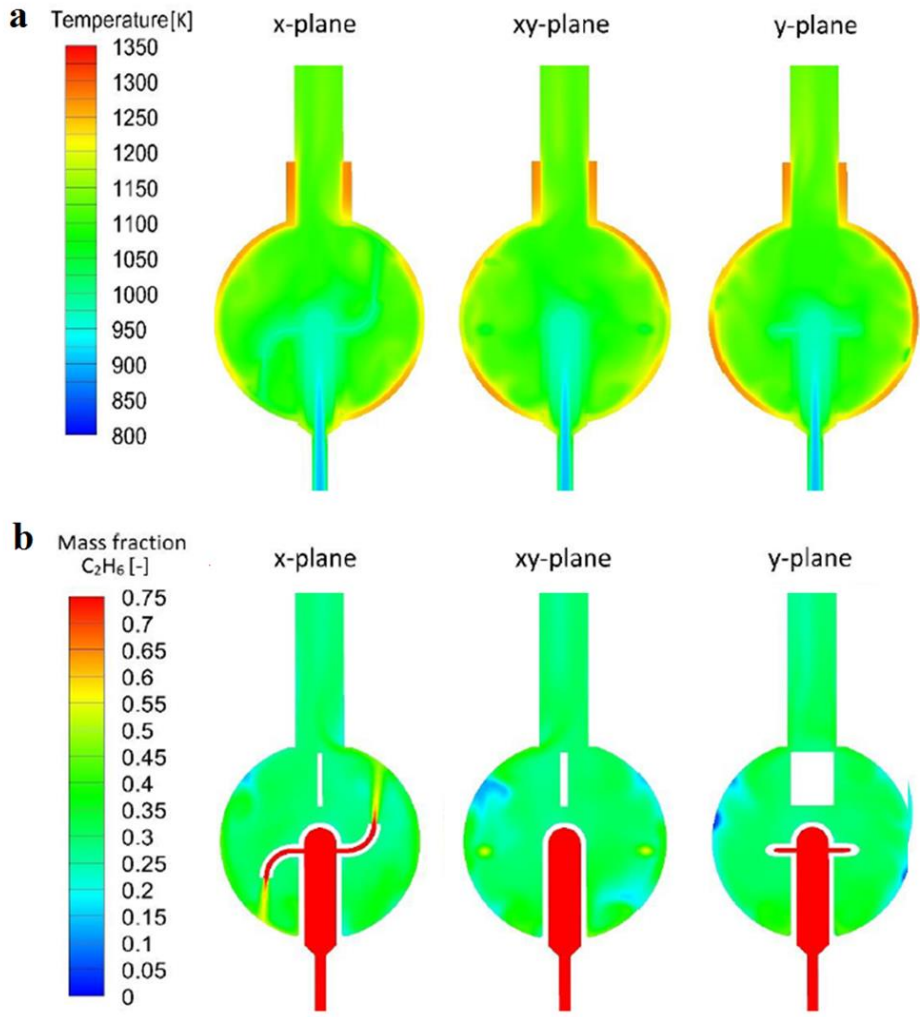

Figure B. 3: Cross section fields of temperature (a) and ethane mass fraction (b) for ethane cracking experiments in the JSR[15]

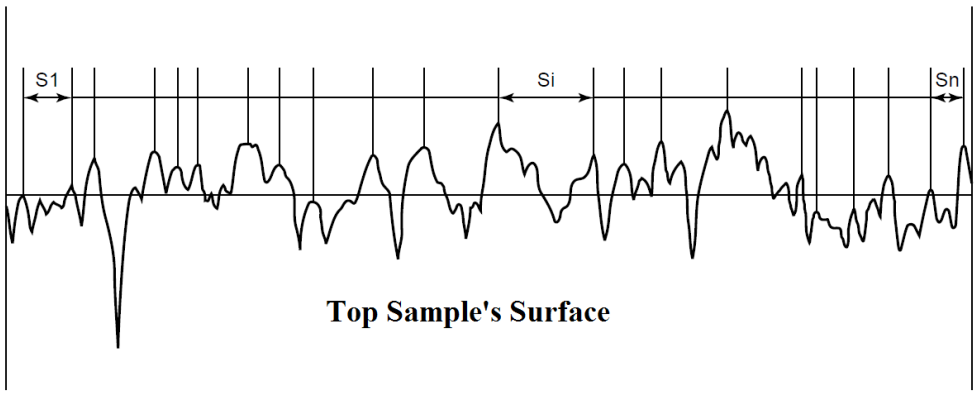

Figure B. 4: Local peaks spacing (Si)[16]

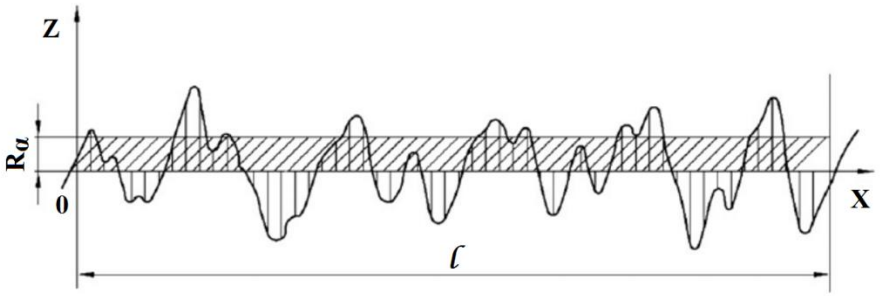

Figure B. 5: Illustration of the determination of the surface roughness. Shown is the height profile of the surface measured over a distance l on the surface with Z(0), the mean value of the measured height profile. R_α, the arithmetic average of the absolute deviations of Z(x) from Z(0), is also indicated.

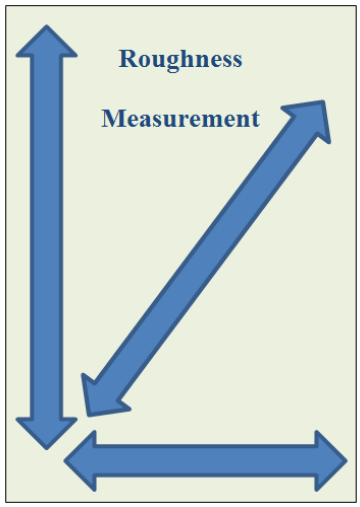

Figure B. 6: Illustration of the procedure used to measure the roughness of the tested coupons.

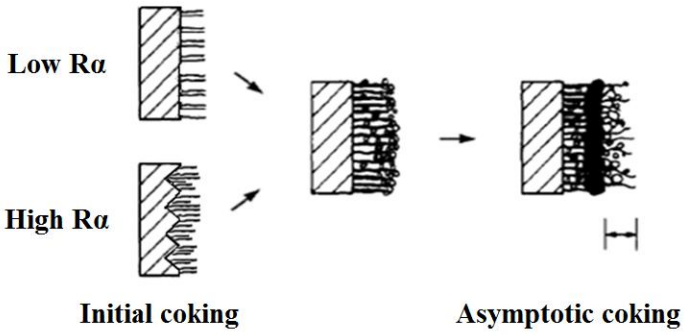

Figure B. 7: Graphical illustration of the limited effect of the initial surface roughness on the asymptotic coking behavior [3]

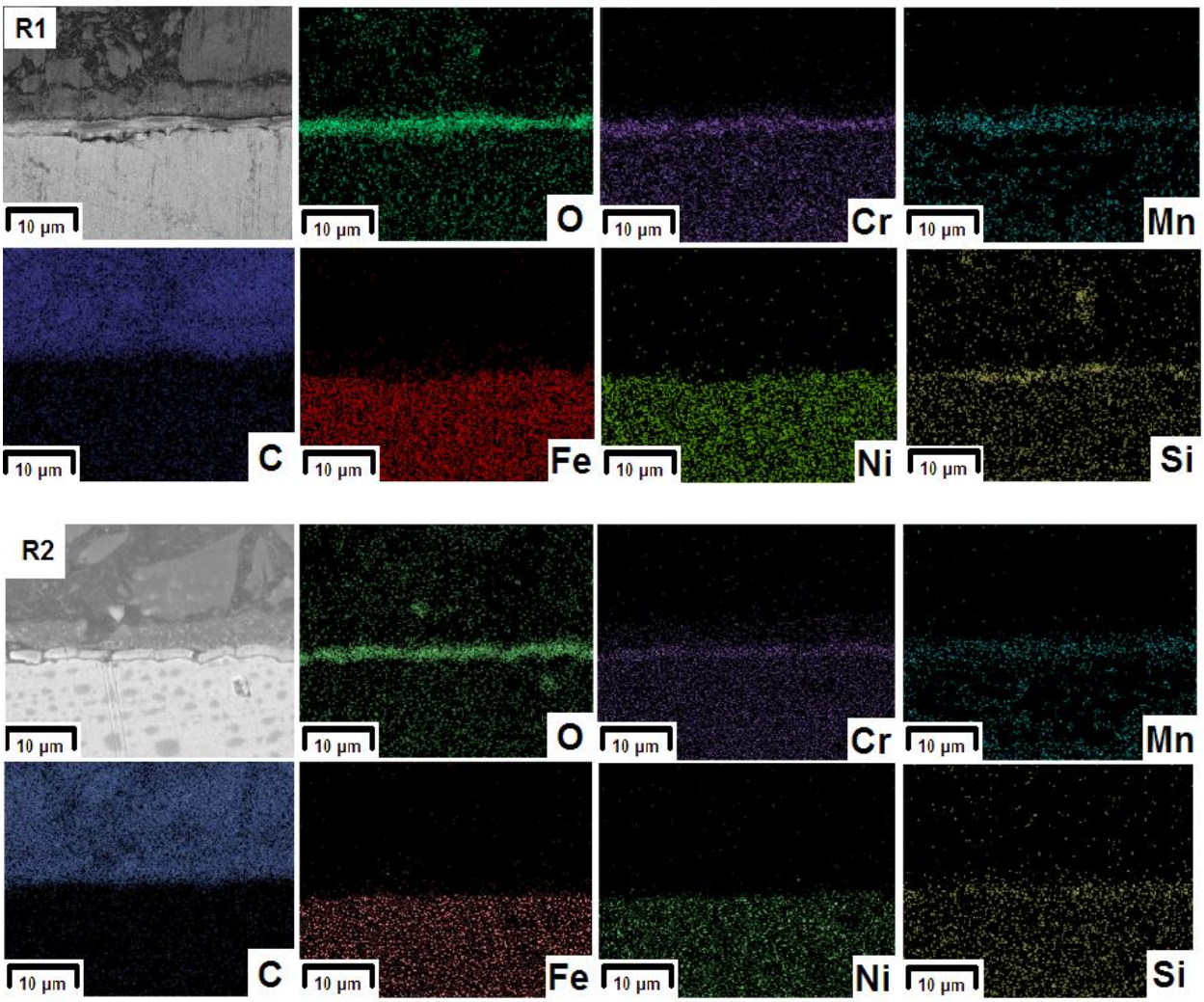

Figure B. 8: Elemental mappings of the coked samples obtained after 1 hour of cracking in the 8th cracking cycle for an initial surface roughness of R1 (0.15 µm), R2 (0.75 µm), R3 (1.3 µm) and R4 (2.6 µm). Magnification: 3000x; Accelerating Voltage: 15 kV; Steam cracking of Ethane: F_{HC} = 29.18 10^{-6} kg s^{-1}, δ = 0.33 kg_{H2O} kg^{-1}_{HC}, $T_{reactor}$ = 1173 K, P = 101.35 kPa, F_{H2O} = 9.72 10^{-6} kg s^{-1}, 8 cracking cycles

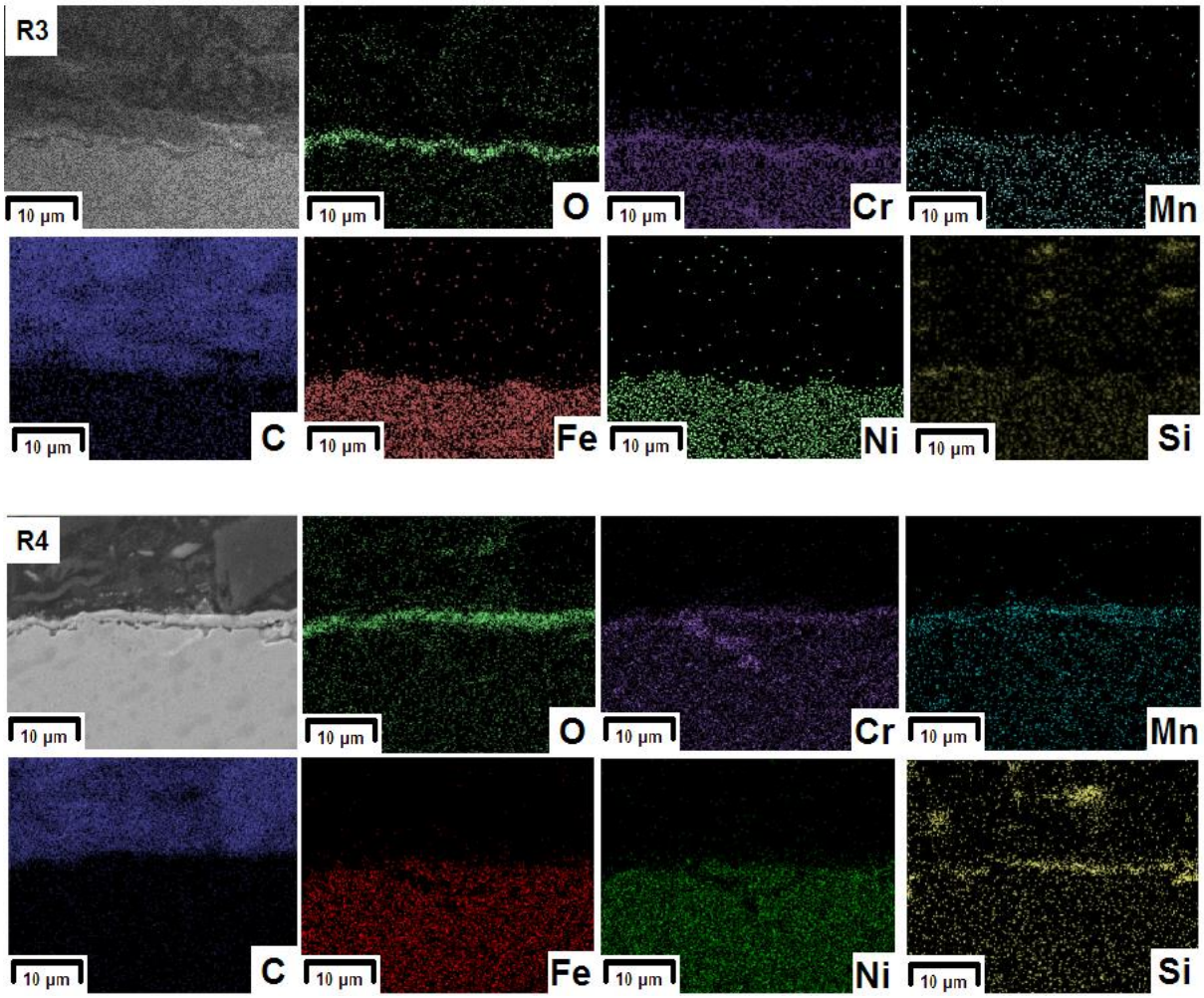

Figure B. 9: Elemental mappings of the coked samples obtained after 1 hour of cracking in the 8th cracking cycle for an initial surface roughness of R1 (0.15 µm), R2 (0.75 µm), R3 (1.3 µm) and R4 (2.6 µm). Magnification: 3000x; Accelerating Voltage: 15 kV; Steam cracking of Ethane: F_{HC} = 29.18 10^{-6} kg s^{-1}, δ = 0.33 kg_{H2O} kg^{-1}_{HC}, $T_{reactor}$ = 1173 K, P = 101.35 kPa, F_{H2O} = 9.72 10^{-6} kg s^{-1}, 8 cracking cycles

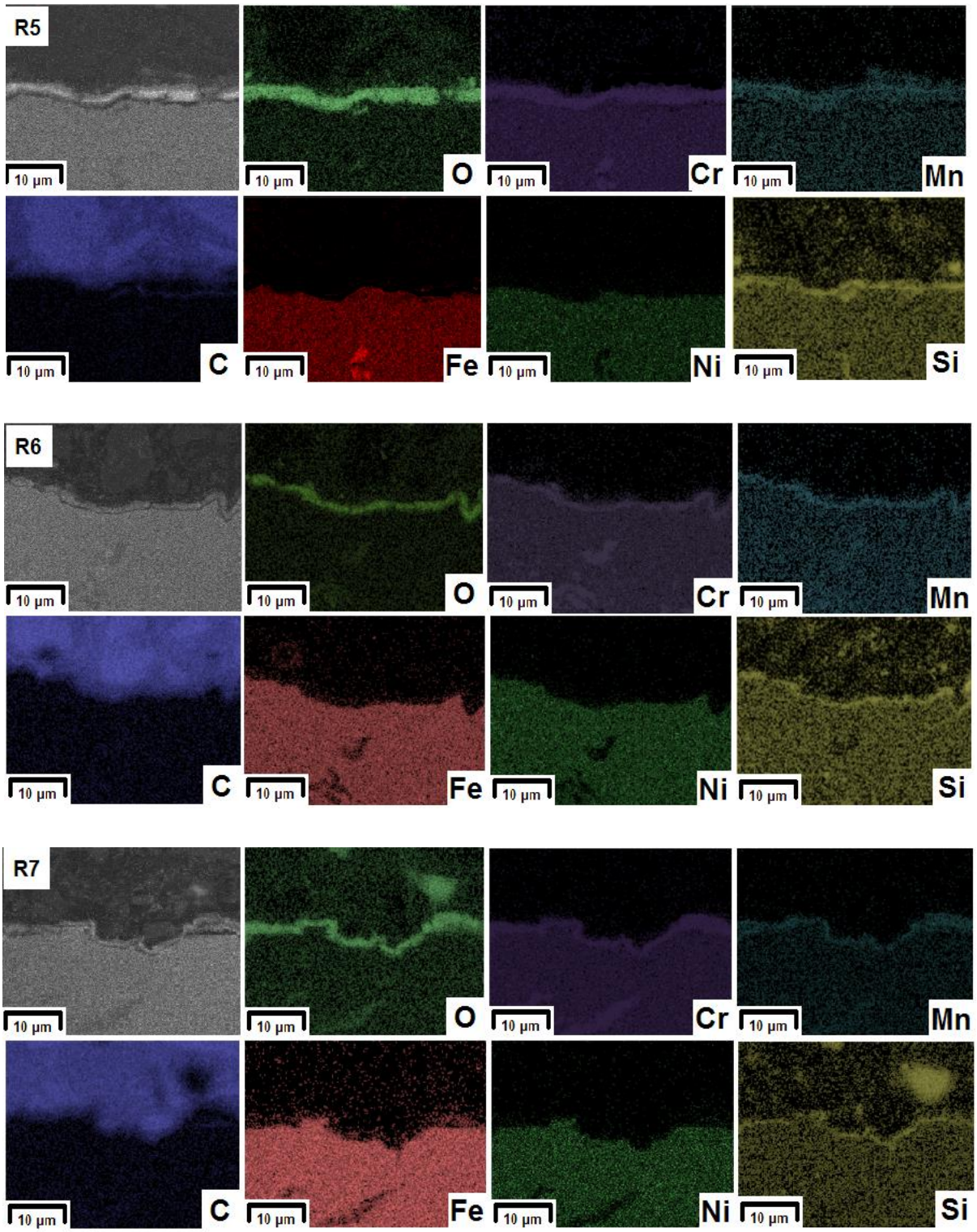

Figure B. 10: Elemental mappings of the coked samples for an initial surface roughness of R5 (3.9 µm), R6 (5.1 µm) and R7 (7.0 µm). Magnification: 3000x; Accelerating Voltage: 15 kV; Steam cracking of Ethane: F_{HC} = 29.18 10^{-6} kg s^{-1}, δ = 0.33 kg_{H2O} kg^{-1}_{HC}, $T_{reactor}$ = 1173 K, P = 101.35 kPa, F_{H2O} = 9.72 10^{-6} kg s^{-1}, 8 cracking cycles

Table B. 1: Overview of the cyclic aging experimental procedure

Process step	Duration	Temperature (K)	Gas feed flow (10^{-6} kg s^{-1})			Water flow (10^{6} kg s^{-1})
			N_2	Ethane	Air	
Preoxidation	12-14 hours	1023	-	-	9.575	-
High-Temperature Preoxidation	30-40 minutes	Heating up from 1023 to 1173	9.683	-	11.862	-
Steam treatment	15 minutes	1173	-	-	11.862	6.7
1st cc	6 hours	1173	-	29.167	-	9.7
Decoking	30-40 minutes	Heating up from 1023 to 1173	9.683	-	11.862	-
Steam treatment	15 minutes	1173	-	-	11.862	6.7
2nd cc	6 hours	1173	-	29.167	-	9.7
Decoking	30-40 minutes	Heating up from 1023 to 1173	9.683	-	11.862	-
Steam treatment	15 minutes	1173	-	-	11.862	6.7
3rd cc	6 hours	1173	-	29.167	-	9.7
Decoking	30-40 minutes	Heating up from 1023 to 1173	9.683	-	11.862	-
Steam treatment	15 minutes	1173	-	-	11.862	6.7
Cyclic aging	Consists of 4 cycles of: o Heating up from 1023 to 1173 K o Cracking at 1173 K (1 hour) o Decoking from 1023 to 1173 K o Steam treatment at 1173 K (15 minutes)					
8th cc	6 hours	1173	-	29.167	-	9.7
Decoking	30-40 minutes	Heating up from 1023 to 1173	9.683	-	11.862	-
Steam treatment	15 minutes	1173	-	-	11.862	6.7
Cooling down	100 K /h	To ambient temperature under He	-	-	-	-

During stabilization points a stable helium flow of 0.14 10^{-6} kg s^{-1} is fed

Table B. 2: Process Conditions, Coking rates and Product Yields of Roughness Study; Steam cracking of Ethane: F_{HC} = 29.18 10^{-6} kg s^{-1}, δ = 0.33 kg_{H2O} kg^{-1}_{HC}, $T_{reactor}$ = 1173 K, P = 101.35 kPa, F_{H2O} = 9.72 10^{-6} kg s^{-1}, 8 cracking cycles

Experiment	**R1**	**R2**	**R3**	**R4**	**R5**	**R6**	**R7**
R_α Roughness[a] (μm)	0.15±0.02	0.75±0.15	1.3±0.2	2.6±0.2	3.9±0.3	5.1±0.3	7.0±0.4
CC[b]	**Mass of coke [10^{-6} kg]**						
1	1.1±0.1	1.3±0.1	1.2±0.1	1.2±0.1	1.4±0.1	1.4±0.1	1.6±0.2
2	1.2±0.1	1.2±0.1	1.2±0.1	1.2±0.1	1.5±0.2	1.6±0.2	1.7±0.2
3	1.2±0.1	1.2±0.1	1.4±0.1	1.4±0.1	1.6±0.2	1.8±0.2	1.8±0.2
4	0.5±0.1	0.5±0.1	0.6±0.1	0.7±0.1	0.8±0.1	1.5±0.2	2.3±0.2
5	0.6±0.1	0.6±0.1	0.7±0.1	0.9±0.1	1.4±0.1	1.4±0.1	1.9±0.2
6	0.5±0.1	0.6±0.1	0.7±0.1	0.8±0.1	1.6±0.2	2.6±0.3	2.9±0.3
7	0.4±0.1	0.5±0.1	0.5±0.1	0.8±0.1	1.4±0.1	2.1±0.2	2.8±0.3
8	1.17±0.1	1.2±0.1	1.2±0.1	1.6±0.2	2.0±0.2	3.0±0.3	3.2±0.3
CC	**$r_{initial}$ [10^{-7} kg s^{-1} m^{-2}]**						
1	3.8±0.4	6.8±0.7	7.0±0.7	6.1±0.6	7.8±0.8	8.9±0.9	12.1±1.2
2	5.8±0.6	6.7±0.7	6.7±0.7	6.1±0.6	9.8±1.0	9.8±1.0	13.8±1.4
3	6.8±0.7	6.9±0.7	8.3±0.9	9.5±1.0	11.4±1.1	14.4±1.4	14.3±1.4
4	7.1±0.7	7.5±0.8	8.2±0.9	9.4±1.0	11.1±1.1	21.1±2.1	32.8±3.3
5	7.9±0.8	8.5±0.9	9.3±1.0	13.2±1.3	19.8±2.0	19.8±2.0	26.2±2.6
6	7.0±0.7	8.4±0.8	9.7±1.0	11.2±1.1	22.4±2.2	37.4±3.7	41.7±4.2
7	6.0±0.6	6.5±0.7	6.7±0.7	11.2±1.1	19.4±2.0	29.2±2.9	39.4±3.9
8	5.8±0.6	6.2±0.6	6.3±0.7	12.1±1.2	17.3±1.7	31.3±3.1	34.4±3.4
CC	**$r_{asymptotic}$ [10^{-7} kg s^{-1} m^{-2}]**						
1	2.2±0.2	2.3±0.2	2.2±0.2	2.2±0.2	2.3±0.2	2.3±0.2	2.1±0.2
2	2.2±0.2	2.1±0.2	2.2±0.2	2.1±0.2	2.3±0.2	2.5±0.3	2.2±0.2
3	2.1±0.2	2.1±0.2	2.3±0.2	2.1±0.2	2.2±0.2	2.3±0.2	2.3±0.2
8	2.2±0.2	2.2±0.2	2.1±0.2	2.1±0.2	2.2±0.2	2.2±0.2	2.3±0.2
Components	**Averaged product Yields over 8 CC[wt % dry]**						
H_2	4.2±0.1	4.29±0.1	4.28±0.05	4.29±0.1	4.26±0.1	4.28±0.1	4.31±0.1
CO	0.06±0.01	0.07±0.01	0.08±0.01	0.08±0.01	0.09±0.01	0.09±0.01	0.09±0.01
CO_2	0.002±0.001	0.002±0.001	0.002±0.001	0.002±0.001	0.002±0.001	0.003±0.001	0.003±0.001
CH_4	7.0±0.1	7.3±0.2	7.1±0.2	7.2±0.2	7.1±0.1	7.1±0.1	7.2±0.2
C_2H_6	30.2±0.5	29.5±0.6	29.9±0.5	29.9±0.5	30.0±0.5	29.9±0.5	29.6±0.5
C_2H_4	49.9±0.3	50.2±0.3	49.8±0.3	50.1±0.3	50.1±0.3	50.1±0.2	50.1±0.2
C_3H_8	0.1±0.02	0.12±0.02	0.11±0.02	0.12±0.02	0.12±0.02	0.11±0.02	0.11±0.02
C_3H_6	0.74±0.02	0.74±0.02	0.75±0.02	0.75±0.02	0.75±0.02	0.74±0.02	0.74±0.02
C_2H_2	1.43±0.04	1.44±0.05	1.43±0.05	1.44±0.05	1.43±0.05	1.44±0.05	1.44±0.05
1,3-C_4H_6	1.9±0.1	2.0±0.1	2.0±0.1	2.0±0.1	2.0±0.1	2.0±0.1	2.0±0.1
benzene	2.5±0.1	2.6±0.1	2.5±0.1	2.6±0.1	2.6±0.1	2.5±0.1	2.6±0.1

[a] roughness before pretreatment, [b] cracking cycle

Table B. 3: Theoretical range of the arithmetic range of the mean spacing per surface roughness.[16]

R_a µm [10^{-3} mm]	Smin [10^{-3} mm]	Smax [10^{-3} mm]
0.15	0.0013	0.04
0.75	0.04	0.13
1.3	0.13	0.4
2.6	0.4	1.3
3.9	0.4	1.3
5.1	0.4	1.3
7	0.4	1.3

References

1. Kopinke, F. D.; Zimmermann, G.; Nowak, S., On the mechanism of coke formation in steam cracking—conclusions from results obtained by tracer experiments. *Carbon* **1988,** 26, (2), 117-124.
2. Cai, H.; Krzywicki, A.; Oballa, M. C., Coke formation in steam crackers for ethylene production. *Chemical Engineering and Processing: Process Intensification* **2002,** 41, (3), 199-214.
3. Albright, L. F.; Marek, J. C., Mechanistic model for formation of coke in pyrolysis units producing ethylene. *Ind. Eng. Chem. Res.* **1988,** 27, (5), 755-759.
4. Lahaye, J.; Badie, P.; Ducret, J., Mechanism of carbon formation during steamcracking of hydrocarbons. *Carbon* **1977,** 15, (2), 87-93.
5. Baker, R. T. K.; Yates, D. J. C.; Dumesic, J. A., Filamentous Carbon Formation over Iron Surfaces. In *Coke Formation on Metal Surfaces*, AMERICAN CHEMICAL SOCIETY: 1983; Vol. 202, pp 1-21.
6. Lyle, F. A.; Baker, R. T. K., *Coke Formation on Metal Surfaces*. AMERICAN CHEMICAL SOCIETY: 1983; Vol. 202, p 332.
7. Figueiredo, J. L., Reactivity of coke deposited on metal surfaces. *Materials and Corrosion* **1999,** 50, (12), 696-699.
8. Snoeck, J.-W.; Froment, G.; Fowles, M., Filamentous carbon formation and gasification: thermodynamics, driving force, nucleation, and steady-state growth. *Journal of Catalysis* **1997,** 169, (1), 240-249.

9. Bonnet, F.; Ropital, F.; Berthier, Y.; Marcus, P., Filamentous carbon formation caused by catalytic metal particles from iron oxide. *Materials and Corrosion* **2003,** 54, (11), 870-880.
10. Ranzi, E.; Dente, M.; Goldaniga, A.; Bozzano, G.; Faravelli, T., Lumping procedures in detailed kinetic modeling of gasification, pyrolysis, partial oxidation and combustion of hydrocarbon mixtures. *Progress in Energy and Combustion Science* **2001,** 27, (1), 99-139.
11. Kopinke, F. D.; Zimmermann, G.; Reyniers, G. C.; Froment, G. F., Relative rates of coke formation from hydrocarbons in steam cracking of naphtha. 2. Paraffins, naphthenes, mono-, di-, and cycloolefins, and acetylenes. *Ind. Eng. Chem. Res.* **1993,** 32, (1), 56-61.
12. Wauters, S.; Marin, G. B., Computer generation of a network of elementary steps for coke formation during the thermal cracking of hydrocarbons. *Chemical Engineering Journal* **2001,** 82, (1–3), 267-279.
13. Reyniers, G. C.; Froment, G. F.; Kopinke, F.-D.; Zimmermann, G., Coke Formation in the Thermal Cracking of Hydrocarbons. 4. Modeling of Coke Formation in Naphtha Cracking. *Ind. Eng. Chem. Res.* **1994,** 33, (11), 2584-2590.
14. Bach, G.; Zimmermann, G.; Kopinke, F.-D.; Barendregt, S.; van den Oosterkamp, P.; Woerde, H., Transfer-Line Heat Exchanger Fouling during Pyrolysis of Hydrocarbons. 1. Deposits from Dry Cracked Gases. *Industrial & Engineering Chemistry Research* **1995,** 34, (4), 1132-1139.
15. Reyniers, P. A.; Sarris, S. A.; Marin, G. B.; Van Geem, K. M., Computational Fluid Dynamic Design of Jet Stirred Reactors for Measuring Intrinsic Kinetics of Gas-Phase and Gas-Solid Reactions. *International Journal of Chemical Kinetics* **2016,** 48, (9), 556-569.
16. ltd, B. r. t., MITUTOYO SURFTEST SJ201P - Surface roughness tester Manual. In *178*, www.brw.ch, 2008.
17. Plehiers, P. M.; Reyniers, G. C.; Froment, G. F., Simulation of the run length of an ethane cracking furnace. *Ind. Eng. Chem. Res.* **1990,** 29, (4), 636-641.
18. Geem, K. M. V.; Dhuyvetter, I.; Prokopiev, S.; Reyniers, M.-F.; Viennet, D.; Marin, G. B., Coke Formation in the Transfer Line Exchanger during Steam Cracking of Hydrocarbons. *Ind. Eng. Chem. Res.* **2009,** 48, (23), 10343-10358.
19. Reyniers, G. C. Cokesvorming bij de Thermische Kraking van Koolwaterstoffen. Rijksuniversiteit Gent, 1992.

20. Bennett, M. J.; Price, J. B., Oxidation of an Ethylene Steam Cracker Pyrolysis Tube Deposit in Water Vapor and Its Enhancement by Inorganic Catalysts. In *Coke Formation on Metal Surfaces*, American Chemical Society: 1983; Vol. 202, pp 59-87.
21. Van Geem, K. M.; Reyniers, M. F.; Pyl, S. P.; Marin, G. B., Effect of Operating Conditions and Feedstock Composition on Run Length of Steam Cracking Coils. In *(2009) AIChE 2009 Spring National Meeting*, Tampa, FL, 2009.
22. Schietekat, C. M.; Sarris, S. A.; Reyniers, P. A.; Kool, L. B.; Peng, W.; Lucas, P.; Van Geem, K. M.; Marin, G. B., Catalytic Coating for Reduced Coke Formation in Steam Cracking Reactors. *Ind. Eng. Chem. Res.* **2015,** 54, (39), 9525-9535.
23. Muñoz Gandarillas, A. E.; Van Geem, K. M.; Reyniers, M.-F.; Marin, G. B., Influence of the Reactor Material Composition on Coke Formation during Ethane Steam Cracking. *Ind. Eng. Chem. Res.* **2014,** 53, (15), 6358-6371.
24. Muñoz Gandarillas, A. E.; Van Geem, K. M.; Reyniers, M.-F.; Marin, G. B., Coking Resistance of Specialized Coil Materials during Steam Cracking of Sulfur-Free Naphtha. *Ind. Eng. Chem. Res.* **2014,** 53, (35), 13644-13655.
25. Mahamulkar, S.; Yin, K.; Agrawal, P. K.; Davis, R. J.; Jones, C. W.; Malek, A.; Shibata, H., Formation and Oxidation/Gasification of Carbonaceous Deposits: A Review. *Ind. Eng. Chem. Res.* **2016**.
26. Albright, L. F.; Marek, J. C., Mechanistic Model for Formation of Coke in Pyrolysis Units Producing Ethylene. *Ind. Eng. Chem. Res.* **1988,** 27, (5), 755.

Appendix C. Supplementary information to Chapter 4.

This Appendix contains data to be published as supporting information of the manuscript :

Experimental study of coke formation of innovative super alloys

Sarris, S. A.; Patil, M.; Reyniers, M.-F.; Marin, G. B.; Van Geem, K. M.

To be submitted

Cross section analysis

For all the coked samples cross sectional analysis has been performed by means of SEM and EDX. For better interpretation of the results, this discussion has been organized in five different sections based on the five cracking different conditions applied.

Blank experiments

From Figure C. 1 to Figure C. 4, it is clear that 35/45 Cr/Ni alloy has thicker oxides formed on its top surface than the 25/35 Cr/Ni one. For both samples a thickness of 1 to 2 μm is observed. The thickness of the Al-content alloy is roughly 1 μm consisting mainly of Al and O. A thick and very homogeneous oxide mainly of Cr and O is observed for the 40/48 Cr/Ni alloy.

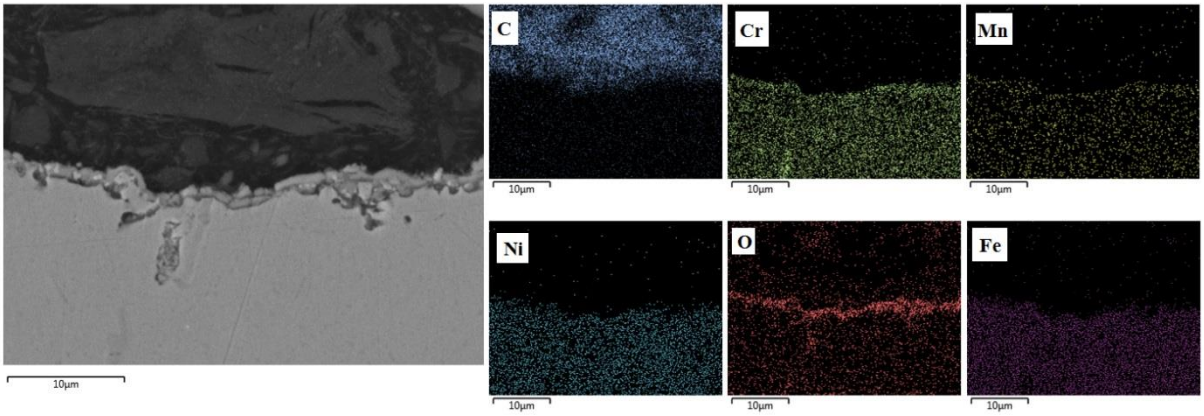

Figure C. 1: 25/35 Cr/Ni alloy after aging Blank steam cracking conditions

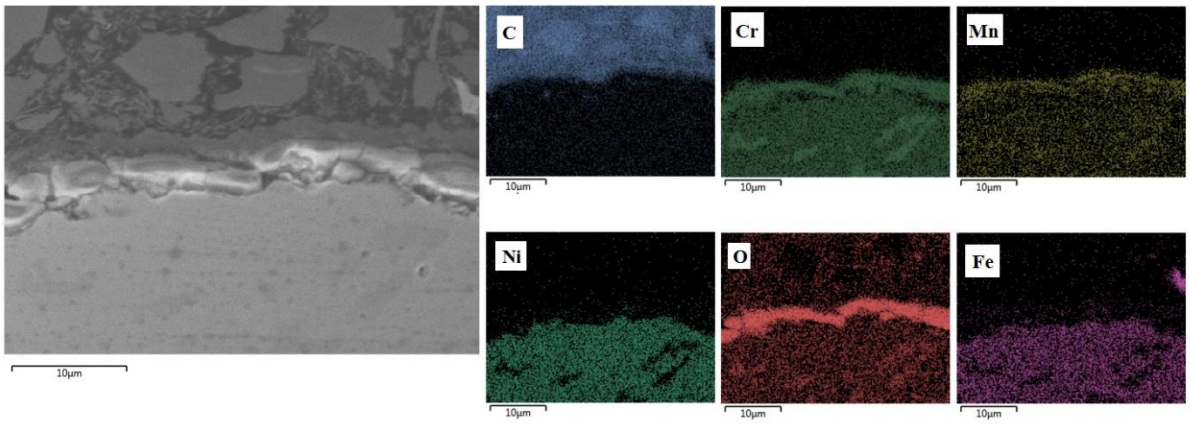

Figure C. 2: 35/45 Cr/Ni alloy after aging Blank steam cracking conditions

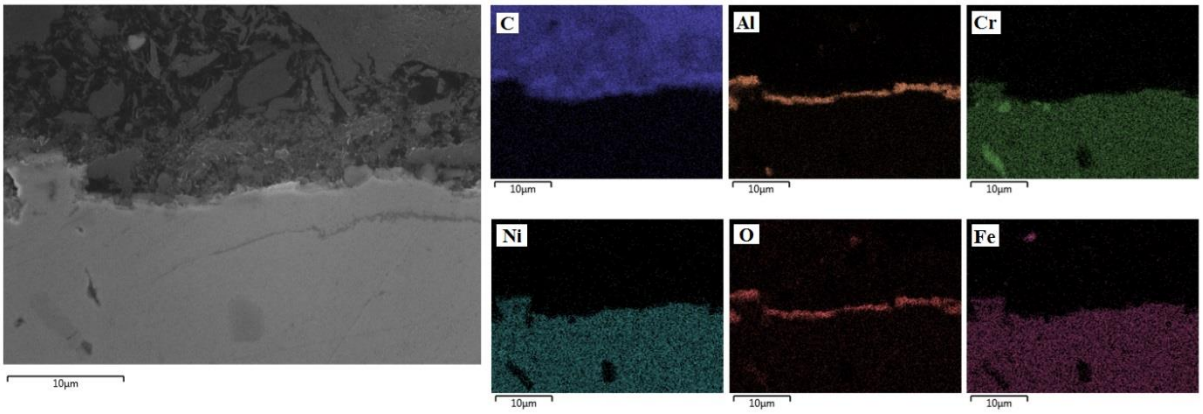

Figure C. 3: Al-content alloy after aging Blank steam cracking conditions

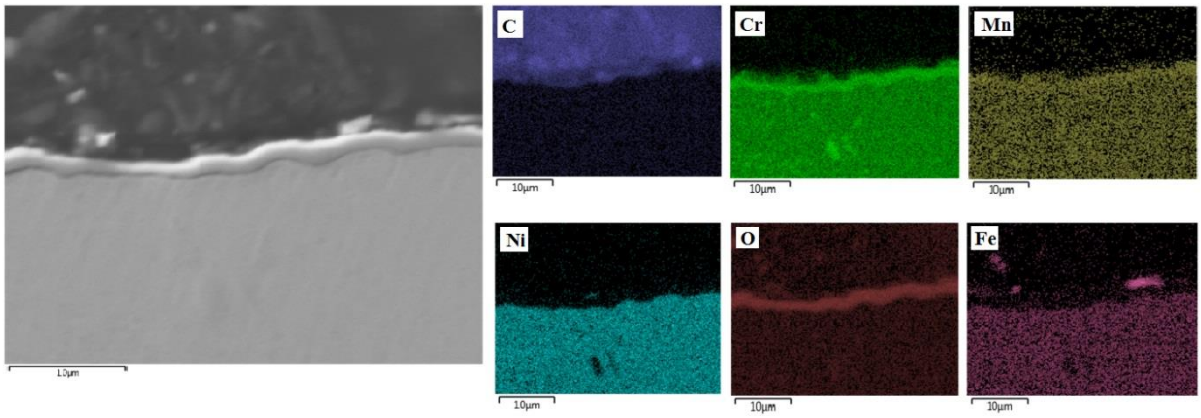

Figure C. 4: 40/48 Cr/Ni alloy after aging Blank steam cracking conditions

Continuous addition of DMDS experiments

In Figure C. 5 to Figure C. 8, the cross sectional images of the coked samples after application of aging continuous addition of DMDS experiments are illustrated. In comparison with the blank conditions, the 25/35 and 35/45 Cr/Ni alloy shows similar oxide thickness. For the Al-content alloy the thickness seems rather suppressed to less than 1 µm. The thickness of the 40/48 Cr/Ni alloy appears also stable, with oxides consisting both of Cr and Mn.

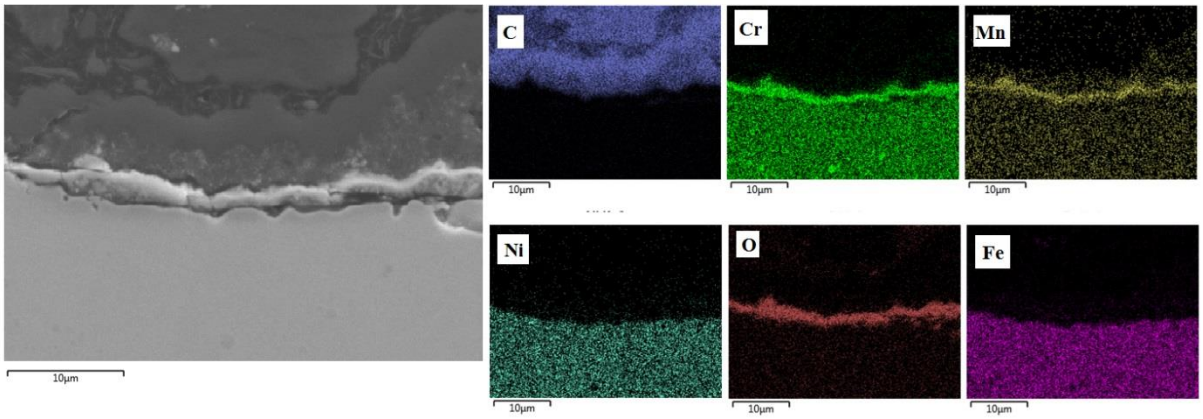

Figure C. 5: 25/35 Cr/Ni alloy after aging CA steam cracking conditions

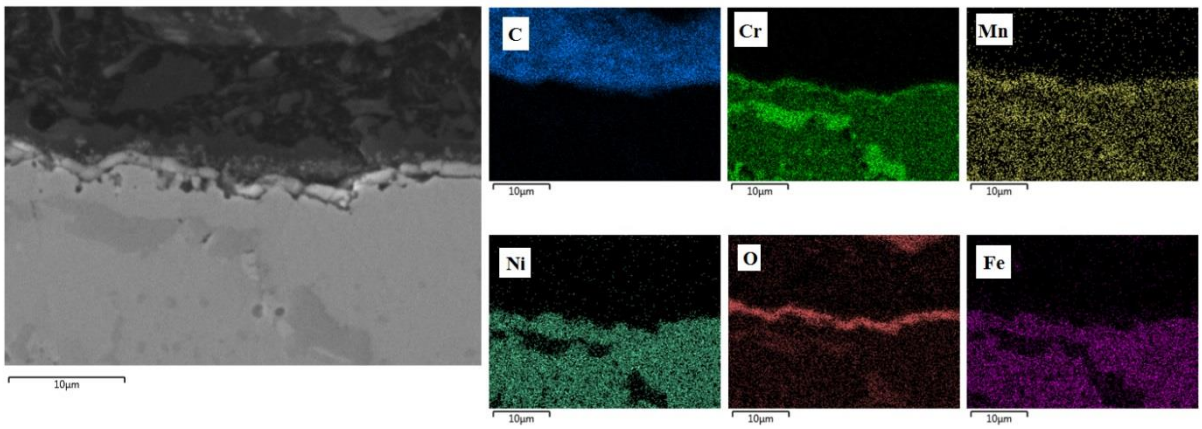

Figure C. 6: 35/45 Cr/Ni alloy after aging CA steam cracking conditions

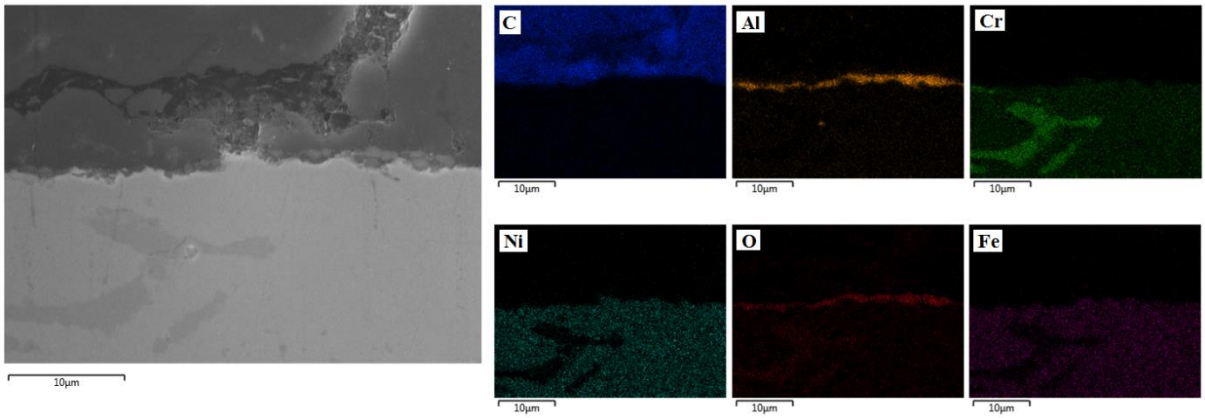

Figure C. 7: Al-content alloy after aging CA steam cracking conditions

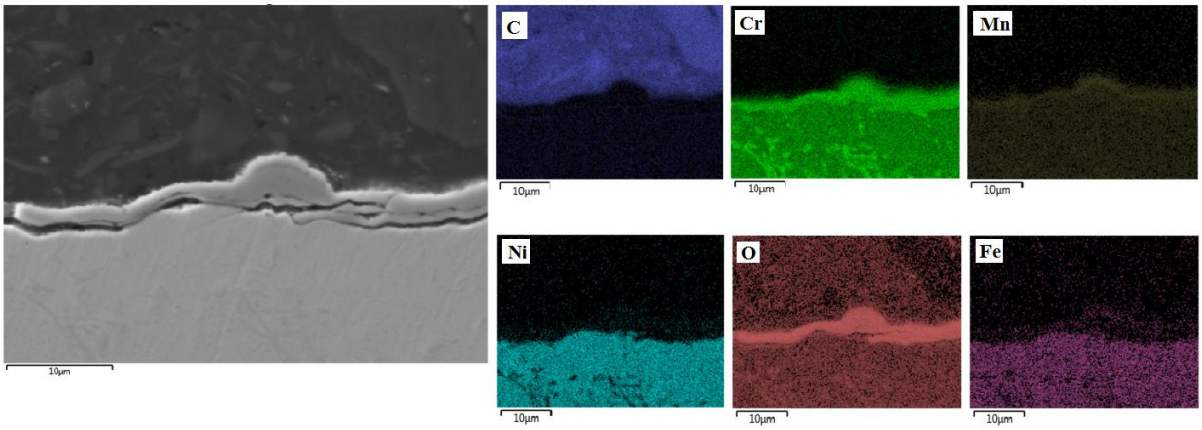

Figure C. 8: 40/48 Cr/Ni alloy after aging CA steam cracking conditions

Presulfiding experiments

Similarly with the above-mentioned conditions, 25/35 and 35/45 Cr/Ni alloys show a uniform surface oxidation with the latter indicating thicker oxides – see Figure C. 9 to Figure C. 12. Overall, the thickness is decreased by the addition of a presulfiding step before cracking for all the alloys, but no significant effect on the homogeneity is noticed except from the 25/35 Cr/Ni. For the Al-content alloy, also Cr is identified in the oxides formed.

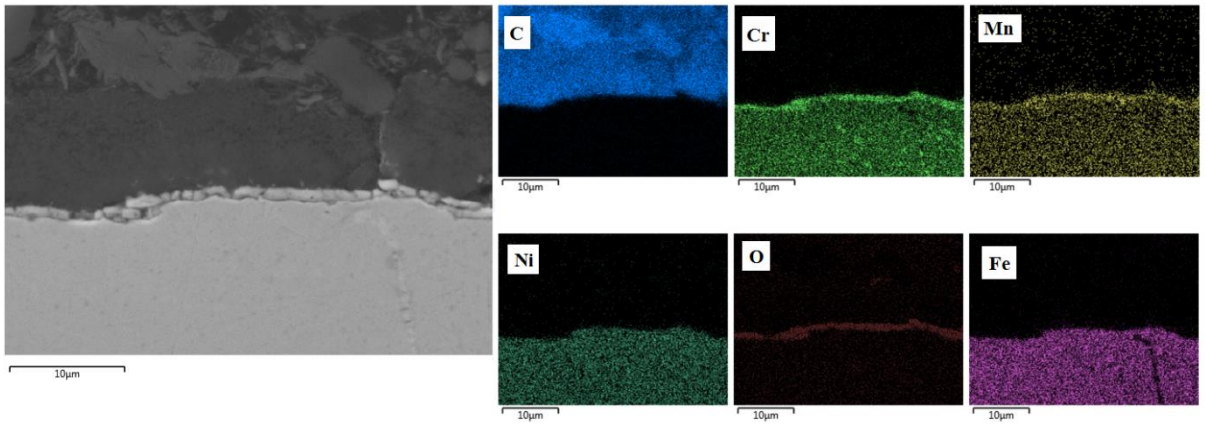

Figure C. 9: 25/35 Cr/Ni alloy after aging PreS steam cracking conditions

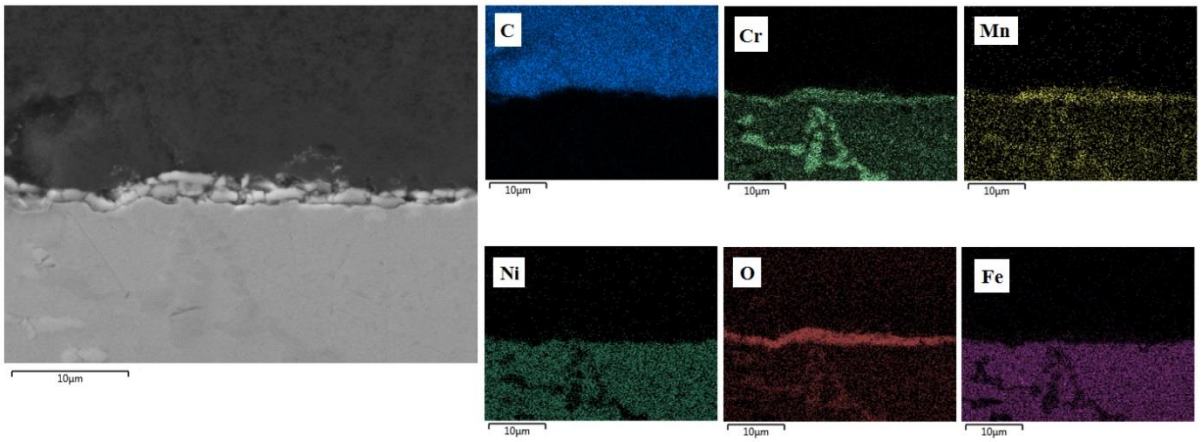

Figure C. 10: 35/45 Cr/Ni alloy after aging PreS steam cracking conditions

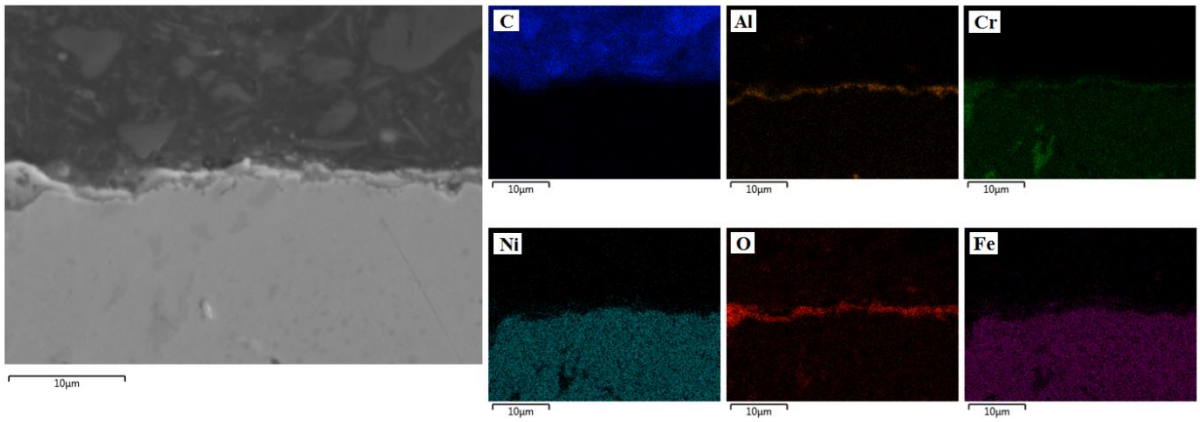

Figure C. 11: Al-content alloy after aging PreS steam cracking conditions

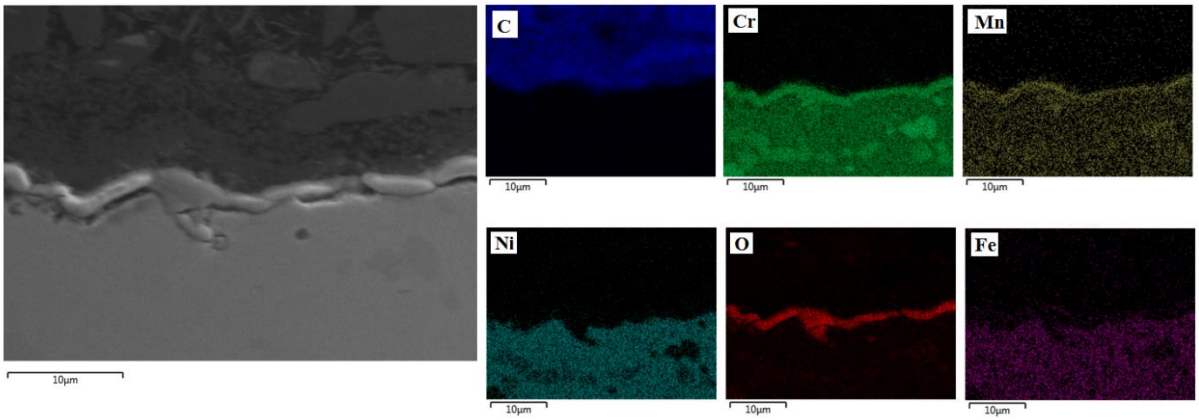

Figure C. 12: 40/48 Cr/Ni alloy after aging PreS steam cracking conditions

Continuous addition of DMDS combined with Presulfiding

Judging by Figure C. 13 to Figure C. 16, the oxides thickness decrease after application of a presulfiding step is also noticed for all the alloys when continuous addition of DMDS is applied during cracking. The homogeneity of the oxides is still acceptable, leaving no catalytic elements in contact with the gas phase.

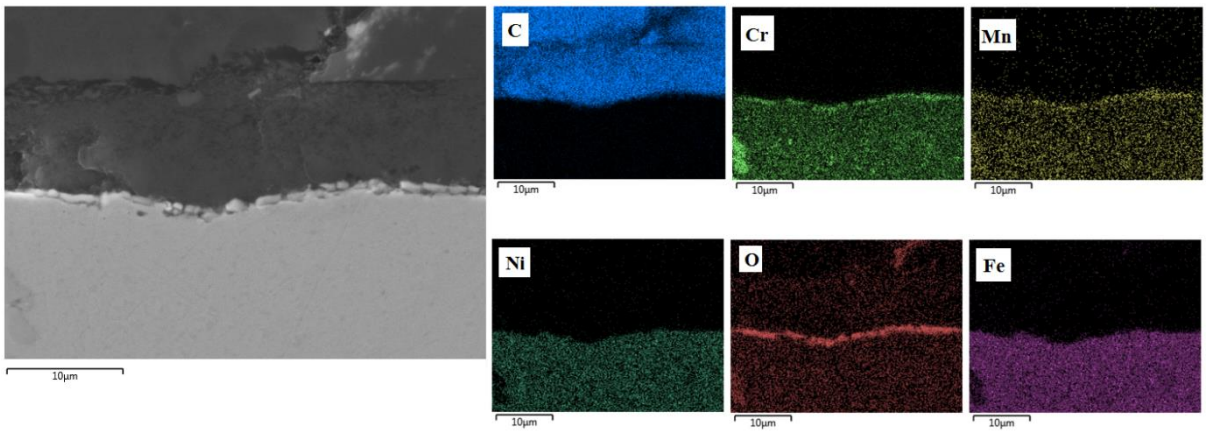

Figure C. 13: 25/35 Cr/Ni alloy after aging CA+PreS steam cracking conditions

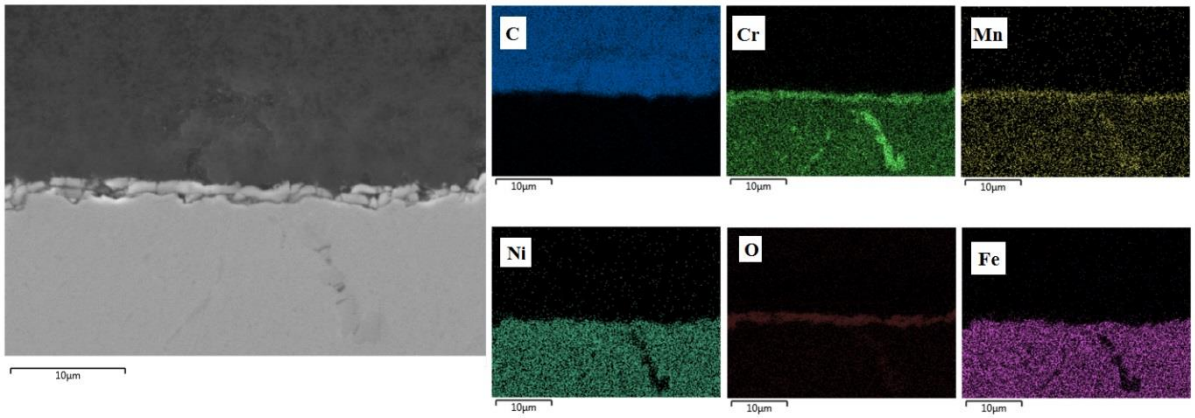

Figure C. 14: 35/45 Cr/Ni alloy after aging CA+PreS steam cracking conditions

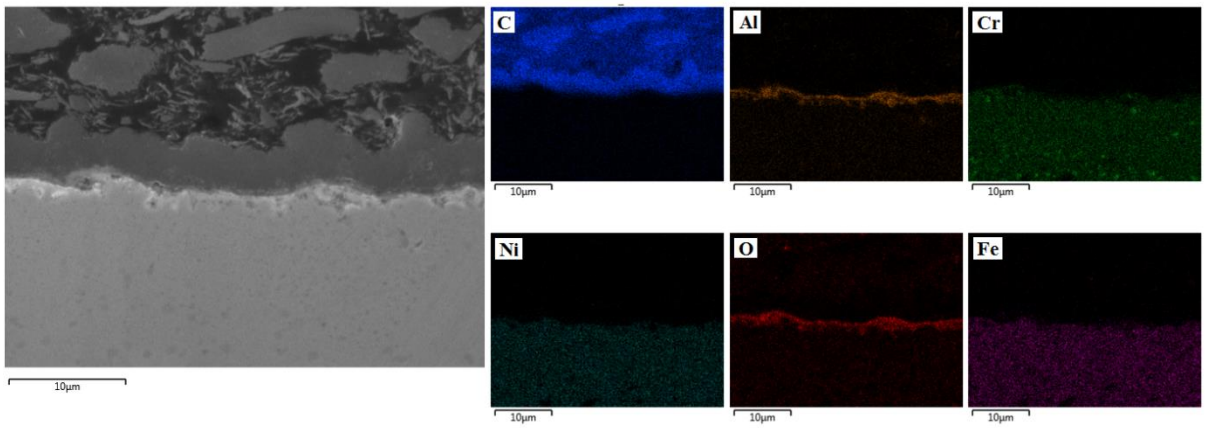

Figure C. 15: Al-content alloy after aging CA+PreS steam cracking conditions

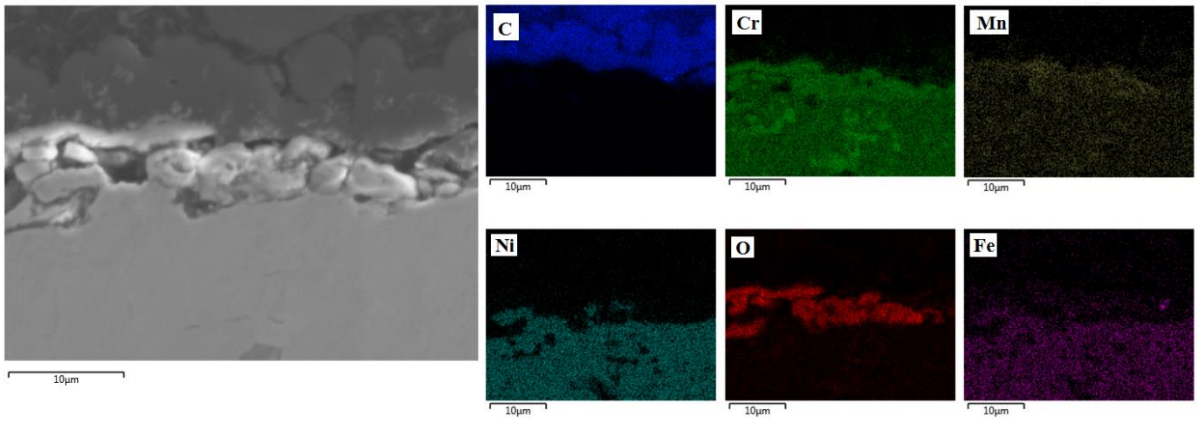

Figure C. 16: 40/48 Cr/Ni alloy after aging CA+PreS steam cracking conditions

Continuous addition of DMDS at high temperature

The most significant differences are observed when a higher cracking temperature is applied on the samples, as illustrated in Figure C. 17 to Figure C. 20. The Cr/Ni alloys seem to form thicker oxides, during cracking, keeping their homogeneity stable. However, only the bulk of the 40/48 Cr/Ni alloy is not affected by the higher cracking temperature. The rest of the samples suffer from internal oxidation. Especially, the Al-content alloy is now covered by a thick Chromium oxide that underneath is overlaying with Al, Fe or Ni. Apparently, the latter phenomenon, is what makes the Al-content performing better under high temperature conditions. On top, the existence of the Chromium oxides help with the anti-coking performance, while the Aluminum oxide under that possibly helps with its stability at higher temperatures [1]. The latter observation confirms the conclusion of the cracking experiments. The 40/48 Cr/Ni alloy is highly suggested candidate as industrial tube material.

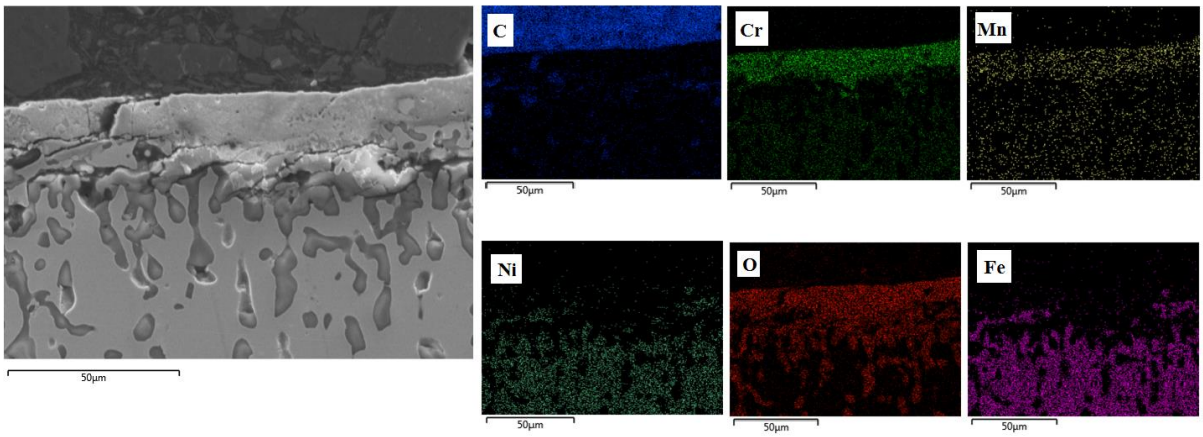

Figure C. 17: 25/35 Cr/Ni alloy after aging CA HT steam cracking conditions

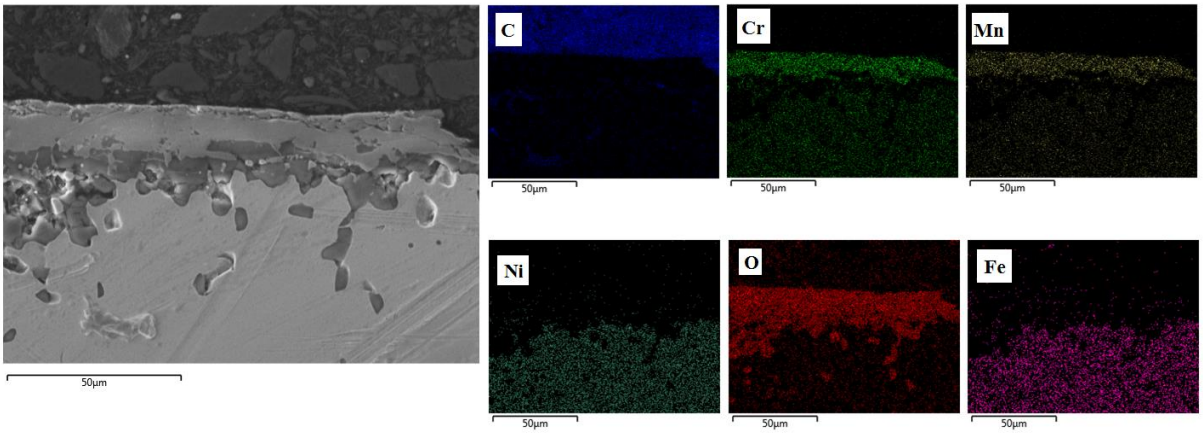

Figure C. 18: 35/45 Cr/Ni alloy after aging CA HT steam cracking conditions

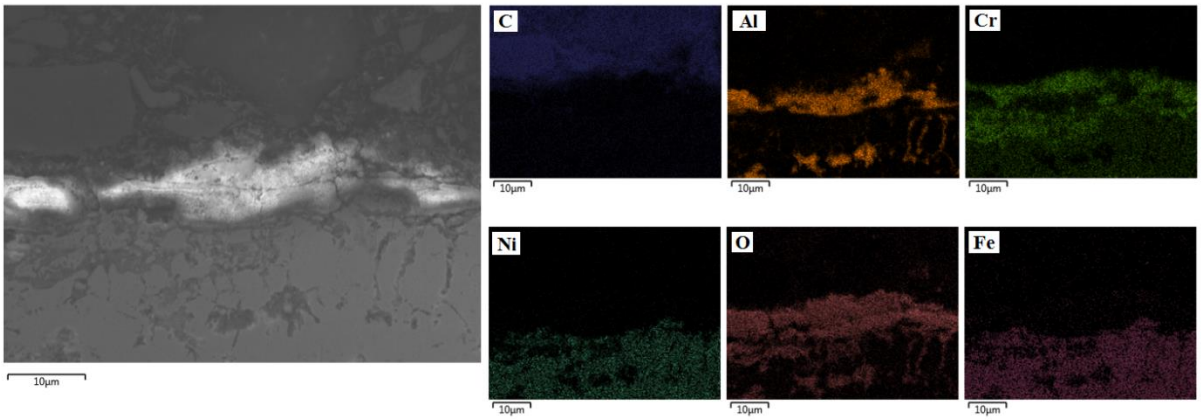

Figure C. 19: Al-content alloy after aging CA HT steam cracking conditions

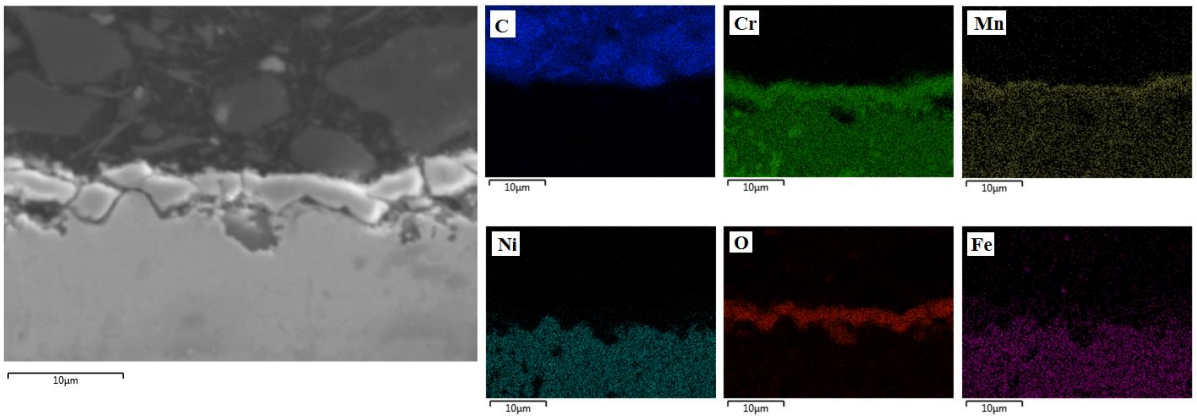

Figure C. 20: 40/48 Cr/Ni alloy after aging CA HT steam cracking conditions

Table C. 1: Experimental results and process conditions of the Blank cracking experiments

Experiment		Blank			
		25/35 Cr/Ni	35/45 Cr/Ni	40/48 Cr/Ni	Al-content
Conditions	**Ethane Flow [10^{-6} kg s^{-1}]**			29.17	
	Steam Flow [10^{-6} kg s^{-1}]			9.72	
	CA DMDS amount (ppmw S/HC)			-	
	PreS DMDS amount (ppmw DMDS/H_2O)			-	
	Temperature (K)			1173	
	Pressure			1.02	
	dillution			0.33	
Initial coking rate [10^{-6} kg/s/m^2]	**cc**				
	1	0.71	0.50	0.44	1.04
	2	0.67	0.79	0.74	1.77
	3	0.86	0.62	0.58	1.87
	4	0.85	0.55	0.54	1.93
	5	0.96	0.64	0.62	2.02
	6	0.97	0.66	0.64	1.90
	7	0.67	0.57	0.55	1.79
	8	0.63	0.50	0.46	1.82
Asymptotic coking rate [10^{-6} kg/s/m^2]	**cc**				
	1	0.22	0.15	0.14	0.38
	2	0.22	0.17	0.17	0.41
	3	0.23	0.15	0.14	0.47
	8	0.21	0.16	0.15	0.52
Yields (wt%)	**wt(%)**				
	H_2	4.23	4.25	4.22	4.26
	CO_2	0.006	0.006	0.003	0.007
	CO	0.053	0.050	0.045	0.060
	CH_4	6.99	7.09	6.99	7.02
	C_2H_6	30.13	30.03	30.11	30.03
	C_2H_4	49.88	49.95	49.86	49.88
	C_3H_8	0.11	0.11	0.11	0.11
	C_3H_6	0.74	0.75	0.74	0.75
	C_2H_2	1.38	1.39	1.39	1.38
	1,3-C_4H_6	2.02	2.00	1.98	1.99
	Benzene	2.46	2.46	2.46	2.46

Table C. 2: Experimental results and process conditions of the PreS cracking experiments

	Experiment	PreS			
		25/35 Cr/Ni	35/45 Cr/Ni	40/48 Cr/Ni	Al-content
Conditions	**Ethane Flow [10^{-6} kg s^{-1}]**		29.17		
	Steam Flow [10^{-6} kg s^{-1}]		9.72		
	CA DMDS amount (ppmw S/HC)		-		
	PreS DMDS amount (ppmw DMDS/H_2O)		500		
	Temperature (K)		1173		
	Pressure		1.02		
	dillution		0.33		
Initial coking rate [10^{-6} kg/s/m^2]	**cc**				
	1	0.63	0.65	0.67	1.04
	2	0.87	0.85	0.82	1.06
	3	1.04	1.06	0.68	1.53
	4	0.91	0.81	0.81	2.19
	5	1.68	1.46	0.91	2.48
	6	2.34	1.64	0.87	1.62
	7	2.71	1.71	0.71	1.61
	8	1.36	1.26	0.68	1.83
Asymptotic coking rate [10^{-6} kg/s/m^2]	**cc**				
	1	0.57	0.54	0.28	0.55
	2	0.45	0.42	0.35	0.29
	3	0.51	0.49	0.36	0.37
	8	0.63	0.53	0.34	0.56
Yields (wt%)	**wt(%)**				
	H_2	4.26	4.27	4.24	4.25
	CO_2	0.004	0.004	0.002	0.004
	CO	0.041	0.038	0.027	0.060
	CH_4	7.11	7.11	6.98	7.13
	C_2H_6	29.84	29.94	30.12	29.85
	C_2H_4	50.06	50.09	49.96	50.23
	C_3H_8	0.11	0.11	0.11	0.12
	C_3H_6	0.76	0.76	0.74	0.77
	C_2H_2	1.41	1.41	1.38	1.42
	1,3-C_4H_6	2.02	2.01	2.02	1.99
	Benzene	2.48	2.48	2.46	2.48

Table C. 3: Experimental results and process conditions of the CA cracking experiments

Experiment		CA			
		25/35 Cr/Ni	35/45 Cr/Ni	40/48 Cr/Ni	Al-content
Conditions	**Ethane Flow [10^{-6} kg s^{-1}]**	29.17			
	Steam Flow [10^{-6} kg s^{-1}]	9.72			
	CA DMDS amount (ppmw S/HC)	41			
	PreS DMDS amount (ppmw DMDS/H_2O)	-			
	Temperature (K)	1173			
	Pressure	1.02			
	dillution	0.33			
Initial coking rate [10^{-6} kg/s/m^2]	**cc**				
	1	3.03	2.07	0.94	1.13
	2	4.74	1.44	0.60	1.28
	3	4.23	2.11	0.92	1.26
	4	5.85	1.78	0.91	1.64
	5	6.45	1.83	1.39	1.55
	6	6.42	1.80	0.96	1.58
	7	6.39	1.77	0.84	1.64
	8	5.29	2.20	0.99	1.24
Asymptotic coking rate [10^{-6} kg/s/m^2]	**cc**				
	1	1.53	1.11	0.72	0.74
	2	1.43	1.00	0.48	0.75
	3	1.61	1.02	0.67	0.79
	8	2.47	1.23	0.40	0.79
Yields (wt%)	**wt(%)**				
	H_2	4.25	4.23	4.21	4.27
	CO_2	0.003	0.00	0.002	0.004
	CO	0.010	0.01	0.010	0.011
	CH_4	7.05	7.11	7.17	7.05
	C_2H_6	30.15	30.20	30.16	30.21
	C_2H_4	49.80	49.84	49.93	49.77
	C_3H_8	0.11	0.11	0.11	0.11
	C_3H_6	0.76	0.77	0.78	0.76
	C_2H_2	1.38	1.41	1.45	1.38
	1,3-C_4H_6	2.03	2.00	1.97	2.03
	Benzene	2.55	2.59	2.62	2.55

Table C. 4: Experimental results and process conditions of the PreS cracking experiments

	Experiment	CA + PreS			
		25/35 Cr/Ni	35/45 Cr/Ni	40/48 Cr/Ni	Al-content
Conditions	**Ethane Flow [10^{-6} kg s^{-1}]**	29.17			
	Steam Flow [10^{-6} kg s^{-1}]	9.72			
	CA DMDS amount (ppmw S/HC)	41			
	PreS DMDS amount (ppmw DMDS/H_2O)	500			
	Temperature (K)	1173			
	Pressure	1.02			
	dillution	0.33			
Initial coking rate [10^{-6} kg/s/m^2]	**cc**				
	1	6.28	2.32	1.08	1.19
	2	3.39	1.61	1.05	1.42
	3	3.63	2.36	1.06	1.60
	4	5.28	1.87	1.11	2.04
	5	5.78	1.92	1.62	1.96
	6	6.43	1.89	1.26	2.10
	7	4.12	1.86	1.06	1.96
	8	5.42	2.31	1.10	1.72
Asymptotic coking rate [10^{-6} kg/s/m^2]	**cc**				
	1	4.17	1.15	0.80	0.87
	2	2.79	1.06	0.72	0.86
	3	2.91	1.10	0.72	1.06
	8	2.89	1.38	0.53	1.02
Yields (wt%)	**wt(%)**				
	H_2	4.28	4.26	4.29	4.24
	CO_2	0.003	0.002	0.002	0.003
	CO	0.011	0.010	0.010	0.010
	CH_4	7.08	7.05	7.08	7.05
	C_2H_6	30.02	30.21	30.12	29.99
	C_2H_4	49.87	49.76	49.87	50.04
	C_3H_8	0.11	0.11	0.11	0.11
	C_3H_6	0.76	0.77	0.74	0.76
	C_2H_2	1.39	1.38	1.39	1.38
	1,3-C_4H_6	2.03	2.03	2.03	2.03
	Benzene	2.54	2.55	2.54	2.55

Table C. 5: Experimental results and process conditions of the PreS cracking experiments

	Experiment	**CA HT**			
		25/35 Cr/Ni	**35/45 Cr/Ni**	**40/48 Cr/Ni**	**Al-content**
Conditions	**Ethane Flow [10^{-6} kg s^{-1}]**	29.17			
	Steam Flow [10^{-6} kg s^{-1}]	9.72			
	CA DMDS amount (ppmw S/HC)	41			
	PreS DMDS amount (ppmw DMDS/H_2O)	-			
	Temperature (K)	1223			
	Pressure	1.02			
	dillution	0.33			
Initial coking rate [10^{-6} kg/s/m^2]	**cc**				
	1	7.58	4.01	1.19	1.69
	2	11.86	3.95	1.47	2.06
	3	10.57	3.97	1.16	1.95
	4	14.61	8.53	1.27	3.11
	5	16.14	8.69	1.79	7.04
	6	16.04	7.10	1.52	2.53
	7	15.97	8.09	1.24	1.97
	8	13.23	4.95	1.17	3.24
Asymptotic coking rate [10^{-6} kg/s/m^2]	**cc**				
	1	3.83	2.20	0.87	0.80
	2	3.57	2.28	0.94	1.01
	3	4.02	2.91	0.76	1.06
	8	6.19	3.38	0.66	2.10
Yields (wt%)	**wt(%)**				
	H_2	5.17	5.22	5.23	5.19
	CO_2	0.008	0.006	0.006	0.007
	CO	0.081	0.070	0.040	0.087
	CH_4	12.91	12.86	12.86	12.76
	C_2H_6	15.86	15.97	15.95	16.02
	C_2H_4	47.58	47.59	47.67	47.69
	C_3H_8	0.08	0.08	0.08	0.08
	C_3H_6	0.68	0.68	0.68	0.68
	C_2H_2	3.57	3.54	3.56	3.56
	1,3-C_4H_6	2.12	2.11	2.12	2.13
	Benzene	6.12	6.11	6.12	6.08

References

1. Jakobi, D.; Karduck, P.; von Richthofen, A. F., The High-Temperature Corrosion Resistance of Spun-Cast Materials for Steam-Cracker Furnaces-A Comparative Study of Alumina-and Chromia-Forming Alloys. *CORROSION* **2013**.

Appendix D. Supplementary information to Chapter 6.

This Appendix contains data to be published as supporting information of the manuscript :

Al-based barrier coating for coke reduction in Steam Crackers

Stamatis A. Sarris, Steffen H. Symoens, Natalia Olahova, Reyniers, M.-F.; Marin, G. B.; Van Geem, K. M.

To be submitted

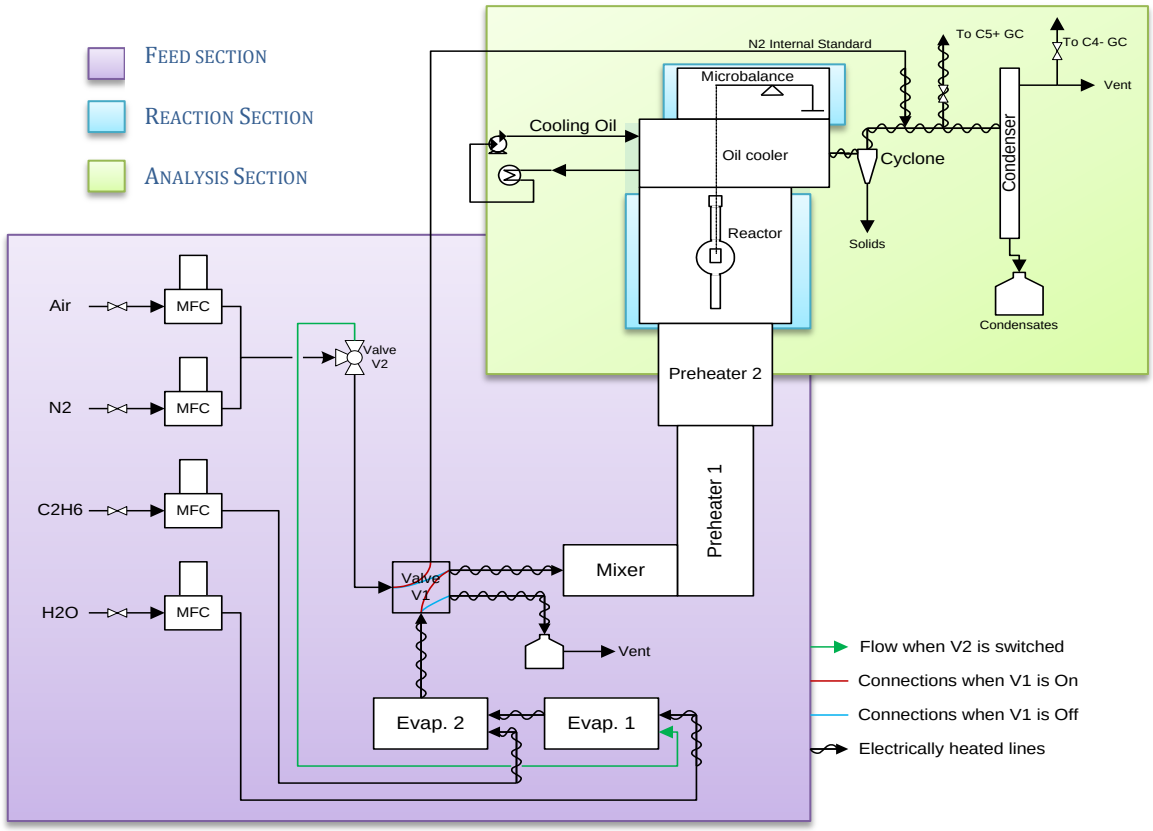

Figure D. 1: Schematic representation of the JSR set-up

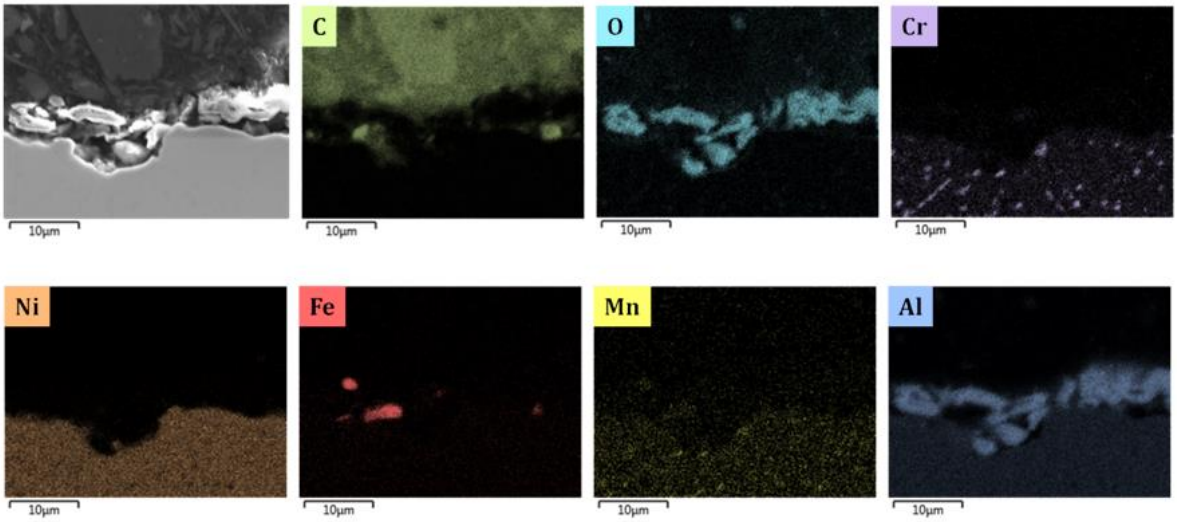

Figure D. 2: Cross-sectional elemental mappings of a fresh CoatAlloy coupon at 3000x and 15 kV.

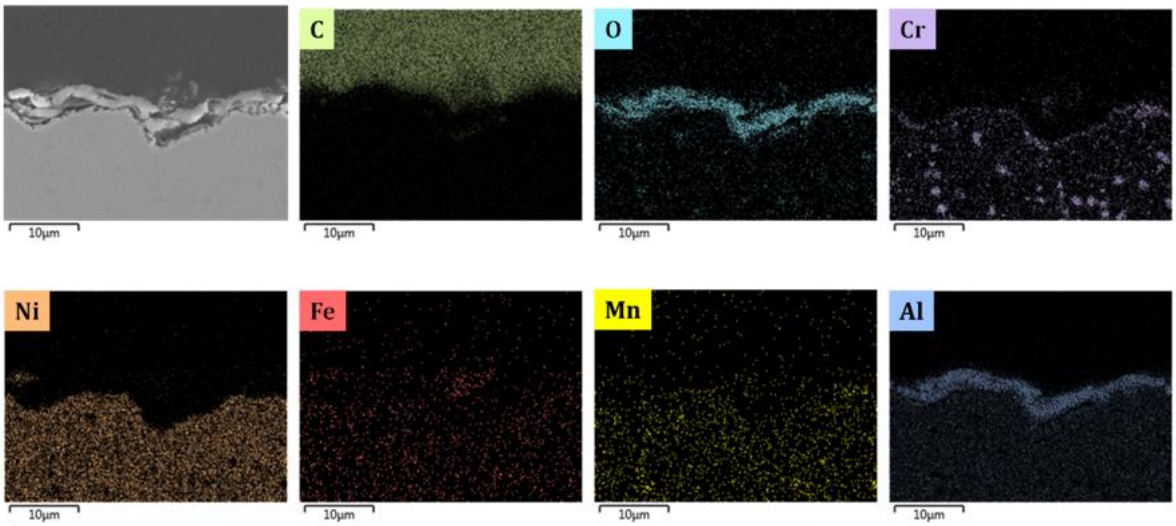

Figure D. 3: Cross-sectional elemental mapping of the CoatAlloy coupon subjected to pre-nitration at 3000x and 15 kV.

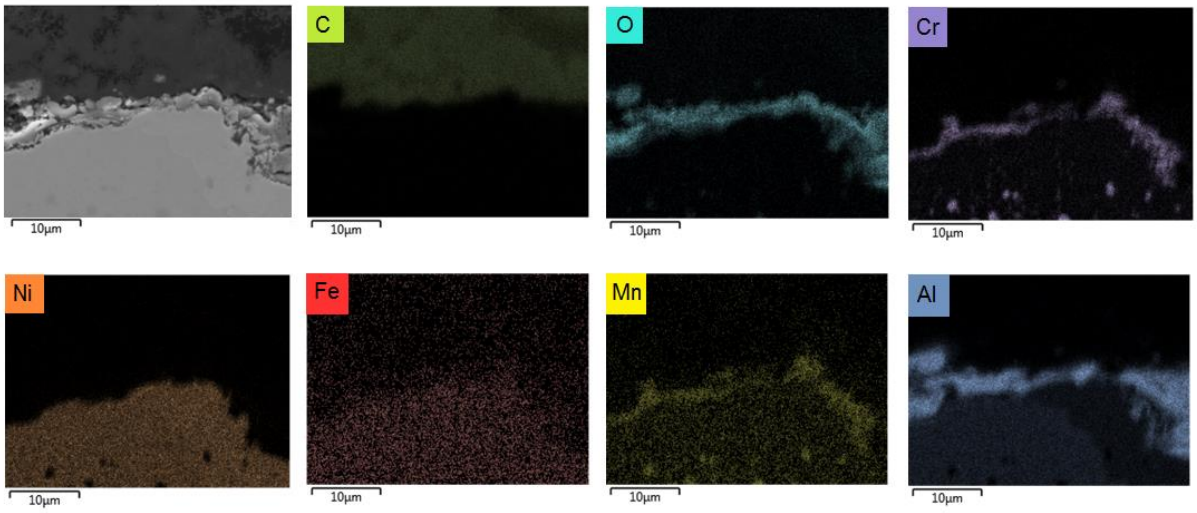

Figure D. 4: Cross-sectional elemental mappings of CoatAlloy after application of the typical pretreatment at a magnification of 3000x and a voltage of 15 kV.

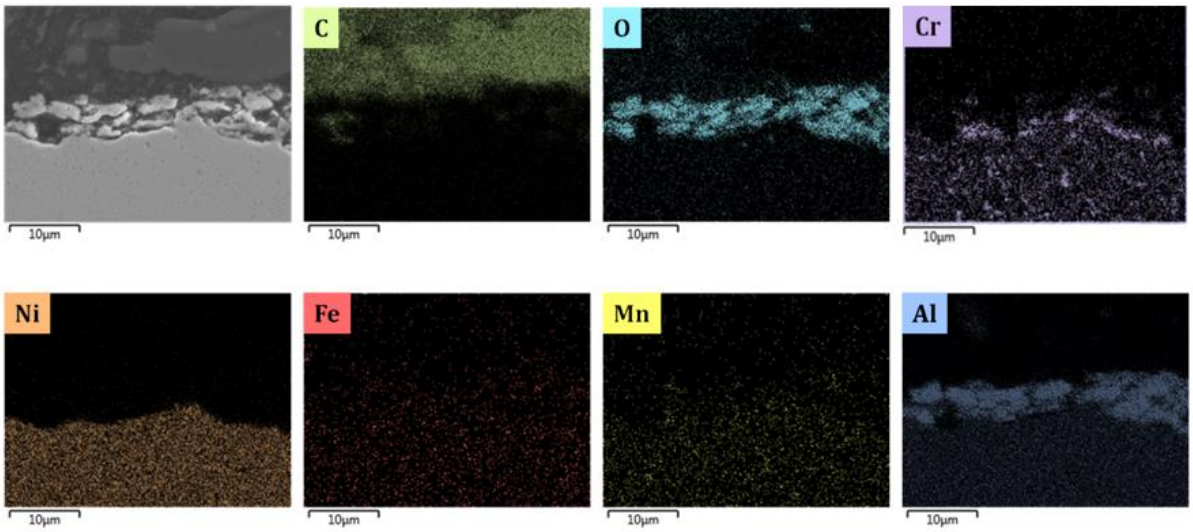

Figure D. 5: Cross-sectional elemental mappings of the CoatAlloy coupon subjected to the improved pretreatment at 3000x and 15 kV.

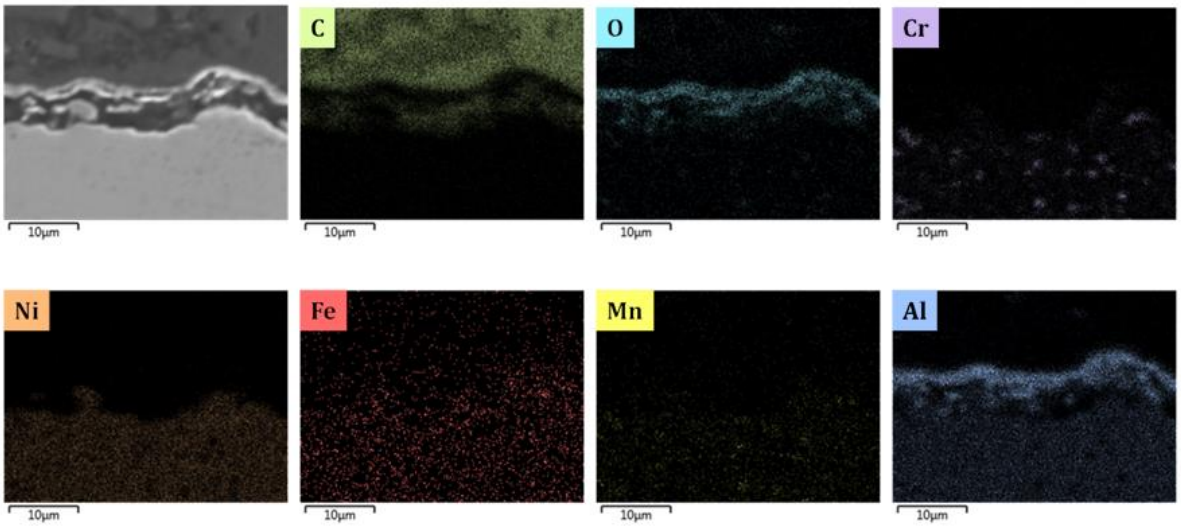

Figure D. 6: Cross-sectional elemental mapping of the CoatAlloy coupon subjected to improved pretreatment followed by presulfiding at 3000x and 15 kV

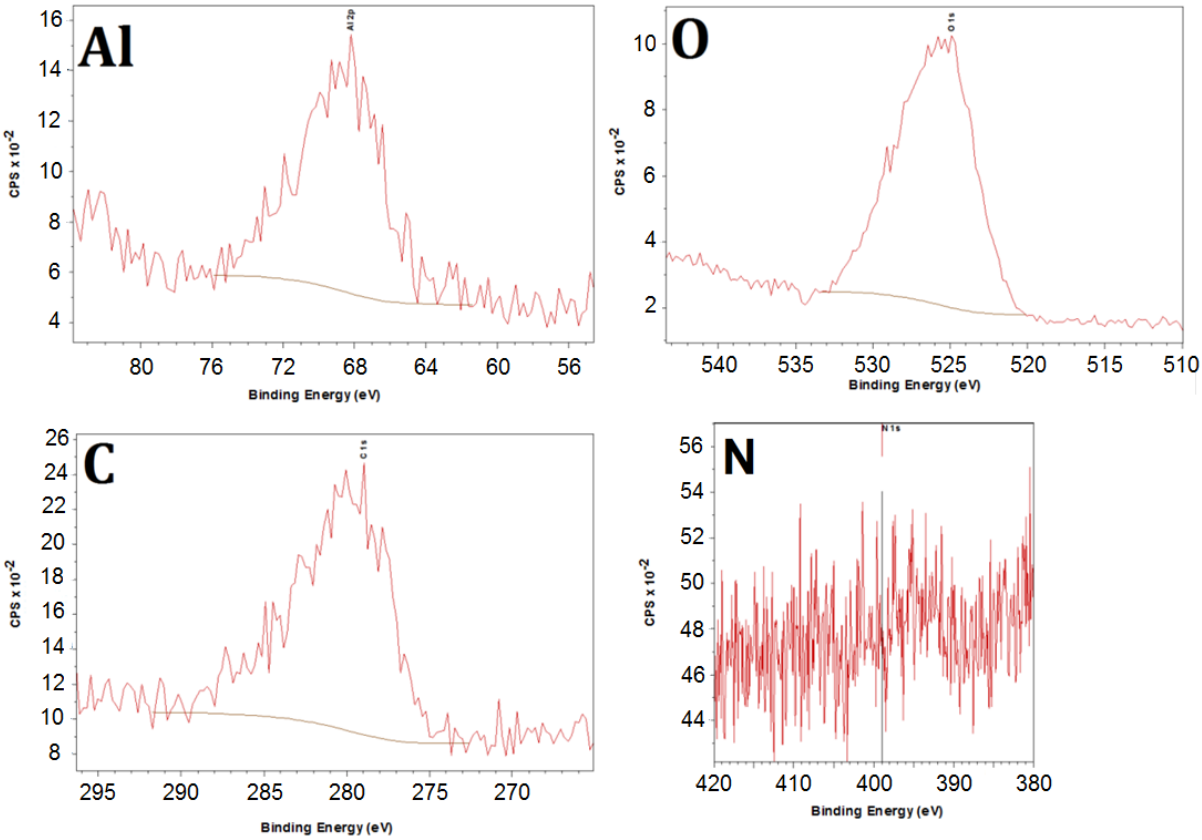

Figure D. 7: CoatAlloy sample on XPS analysis. Integrated spectra for C, O, N and Al

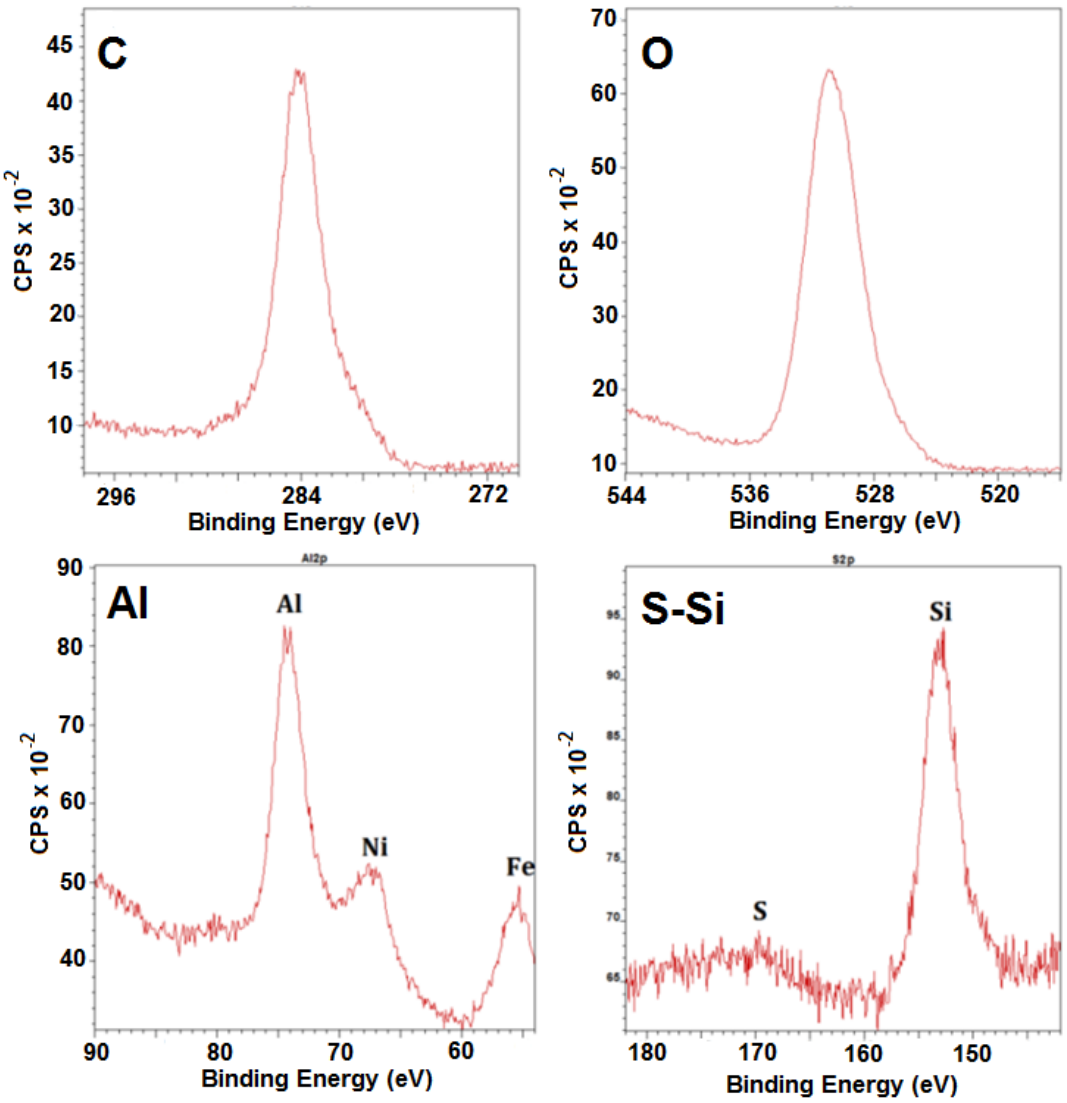

Figure D. 8: XPS-spectra for the different elements in sulfided coated coupon.

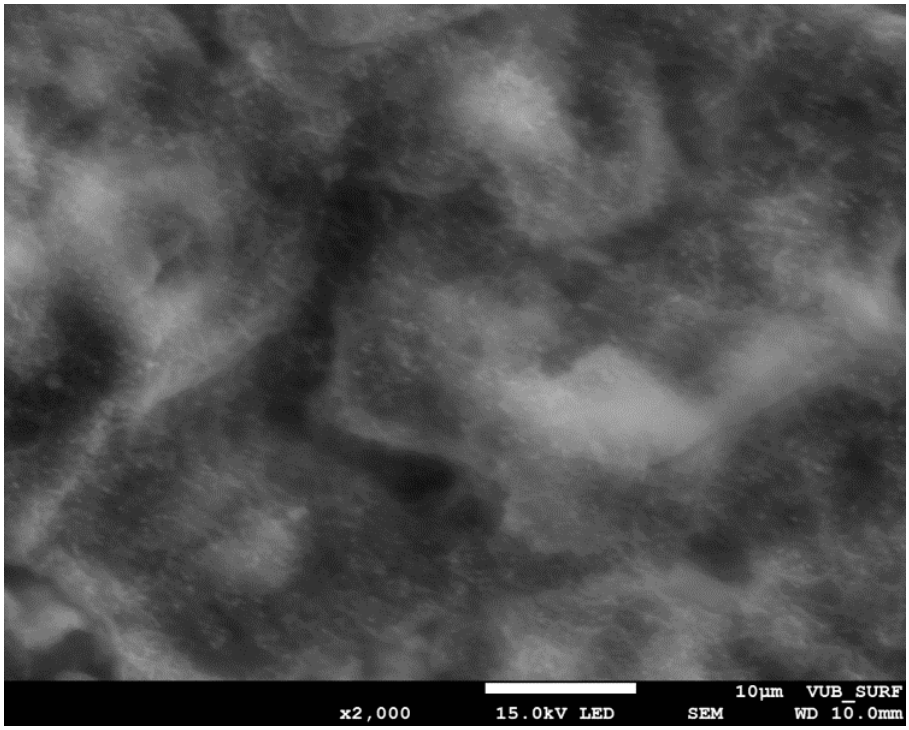

Figure D. 9: Picture of CoatAlloy surface subjected to N_2. Magnification: 2000x, Acceleration Voltage: 15kV

Table D. 1: Overview of the cracking experiments

Material	**25/35 Cr/Ni**	**CoatAlloy**	**CoatAlloy**	**25/35 Cr/Ni**	**CoatAlloy**	**25/35 Cr/Ni**	**CoatAlloy**	**25/35 Cr/Ni**	**CoatAlloy**
Pretreatment	**optimized**	**standard**	**only steam**	**standard**	**only steam**	**standard**	**only steam**	**standard**	**only steam**
id		**Blank**		**PreS**		**CA**		**CA+PreS**	
Cracking Temperature (K)		1173		1173		1173		1173	
N_2 during stabilization		no		no		no		no	
dilution		0.33		0.33		0.33		0.33	
CA DMDS (ppmw S per HC)		0		0		41		41	
PreS (ppmw DMDS per H_2O)		0		500		0		500	
cc				**Coke formed (mg)**					
1	1.29	2.01	1.61	2.46	5.60	7.55	14.28	19.15	36.16
2	1.26	2.08	1.65	2.18	3.83	8.38	16.89	12.24	36.04
3	1.41	2.47	1.93	2.52	4.71	8.66	11.52	12.84	37.09
4	0.60	1.26	0.96	0.64	1.77	4.12	2.39	3.73	4.68
5	0.67	1.97	1.50	1.19	1.66	4.55	2.34	4.08	4.52
6	0.69	1.18	0.94	1.65	1.88	4.53	2.54	4.54	4.47
7	0.47	1.17	0.91	1.91	1.51	4.51	2.44	2.91	4.73
8	1.19	5.08	4.13	2.84	4.97	11.46	9.69	11.21	16.42
cc				**Initial coking rate [10^{-6} kg/s/m^2]**					
1	0.71	0.72	0.48	0.63	1.52	3.03	5.15	6.28	8.79

2	0.67	0.73	0.49	0.87	1.30	4.74	7.07	3.39	8.72
3	0.86	0.83	0.55	1.04	1.86	4.23	3.26	3.63	8.80
4	0.85	1.56	1.04	0.91	1.95	5.85	2.69	5.28	4.93
5	0.96	2.44	1.63	1.68	1.82	6.45	2.63	5.78	4.50
6	0.97	1.46	0.98	2.34	2.31	6.42	2.82	6.43	4.70
7	0.67	1.44	0.96	2.71	1.87	6.39	2.71	4.12	4.86
8	0.63	2.56	1.71	1.36	1.77	5.29	4.40	5.42	5.03
cc	**Asymptotic coking rate [10^{-6} kg/s/m^2]**								
1	0.22	0.35	0.24	0.57	0.87	1.53	2.14	4.17	6.85
2	0.22	0.37	0.24	0.45	0.55	1.43	2.04	2.79	6.86
3	0.23	0.44	0.30	0.51	0.61	1.61	1.85	2.91	7.14
8	0.21	0.74	0.50	0.53	0.73	2.17	1.01	2.09	2.67
component	**Averaged Yields (wt %)**								
H_2	4.24	4.26	4.23	4.26	4.23	4.25	4.23	4.26	4.24
CO_2	0.006	0.007	0.006	0.004	0.004	0.003	0.003	0.002	0.003
CO	0.05	0.11	0.09	0.04	0.08	0.01	0.01	0.01	0.01
CH_4	6.99	7.13	7.13	7.11	7.16	7.05	7.14	7.08	7.17
C_2H_6	30.13	29.88	29.94	29.84	29.86	30.21	29.96	30.02	29.88
C_2H_4	49.86	50.18	50.31	50.06	50.39	49.76	50.42	49.87	50.41
C_3H_8	0.11	0.11	0.12	0.11	0.12	0.11	0.12	0.11	0.12
C_3H_6	0.74	0.76	0.75	0.76	0.77	0.76	0.77	0.76	0.77
C_2H_2	1.38	1.39	1.37	1.41	1.43	1.38	1.41	1.39	1.42
1,3-C_4H_6	2.00	2.05	1.95	2.02	1.97	2.03	2.07	2.03	1.97
Benzene	2.46	2.46	2.49	2.48	2.49	2.55	2.47	2.54	2.48

*In all coking results a 10% error should be accounted

List of publications

Journal Papers

Optimization of the in-situ pretreatment of high temperature Ni-Cr Alloys for Ethane steam cracking
Stamatis A. Sarris, Natalia Olahova, Kim Verbeken, Marie-Françoise Reyniers, Guy B. Marin, Kevin M. Van Geem
Ind. Eng. Chem. Res., 2017, 56 (6), pp 1424–1438
Publication Date (Web): January 17, 2017 (Article)
DOI: 10.1021/acs.iecr.6b04537

Impact of initial surface roughness and aging on coke formation during Ethane Steam Cracking
Stamatis A. Sarris, Steffen H. Symoens, Natalia Olahova, Kim Verbeken, Marie-Françoise Reyniers, Guy B. Marin, Kevin M. Van Geem
Ind. Eng. Chem. Res., 2017, 56 (44), pp 12495–12507
Publication Date (Web): October 16, 2017 (Article)
DOI: 10.1021/acs.iecr.7b02479

Experimental study of coke formation of innovative super alloys
Stamatis A. Sarris, Manjunath Patil, Marie-Françoise Reyniers, Guy B. Marin, Kevin M. Van Geem
To be submitted

Ti-base alloy coking behavior during steam cracking of ethane
Stamatis A. Sarris, Manjunath Patil, Marie-Françoise Reyniers, Guy B. Marin, Kevin M. Van Geem
To be submitted

Al-based barrier coating for coke reduction in Steam Crackers
Stamatis A. Sarris, Steffen H. Symoens, Marie-Françoise Reyniers, Guy B. Marin, Kevin M. Van Geem
To be submitted

Effect of long-term high temperature oxidation on coking behavior and microstructure of Ni-Cr alloys
Stamatis A. Sarris, Manjunath Patil, Reyniers, M.-F.; Marin, G. B.; Van Geem, K. M.
To be submitted

Catalytic Coating for Reduced Coke Formation in Steam Cracking Reactors
Carl M. Schietekat, Stamatis A. Sarris, Pieter A. Reyniers, Lawrence B. Kool, Wenqing Peng, Patrick Lucas, Kevin M. Van Geem, and Guy B. Marin
Ind. Eng. Chem. Res., 2015, 54 (39), pp 9525–9535
Publication Date (Web): September 14, 2015 (Article)
DOI: 10.1021/acs.iecr.5b02263

Computational Fluid Dynamic Design of Jet Stirred Reactors for Measuring Intrinsic Kinetics of Gas-Phase and Gas-Solid Reactions
Pieter A. Reyniers, Stamatis A. Sarris, Guy B. Marin, Kevin M. Van Geem
First published: 11 July 2016
DOI: 10.1002/kin.21016

CoatAlloy ™ Barrier Coating for Reduced Coke Formation in Steam Cracking Reactors: Experimental Validation and Simulations
Natalia Olahova, Steffen H. Symoens, Marko Dokic, Nenad Ristic, Stamatis A. Sarris, Marie-Françoise Reyniers, Mathieu Couvrat, Fanny Riallant, Hugues Chasselin, Kevin Van Geem
Submitted on 14th of November 2017 on Ind. Eng. Chem. Res.

Coking tendency of 25Cr-35Ni alloys: influence of temperature, sulfur addition and cyclic aging
Natalia Olahova, Stamatis A. Sarris, Marie-Françoise Reyniers, Kevin Van Geem
Submitted on 15th of November 2017 on Ind. Eng. Chem. Res.

Oral presentations

Al-based Coating for Coke Reduction during Ethane Steam Cracking
Stamatis A. Sarris[1], Natalia Olahova[1], Marko Djokic[1], Mathieu Couvrat[2], Fanny Riallant[2], Hugues Chasselin[2], Marie-Françoise Reyniers[1], Guy B. Marin[1], Kevin M. Van Geem[1]
(1)Laboratory for Chemical Technology (LCT), Ghent University, Ghent, Belgium,
(2)Manoir Industries, Paris, France
2016 AIChE Annual Meeting, San Francisco, CA, November 13-18 2016

Ti-Base Alloy Coking Behavior during Steam Cracking of Ethane
Stamatis A. Sarris, Kevin M. Van Geem, Marie-Françoise Reyniers, Guy B. Marin
2016 AIChE Annual Meeting, San Francisco, CA, November 13-18 2016

Poster presentations

Experimental study of catalytic coating for reduced coke formation
Stamatis A. Sarris, Carl M. Schietekat , Lawrence B. Kool, Wenqing Peng, Patrick Lucas, Kevin M. Van Geem, Guy B. Marin